AN ABSTRACT OF THE THESIS OF

__John M. O'Connor__ for the degree of __Doctor of Philosophy__ in
__Oceanography__ presented on __May 31, 1991__
Title:_____The Evolution of South Atlantic Hot Spot Systems:_____
_____An Integrated Geochronological and Geochemical Investigation_____
Redacted for Privacy

Abstract approved:_____

David M. Christie

The time-space and geochemical evolution of the volcanic traces generated by the Walvis and St. Helena hot spots have important implications for reconstructing plate motions over mantle-fixed hot spots, and for understanding the geochemical structure of the mantle. Assuming that the Walvis and St. Helena hot spots are both broad and diffuse (i.e., greater than 500 km in diameter), two Euler poles are sufficient to reconstruct African plate migration such that predicted geometries and ages of the volcanic traces generated by these hot spots accord with the observed trends of the Walvis Ridge, the St. Helena Seamount Chain, and in the case of the Reunion hot spot, the Mascarene Plateau. The velocity of the African plate is calculated from the distribution of ^{40}Ar-^{39}Ar basement ages along these volcanic traces and incorporates an uncertainty of 4.5°, due to the inferred broad, diffuse nature of the associated hot spots. Westward migration of the South Atlantic spreading-axis away from the St. Helena and Walvis hot spots, beginning between 80 and 70 Ma, changed the plate tectonic setting in which the Walvis Ridge and the St. Helena Chain were forming simultaneously from on-axis to intraplate.

Hyperbolic Nd-Pb, Sr-Pb, and linear Pb-Pb isotopic covariations in lavas dredged from the St. Helena Chain suggest a continuum of mixing between HIMU and EM 1 mantle components. Mixing between depleted mantle (i.e. DMM) and compositions from the HIMU–EM 1 continuum best explains the enigma of a single St. Helena Seamount sample plotting below this two-component mixing array. Basalt drilled from Cretaceous seafloor formed close to the Walvis hot spot was apparently derived from a mixture of EM1, HIMU, and DMM. Three mantle components (HIMU, EM1, and DMM) are therefore available to the St. Helena and Walvis hot spot sources. Finally, it is suggested that variability in plume temperature plays a significant role in controlling the isotopic composition of hot spot lavas, leading to the association of predominantly EM 1-like

lavas with hot, vigorous plumes and, conversely, predominantly more HIMU-like lavas with cooler, less vigorous plumes.

The Evolution of South Atlantic Hot Spot Systems:
An Integrated Geochronological and Geochemical Investigation

by

John M. O'Connor

A THESIS

submitted to

Oregon State University

in partial fulfillment of
the requirements for the
degree of

Doctor of Philosophy

Completed May 31, 1991

Commencement June 1992

APPROVED:

Redacted for Privacy

Professor of Oceanography in charge of major

Redacted for Privacy

Dean of College of Oceanography

Redacted for Privacy

Dean of Graduate School

Date thesis is presented   May 31, 1991

Presented by   John M. O'Connor

To Angelika and my parents

ACKNOWLEDGEMENTS

TABLE OF CONTENTS

Table of contents (continued)

Table of contents (continued)

List of Figures (continued)

CHAPTER III

List of Figures (continued)

CHAPTER IV

LIST OF TABLES

THE EVOLUTION OF SOUTH ATLANTIC HOT SPOT SYSTEMS: AN INTEGRATED GEOCHRONOLOGICAL AND GEOCHEMICAL INVESTIGATION

I. INTRODUCTION TO THESIS

Hot spot volcanism and the opening of the South Atlantic

This thesis investigates the phenomenon of hot spot volcanism as it is expressed by the time-space evolution, and compositional variability, of prominent South Atlantic aseismic ridges, seamount chains, and oceanic islands. The two longest hot spot-generated volcanic lineaments on the African plate, both in time and space, are the Walvis Ridge and the sub-parallel St. Helena Seamount Chain (South Atlantic Ocean). The Rio Grande Rise and the Pernambuco-Bahia Seamounts (all on the South American lithospheric plate) formed in conjunction with these lineaments during the period that the South Atlantic spreading-axis was located astride, or close to, the Walvis and St. Helena hot spots, respectively.

These South Atlantic hot spot-generated volcanic traces are of particular interest as their lavas characterize two isotopically distinct mantle components (i.e., HIMU and EM 1). In addition, continental rifting in the vicinity of the Walvis hot spot was accompanied by the eruption of the massive Parana (Brazil) and Etendeka (Namibia) continental flood basalt flows. The results and conclusions of this investigation are reported in the following three manuscripts.

Chapter II (Manuscript 1)

The distribution of ^{40}Ar-^{39}Ar incremental heating ages determined for basalts dredged and drilled from the Walvis Ridge and the Rio Grande Rise indicates that the Walvis Ridge and the Rio Grande Rise formed as the African and South American plates, respectively, migrated away from a spreading-axis-centered hot spot. The orientations of the Walvis Ridge and other African plate hot spot traces, define the locations of Euler poles which describe the direction of African plate motion over hot spots; the time-space distribution of radiometric ages along the Walvis Ridge records African plate velocity about these poles, since the South Atlantic began to open. This model assumes that the hot spot responsible for the formation of the Walvis Ridge-Rio Grande Rise is centered now beneath the island of Tristan da Cunha.

Beginning at about 70 Ma the South Atlantic spreading axis began to migrate westward, away from the Tristan da Cunha hot spot, leading to a transition from on-axis to intraplate hot spot volcanism along the Walvis Ridge.

Chapter III (Manuscript 2)

The time-space evolution of the St. Helena Seamount Chain and the Gough Lineament (Walvis Ridge), as defined by the distribution of ^{40}Ar-^{39}Ar incremental heating ages for dredged seamount samples along these features, significantly improves reconstruction of African plate motion over hot spots. The most important contributions of this manuscript are to propose that the St. Helena and Walvis hot spots are broad and diffuse (>500 km in diameter), far larger than suggested by the size of an individual ocean island such as St. Helena or Tristan da Cunha, and to incorporate this proposition into a model of African plate motion over hot spots. African plate velocity about these poles is estimated from the combined distribution of ^{40}Ar-^{39}Ar ages along the St. Helena Chain, Walvis Ridge, and the Mascarene Plateau. A systematic uncertainty of 4.5° or 500 km is allowed in these calculations due to the broad and diffuse nature of the associated hot spots. African plate velocity appears to have decreased from ~0.25 to ~0.11 deg/m.y. between ~31 and 0 Ma. A simultaneous transition to intraplate hot spot volcanism occurred along the St. Helena Chain and the Walvis Ridge, beginning between 80 and 70 Ma, in response to a westward migration of the South Atlantic spreading-axis away from the St. Helena and Walvis hot spots.

Chapter IV (Manuscript 3)

Variability in Sr, Nd, and Pb isotopic ratios for rock samples dredged from the St. Helena, Bahia, and Pernambuco Seamounts indicates a mixing continuum between HIMU and EM 1 mantle components, which are typified by the compositions of lavas from the island of St. Helena, and the Walvis Ridge, respectively. Interaction between depleted mantle (DMM) and this mixing array is also indicated by the composition of a St. Helena Seamount sample. Basalt drilled from abyssal seafloor, north of the easternmost Walvis Ridge, was derived from HIMU, as well as EM 1 and DMM mantle components. It is therefore concluded that HIMU, EM 1, and DMM, are available to the Walvis and St. Helena hot spot sources, supporting the suggestion that these components are available to the majority of hot spot sources. Finally, it is suggested that variability in plume temperature and vigor may dictate the relative proportions of HIMU, EM 1, and DMM in Atlantic hot spot lavas.

II. EVOLUTION OF THE WALVIS RIDGE–RIO GRANDE RISE HOT SPOT SYSTEM: IMPLICATIONS FOR AFRICAN AND SOUTH AMERICAN PLATE MOTIONS OVER PLUMES

John M. O'Connor and Robert A. Duncan

ABSTRACT

Crystallization ages of volcanic rocks, dredged or drilled from the Walvis Ridge (ten sites) and the Rio Grande Rise (one site), have been determined by the ^{40}Ar-^{39}Ar incremental heating technique. The fundamentally age-progressive distribution of these basement ages suggests a common hot spot source for volcanism on the island of Tristan da Cunha, along the Walvis Ridge and Rio Grande Rise, and for the formation of the continental flood basalts located in Namibia (Africa) and Brazil (South America). The Walvis Ridge–Rio Grande Rise volcanic system evolved along a section of the South Atlantic spreading-axis, as the African and South American plates migrated apart, astride, or in close proximity to, an upwelling plume. Reconstructions of the spatial relationship between the spreading-axis, the Tristan hot spot, and the evolving Walvis Ridge–Rio Grande Rise volcanic feature show that, at about 70 Ma, the spreading-axis began to migrate westward, away from the hot spot. The resulting transition to intraplate hot spot volcanism along the Walvis Ridge (and associated termination of Rio Grande Rise formation) also involved a northward migration of previously formed African seafloor over the hot spot. Rotation parameters for African motion over fixed hot spots (i.e., absolute motion) have been recalculated such that the predicted trail of the Tristan hot spot agrees with the distribution of radiometric and fossil basement ages along the Walvis Ridge. African absolute motion has been extended to the South and North American plates, by the addition of relative motion reconstruction poles.

INTRODUCTION

Apart from the mid-Atlantic spreading-axis, the Walvis Ridge (Figure II.1a) and Rio Grande Rise (Figure II.1b) are the two most prominent bathymetric features in the South Atlantic basin. Broadly speaking, the Walvis Ridge and the Rio Grande Rise form a V-shaped pair of volcanic lineaments, whose axis of symmetry is the South Atlantic spreading-center (Figure II.2). Morgan [1971, 1972], following Wilson [1963], related the formation of these volcanic trails to hot spot volcanism, presently active beneath the ocean island of Tristan da Cunha.

The Walvis Ridge can be subdivided into three morphologically distinct regions, two of which appear to have a comparable or "mirror image" region on the Rio Grande Rise. The broad eastern plateau of the Walvis Ridge projects seaward from the African coast to about 5°E. This plateau initially evolved in conjunction with the Torres Arch, later with the broad plateau of the Rio Grande Rise, and finally with the northeastern shoulder of the Rio Grande Rise. The central section of the Walvis Ridge (about 5°E to 2°W) includes three distinct, subparallel NE-trending ridges, which formed in conjunction with the eastern, N-S ridge of the Rio Grande Rise. Finally, the Walvis Ridge merges into a line of large seamounts, which extends southwestward from the central section of the Walvis Ridge toward Tristan da Cunha. A corresponding seamount chain does not appear to exist on the South

Figure II.1a. Bathymetry for the Walvis Ridge, contoured in 1000 m intervals [after Needham et al., 1986].
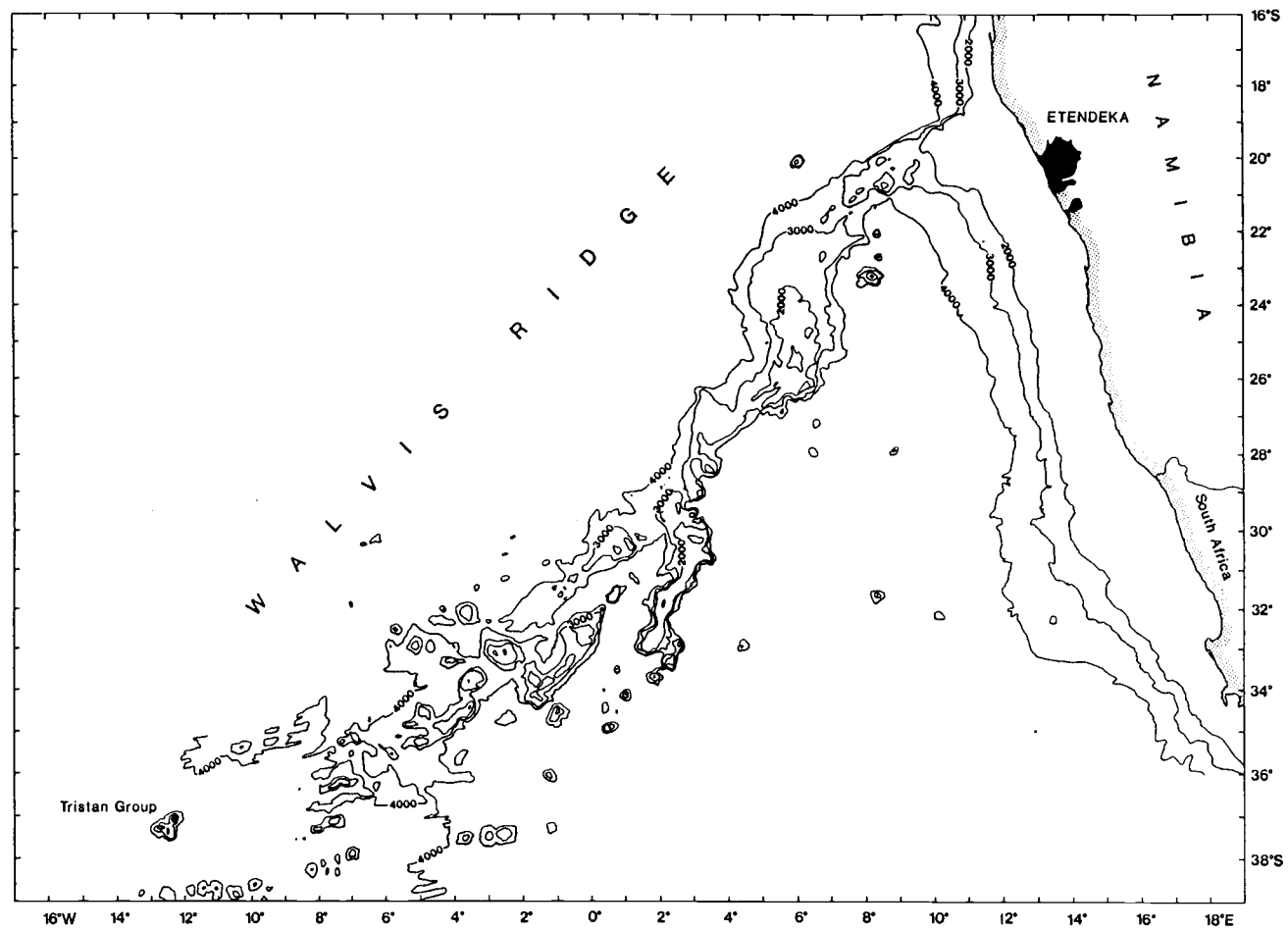
Figure II.1a

Figure II.1b. Bathymetry for the Rio Grande Rise, contoured in 1000 m intervals [after Cherkis et al., 1989]. Mercator projections.
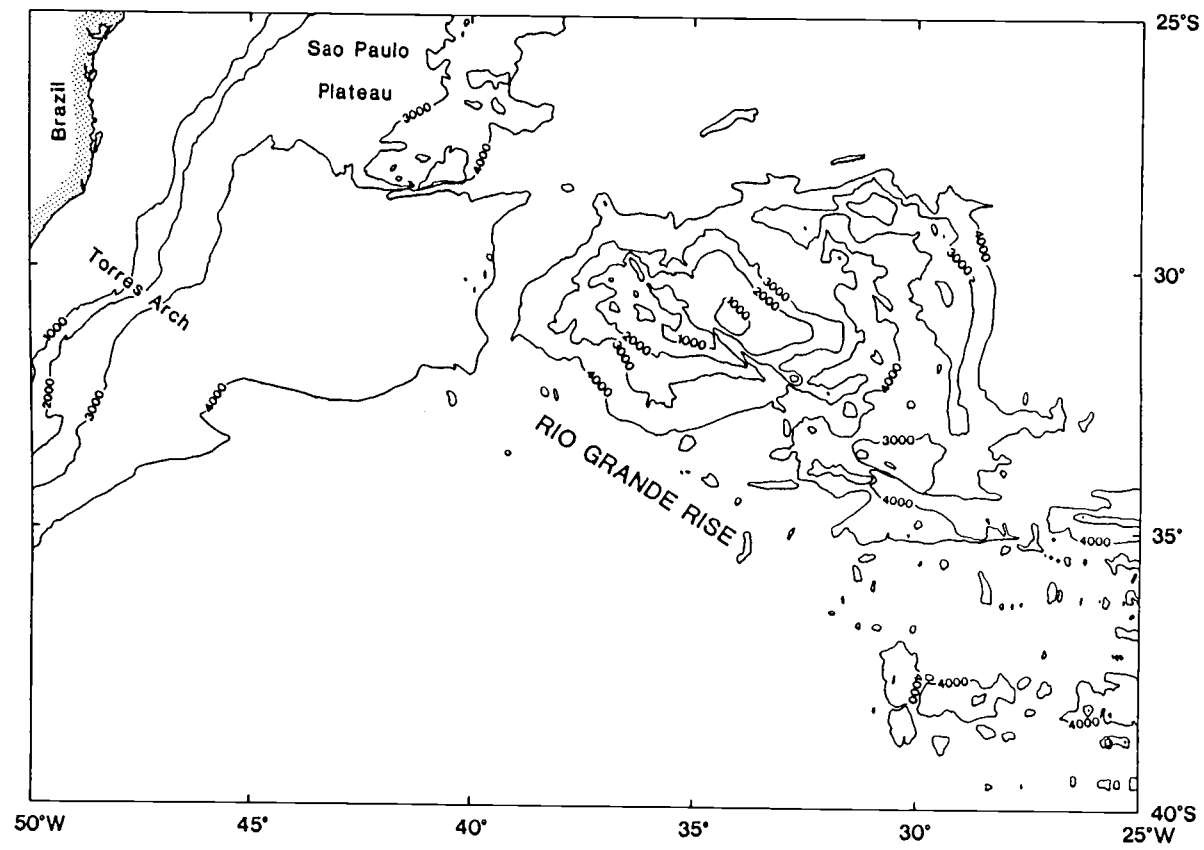
Figure II.1b

Figure II.2. Solid circles show the locations of the sample sites from which the rocks analyzed in this study were recovered. Seafloor spreading anomalies and fracture zones are from Cande et al. [1989]. A fossil spreading center south of the Rio Grande Rise is shown by a "railroad track". The location to which the spreading-axis jumped, between C32 and C30 times, is shown as a line of open circles on both the Rio Grande Rise and the Walvis Ridge. Mercator projection.
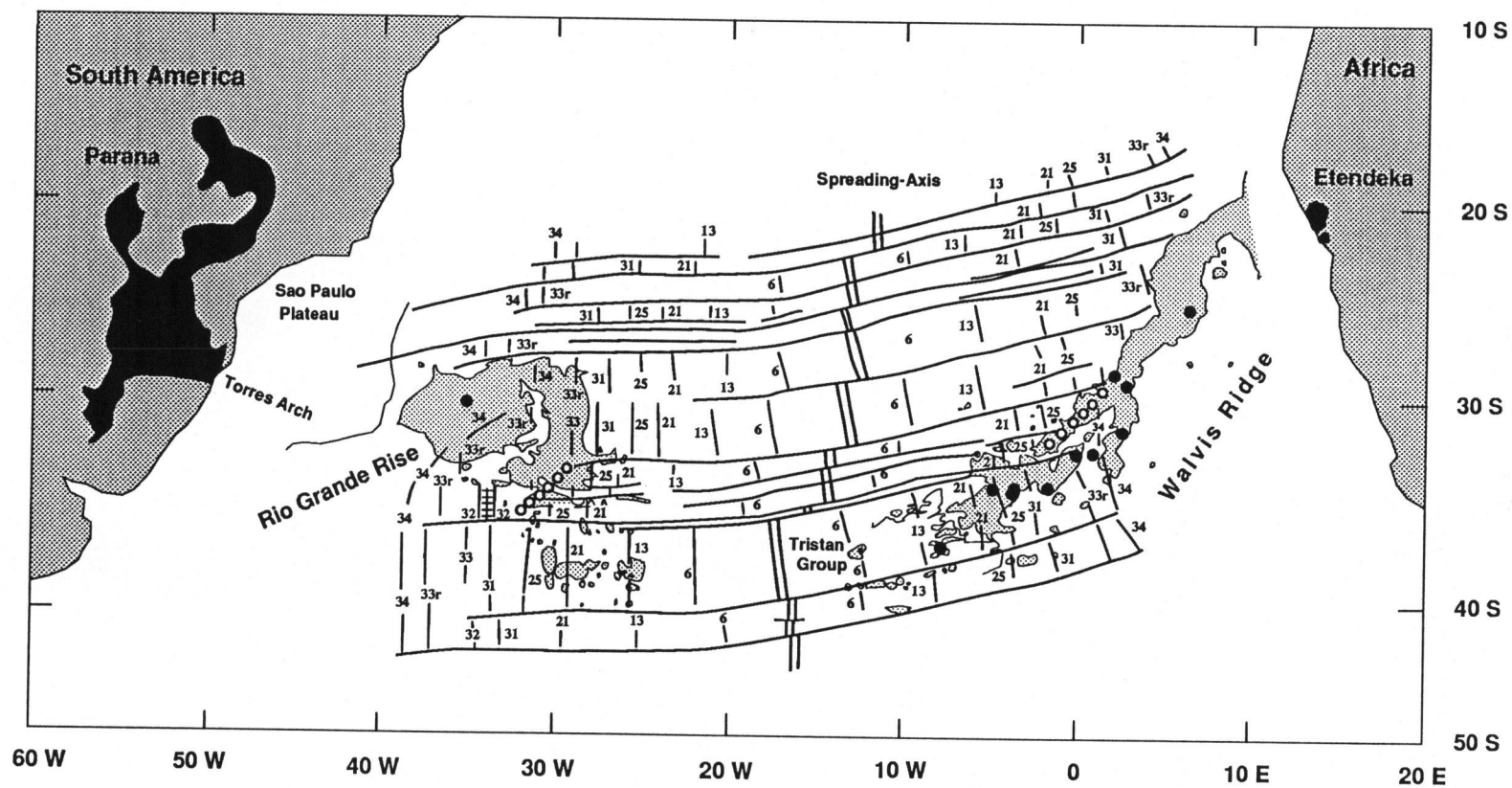
Figure II.2

American plate; however, the Zapiola Seamount Complex, located to the south of the Rio Grande Rise may be related in some way to the Tristan hot spot.

The island of Tristan da Cunha is located ~550 km to the east of the present day spreading-axis, on C6 oceanic crust (19 Ma after the time scale of Kent and Gradstein [1986], used throughout this discussion). Apparent K-Ar ages ranging from 0.01 ± 0.02 Ma to 0.21 ± 0.01 Ma have been determined for this island [McDougall and Ollier, 1982], with the most recent volcanic eruption having occurred in 1962 [Barker, 1964].

This paper reports the results of sixteen ^{40}Ar-^{39}Ar incremental heating studies of volcanic rocks recovered from ten locations distributed along the Walvis Ridge and a single sample site located on the Rio Grande Rise (Figure II.2). The changing spatial relationship between the spreading-axis, the Tristan hot spot, and the evolving structure of the Walvis Ridge–Rio Grande Rise system, has been reconstructed for selected times. These reconstructions provide new insights into the influence of hot spot and spreading-axis interactions on the structural and compositional evolution of the Walvis Ridge–Rio Grande Rise volcanic system. Previously estimated finite reconstruction poles for African plate motion over hot spots (i.e., absolute motion) have been adjusted such that the predicted track of the Tristan hot spot on the African plate reconstructs the distribution of the new Walvis Ridge basement ages. The absolute motions of the South and North American plates have, in turn, been calculated by the addition of appropriate relative motion reconstruction poles.

GEOLOGICAL SETTING

The Parana (southeast Brazil) and the Etendeka (southwest Africa) continental flood basalts (Figure II.2) represent the earliest known manifestation of the hot spot responsible for forming the Walvis Ridge–Rio Grande Rise. These flood basalt fields are shown to have formed as adjoining neighbors, on reconstruction of the South Atlantic for early Cretaceous time [Rabinowitz and LaBrecque, 1979] and Figure II.9a. Geochemical and isotopic data support a common source for the Parana–Etendeka and Walvis Ridge basalts [Hawkesworth et al., 1986]. K-Ar ages ranging from 114 to 196 Ma have been reported for the Etendeka lavas [Siedner and Miller, 1968; Siedner and Mitchell, 1976]. Erlank et al. [1984] have recognized three petrographic units within these basaltic lavas: the coastal Albin type, the widespread and voluminous Tafelberg type, and in the faulted coastal zone, late stage cross-cutting dolerite dikes which have been grouped as the Horingbaai type. K-Ar ages for these three units range from 88 to 377 Ma. The authors attribute these anomalously high K-Ar ages (as indicated by stratigraphic relationships) to excess argon "inherited" at the time of crystallization. Feldspar separates taken from two fresh Horingbaai dolerites yielded fairly convincing ^{40}Ar-^{39}Ar plateau ages of 125, and 125 to 130 Ma [Erlank et al., 1984]. These late stage intrusives may represent a final upwelling of continental hot spot volcanism immediately preceding the initiation of Walvis Ridge construction. In Brazil, Parana volcanism also appears to have peaked at between 120 and 130 Ma

[Amaral et al., 1966; McDougall and Ruegg, 1966; Melfi, 1967; Siedner and Mitchell, 1976; Cordani et al., 1980].

Based on the results of seismic reflection profiling, Austin and Uchupi [1982] have suggested that the South Atlantic began to open in the form of a northward propagating rift. The oldest seafloor spreading anomaly identified in the South Atlantic at the latitude of Capetown is M11 (133 Ma), while the oldest anomaly recognized off of the Namibian coast is M4 (126 Ma) [Cande et al., 1989]. As the Etendeka and Parana flood basalts appear to have erupted at about the same time that the northward-propagating South Atlantic rift reached the latitude of Namibia, a close association may have existed between hot spot volcanism and continental rifting. However, due to uncertainty in locating the continent-ocean boundary [e.g. Rabinowitz, 1976, 1978; Scrutton, 1978], it is presently difficult to determine whether or not, on reconstruction of the African and South American plates to a prerifting configuration, overlapping or misfit exists at the latitude of the Walvis Ridge–Rio Grande Rise. The existence of such an overlap would suggest that crustal stretching occurred in response to doming of the continental lithosphere by the upwelling plume, so supporting a relationship between rifting and hot spot volcanism. Morgan [1972], Anderson [1982] and White and McKenzie [1989] have suggested such a cause and effect relationship between Atlantic basin hot spots and the initiation of continental rifting.

The Walvis Ridge extends southwestward from the Etendeka flood basalts to about 10°E in the form of thinned continental crust, as shown by seismic reflection studies [Sibuet et al., 1984]. This portion of the ridge is characterized by internal basement reflectors which dip to the west, while still further to the west (10°E to 8°E) the acoustic basement changes to that of typical oceanic crust [Sibuet et al., 1984]. On the South American margin, the Parana lavas stretch seaward toward the Vema Channel in the form of the Torres Arch (Figure II.1b) [Kowsmann et al., 1977; Kumar, 1979].

The present day position of the spreading-axis in the latitudes of the Walvis Ridge and Rio Grande Rise is asymmetric with respect to the coasts of Africa and South America; i.e., the spreading-axis is located closer to the African than to the South American coast (Figure II.2). The southern boundary of this spreading-axis asymmetry would appear to be the unnamed fracture zone located to the north of Tristan da Cunha (Figure II.2). This asymmetry has been attributed to a succession of easterly and southeasterly spreading-axis migrations [Mascle and Phillips, 1972; Sclater and McKenzie, 1973; Ladd, 1974, 1976], which began prior to C34 (84 Ma) time. The first recorded eastward migration of the spreading-axis occurred to the north of the Walvis Ridge–Torres Arch lineament at early Albian–late Aptian time (97.5 to 115 Ma) [Leyden et al., 1976; Ponte and Asmus, 1976; Cande and Rabinowitz, 1978, 1979; Rabinowitz and LaBrecque, 1979; Kumar and Gamboa, 1979]. The primary evidence for the timing of this axis jump is the asymmetric distribution of continental margin salt deposits, which are more extensive in the Brazilian compared with the Angolan basin. African plate Mesozoic magnetic anomalies located to the north of the Rio Grande Fracture Zone were transferred westward to

13

the Sao Paulo plateau [Cande and Rabinowitz, 1978, 1979]; however, to the south of this fracture zone Mesozoic anomalies remained on the African plate [Rabinowitz, 1976]. The timing and location of the beginning of this second phase of spreading-axis migrations are not well constrained.

LaBrecque et al. [1984] mapped younger anomalies extending progressively southward and terminating against the northern flank of the Walvis Ridge (Figure II.2) and proposed that a southwardly propagating spreading-axis was involved in the formation of the Walvis Ridge–Rio Grande Rise volcanic system. Barker [1984] suggested that such easterly and southerly migrations of the spreading-axis represent a "recapturing process" of the westward drifting spreading-axis, by the Tristan da Cunha hot spot. Such spatial readjustments of the spreading-axis may therefore represent a process by which the axis maintained its position on, or close to, the Tristan hot spot for the duration of Rio Grande Rise formation.

Detrick and Watts [1979] and Humphris and Thompson [1983] have proposed that at about 80 Ma the mid-Atlantic axis began a westward migration away from the hot spot. The resulting transition to intraplate hot spot volcanism along the Walvis Ridge also involved a pronounced east-southeast ridge crest jump, sometime between anomaly 32 (71.4 Ma) and anomaly 30 (67 Ma) times, which has been mapped south of the Rio Grande Rise (Figure II.2) [Cande et al., 1988; after J. L. LaBrecque and J. M. Brozena, manuscript in preparation]. This ridge jump left a fossil spreading center roughly 200 km long, the location of which is consistent with a southward propagating rift model for spreading-axis involvement in the formation of the Walvis Ridge–Rio Grande Rise [LaBrecque et al., 1984].

SAMPLE SELECTION

The petrology and geochemistry of the Walvis Ridge and Rio Grande Rise samples selected for age determinations have been reported by Humphris and Thompson [1982, 1983], Thompson and Humphris [1984], and Richardson et al. [1982, 1984]. Overall, the Walvis Ridge and Rio Grande Rise samples range in composition from tholeiitic to alkalic basalts. These rocks generally contain phenocrysts of plagioclase feldspar up to 8 mm long and, less commonly, titaniferous augite in a groundmass composed of laths of plagioclase, granular pyroxene, Fe-oxides, and glass. Rock compositions contain between 1.0 and 4.8% MgO (dredged samples) and 0.9 and 7.2% MgO (drilled samples), representing liquids that are far evolved from primary melts. Brief sample descriptions and sample site coordinates are given in Table II.1, with sample site locations shown in Figures II.2 and II.5.

Most of the rocks show patchy alteration of the groundmass to low-temperature Fe-oxides and clay minerals. This appears to have affected mainly the groundmass, but in some cases even the pyroxene microphenocrysts are replaced. Glass has devitrified, and very finely crystallized mesostasis (as much as 40% by volume of some samples) has altered in places to smectites and zeolites. This is

TABLE II.1. Walvis Ridge and Rio Grande Rise Basalts Used for ^{40}Ar-^{39}Ar Age Determinations

Sample	Location (°S, °E)	Depth, m	Description
Walvis Ridge			
AII-93-3-1	37° 05.7', -7' 46.7'	2600-2000	vesicular pl-basalt
AII-93-3-25	37° 05.7', -7° 46.7'	2600-2000	vesicular pl-basalt
AII-93-5-3	34° 17.3', -5° 01.5'	3100-3000	vesicular pl-basalt
AII-93-7-1	34° 30.1', -3° 37.6'	2200-2100	alkali pl-basalt
AII-93-8-11	34° 29.9', -3° 28.7'	2000-1500	alkali basalt
AII-93-10-11	34° 20.1', -1° 34.4'	2300-2000	basalt
AII-93-11-8	32° 58.2', -0° 01.1'	3100-1600	vesicular basalt
V29-9-1	32° 38.0', 1° 07.0'	3500	pl-basalt
AII-93-14-1	31° 59.6', 2° 23.6'	2300-1600	vesicular basalt
AII-93-14-19	31° 59.6', 2° 23.6'	2300-1600	aphyric basalt
AII-93-21-1	25° 26.1', 6° 42.2'	3200-2600	pl-basalt
DSDP 74-525-57-5, 104-106 -6, 41-43	29° 04.2', 2° 59.1'	3087	aphyric tholeiitic basalt
DSDP 74-528-40-5, 70-75	28° 31.5', 2° 19.4'	4280	phyric pl-basalt
DSDP 74-528-41-2, 40-42	28° 31.5', 2° 19.4'	4291	aphyric basalt
Rio Grande Rise			
DSDP 72-516F-128-1, 22-24	30° 16.6', -35°17.1'	1268	phyric basalt
DSDP 72-516F-128-1, 104-107	30° 16.6', -35°17.1'	1268	phyric basalt

further demonstrated by the moderately high total volatile contents (CO_2 plus H_2O+), which range from 1.2 to 3.9%. Olivine is rarely present as a phenocryst phase or in the groundmass.

Much of the potassium in these rocks is likely to reside in the variably altered groundmass. The radiogenic ^{40}Ar ($^{40}Ar*$) generated by the decay of ^{40}Ar at these sites (after crystallization) can be lost both by diffusion and the low-temperature formation of clay minerals, resulting in erroneously young conventional K-Ar ages [Schlanger et al., 1984]. Smectites and zeolites crystallize from volcanic glass, infill vesicles and replace primary minerals.

Other complications encountered in applying the K-Ar technique to the dating of submarine volcanic rocks may arise from the fact that glassy submarine lavas may contain excess ^{40}Ar, due to the retention of mantle-derived Ar in magma erupted under high hydrostatic pressure [e.g., Dalrymple and Moore, 1968; Dalrymple and Lanphere, 1969; Dymond, 1970; Aumento, 1971]. Metasomatic addition of K, derived from seawater, to grain surfaces [Melson and Thompson, 1973; Seidemann, 1977] may lead to erroneously young K-Ar age determinations.

The available Walvis Ridge and Rio Grande Rise samples were examined in thin section in order assess the original igneous texture, crystallinity, and subsequent degree of alteration of the potassium-bearing phases. While no sample was regarded as being ideal for radiometric dating purposes, well-crystallized samples, displaying the lowest degrees of groundmass alteration, were selected for ^{40}Ar-^{39}Ar age incremental heating studies.

AGE MEASUREMENT METHODS

The ^{40}Ar-^{39}Ar method is based on the generation of ^{39}Ar from ^{39}K by the irradiation of K-bearing samples with neutrons in a nuclear reactor. The principles of this method of dating have been presented by Dalrymple and Lanphere [1971], Dalrymple et al. [1981a], and McDougall and Harrison [1988]. Samples selected for age studies were crushed after the removal of any obvious surface weathering and vesicle fillings. The 0.5 to 1.0 mm rock fragments were retained for dating experiments, ultrasonically washed in distilled H_2O, and dried. About one gram of each of the samples was encapsulated in an evacuated quartz vial and irradiated in the central thimble position of the U.S. Geological Survey TRIGA reactor for 15 hours at 1 MW power level, using the procedures described by Dalrymple et al. [1981a]. A hornblende flux monitor of known age (Mmhb-1), [Samson and Alexander, 1987] was irradiated with the basalts in order to determine the neutron flux density and the capture cross section of ^{39}Ar for neutrons during the irradiation, i.e., the efficiency of conversion of ^{39}K to ^{39}Ar expressed as the J-factor (Table II.2).

Samples and standards were individually placed in an outgassed Mo crucible, which was then heated in a high-vacuum extraction line. The standards were fused in a single heating step, while the basalts were incrementally heated in a series of five steps (each of 30 min duration) and then melted during a sixth and final step. The isotopic composition of argon (^{40}Ar, ^{39}Ar, ^{37}Ar and ^{36}Ar) released

from each individual heating or fusion step was measured immediately by means of an AEI MS-10S mass spectrometer, after active gases had been removed by cooling Ti-TiO$_2$ getters. The apparent ages of the individual heating steps were calculated from the measured $^{40}Ar^*$ to ^{39}Ar ratios, after corrections for all interfering nuclear reactions had been applied using the equation of Brereton [1970]. Hence an age-temperature spectrum was obtained for each sample, based on the $^{40}Ar^*/^{39}Ar$ compositions of the gas fractions released incrementally, from low to high temperature sites. Argon isotopic data and apparent ages are given in Table 2.

RESULTS

The most common age-temperature spectrum observed in this study consists of a middle temperature plateau bounded by higher ages at the low temperature steps, and conversely, by lower ages at the high temperature steps (e.g., Figure II.3e). Turner and Cadogan [1974] first proposed that such an "inverse staircase" age-temperature profile might result from neutron-capture recoil of ^{39}Ar from K-rich to K-poor sites within fine-grained basalts, during irradiation. Because the low-temperature sites are K-rich, recoil effects may lead to the transfer of ^{39}Ar (but not $^{40}Ar^*$) from low temperature (i.e., alteration minerals and groundmass) to high-temperature sites (e.g., feldspar and pyroxene), resulting in a descending age-temperature release pattern. Dalrymple and Clague [1976], Seidemann [1978], and McDougall and Duncan [1988] have shown that significant amounts of ^{39}Ar may be lost from slightly altered volcanic rocks during the irradiation process. Thus, in conjunction with the loss of $^{40}Ar^*$ discussed earlier, ^{39}Ar may also be lost from, or relocated within, a multiphase sample.

Examination of apparent K/Ca ratios can be helpful in identifying the mineral phases that are contributing to different regions of the age spectrum [Walker and McDougall, 1982] (e.g., Figure II.3f). With respect to the study reported here, low temperature steps generally correspond to high K/Ca phases, characteristic of K-rich alteration products such as smectite. The high apparent ages of these initial heating steps may reflect the loss or redistribution of ^{39}Ar due to neutron-induced recoil effects. The lower K/Ca values of the middle to high temperature steps are characteristic of unaltered, low K phases such as plagioclase. The plateau ages usually evident at these heating steps may be attributed to the diffusion of ^{40}Ar and ^{39}Ar from such unaltered phases. The highest temperature spectrum steps are commonly lower in age than that of the mid-temperature plateau and correspond to very low K/Ca ratios, which are characteristic of low K-phases, such as pyroxene. Recoil-induced addition of ^{39}Ar from low temperature high K-phases to K-poor high temperature phases, might account for such erroneously young ages in the age spectra.

Dalrymple et al. [1981b] suggested that, in cases where ^{39}Ar recoil is evident, the best age estimate for a sample comes from summing the gas composition of all the heating steps into a "recalculated" $^{40}Ar-^{39}Ar$ total fusion age. This calculation is based on the assumption that phases which lose ^{39}Ar during irradiation have also lost their $^{40}Ar^*$ over geological time. However, since

TABLE II.2a. Argon Isotopic Data for Walvis Ridge and Rio Grande Rise Whole Rock Samples

Increment	$^{40}Ar/^{36}Ar$	$^{40}Ar/^{39}Ar$	$^{37}Ar*/^{40}Ar$	% Radiogenic ^{40}Ar	$\%^{39}Ar$ of Total	Age ± 1 σ x 10^6 years
			Sample AII-93-3-1, J = 0.00368			
1	339.8	65.520	0.0159	13.2	9.9	56.4 ± 2.2
2	404.0	19.140	0.0816	27.5	17.0	34.6 ± 0.5
3	952.8	6.278	0.4944	72.7	26.9	30.1 ± 0.2
4	1492.6	4.959	0.7498	85.9	25.2	28.4 ± 0.2
5	1076.2	4.120	0.9291	79.6	10.1	21.7 ± 0.3
6	340.0	2.948	7.3437	70.2	11.0	13.9 ± 0.5
			Sample AII-93-3-25, J = 0.00368			
1	322.7	61.240	0.0121	8.5	10.9	34.4 ± 3.4
2	356.7	29.520	0.0640	17.6	15.2	34.3 ± 0.8
3	669.0	7.763	0.4805	59.5	26.7	30.5 ± 0.3
4	1443.3	5.590	0.6147	84.2	26.6	31.3 ± 0.2
5	974.0	4.515	0.5951	74.2	9.5	22.1 ± 0.3
6	466.7	4.133	4.0620	68.2	11.2	18.8 ± 0.2
			Sample AII-93-5-3, J = 0.00368			
1	359.5	46.900	0.0230	18.0	2.4	55.1 ± 1.0
2	371.6	31.250	0.0250	20.7	7.9	42.4 ± 0.6
3	8211.2	6.060	0.2164	98.0	28.2	39.0 ± 0.6
4	3474.4	6.985	0.1503	92.6	26.7	42.5 ± 0.3
5	3397.8	6.259	0.1196	92.2	16.9	37.9 ± 0.3
6	17197.0	6.377	0.8137	89.1	17.9	37.5 ± 0.2
			Sample AII-93-7-1, J = 0.00368			
1	363.1	36.600	0.0200	18.7	13.0	45.0 ± 2.3
2	392.2	26.900	0.0449	25.0	15.2	44.0 ± 0.9
3	654.9	10.500	0.2036	56.4	18.2	39.0 ± 0.2
4	1926.0	6.501	0.6132	89.3	26.4	38.3 ± 0.2
5	1132.7	5.820	0.7350	79.5	18.1	30.5 ± 0.2
6	481.4	4.762	3.6127	66.7	9.1	21.2 ± 0.4
			Sample AII-93-8-11, J = 0.00368			
1	389.1	34.769	0.0348	24.3	19.1	55.3 ± 17.9
2	373.6	36.660	0.0522	21.3	12.0	51.2 ± 1.4
3	784.8	8.517	0.5394	66.5	24.0	37.3 ± 0.2
4	1148.2	6.722	0.8279	80.6	16.1	35.8 ± 0.4
5	732.9	5.313	1.0019	67.4	16.1	23.7 ± 0.1
6	537.7	4.565	2.5495	64.8	14.7	19.7 ± 0.3
			Sample AII-93-10-11, J = 0.00341			
1	509.9	24.890	0.0319	42.3	25.0	63.6 ± 0.4
2	571.4	18.420	0.0872	48.9	9.7	54.7 ± 0.3
3	561.2	18.000	0.1533	48.5	10.3	53.0 ± 0.4
4	529.2	16.830	0.2173	45.8	11.7	46.5 ± 0.4
5	513.0	16.800	0.2529	45.4	8.6	45.4 ± 0.6
6	475.0	18.390	0.4143	41.0	34.7	46.0 ± 0.3
			Sample AII-93-11-8, J = 0.00320			
1	1485.0	14.900	0.0158	80.2	13.4	67.5 ± 0.4
2	30782.6	11.290	0.0102	99.1	24.6	63.5 ± 0.8
3	58224.5	11.570	0.0108	99.6	28.3	65.3 ± 0.5
4	26671.7	11.400	0.0187	99.0	17.1	64.0 ± 0.4
5	13009.2	11.250	0.0579	98.1	11.7	62.6 ± 0.3
6	5467.1	11.260	0.0815	95.2	4.9	60.9 ± 0.3
			Sample V29-9-1, J = 0.00262			
1	340.3	105.300	0.0073	13.2	16.1	64.6 ± 1.4
2	337.9	81.740	0.0157	12.7	14.0	48.3 ± 2.0
3	371.5	53.580	0.0493	20.8	25.7	52.1 ± 0.5
4	380.3	45.100	0.0984	23.1	24.5	48.6 ± 0.5
5	302.1	181.400	0.0292	2.4	8.7	20.6 ± 1.3
6	292.4	151.870	0.1846	0.4	11.0	2.8 ± 1.7

TABLE II.2a. (continued)

Increment	$^{40}Ar/^{36}Ar$	$^{40}Ar/^{39}Ar$	$^{37}Ar*/^{40}Ar$	% Radiogenic ^{40}Ar	%^{39}Ar of Total	Age ± 1 σ x 10^6 years
			Sample AII-93-14-1, J = 0.00320			
1	602.8	23.460	0.0394	51.3	12.4	68.2 ± 0.4
2	10398.0	11.350	0.9980	97.9	14.6	63.1 ± 0.4
3	22614.3	11.030	0.0679	99.2	27.9	62.1 ± 0.3
4	28535.1	10.850	0.0037	99.2	20.9	61.1 ± 0.3
5	8278.9	10.490	0.0691	96.9	12.5	57.8 ± 0.3
6	3229.6	10.900	0.1022	91.6	11.8	56.8 ± 0.4
			Sample AII-93-14-19, J = 0.00368			
1	439.4	38.200	0.0135	32.8	10.3	81.5 ± 4.0
2	1183.0	13.910	0.0507	75.4	7.2	68.3 ± 0.4
3	7882.0	10.070	0.0891	96.9	27.7	63.6 ± 0.3
4	18683.4	9.495	0.0802	99.0	39.4	61.4 ± 0.3
5	3838.2	9.109	0.1050	93.1	8.4	55.4 ± 0.3
6	2549.5	8.255	0.6993	93.8	6.9	50.9 ± 0.5
			Sample DSDP 525A-57-5, J = 0.00341			
1	1795.1	15.790	0.1190	84.4	16.6	80.3 ± 0.5
2	5600.9	14.320	0.0900	95.4	14.5	82.2 ± 0.4
3	6807.2	13.606	0.1862	97.1	23.5	79.6 ± 0.4
4	4512.4	13.790	0.2129	95.1	21.0	79.0 ± 0.4
5	5178.7	13.300	0.1198	95.2	17.7	76.3 ± 0.4
6	1866.4	13.700	0.8566	90.8	6.6	75.3 ± 0.5
			Sample DSDP 528-40-5 (73-75), J = 0.00341			
1	419.4	45.380	0.0887	30.3	7.2	82.7 ± 0.5
2	869.8	19.970	0.2555	68.0	11.1	81.9 ± 0.4
3	883.5	18.130	0.4984	70.4	13.5	77.3 ± 0.4
4	641.3	22.590	0.3894	56.9	20.2	77.9 ± 0.4
5	1010.2	16.350	0.2826	72.9	26.4	72.1 ± 0.4
6	1365.9	13.320	1.3602	88.9	21.7	72.3 ± 0.4
			Sample DSDP 528-41-2 (40-42), J = 0.00341			
1	3212.4	10.953	0.0538	91.2	17.6	60.5 ± 0.3
2	9613.1	10.881	0.0785	97.5	13.6	64.1 ± 0.8
3	5510.4	11.645	0.0566	95.3	17.5	66.9 ± 0.5
4	915.4	17.902	0.0173	67.8	14.8	73.2 ± 0.4
5	6957.0	10.000	0.0373	95.9	21.5	58.1 ± 0.3
6	3308.4	9.555	0.2873	93.2	14.9	54.1 ± 0.3
			Sample AII-93-21-1, J = 0.002620			
1	440.7	55.310	0.0106	33.0	2.8	84.3 ± 0.7
2	480.4	52.740	0.0085	38.5	7.9	93.6 ± 0.8
3	467.9	59.250	0.0083	36.9	21.5	100.5 ± 1.1
4	484.7	40.550	0.0303	39.3	19.1	73.9 ± 3.5
5	848.2	19.800	0.2334	67.0	22.8	61.8 ± 0.3
6	445.6	23.583	0.2478	35.9	26.1	39.4 ± 0.3
			Sample DSDP 516F-128-1 (22-24), J = 0.002785			
1	509.5	51.590	0.0188	42.1	5.4	106.1 ± 1.8
2	581.9	40.100	0.0163	49.4	10.8	96.9 ± 0.6
3	761.0	32.500	0.0969	61.9	24.4	98.6 ± 0.6
4	1185.8	23.450	0.2542	77.0	22.8	88.9 ± 0.5
5	678.4	26.840	0.3936	59.5	17.9	79.1 ± 0.5
6	419.9	36.090	1.4133	40.6	18.6	74.7 ± 0.6

TABLE II.2a. (continued)

Increment	$^{40}Ar/^{36}Ar$	$^{40}Ar/^{39}Ar$	$^{37}Ar*/^{40}Ar$	% Radiogenic ^{40}Ar	$\%^{39}Ar$ of Total	Age $\pm 1\,\sigma$ x 10^6 years
all	Sample DSDP 516F-128-1 (104-107). J = 0.002785					
1	534.2	67.210	0.0198	44.8	15.1	145.5 ± 1.1
2	756.0	35.510	0.0760	61.5	22.8	106.7 ± 0.6
3	1377.4	22.130	0.2410	87.6	22.5	87.6 ± 0.4
4	1358.4	20.050	0.3920	81.3	14.7	80.5 ± 0.4
5	881.5	22.100	0.4537	70.0	10.8	76.5 ± 0.4
6	476.6	32.100	1.0919	40.8	14.1	66.1 ± 0.5

Here, $\lambda = 5.53 \times 10^{-10}$/year. Ratios in table have not been corrected for neutron interferences.

Correction factors: $(^{36}Ar/^{37}Ar)$ Ca = 0.000264; $(^{39}Ar/^{37}Ar)$ Ca = 0.000673; $(^{40}Ar/^{39}Ar)$ K = 0.0006.

* Corrected for decay since neutron irradiation $(\lambda\,^{37}Ar = 1.975 \times 10^{-2}$/day).

TABLE II.2b. Age Calculations From Argon Isotopic Data

	Plateau Calculation			Isochron Calculation			
Sample	Age (m.y.) ± 1σ	Steps Used	% of Total ^{39}Ar	Age (m.y.) ± 1σ	Steps Used	Intercept	Recalculated Total Fusion Age (m.y.) ± 1σ
AII-93-3-1	29.2 ± 0.2	2, 3, 4	69.1	28.4 ± 0.6	1, 2, 3, 4	317.4 ± 5.2	30.3 ± 0.3
AII-93-3-25	31.0 ± 0.2	1, 2, 3, 4	79.2	30.8 ± 0.4	1, 2, 3, 4	299.9 ± 3.6	29.5 ± 0.4
AII-93-5-3	38.7 ± 0.2	2, 3, 4, 5, 6	97.6	38.2 ± 1.1	1, 2, 3, 4, 5, 6	309.4 ± 9.2	40.1 ± 0.3
AII-93-7-1	38.5 ± 0.2	3, 4	44.6	38.0 ± 0.2	1, 2, 3, 4	307.6 ± 1.5	37.2 ± 0.4
AII-93-8-11	37.2 ± 0.2	1, 2, 3, 4	69.0	35.6 ± 0.3	1, 2, 3, 4	321.8 ± 4	37.5 ± 3.5
AII-93-10-11	46.2 ± 0.3	4, 5, 6	55.0	49.2 ± 5.5	4, 5, 6	280.9 ± 26	52.0 ± 0.3
AII-93-11-8	64.1 ± 0.3	2, 3, 4, 5	81.7	62.0 ± 1.3	1, 2, 3, 4, 5, 6	384.0 ± 44	64.4 ± 0.4
V29-9-1	50.3 ± 0.4	2, 3, 4	64.0	50.0 ± 7.1	2, 3, 4	295.6 ± 10.6	44.6 ± 0.5
AII-93-14-1	61.4 ± 0.3	2, 3, 4	63.4	60.2 ± 1.0	2, 3, 4	949.0 ± 556	61.6 ± 0.3
AII-93-14-19	61.5 ± 0.3	3, 4	67.0	59.9 ± 2.0	2, 3, 4, 5, 6	389.0 ± 90	63.4 ± 0.5
DSDP 525A-57-5, 104-106							
DSDP 525A-57-5, 41-43	79.4 ± 0.4	3, 4	62.3	82.0 ± 1.9	1, 2, 3, 4	288.0 ± 128	79.1 ± 0.4
DSDP 528-40-5 (73-75)	77.6 ± 0.5	3, 4	33.6	79.1 ± 6.3	1, 2, 3, 4	296.8 ± 45	75.9 ± 0.5
DSDP 528-41-2 (40-42)							62.5 ± 0.3
AII-93-21-1							69.8 ± 0.8
DSDP 516F-128-1 (22-24)				87.2 ± 8.9	1, 2, 3, 4, 5, 6	293.2 ± 41.9	88.7 ± 0.5
DSDP 516F-128-1 (104-107)							95.5 ± 0.5

^{39}Ar recoil may be an incomplete process, a total fusion age which is not supported by both a clear plateau (particularly for the middle temperature steps) and a well constrained isochron age, must be interpreted cautiously. Other criteria, such as the consistency of ages for multiple samples from the same locality or independent geological constraints, can increase confidence in such total fusion ages.

Weighted mean plateau ages have been calculated for samples yielding an age-temperature plateau, primarily for middle temperature heating steps. These middle temperature sites are considered to be least disturbed by the loss or addition of ^{39}Ar resulting from recoil effects, as discussed above. The slope formed by the correlation of the ^{40}Ar/^{36}Ar and ^{39}Ar/^{36}Ar ratios for selected heating steps yielded an ^{40}Ar*/^{39}Ar ratio, from which an isochron age was determined for most samples. Ideally, the ^{40}Ar/^{36}Ar intercept of such isochrons should reflect the composition of the rock at the time of crystallization, i.e., 295.5, consisting of only atmospheric argon without any contribution from potassium decay. Isochron slopes and intercepts were calculated using the least squares fitting technique of York [1969], which allows for correlated errors in both ^{40}Ar/^{36}Ar and ^{39}Ar/^{36}Ar isotopic ratios. Errors involved in measuring Ar ratios and J-factors (a typical error of 0.5% has been assigned) and in making corrections for interfering nuclear reactions were combined to yield a standard deviation for each heating age. The most reliable age-temperature spectrum and isochron plot for each sample site are shown in Figure II.3. Plots of ^{36}Ar/^{40}Ar versus ^{39}Ar/^{40}Ar (inverse diagram) produced the same results as those estimated from isochron plots, as demonstrated by Dalrymple et al. [1988].

Samples AII-93-3-1 and AII-93-3-25 are from the same dredge haul and have very similar compositions [Humphris and Thompson, 1982]. Sample 3-1 produced a plateau age of 29.2 ± 0.2 Ma (69.1% of the total ^{39}Ar released), an isochron age of 28.4 ± 0.6 Ma (intercept of 317 ± 5.2), and a recalculated total fusion age of 30.3 ± 0.3 Ma. Sample 3-25 yielded a distinct middle temperature age plateau of 31.0 ± 0.2 Ma (79.2% of the total ^{39}Ar released) (Figure II.3a) and an isochron age of 30.8 ± 0.4 Ma (intercept of 299.9 ± 3.6) (Figure II.3b). The total fusion age is 29.5 ± 0.4 Ma. The best estimate of the apparent age of this site is considered to be between 30 and 31 Ma.

Sample AII-93-5-3 produced a plateau age of 38.7 ± 0.2 Ma (97.6% of the total ^{39}Ar released) (Figure II.3c), an isochron age of 38.2 ± 1.1 Ma (intercept of 309 ± 9.2) (Figure II.3d), and a recalculated total fusion age of 40.1 ± 0.3 Ma. The crystallization age at this site appears to be well constrained at between 39 and 40 Ma.

Samples AII-93-8-11 and AII-93-7-1 are from separate dredge hauls from the same volcano. Sample 8-11 yielded a middle temperature plateau age of 37.2 ± 0.2 (69% the total ^{39}Ar released), an isochron age of 35.6 ± 0.3 Ma (intercept of 322 ± 4.0), and a recalculated total fusion age of 37.5 ± 3.5 Ma. Sample 7-1 results show a middle temperature plateau age of 38.5 ± 0.2 Ma (45% of the total 39Ar) (Figure II.3e), an isochron age of 38.0 ± 0.2 Ma (intercept of 308 ± 1.5) (Figure II.3g), and a recalculated total fusion age of 37.2 ± 0.4 Ma. The best estimate of the age of this volcano is between 38 and 39 Ma.

Figure II.3. Age-temperature spectra and $^{40}Ar/^{36}Ar$-$^{39}Ar/^{36}Ar$ correlation diagrams for basaltic samples from the Walvis Ridge. Age bands in spectra plots are the measured heating step ages ± 2σ. Errors on plateau ages are ± 1σ. The numbered points on the correlation diagrams correspond to the individual heating steps. Solid boxes in correlation diagrams indicate heating steps used in isochron calculations. A single representative K/Ca release spectrum diagram is also shown.

Figure II.3a

23
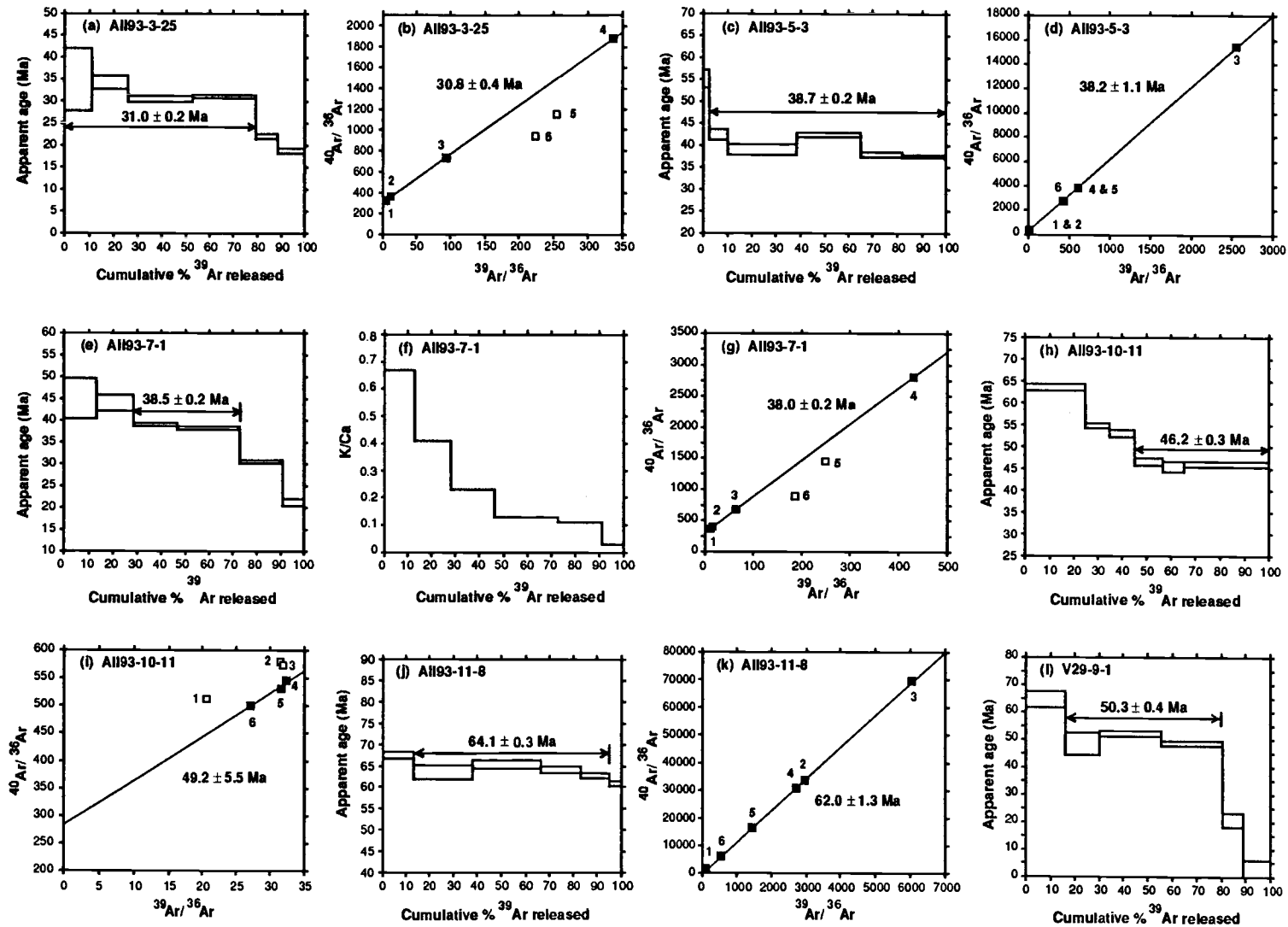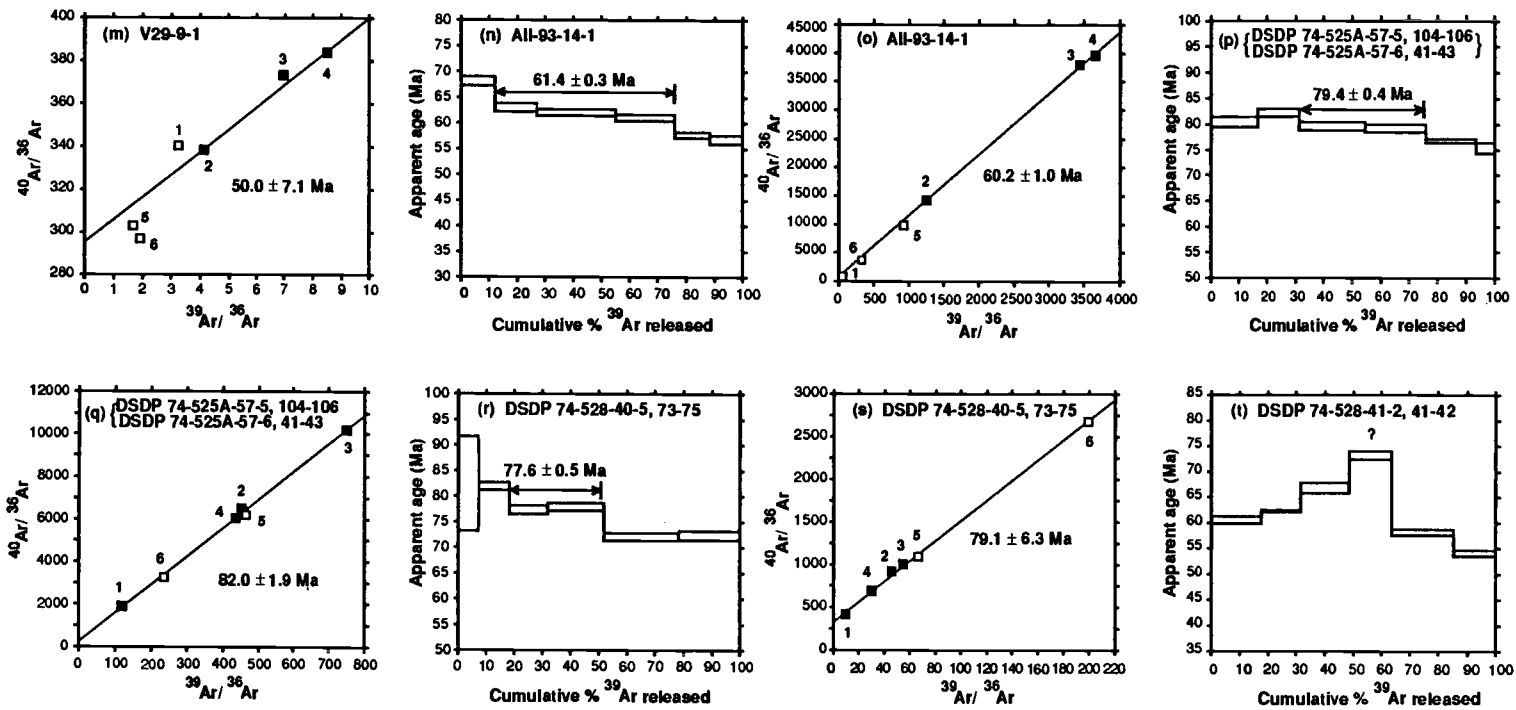
Figure II.3 (continued)

The crystallization ages of dredged samples AII-93-5, 7 and 8 (38 to 40 Ma) are supported by results from the nearby Deep Sea Drilling Project (DSDP) site 359, which encountered volcanic tuff dated radiometrically (K-Ar) at 40.3 ± 1.0 Ma [Fodor et al., 1977].

Sample AII-93-10-11 showed evidence in its argon release pattern of ^{39}Ar recoil; however, we tentatively identify a questionable plateau age of 46.2 ± 0.3 Ma (the final 55% of the total ^{39}Ar released) (Figure II.3h). An isochron age of 49.2 ± 5.5 Ma (intercept of 281 ± 26) has been calculated using the heating steps which were included in the plateau age calculation (Figure II.3i). The proportion of radiogenic ^{40}Ar released during this experiment was low, not exceeding 50% for any of the six heating steps. The recalculated total fusion age of 52.0 ± 0.3 Ma provides a minimum estimate of the age of this sample site.

Sample AII-93-11-8 yielded a good plateau age of 64.1 ± 0.3 Ma (81.7% of the total ^{39}Ar released) (Figure II.3j), a well-constrained isochron age of 62.0 ± 1.3 Ma (intercept of 384 ± 44) (Figure II.3k), and a recalculated total fusion age of 64.4 ± 0.4 Ma. The apparent age of this sample site is 64 Ma.

Sample V29-9-1 results show a middle temperature plateau age of 50.3 ± 0.4 Ma (64% of the total ^{39}Ar released) (Figure II.3l) and a somewhat poorly constrained isochron age of 50.0 ± 7.1 Ma (intercept of 296 ± 11) (Figure II.3m). The recalculated total fusion age of 44.6 ± 0.5 Ma is significantly lower than the plateau age. The percentage radiogenic ^{40}Ar released during incremental heating was very low, reaching a maximum of 21%. The best estimate of the age of this sample is taken to be the 50.0 ± 0.4 Ma plateau age.

Samples AII-93-14-19 and AII-93-14-1 are from the same dredge haul. Sample 14-19 yielded a plateau age of 61.5 ± 0.3 Ma (67% of the total ^{39}Ar released), an isochron age of 59.9 ± 2.0 Ma (intercept of 389 ± 90), and a total fusion age of 63.4 ± 0.5 Ma. Sample 14-1 produced a reasonable plateau age of 61.4 ± 0.3 Ma (63.4% of the total ^{39}Ar released) (Figure II.3n), an isochron age of 60.2 ± 1.0 Ma (intercept of 949 ± 556) (Figure II.3o), and a total fusion age of 61.6 ± 0.3 Ma. The crystallization age of this site is between 61 and 62 Ma.

DSDP Transect of the Walvis Ridge

DSDP sites 525A, 528, and 527 constitute a SE-NW transect across the Walvis Ridge (Figure II.2). The ages of drilled basalts recovered from sites 525A and 528 are broadly constrained by magneto-biostratigraphic information from the overlying sediments [Manivit, 1984; Chave, 1984]. These data provide minimum estimates on the formation ages of the underlying basement and so act as an independent control on ^{40}Ar-^{39}Ar incremental heating age determinations.

Rock chips from core intervals DSDP 74-525A-57-5, 104-106 and DSDP 74-525A-57-6, 41-43 were combined, yielding a convincing middle temperature plateau age of 79.4 ± 0.4 Ma (62.3% of the total ^{39}Ar released) (Figure II.3p), an isochron age of 82.0 ± 1.9 Ma (intercept of 288 ± 128)

(Figure II.3q), and a recalculated total fusion age of 79.1 ± 0.4 Ma. The apparent age of DSDP 525A basement is 79 Ma. This ^{40}Ar-^{39}Ar incremental heating age is compatible with the biostratigraphically constrained early Maestrichtian to late Campanian (between ~73 and 78 Ma) sediments which immediately overlie site 525A basement [Manivit, 1984]. Magnetostratigraphic correlation indicates that 525A basement formed within magnetic C32 (~ 72 to 74 Ma) [Chave, 1984].

Sample DSDP 74-528-40-5, 73-75 (located to the northwest of DSDP site 525A) produced an indistinct age-temperature plateau of 77.6 ± 0.5 Ma (33.6% of the total ^{39}Ar released) (Figure II.3r), an isochron age of 79.1 ± 6.3 Ma (intercept of 297 ± 45) (Figure II.3s), and a recalculated total fusion age of 75.9 ± 0.5 Ma. A best estimate of the apparent crystallization age at this site is between 78 and 79 Ma. This radiometric age range is somewhat older than the age of overlying sediments, which have been biostratigraphically constrained at middle Maestrichtian age (between ~72 and 69 Ma) [Manivit, 1984], with a corresponding magnetostratigraphic assignment of C31 to C32 times (~ 69 to 74 Ma) [Chave, 1984].

The age-temperature release spectrum of sample DSDP 528-41-2, 40-42 contrasts with the generally plateau-like or inverse staircase release spectra which are characteristic of the samples examined in this study. Heating step ages increase to a maximum for a middle temperature step (73.2 ± 0.4 Ma) and then decrease again to approximately the age of the first heating step, so forming an arched release pattern (Figure II.3t). This age-release spectrum may reflect significant loss of ^{40}Ar* from this sample. The recalculated total fusion age is 62.5 ± 0.3 Ma, which is substantially lower than the radiometric age of the overlying sample (DSDP 528-40-5). It was therefore concluded that the apparent total fusion age of DSDP 528-41-2 is erroneously young; this result clearly demonstrates the pitfalls of conducting single step total fusion rather than incremental heating ^{40}Ar-^{39}Ar experiments on seawater altered whole rock basalts. Such an arched release spectrum (Figure II.3t) may prove to be characteristic of such erroneously young total fusion ages.

Sample AII-93-21-1, recovered from the most northeasterly of the sample sites investigated in this study, produced an extreme example of an inverse staircase age-temperature spectrum, and did not produce a recognizable age plateau. The percentage of radiogenic ^{40}Ar released during incremental heating was low, 60% being the maximum value attained. The recalculated total fusion age of 69.8 ± 0.8 Ma is the best age estimate for this sample site; this apparent age probably represents a minimum estimate, rather than the true sample age.

The oldest age determined for the Walvis Ridge is provided by DSDP 363, where drilling encountered lower Aptian (about 113 to 119 Ma) sediments, a short distance above the inferred basaltic basement [Bolli et al., 1978]. To a first approximation the age of Walvis Ridge basement increases linearly with increasing distance from Tristan da Cunha (Figure II.4), thus linking recent hot spot volcanism on Tristan da Cunha, via the Walvis Ridge, to its 120-130 Ma expression on the Namibian coast, the Etendeka continental flood basalt field.

Figure II.4. All available basement age constraints for the Walvis Ridge and Rio Grande Rise are plotted against their respective distances along volcanic trail, from Tristan da Cunha. A straight line has been fitted to these data, with an age of 0 Ma assigned to Tristan da Cunha. Migration rates for the African and South American plates over the Tristan plume have been estimated at 3.1 and 2.9 cm/yr, respectively.

Distance from Tristan da Cunha along volcanic trails (km)
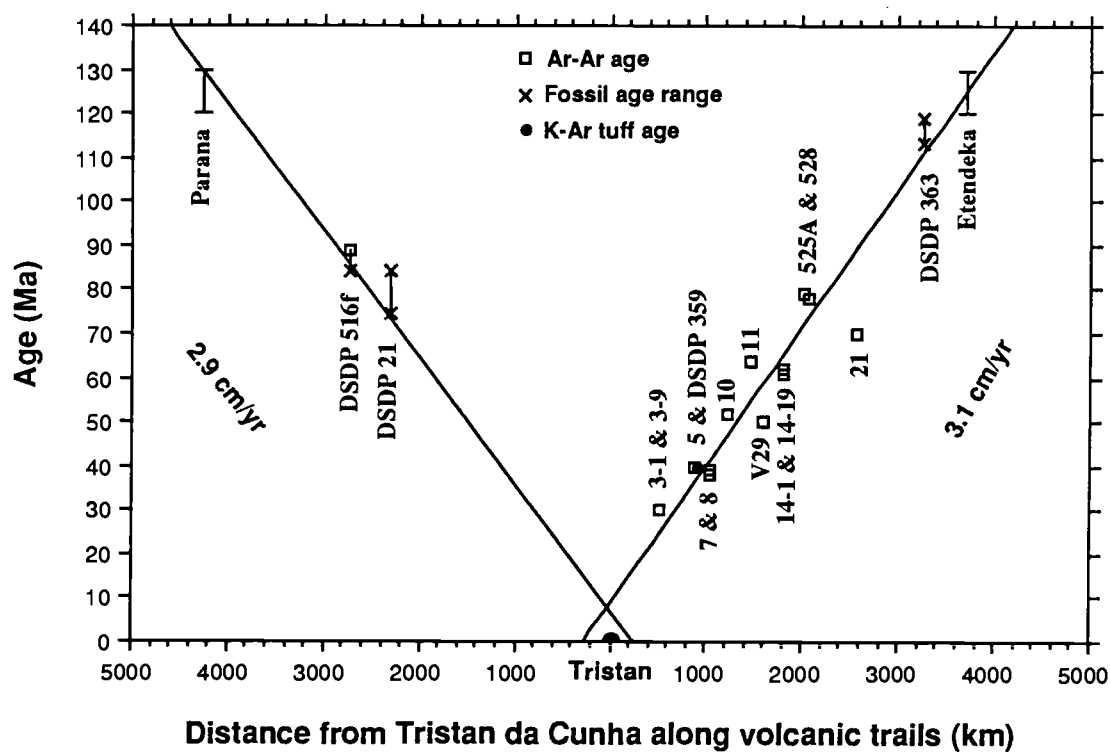
Figure II.4

Rio Grande Rise

Samples DSDP 516F-128-1, 22-24 and DSDP 516F-128-1, 104-107 both failed to produce conclusive plateau ages. The first yielded a recalculated total fusion age of 88.7 ± 0.5 Ma and an isochron age of 87.2 ± 8.9 Ma (intercept of 293 ± 42). The second produced an even more extreme example of an inverse staircase release pattern, with a recalculated total fusion age of 95.5 ± 0.5 Ma. An apparent age of 88 Ma was chosen as the best available constraint on the time of crystallization of this site. DSDP 516F basalts were sampled beneath poorly lithified and recrystallized sediments which have been biostratigraphically dated at between Coniacian to Santonian age (84 Ma to 88.5 Ma) [Weiss, 1983]. Since this time was within the long Cretaceous normal magnetization period, magnetic stratigraphy is not informative. Musset and Barker [1983] also investigated DSDP 516F basalts using the ^{40}Ar-^{39}Ar incremental heating method and concluded that 86.0 ± 4.0 Ma was the best estimate of the age of crystallization.

DSDP site 21, located on the northeastern shoulder of the Rio Grande Rise (Figure II.6), provides a minimum biostratigraphic age of Campanian time (74.5 to 84 Ma) for the underlying basement. This drill hole did not actually reach basement but terminated in shallow water sediments consisting mainly of megafossil fragments; the actual thickness of this rock layer is unknown [Bukry and Bramlette, 1970; Gartner, 1970; Blow, 1970]. The distribution of available Rio Grande Rise basement and fossil ages, in conjunction with present estimates of the narrow age-range of the Parana flood basalts, is compatible with age-progressive volcanism linking the northeastern shoulder of the Rio Grande Rise (~75 to 84 Ma) to 120-130 Ma continental flood basalt volcanism (Figure II.4).

However, volcanism may not have migrated along the Rio Grande Rise in a simple, linear age-progressive fashion. Portions of the Rio Grande Rise–Walvis Ridge system appear to have developed in a manner similar to that of present day Iceland [Vogt and Johnson, 1975; Saemundsson, 1979; Helgason, 1985] and Figure II.9b. Barker [1984] has observed that a sequence of planar dipping reflectors exists beneath the reflector associated with the basalt at the base of DSDP 516F, located on the Rio Grande Rise plateau. When Icelandic plateau basalts eventually become submerged, they will show similar characteristics. Such a dipping reflector sequence is similar to those found along many continental margins and is usually considered to represent a subaerial seafloor spreading facies, composed of sheet lava flows and shallow marine or alluvial sediments. The central plateau of the Rio Grande Rise may therefore have formed along a spreading-axis, which in turn was astride, or in close proximity, to a hot spot, as is the case for Iceland today. Numerous eastward spreading-axis jumps were, in all probability, associated with the formation of the central plateau of the Rise. The eastern, N-S ridge of the Rio Grande Rise has previously been attributed to the eruption of hot material along a segment of the South Atlantic spreading-axis [e.g., Vogt and Johnson, 1975]. The history of interaction between the spreading-axis and the Tristan hot spot is reconstructed in a later section.

An additional complication to understanding the evolution of the Rio Grande Rise arises from an undefined volume of Eocene volcanism identified by Bryan and Duncan [1983], who have dated volcanoclastic, turbiditic horizons at 46 Ma, using the K-Ar dating technique. This enigmatic second phase of volcanism has presently no satisfactory explanation within the context of the hot spot model proposed for the formation of the Walvis Ridge–Rio Grande Rise.

Eruption rates through time of Walvis Ridge–Rio Grande Rise volcanism have yet to be quantitatively estimated. However, significantly more material was emplaced when the spreading-axis was in close proximity to the hot spot (Figure II.9b); the contribution from renewed volcanism on the Rio Grande Rise plateau during the Eocene should be kept in mind when making such an assumption. An obvious explanation is that the Tristan plume decreased in strength through time. Changing eruption rates may also reflect the changing tectonic character of the overriding plate, into which the Tristan magmas were emplaced (i.e., from rifting continental crust, to spreading-axis, to finally, an intraplate environment). Changes in plate thickness and/or velocity may have controlled, in part, the volumes of Tristan magma which erupted. Variations in the dynamics of the plume, and the surrounding mantle, could also have played a contributory role.

ABSOLUTE MOTION MODELING (fixed hot spot reference frame)
Rotation Parameters for African Plate Motion Over Hot Spots

Previously estimated sets of reconstruction parameters for African plate motion over fixed hot spots (i.e., absolute motion) [Morgan, 1981, 1983; Duncan, 1981] have been adjusted such that the predicted trail of the African plate over the Tristan hot spot would reconstruct the distribution of Walvis Ridge basement ages (Figures II.5 and II.6). The geographical coordinates of the adjusted rotation poles were located geometrically by requiring that small circles, when fitted about each pole, should simultaneously fit the geometry of three African plate hot spot lineaments: the Walvis Ridge and the volcanic trails of the Reunion and Marion hot spots. This is illustrated by the fact that the geometry of the predicted tracks for the Tristan, Reunion and Marion hot spots, coincides with that of their postulated volcanic trails (Figure II.7). The Africa/hot spots reconstruction parameters given in Table 3 differ from those of earlier versions, primarily in that the rates of plate motion are now constrained to match the distribution of new basement ages along the Walvis Ridge. The geometry of the predicted trails of the St. Helena and Comores hot spots is also in broad agreement with that of their postulated volcanic trails (Figure II.7).

The principal assumptions made in this particular model are: (1) the Walvis Ridge basement ages and geometry perfectly record the motion of the African plate over hot spots, (2) the ocean island of Tristan da Cunha represents the center of a discrete, small diameter, vertically rising plume, as do the islands of Reunion, and Marion, (3) the geometry of the Reunion, Marion/Prince Edward hot spot trails

Figure II.5. The direction of modeled African/hot spots motion is shown by the heavy line connecting Tristan da Cunha (0 Ma volcanism) to the 120 to 130 Ma Etendeka continental flood basalts. The small solid circles distributed along this line represent the modeled progress of the African plate over the Tristan hot spot at intervals of 10 Ma. Sample sites are shown as large solid circles, along with ages, and site labels in parentheses. Two reconstructions from the period 80 Ma to 120 Ma are presented; the dashed hot spot track follows the geometry of the Walvis Ridge (model B), whereas the solid track (model A) is a linear, best fit to the bathymetry of the northern portion of the Walvis Ridge. The 130 Ma interval point on the hot spot tracks reconstructs the Etendeka basalts to the southeastern edge of a hypothetically large diameter plume, which may have existed at the time of continental rifting. Mercator projection.
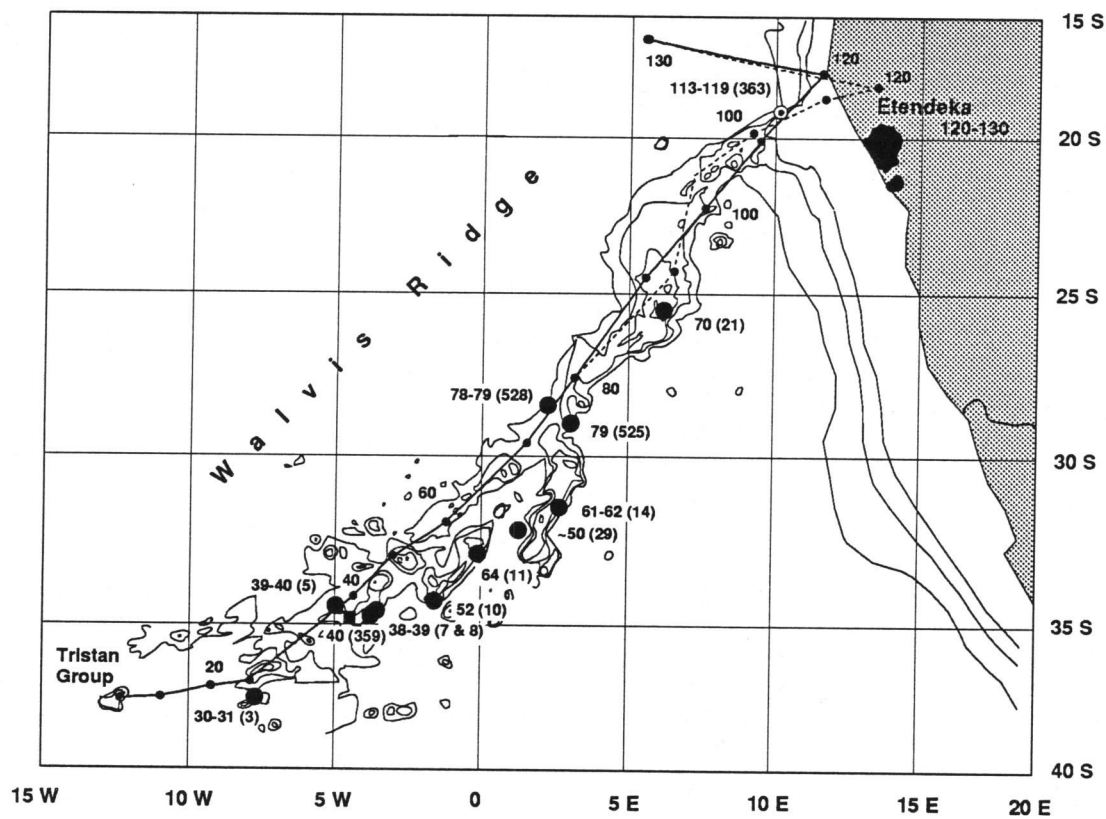
Figure II.5

Figure II.6. Predicted trail of the African and South American plates over the Tristan hot spot. South American/African relative motion [Cande et al., 1988] was added to Africa/hot spots motion given in Table 3. The modeled trail of the Martin Vas plume is also shown. Mercator projection.
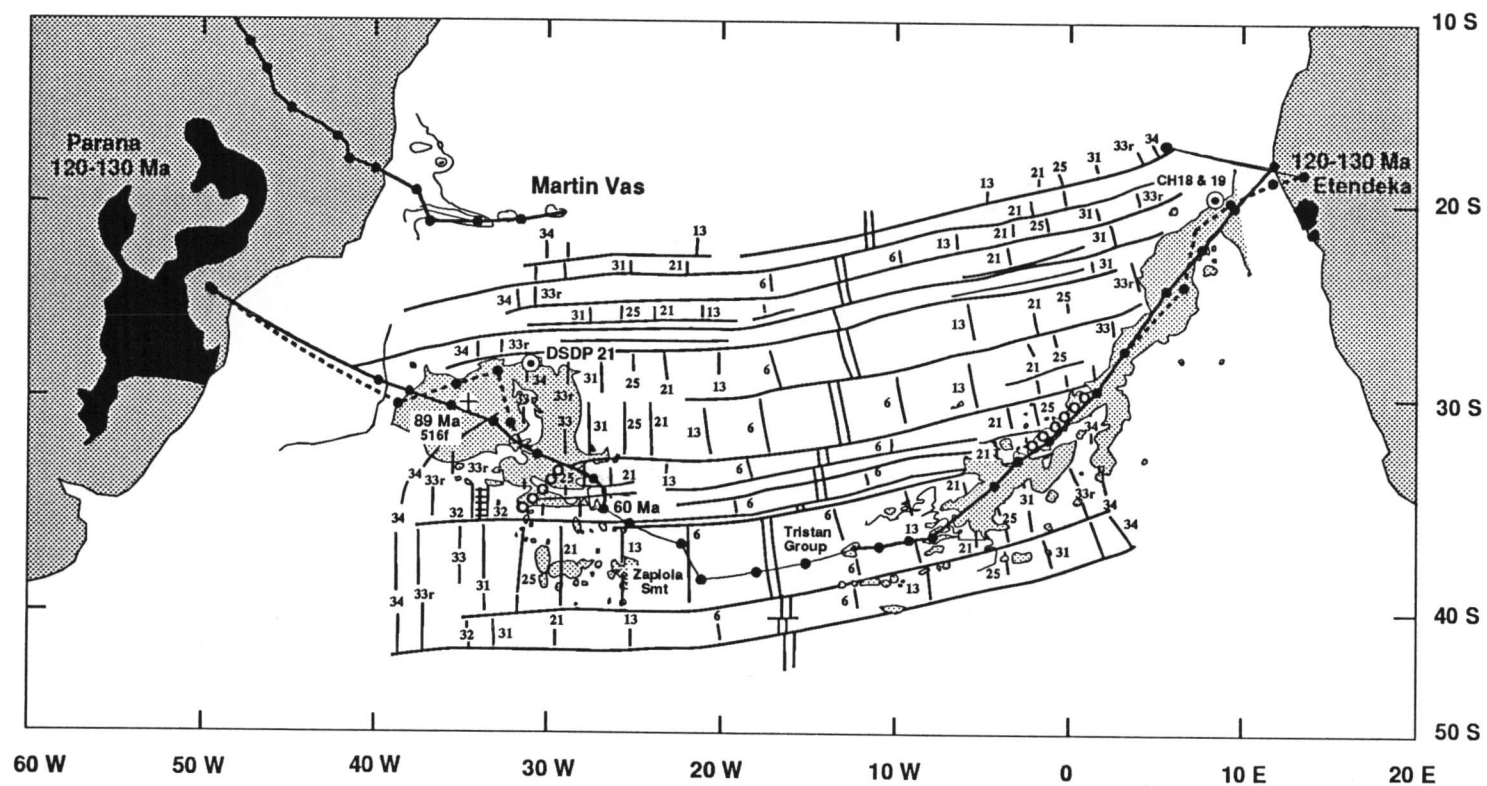
Figure II.6

is accurately known, and (4) there has been no significant wander of these three hot spots with respect to one another.

The Predicted Trail of the Tristan Plume Compared to Walvis Ridge Bathymetry and Age Data

Figure II.5 illustrates the relationship between the modeled trail of the African plate over the Tristan plume and the bathymetry and distribution of all available Walvis Ridge basement ages. A 30 Ma seamount cluster, located due east of Tristan da Cunha, tightly constrains the rotation angle about the 30 Ma finite reconstruction pole. As no volcanic trail is evident between this 30 Ma site and the island of Tristan da Cunha, the 10 and 20 Ma reconstruction poles were calculated by interpolation. The rotation angle about the 40 Ma is very well constrained by age data from three sample sites, and a supporting K-Ar age.

The 50 to 70 Ma portion of the Walvis Ridge consists of a complex series of subparallel volcanic lineaments (Figure II.5). It is somewhat of a quandary as to which of these minor ridges best records the motion of the African plate over the Tristan hot spot. The northern lineament formed along a spreading-axis, in contrast to the two southern lineaments, which formed in an intraplate situation, as will be shown in a later section. While these southern lineaments may in fact accurately record the motion of the African plate over the Tristan plume, the rotation parameters given in Table II.3 have been constrained so as to predict a hot spot trail which follows the northern limb. These rotation parameters predict smooth, linear hot spot trails for other African hot spots which are compatible with the geometry of their postulated volcanic traces. As no basement ages were available for the northern limb, reasonable estimates were made on the basis of the age data available for the southern two limbs, in order to constrain the angles of rotation about the 50, 60, and 70 Ma reconstruction poles. However, significantly more basement sampling is obviously essential in order to better define the tectonic and geochemical evolution of this, and other such complex tectonic regions of the Walvis Ridge–Rio Grande Rise system; increased sampling will reveal which specific portions of the volcanic trails best record the motion of the African plate over the hot spot. The rotation angle about the 80 Ma finite reconstruction pole is well constrained by the 78-79 Ma DSDP transect of the Walvis Ridge.

Between 80 and 120 Ma little reliable age data are available; the enigmatic 70 Ma age for sample AII-93-21 was interpreted as a minimum age and therefore was not used in the estimation of rotation parameters. However, future studies may confirm that reactivation of the volcanic lineament may actually have occurred in this region of the Walvis Ridge. Two sets of rotation parameters have been estimated for Africa/hot spot motion for the period 80 to 120 Ma (Figure II.5). Model A predicts a track which follows the bathymetry for this portion of the Walvis Ridge in basically a linear fashion. In contrast, the track predicted by model B closely follows the curvature of the Walvis Ridge. If, indeed, this section of the Walvis Ridge–Rio Grande Rise system represents a twin of present day Iceland (to be discussed in the following section), the changing curvature of the Walvis Ridge does not,

Table II.3. Finite Reconstruction Poles for African Plate
Motion Over Hot Spots

Age, Ma	Latitude, °N	Longitude, °E	Angle*
Model A (Linear Fit Through NE Walvis Ridge)			
10	52.0	-16.3	-1.0
20	51.4	-24.3	-2.4
30	51.5	-23.3	-3.5
40	47.3	-45.9	-7.1
50	45.7	-50.9	-8.7
60	44.9	-50.7	-10.6
70	43.6	-54.2	-14.0
80	42.4	-57.5	-16.4
90	40.0	-59.6	-20.2
100	39.7	-60.6	-23.2
110	39.4	-61.3	-26.0
120	41.5	-64.9	-29.2
130	32.8	-73.3	-26.4
Model B (Following the Curvature of NE Walvis Ridge Bathymetry)			
90	41.2	-58.7	-21.0
95	38.6	-64.2	-23.8
100	40.2	-64.5	-26.1
110	40.9	-61.6	-28.5
120	41.1	-58.0	-30.0

*Negative angles indicate counterclockwise rotation.

in all probability, record changes in the direction of African plate motion over hot spots. Following this reasoning, model A is a preferable model and so will be used in following discussions.

At ~130 Ma the initial expression of the Tristan plume on the surface of the rifting African and South American plates was in the form of the Parana–Etendeka continental flood basalt (Figure II.9a). These lavas may have erupted in response to the rapid partial melting of the large diapiric head of the Tristan plume [Richards et al., 1989]. Subsequent volcanism linked to the Tristan plume, i.e., the Walvis Ridge–Rio Grande Rise, are possibly related to smaller volumes of plume material rising through the conduit or "tail", formed by the diapir. Alternatively, the Parana-Etendeka basalts may have been formed by the pressure-release melting of the upper mantle, which would have occurred if continental rifting commenced in a region warmed by a hot spot, previously unable to penetrate the lithosphere [White and McKenzie, 1989; Cox, 1989]. A 130 Ma Africa/hot spots reconstruction pole was estimated such that the Etendeka basalt field would straddle, on reconstruction, the eastern edge of such a large hot spot (Figure II.9a).

An additional constraint on the reliability of the adjusted rotation parameters is that the predicted trail of the South American plate over the Tristan plume should be in reasonable agreement with the evolutionary history of the Rio Grande Rise, as it is presently understood. South American plate motion over hot spots has been reconstructed by the addition of South America/Africa finite reconstruction poles [Cande et al., 1988] to African motion over hot spots. Figure II.6 shows that the hot spot track predicted by model A trends in a linear, NW-SE direction through the Rio Grande Rise. Model B, which more closely follows the bathymetry of the Walvis Ridge, predicts a more northerly trending track until 100 Ma when it changes direction to the west. Africa/hot spots rotation parameters do not predict a trail for the South American plate over the Tristan plume, which follows the N-S ridge of the eastern Rio Grande Rise (Figure II.6). However, as will be shown in a later section, this portion of the rise probably formed along a southwardly propagating spreading-axis (Figure II.9b), and so did not record the true direction of South American plate motion over the Tristan hot spot. This point illustrates the critical importance of accurately understanding the evolutionary history of individual hot spot-related volcanic trails, in the estimation of valid absolute motion reconstruction parameters.

Support for a NW-SE trending hot spot track through the Rio Grande Rise is provided by recent studies of the South Atlantic geoid. At short wavelengths, seafloor topography and variations in the geoid are strongly correlated and so provide a better constraint on seafloor topography in poorly surveyed areas, such as the South Atlantic. A map of short-wavelength regional undulations in the amplitude of the geoid shows a good correlation between the bathymetry of the Walvis Ridge and its topography determined from the geoid [Gibert et al., 1989; Plate 1]. The geoid-inferred topography of the Rio Grande Rise, however, forms an elongated NW-SE trending lineament, as predicted by the hot spot track, which does not correlate well with available bathymetry (Figure II.1b). A NW-SE trending volcanic trail is more symmetrical with respect to the Walvis Ridge than is the bathymetry of the Rio

Grande Rise. Fleitout et al. [1989] have detected numerous small-wavelength elongated features on filtered geoid and topography maps of the South Atlantic. A number of these features are orientated at N50°E for the African plate, and N65°W for the South American plate: this agrees with the geometries of the predicted hot spot trails shown in Figure II.6. The authors attribute these elongated features to magmatic traces left over a large number of convecting plumes, which record the directions of African and South American absolute plate motions.

African and South American Plate Motions Over South Atlantic and Indian Ocean Hot Spots

The island of Reunion is composed of two volcanoes, the dormant Piton des Neiges (>2 to 0.02 Ma [McDougall, 1971; Chevallier and Vatin-Perignon, 1982; Gillot and Nativel, 1984]) and Piton de la Fournaise, which began to erupt earlier than 0.5 Ma and is presently one of the most active volcanoes in the world [McDougall, 1971; Gillot and Nativel, 1989]. Morgan [1981] proposed that Reunion locates a hot spot, which formed the island of Mauritius (7-8 Ma [McDougall, 1971]) and the volcanic ridge extending northward beneath the Mascarene Plateau. On the Indian plate, the trail of the Reunion hot spot consists of the Chagos Bank, the Maldive and Laccadive islands, and the Deccan continental flood basalts. Thus, the track of the Reunion hot spot stretches for ~5,000 km from Reunion to the flood basalts of western India. The age progressive character of this hot spot lineament has been confirmed by recent biostratigraphic and magnetostratigraphic data [Backman et al., 1988], radiometric dating [Duncan and Hargraves, 1990], and isotopic studies [White et al., 1990]. Biostratigraphic and magnetostratigraphic information provides an age estimate of between chrons C13N-1 and C13N-2 time (~36 Ma) for Ocean Drilling Program (ODP) site 706 basalts, located at the northeastern margin of the Nazareth Bank (Figure II.7). Extending northward from this plateau is the Saya de Malha Bank, dated at 47 Ma by ^{40}Ar-^{39}Ar radiometric age determination of basalt recovered from industrial drill site SM-1 (located between ODP sites 706 and 707, Figure II.7). Duncan and Hargraves [1990] have shown that this bank formed simultaneously with the Chagos Bank (48 Ma) on the Indian plate, and that these features were separated by the initiation of seafloor spreading at about 36 Ma along the Central Indian Ridge. The volcanic ridge connecting the Saya de Malha Bank with the Seychelles Bank has been biostratigraphically and magnetostratigraphically dated at ODP site 707 as C26R, between 62 and 63 Ma, and at ~64 Ma by radiometric dating. This ridge is considered to have formed along the southwestern edge of the Deccan Traps, and to have been rifted away from India as the Arabian Sea began to open (Duncan and Hargraves, 1990].

The Africa/hot spots reconstruction parameters given in Table 3 have been estimated in such a manner as to predict a trail for the Reunion plume that would follow the geometry of the Mascarene Plateau (for the period between 0 and about 36 Ma). However, the predicted rate of migration of the African plate over the Reunion plume (Figure II.7) is somewhat slower than that indicated by available basement age data for its volcanic trail (Figure II.7). Relative motion between the Reunion and Tristan

Figure II.7. The trails of all South Atlantic and Indian Ocean hot spots located on the African and South American plates are shown. Thin portions of modeled hot spot tracks illustrate the connection between volcanic trails which are linked to a common hot spot, and do not correspond to actual volcanic trails. Biostratigraphic and magnetostratigraphic ages shown for the Mascarene Plateau are from Backman et al. [1988]; drill site numbers are shown in parentheses. K-Ar age range for Mauritius is from McDougall [1971]. Mercator projection.
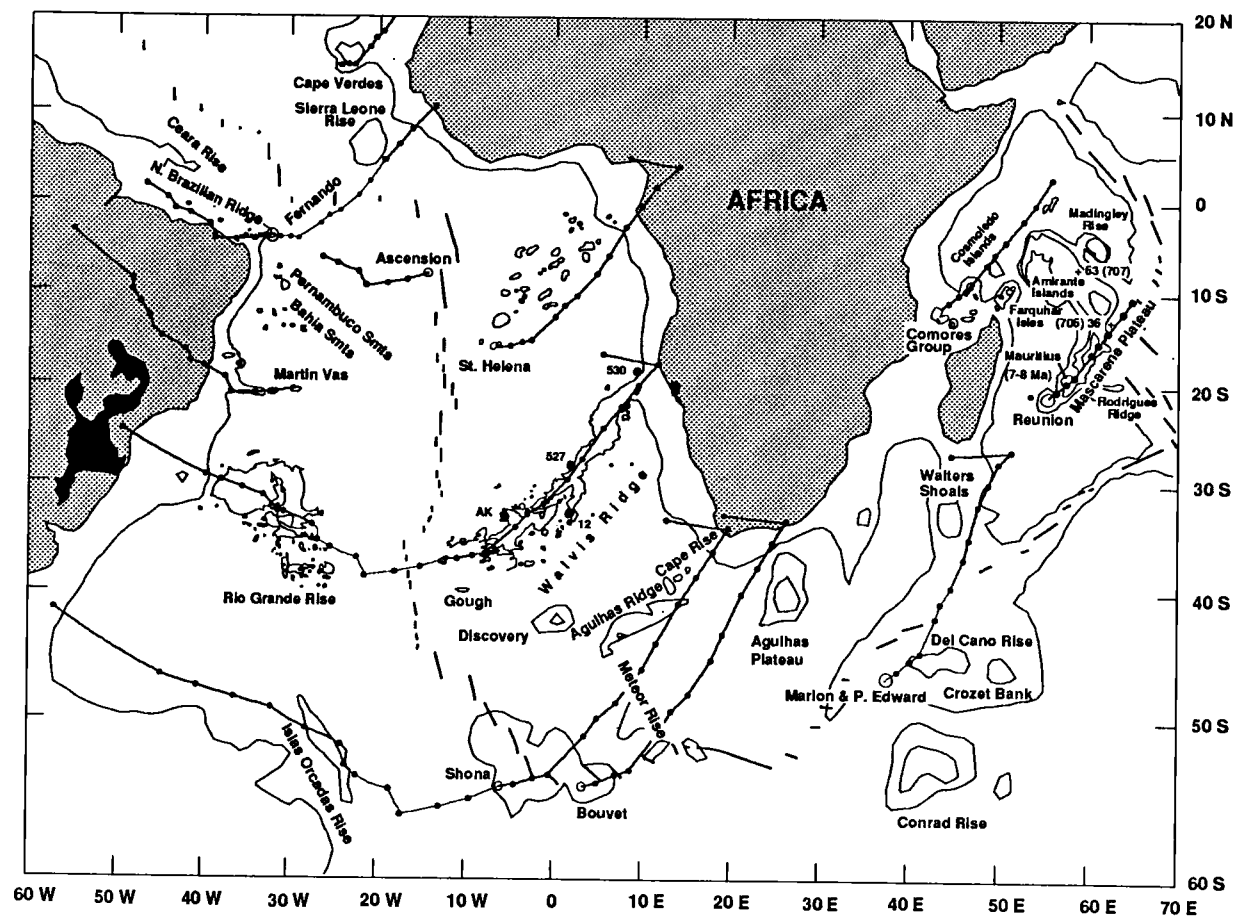
Figure II.7

hot spot could explain this misfit. An alternative explanation might involve relative motion across the east African rift zone, i.e., the western boundary of the Somalia plate, which could have added an easterly component of motion to Somalia plate migration over the Reunion plume [Emerick and Duncan, 1982].

The geometry of the predicted trail of the Comores hot spot is in general agreement with that of its postulated volcanic trail, the Comores, Cosmoledo, Farquhar and Amirante island groups, and the Tertiary igneous activity located at the northeastern region of the Seychelles continental block [Emerick and Duncan, 1982]. This intense episode of widespread igneous activity in the Seychelles Islands, first noted by Baker and Miller [1963], has been dated at 63 Ma by MacIntyre et al. [1985]; this age is in good agreement with that predicted by the Comores hot spot trail (Figure II.7). The zero age location of the Comores plume is assumed to be beneath the island of Grande Comore. As is the case with the Reunion hot spot, extension across the East African rift zone could also have augmented the rate at which the Somalia plate migrated over this hot spot.

Africa/hot spots reconstruction parameters were also constrained to follow closely as possible, the trail of the African plate over the Marion/Prince Edward plume. However, there is a small degree of misfit between the predicted trail and the somewhat indistinct volcanic trail of the Marion/Prince Edward plume, the Walters Shoals and the Madagascar Ridge. The postulated zero age location of this hot spot trail is the volcanically active Marion Island, located on the Antarctica plate (Figure II.7).

Hartnady and le Roex [1985] have proposed the existence of a hot spot, known as Shona, located near the southernmost tip of the South Atlantic spreading-axis, in close proximity to the Bouvet hot spot (Figure II.7). The authors support the existence of such a hot spot with geochemical data, which distinguish between the composition of Bouvet and Shona magmas. The zigzag shape of the Cape Rise–Meteor Rise lineament has been attributed to the crossing of the Shona hot spot by the active transform segment of the Falkland-Agulhas Fracture Zone in Late Mesozoic times [Hartnady and le Roex, 1985]. The relationships between the predicted trail of the Shona hot spot, on the African and South American plates, and the geometries of the Meteor and Islas Orcadas Rises, respectively, suggest that both of these features were formed simultaneously, at about 60 Ma (as suggested by LaBrecque [1986]) by the Shona hot spot (Figure II.7). Basal sediments on the Islas Orcadas Rise (ODP site 702) show that this feature is >61 Ma and so is possibly Late Cretaceous [Ciesielski et al., 1988]. The oldest in-situ or reworked microfossils at ODP site 703, located on the Meteor Rise are Eocene, in contrast to the Late Cretaceous microfossils found on the Islas Orcadas Rise [Ciesielski et al., 1988]. This age difference has been attributed to the Meteor Rise having experienced more recent volcanism, which would account for its shallower basement and more rugged relief. An additional constraint on the age of these features is given by the fact that the oldest anomaly bounding the east side of the Islas Orcadas Rise, and the corresponding west side of the Meteor Rise, is anomaly 24 (55 Ma) [Cande et al., 1989].

The Trinadade–Columbia seamount chain represents the trail of the South American plate over the Martin Vas hot spot [Herz, 1977] (Figure II.6). Ages of 0.7 Ma and 0.2 to 3 Ma have been determined for Martin Vas and its adjoining island to the west, Trinadade, respectively [Herz, 1977]. The predicted trail of this hot spot follows the Trinadade–Columbia seamount chain and broadly agrees with the 42-52 K-Ar age range determined for the Abrolhos archipelago, located somewhat to the north of the Trinadade–Columbia lineament [Herz, 1977, Figure 1]. In addition to the Abrolhos archipelago, the Hotspur, Rodgers, and Minerve Seamounts are located along the northern fringe of the Trinadade–Columbia seamount chain, while to the south, is located the Almirante Saldanha seamount [Cherkis et al., 1989]. This broad zone of seamounts may indicate that, as the continental margin of the South American plate migrated over the Martin Vas plume, a wide diameter hot spot was in existence. Such a suggestion is supported by the fact that this hot spot track coincides in age with a group of alkalic igneous intrusions on the Goiania Arch ranging in age from 70 to 95 Ma [Neill, 1973], as noted by Hartnady and le Roex [1985]. About 200-300 km southeastward, a series of alkalic intrusions between Pocos de Caldas (63-80 Ma) and Cabo Frio (51 Ma) [Neill, 1973] have also been attributed to the Martin Vas plume [Hartnady and le Roex, 1985]; these continental intrusives are in broad agreement with the ages predicted for the Martin Vas hot spot. A series of three dated kimberlite deposits (80, 86 and 122 Ma) [Crough et al., 1980, Figure II.6] also coincide with the predicted trail ages for the hot spot. In addition, Crough et al. [1980] pointed out that the trail of the Martin Vas hot spot coincides with most of the alluvial diamond deposits in Brazil. The ages of these alluvial deposits are still uncertain, however, some geological evidence suggests a Cretaceous age [Svisero et al., 1979], but other deposits are considered to be Precambrian.

The modeled trail of the St. Helena hot spot follows the southern boundary of its postulated volcanic trail, a broad NE-SW swath of seamounts and ridges. K-Ar ages of between 14 and 8 Ma have been determined for St. Helena [Baker et al., 1967], although new data indicate an age range of between 9-7 Ma [Chaffey et al., 1989]. The misfit between the predicted trail of the St. Helena plume and its volcanic trail may be explained by uncertainty in accurately locating the zero age center of the upwelling plume. An alternative explanation could be that Helena and Tristan hot spots are of significantly wider diameters (~500 km) than has been assumed for the purposes of this discussion [O'Connor, 1989].

An age range of 1.81 to 12.3 Ma has been determined for the island of Fernando de Noronha [Cordani, 1970]. The modeled trail of the Fernando de Noronha hot spot on the African plate coincides with the Sierra Leone Rise, although the predicted trail passes somewhat to the south of this feature (Figure II.7). On the basis of both ocean drilling, and its distance from the spreading-axis, Kumar and Embley [1977] suggested that the Ceara Rise originated in conjunction with the Sierra Leone Rise, at approximately 80 Ma, as shown by Sibuet and Mascle [1978]. The predicted trail of the African plate over the Fernando plume supports the suggestion that the Ceara and the Sierra Leone rises were formed

simultaneously by the Fernando hot spot, at about 80 Ma (Figure II.8); the North Brazilian Ridge may also have been formed by this particular plume. At the intersection of the Fernando de Norhona lineament and the South American continent near Fortaleza, Tertiary volcanic centers have been identified and attributed to the Fernando hot spot [Almeida, 1958; Vandoros and Oliveira, 1968]. Rb/Sr ages yielded an age of 34 ± 2 Ma [Guimaraes et al., 1982], and five K-Ar analyses yielded an age of 28.7 ± 2.5 Ma. [Vandoros and Oliveira, 1968]. Recent K-Ar dating of these volcanics indicates an age range of 26 to 36 Ma (unpublished data), in broad agreement with the age predicted by the trail of the Fernando hot spot (Figure II.7).

Ascension Island is located on the South American plate, in close proximity to the mid-Atlantic spreading-axis (Figure II.7). The presence of unweathered basalt flows suggests that there has been volcanic activity on this island within the past few hundred years. Nine K-Ar ages from widely distributed sample sites, range from ages too young to be accurately dated by the K-Ar technique, to a maximum of 1.9 Ma (unpublished data). Two undated seamounts located at 9° 04°S, 19° 40°W and 8°29°S, 17° 07.6°W, some 570 and 300 km west of Ascension, respectively [e.g., Cherkis et al., 1989], are located along the predicted trail of the Ascension plume on the South American plate (Figure II.7). The predicted ages of these two seamounts are ~20 and ~10 Ma, respectively.

North American Plate Motion Over Hot Spots

North American plate motion over hot spots has been reconstructed by the addition of North America/Africa finite reconstruction poles [Klitgord and Schouten, 1986] to Africa/hot spots motion (Table II.3). A number of interesting observations can be made regarding various central Atlantic hot spot systems, on the basis of this adjusted absolute motion reconstruction (Figure II.8).

The most prominent volcanic trail in the central Atlantic basin is the New England Seamount chain, which probably formed in association with the Muir and Corner seamount complexes (Figure II.8). Radiometric ages for this seamount chain confirm that it is age progressive [Duncan, 1984] (Figure II.8). Previous authors have postulated that the zero age location of the New England hot spot is either the Great Meteor seamount, or a nearby location. However, this study indicates that a zero age position of the New England hot spot needs to be located at, or in the region of 27°N, 43.0°E, on the African plate, for the predicted trail of the North American plate over the New England hot spot to agree broadly with the geometry and distribution of radiometric ages along the New England Seamount lineament. The agreement between the geometries of the hot spot track and the volcanic lineament is nonetheless still poor. The Corner Seamounts formed when the spreading-axis was in close proximity to a hot spot between 80 Ma and 76 Ma [Tucholke and Smoot, 1990] and may also have been formed by the New England hot spot. Interestingly, this postulated location of the New England plume adjoins a large intermediate wavelength anomaly, which straddles the central Atlantic spreading-axis [Vogt et al., 1984] (Figure II.8). Such intermediate wavelength geoid anomalies generally coincide

Figure II.8. The modeled trails of the African, North American and Eurasian plates over postulated hot spots. Tick marks along hot spot trails represent the progress of plates in 10 m.y. intervals. Relative motion parameters for North American/Africa motion [Klitgord and Schouten, 1986], and for Eurasia/North America [Srivastava and Tapscott, 1986] were added to African/hot spots motion (Table II.3). The intermediate wavelength geoid anomaly shown is from Vogt et al. [1984]. Solid circles represent seamounts with a relief greater that 50 fathoms (300 feet) (91 m) [after Epp and Smoot, 1989]. Radiometric ages shown for the New England Seamounts are from Duncan [1984]. Mercator projection.
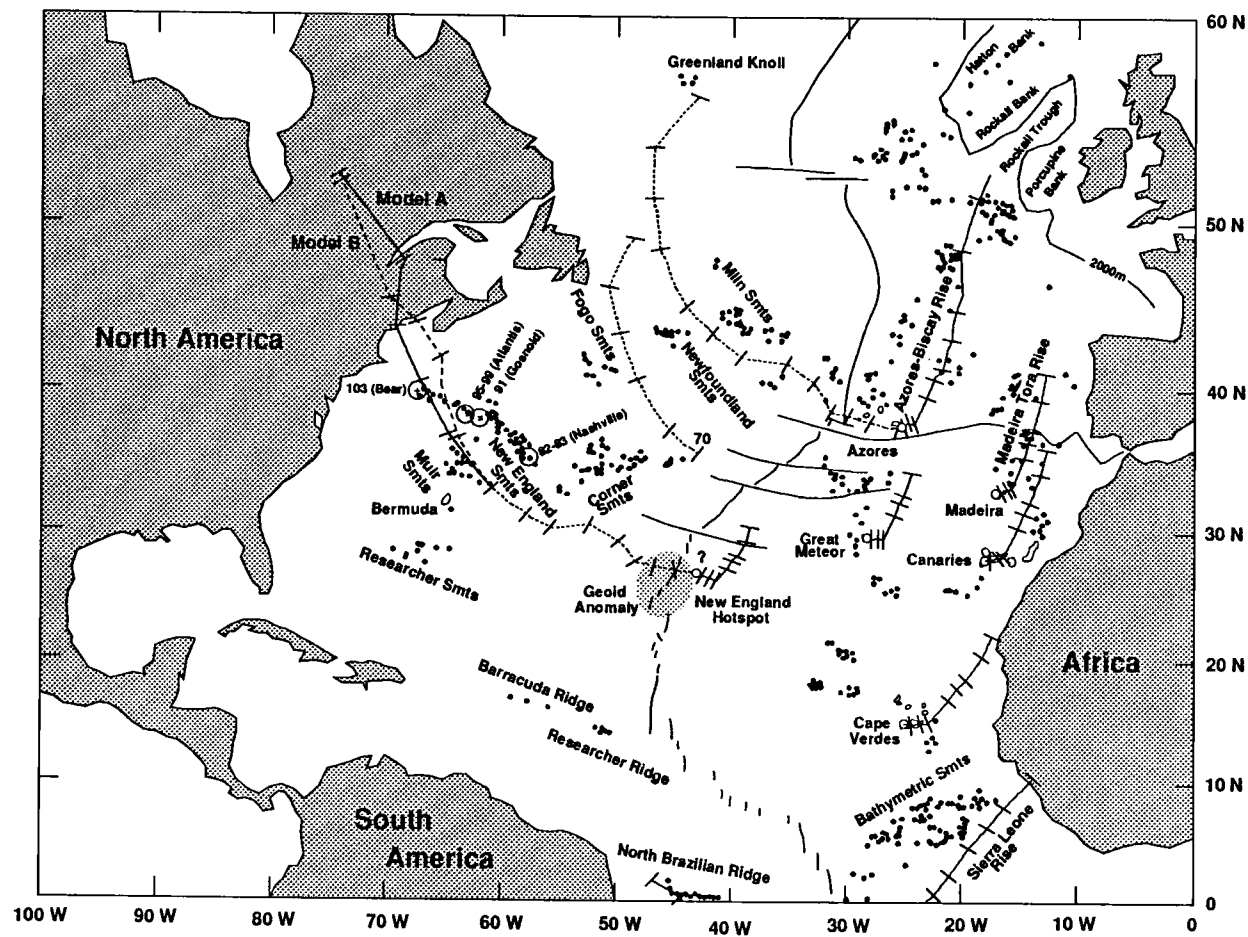
Figure II.8

with major topographic structures such as subduction zones, mid-plate swells, and mid-oceanic ridges, and are considered to reflect sublithospheric processes. There is, however, no convincing evidence to support the existence of this plume from currently available studies of the isotopic and trace element composition of lavas erupting along this section of the mid-Atlantic spreading-axis [Schilling, 1986].

The Mesozoic plutonic complexes of northeastern North America, the White Mountain Intrusives of New England and the Monteregian Hills of Quebec, probably represent a continuation of the trail of the New England hot spot beneath the North American continent, as first proposed by Morgan [1972]. Regional uplift of southeastern Canada and New England in Cretaceous-early Tertiary time has been attributed to the passage of this region of the North American plate over a hot spot [Crough, 1981]. Foland et al. [1988] have reported that the Nd and Sr isotopic signatures of the parental magmas for the New England–Quebec continental plutons are similar to one another, regardless of whether the magma intruded Precambrian or Paleozoic crust, and also similar to those for the New England seamounts, described by Taras and Hart [1987]. Foland and Faul [1977] reported that K-Ar ages, supported by Rb-Sr and U-Pb data, indicate that the White Mountain Intrusives constitute distinct age groups of 230, 200-156, and 124-100 Ma. Morgan [1983] and Crough [1981] accounted for this grouping of ages by suggesting that a series of different hot spots have been active beneath the White Mountain region, with the most recent age period of volcanism associated with the New England hot spot. Foland et al. [1986] and Gilbert and Foland [1986] determined, on the basis of ^{40}Ar-^{39}Ar dating, that the Monteregian Hill centers formed within a short interval of time at 124 Ma. The age distribution along the New England–Quebec plutonic lineament is in very broad agreement with the hot spot track shown in Figure II.8. However, it should be kept in mind that the 120 and 130 Ma rotation poles for Africa/hot spots, on which this reconstruction is based, are not well constrained.

The Great Meteor Seamount (30°N, 29°W) (Figure II.8) may reflect the earlier location of a plume, now extinct, which formed the Newfoundland seamounts and/or Fogo Seamounts (Figure II.8); both of these seamount complexes are located on Cretaceous Quiet Zone to older seafloor [e.g., Klitgord and Schouten, 1986]. The modeled track of this plume assumes a zero age for the Great Meteor Seamount; however, K-Ar ages of 11 Ma and 17 Ma have been determined [Wendt et al., 1976]. An ^{40}Ar-^{39}Ar age of 97.7 ± 1.5 Ma has been determined for trachyte dredged from the Newfoundland seamount [Sullivan and Keen, 1977], compatible with the age predicted by the reconstruction of North American plate motion over a Great Meteor plume (Figure II.8). Earlier activity caused by this hot spot may be marked by 115-145 alkaline intrusions along the coast of Newfoundland [Clark, 1977].

Using the empirical age-depth curve for the Atlantic Ocean crust, Tucholke and Smoot [1990] have shown that the Corner seamounts formed at about 80 Ma to 76 Ma, while on the African plate, the conjugate Cruiser plateau, formed at 76 Ma. Volcanism appears to have migrated northward from Great Meteor Seamount in early Cenozoic time, and then southward to Great Meteor Seamount in the late Cenozoic, with renewed volcanism occurring on some of these seamounts 20 to 30 Ma after their

initial formation over a hot spot. The existence of "intralithospheric conduits" of several hundred kilometers in length may have maintained a link between these seamounts and the hot spot [Tucholke and Smoot, 1990]. If plume material from the Great Meteor and New England plumes were supplied simultaneously to the spreading-axis between 80 Ma and 76 Ma, the combined flow of magma from these two hot spots might account for the construction of the N-S elongated, Corner Seamounts–Cruiser Plateau (Figure II.8).

The motion of the Eurasian plume over the Azores hot spot was calculated by the addition of Eurasian/North America relative motion [Srivastava and Tapscott, 1986] to that of African/hot spots. The predicted trail of the Azores plume intersects the southern opening of the Rockall Trough (Figure II.8) at the 105 Ma location on hot spot track. This result suggests a link between the Azores plume and the initiation of rifting in the Rockall Trough. Srivastava and Tapscott [1986] concluded that the initiation of rifting between the Porcupine Bank and the Orphan Knoll and in the Rockall Trough began at anomaly M0 (118 Ma). From between anomalies M0 and 34 active seafloor spreading was initiated in the North Atlantic and Rockall Trough (all regions south of the Charlie Gibbs Fracture Zone). By anomaly 34 time, seafloor spreading had ceased in the Rockall Trough and commenced to the west in the Labrador Sea. A more recent expression of the Azores plume would appear to be the Azores Biscay Rise (Figure II.8), as first suggested by Morgan [1981]. On the North American plate, the Milne seamounts, located on between approximately anomaly 32 to anomaly 34 seafloor, may record the trail of the Azores plume on the North American plate.

HOT SPOT FIXITY

The cornerstone of all hot spot or absolute motion reconstructions is the assumption that hot spots occur above plumes which rise from, as yet undefined, depth(s) in the mantle to the base of the lithosphere, and that such plumes remain fixed globally with respect to one another over geologically significant periods of time (e.g., 100 m.y.). However, a global extension of the finite reconstruction parameters presented here in order to further test this hypothesis, is beyond the scope of this paper. The research reported here has focused on estimating the most valid set of reconstruction parameters for African plate motion over hot spots, on the basis of presently available data for hot spot generated volcanic lineaments on the African plate. A better understanding of the history of interaction between the mid-Atlantic spreading-axis and the Tristan hot spot has contributed information as to how well particular portions of the Walvis Ridge–Rio Grande Rise volcanic system actually record African and South American plate motions over the Tristan hot spot. Additional constraints on African plate motion over hot spots are, however, critical to further adjustments of African absolute motion. Ongoing radiometric and isotopic studies of basalts recovered from the St. Helena seamount lineament, the seamount chain extending eastward from Gough Island, and additional samples from the Walvis Ridge–Rio Grande Rise, should provide such additional constraints on African plate motion over hot

spots [Chapter III]. Africa/hot spots reconstruction poles given in Table II.3 (adjusted, if necessary, in the light of ongoing studies of South Atlantic volcanic trails) will be extended globally [J. M. O'Connor et al., manuscript in preparation]. Such a study will evaluate differing adjustments to Africa/hot spots reconstruction parameters and lead to a further test as to whether or not hot spots are fixed with respect to one another. While uncertainty ellipses, following the method of Stock and Molnar [1983], have not been calculated for the reconstructions discussed above, typical errors involved in extending African/hot spots motion globally through relative motion plate circuits are ± 100 km [Molnar and Stock, 1987].

SPATIAL RELATIONSHIP BETWEEN THE SPREADING-AXIS AND THE TRISTAN HOT SPOT

For the period of time when the Walvis Ridge–Rio Grande Rise system was forming in a synchronous, age-progressive manner (apart from possible Eocene reactivation), the mid-Atlantic spreading-axis must have been located astride, or in close proximity to the Tristan hot spot. Tristan da Cunha, which is situated on anomaly C6 (19 Ma) African plate seafloor, is located some 550 km east of the present day spreading-axis (Figure II.2). This ~550 km separation between the spreading-axis and the hot spot points to a westward migration of the spreading-axis away from the plume. The absence of a volcanic trail linking the southeastern terminus of the Rio Grande Rise to Tristan da Cunha may best be explained in terms of such a westward migration of the spreading-axis, which eventually shut off the supply of hot material from the upwelling plume. The change in Walvis Ridge morphology from that of aseismic ridge to an indistinct line of discrete seamounts and guyots (Figure II.1a) also reflects, no doubt, this transition from on-axis to intraplate volcanism.

In order to better illustrate the changing spatial relationship between the spreading-axis, the hot spot, and the evolving Walvis Ridge–Rio Grande Rise, a series of reconstructions for selected spreading anomaly times is shown in Figure II.9. If a hot spot-generated seamount or ridge formed at a spreading-axis, it will be surrounded by spreading anomalies of the same age, which may on occasion be mapped onto the hot spot trail (Figure II.2). Conversely, if hot spot magma erupts through older, previously formed seafloor, an age difference will be apparent between the age of the hot spot feature and that of the surrounding seafloor. The age data determined in this study therefore present an excellent opportunity to model the changing spatial relationship between the spreading-axis, the hot spot, and the evolving Walvis Ridge–Rio Grande Rise volcanic system, since anomaly 34 (84 Ma) time.

A suggested prerifting-rifting configuration of Africa, South America, the Parana–Etendeka flood basalts, and a postulated, large diameter hot spot, is shown in Figure II.9a. From anomaly 34 time, spreading anomalies, which were forming at the time of each particular reconstruction, were rotated, along with the Walvis Ridge bathymetry (and African continent), to their respective predrift

Figure II.9a. The shaded region represents a hypothesized, large-diameter hot spot, which formed above the upwelling Tristan plume (open circle) at ~130 Ma. A 130 Ma reconstruction parameter for Africa/hot spots motion was calculated such that the Etendeka flood basalts lie along the southeastern edge of this large diameter plume. The closure parameter of Martin et al. [1981], when combined with this 130 Ma Africa/hot spot rotation parameter, rejoins South America to Africa. Projection is centered on Tristan da Cunha.

10 S
20 S
30 S
40 S
50 S
60 S

SOUTH AMERICA   AFRICA

1500 m African contour
1500 m South American contour

~130 Ma reconstruction

60 W   50 W   40 W   30 W   20 W   10 W   0   10 E   20 E   30 E

Figure II.9a

50
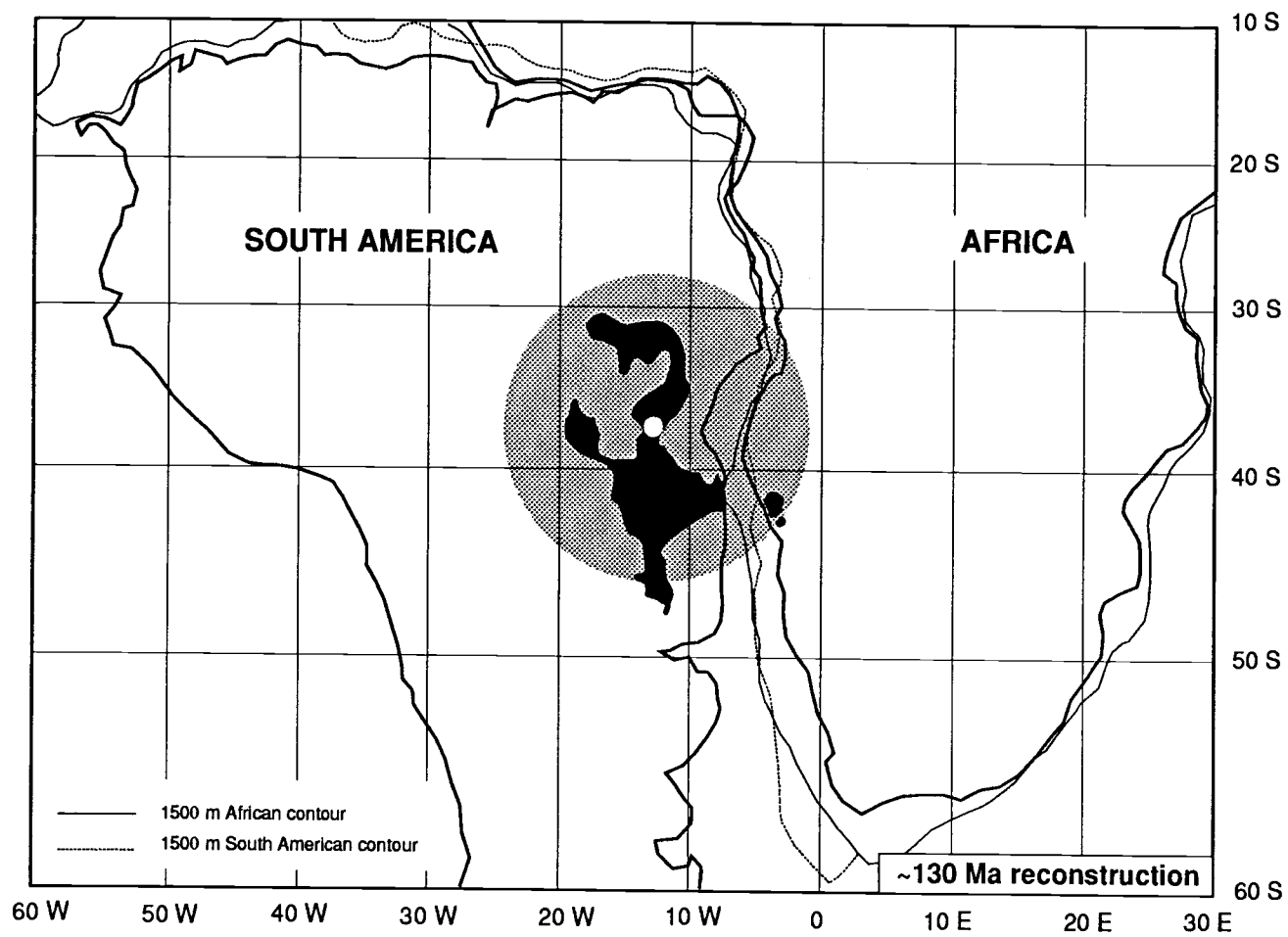
Figure II.9b. A series of reconstructions of the spatial relationship between the spreading-axis, the Tristan hot spot, and the evolving structure of the Walvis Ridge–Rio Grande Rise volcanic system is shown. The projections are centered on the island of Tristan da Cunha (shown as an open circle), i.e., the postulated center of the hot spot. For selected spreading anomaly times the configuration of seafloor spreading anomaly picks (corresponding to the age of the particular reconstruction), Walvis Ridge and Rio Grande Rise bathymetry, and the African and South American continents, have been reconstructed. An Africa/hot spots finite reconstruction pole was calculated for each reconstruction from the rotation parameters given in Table II.3. A corresponding South America/hot spots rotation pole was calculated by the addition of a pertinent South America/Africa relative motion parameter [Cande et al., 1988]. Magnetic anomaly picks are from Cande et al. [1988] with (pluses and small open circles) representing rotated African and South American anomaly picks, respectively. Bathymetry is from the DBDB 10 global bathymetry [National Geophysical Data Center, 1985]. Shaded portions of the Rio Grande Rise represent portions of this feature, which are considered to have formed at the time for which the reconstruction is shown. Dashed bathymetry indicates portions of the Walvis Rise–Rio Grande Rise system which had yet to evolve at the time of the particular reconstruction, and are shown for clarity. Basement ages for the Walvis Ridge–Rio Grande Rise are shown. The letters H, I, and L indicate whether a sample site is characterized by high, intermediate, or low Zr/Nb ratios, respectively, as defined in Figure 10. Mercator projection.
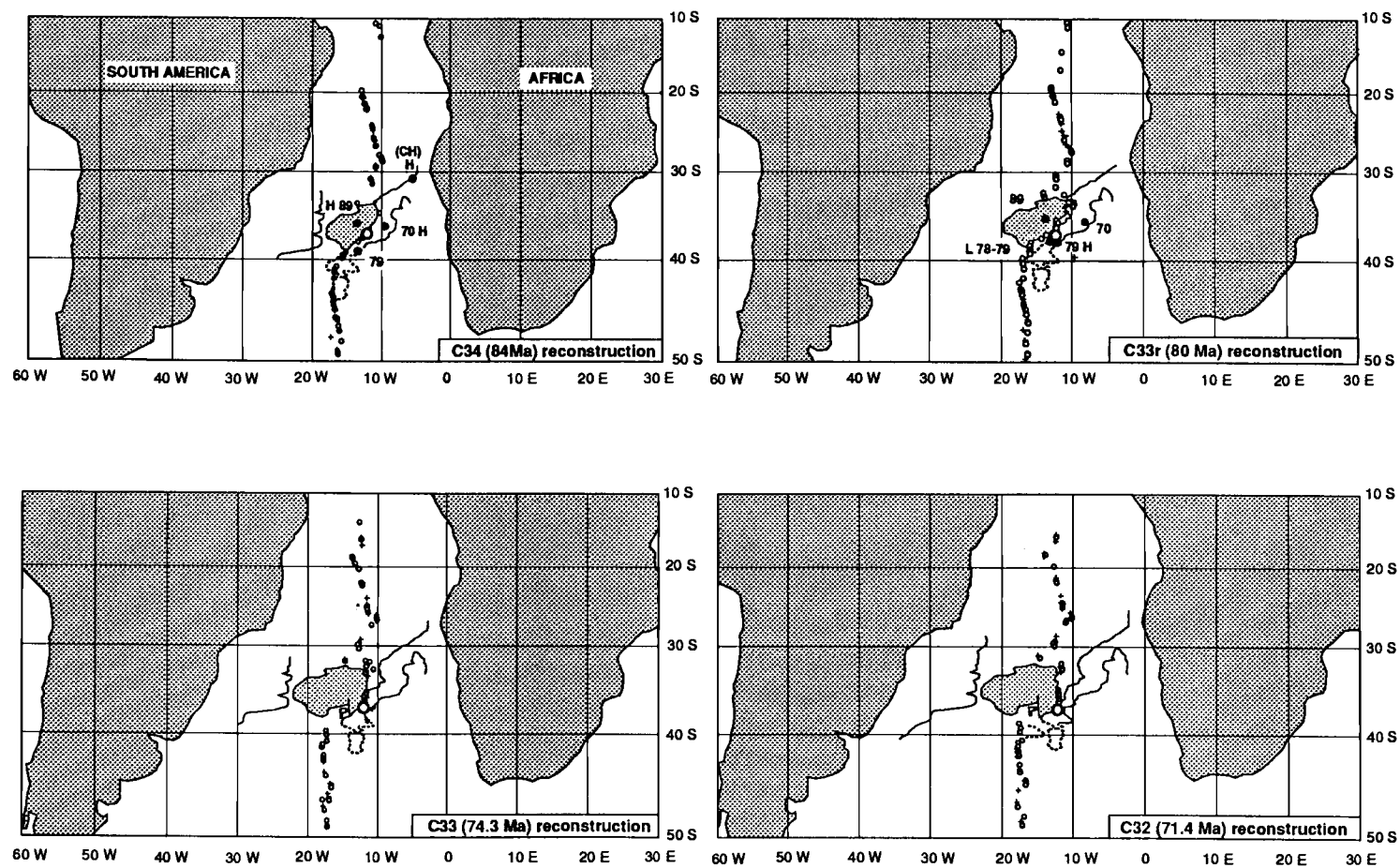
Figure II.9b
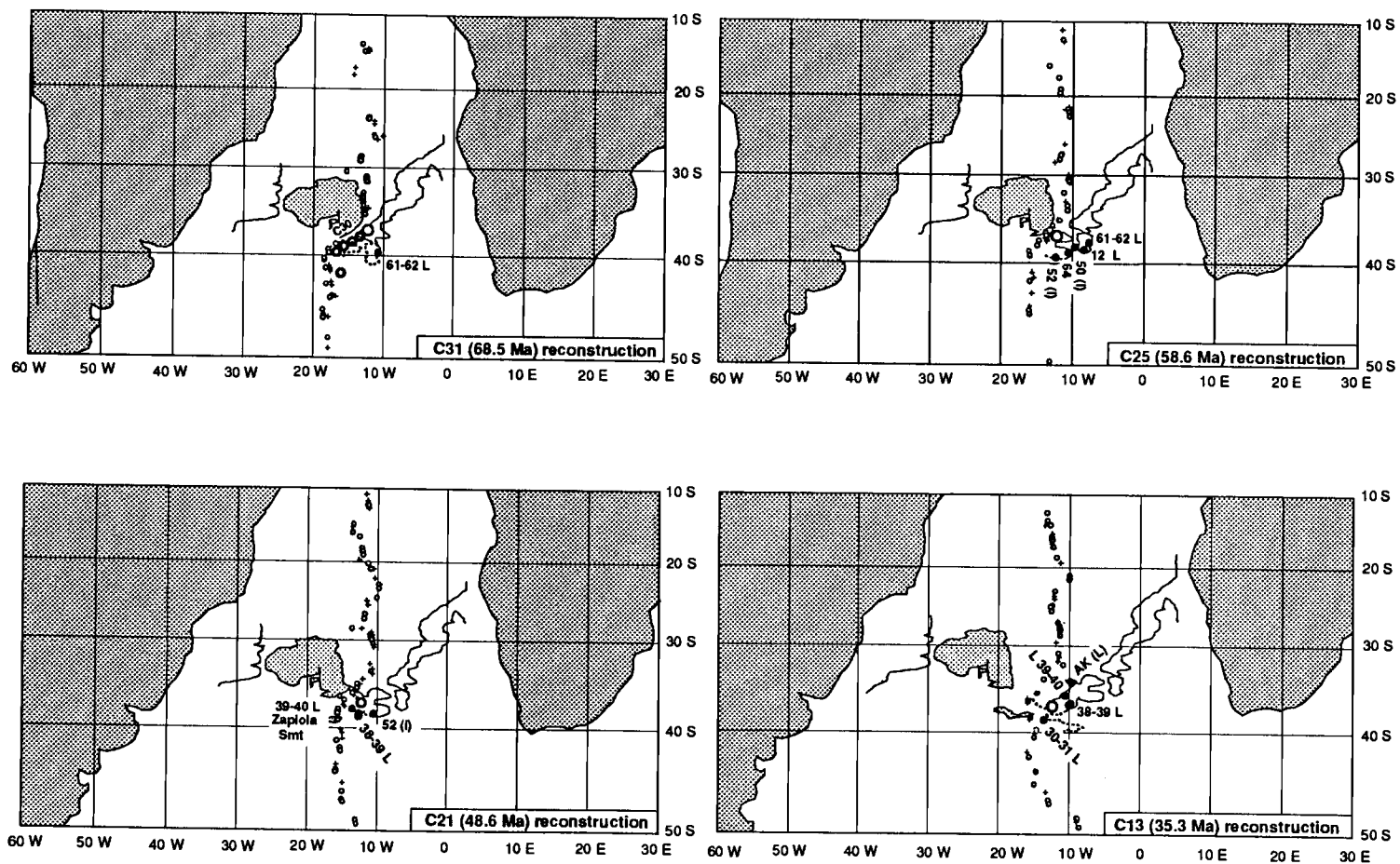
Figure II.9b (continued)

positions. An appropriate rotation parameter was calculated for each reconstruction from the Africa/hot spots finite poles given in Table 3. The corresponding anomaly picks on the South American plate, the Rio Grande Rise bathymetry (and the South American continent) were, in turn, rotated to their conjugate, predrift positions, by the addition of the appropriate South America/Africa relative motion [Cande et al., 1988]. The extent to which the Walvis Ridge–Rio Grande Rise bathymetry had evolved at the time of each reconstruction is constrained primarily by the basement ages reported in this study.

The C34 (84 Ma) reconstruction places the spreading-axis astride the Tristan plume. Large volumes of hot material erupted along this divergent boundary and formed the conjugate western and eastern plateaus of the Rio Grande Rise and the Walvis Ridge, respectively (Figure II.9b). The significant age-offset between seafloor located to the north versus that to the south of the Walvis Ridge (Figure II.2) can be attributed to a prior history of easterly and southeasterly spreading-axis migrations beginning in Albian to late Aptian time, as discussed in an earlier section. The configuration of the spreading-axis, volcanic structure, and the hot spot in anomaly 34 time is strikingly similar to that which exists in present day Iceland.

At C33r (80 Ma) the northeastern shoulder of the Rio Grande Rise and the western edge of the Walvis Ridge plateau were formed. The narrow ridge which extends southward from the Walvis Ridge plateau, was constructed almost as far south as the 78-79 Ma DSDP transect, in conjunction with the western side of the Rio Grande Rise Plateau. Between C33r (80 Ma) and C32 (71.4 Ma) time, this narrow ridge continued to develop in conjunction with the N-S eastern ridge of the Rio Grande Rise. This N-S ridge apparently formed along a spreading-axis, which was continuously propagating southward and southeastward toward the hot spot, apparently in order to retain its position above the upwelling plume. Massive amounts of hot material must have been supplied to the spreading-axis by the plume in order for this massive lineament to have formed within such a relatively short time interval. As the spreading-axis propagated southward it invaded the previously formed seafloor which was in the process of migrating northward over the hot spot. Thus, while the South American plate may in fact have migrated in a NW-SE direction over the hot spot, the N-S ridge of the eastern Rio Grande Rise formed along a southwardly propagating, hot spot-fed spreading-axis, and apparently did not record the true direction of South American plate motion over the plume. As a result of this continued southward propagation, the asymmetry of the spreading-axis became most pronounced between C33r and C32 times.

By C31 (68.5 Ma), or earlier, the Walvis Ridge had commenced to bifurcate into three subparallel lineaments. The northern ridge formed on the spreading-axis, in conjunction with the southeastern terminus of the eastern Rio Grande Rise, while to the southeast a subparallel ridge was forming in an intraplate situation. Between C32 (71.4 Ma) and C30 (66.7 Ma) times a major spreading-axis jump occurred, which may have represented the final effort by the spreading-axis to regain its position over, or close to, the hot spot. Thus, by about C30 (66.7 Ma) time, or earlier, the

northern side of the Walvis Ridge (and the southeastern portion of the Rio Grande Rise) was evolving as a plume-fed spreading-axis, while the southern portion of the Walvis Ridge was forming in an intraplate environment, as older seafloor began to migrate over the hot spot.

By about C21 (48.6 Ma) time, the hot spot could no longer sufficiently augment the volume of hot material upwelling along the westward migrating spreading-axis for continued construction of the Rio Grande Rise. The Zapiola seamount complex began to evolve about this time to the south of the Rio Grande Rise. The migration over the plume of the fracture zone, which represents the southern boundary of spreading-axis asymmetry (located to the north of Tristan da Cunha in Figure II.2), may have switched the flow of plume material from the Rio Grande Rise to the Zapiola seamount region of the spreading-axis. The northward migration of this fracture zone, over the hot spot, could explain why until about C21 (48.6 Ma) the seafloor isochrons identified to the south of the Walvis Ridge were older than those located on and to the north of the ridge (Figure II.2). The subsequent rapid disappearance of this age offset between the seafloor located north and south of the Walvis Ridge is therefore best explained by the combined effects of a westward migration of the spreading-axis away from the hot spot and an associated northward migration over the hot spot of the previously formed African lithosphere.

At C13 (35.3 Ma) the Zapiola Seamount complex ceased to evolve. A mirror image of the Zapiola Complex could have been formed on the African plate by the westward flow of plume material to the spreading-axis, beneath the lithosphere. If such a feature existed it would eventually have been carried over the Tristan plume and have been incorporated into the Walvis Ridge.

There is geochemical evidence to suggest that basaltic magmas, which have erupted at the present day spreading-axis, located due west of Tristan da Cunha, are slightly "enriched" by the continuation of westward flow of plume material beneath the African plate [Humphris et al., 1985]. Such a continuous enrichment of the magmas forming African lithosphere at the latitude of Tristan da Cunha would have varied with increasing separation of the plume and the spreading-axis, which began about 70 Ma. This enriched geochemical signal, trapped in the African plate, might have been mixed into Walvis Ridge magmas, as this variable enriched African lithosphere migrated over the hot spot. Additional information about the history of hot spot and spreading-axis interactions is provided by a number of other approaches (e.g., geochemistry and isostasy) discussed in the following section.

GEOCHEMICAL COMPOSITIONS

Magmas derived from hot spots (ocean island basalts or OIB) and from seafloor spreading-axes (mid-ocean ridge basalts or MORB) are compositionally distinct, especially in certain trace element and isotopic ratios. The compositions of Walvis Ridge–Rio Grande Rise basalts vary in incompatible element abundances and ratios, rare earth elements (REE), and Sr, Nd, Pb isotopic ratios [Humphris and Thompson, 1982, 1983; Richardson et al., 1982, 1984; Thompson and Humphris, 1984; Thompson et al., 1983; Humphris et al., 1985].

A decrease in the Zr/Nb ratio of the hot spot has occurred since the formation of the Etendeka-Parana flood basalts (Figure II.10), which may be related to changes in the plate tectonic environment associated with the westward migration of the spreading-axis (Figure II.9b). The elements Zr and Nb (and also Y and the REE elements) are of particular use in the investigation of magma source regions, as these elements are highly incompatible and their ratio will be influenced only slightly by variations in partial melting and crystal fractionation [Erlank and Kable, 1976; Sun et al., 1979; Pearce and Norry, 1979]. They are also among the trace elements which are most highly resistant to mobilization by seawater alteration [Thompson, 1973].

High Zr/Nb ratios are evident in Etendeka-Parana, DSDP 516F (Rio Grande Rise plateau), CH 18 and CH 19, AII-93-21, V29-11 (eastern Walvis Ridge) and DSDP 525A (central Walvis Ridge) basalts (Figures 5 and 6). Apart from the flood basalts, these high Zr/Nb ratios may be characteristic of an on-axis situation (Figure II.9b), as proposed by Humphris et al. [1985]. In such a tectonic environment large volumes of magma from the upper mantle MORB source region might have diluted the signal of the OIB source, as occurs at the main central rifting zone in Iceland [e.g., Schilling et al., 1982, 1983]. The "enriched" and "depleted" MORB type recovered from the spreading-axis about ~550 km to the west of Tristan da Cunha [Humphris et al., 1985] are the only known volcanic rocks in this region with higher Zr/Nb ratios.

A transition to low Zr/Nb ratios is first recorded within the Walvis Ridge–Rio Grande Rise system at DSDP sites 528 and 527 (79-80 Ma). However, low Zr/Nb basalts have been recovered from DSDP site 530, located about 20 km to the north of the Walvis Ridge (Figure II.7), close to the African coast. Variations in ratios of Zr/Y or Y/Nb, with Zr/Nb, displayed by DSDP 530, 527, and 528 basalts, correspond well with predicted mixing curves calculated for depleted MORB and an enriched, Tristan-type end-member source, in contrast to DSDP 525A and dredged basalts [Humphris and Thompson, 1983]. This points to 527 and 528 basalts having formed at a hot spot-fed spreading ridge, as was the case for 530 basalts, which had formed at an earlier time [Humphris and Thompson, 1983]. A similar pattern of binary mixing between "enriched" (Tristan) and "depleted" (MORB) end-member sources is evident in spreading-axis basalts recovered due west of Tristan da Cunha. This indicates a continued sub-lithospheric connection between the Tristan hot spot and the spreading-axis [Humphris et al., 1985]; however, earlier enrichment or fertilization of the upper mantle by the plume may also be of importance.

The remaining basalts recovered from the Walvis Ridge all exhibit low to intermediate Zr/Nb ratios, characteristic of their having erupted in an intraplate tectonic environment (Figure II.9b). Basalts dredged from the Rio Grande Rise plateau (probably of Eocene age) exhibit low Zr/Nb ratios, in contrast with the underlying, on-axis, high Zr/Nb basement basalts (DSDP 516F) (Figure II.9b).

Low Zr/Nb ratios for the island of Tristan da Cunha may result from the fact that, at very low degrees of partial melting, Zr does not behave as incompatibly as Nb; this could explain why the trend

Figure II.10. Zr/Nb ratios for the Walvis Ridge–Rio Grande Rise hot spot system can be divided into "high", "intermediate", and "low" Zr/Nb basalts. "High" Zr/Nb basalts (apart from present-day spreading-axis basalts) are associated with continental flood and on-spreading-axis, hot spot volcanism. In contrast, "low" Zr/Nb ratios are associated with intraplate hot spot volcanism and hot spot-fed spreading-axis (i.e., DSDP 527 , 528, and 530). Figure 9b illustrates this correlation between decreasing Zr/Nb ratios and the transition from on-spreading-axis to intraplate volcanism, within the Walvis Ridge–Rio Grande Rise system. Gough Island is a recently active volcano located to the southeast of Tristan da Cunha. Sources of data: Parana [Fodor et al., 1985], Etendeka [Marsh, 1987], Walvis Ridge dredges [Humphris and Thompson, 1982, 1983], DSDP 530 and CH18 and 19 [Humphris and Thompson, 1983], DSDP 525A, 527 and 528 [Thompson and Humphris, 1984], DSDP 516F [Thompson et al., 1983; Weaver et al., 1983], Tristan da Cunha [Weaver et al., 1987], Gough Island [le Roex, 1985; Weaver et al., 1987], and MORB [Humphris et al., 1985]. Asterisks denote samples for which ^{40}Ar-^{39}Ar ages have been determined. N = number of analyses for which a mean value has been determined.
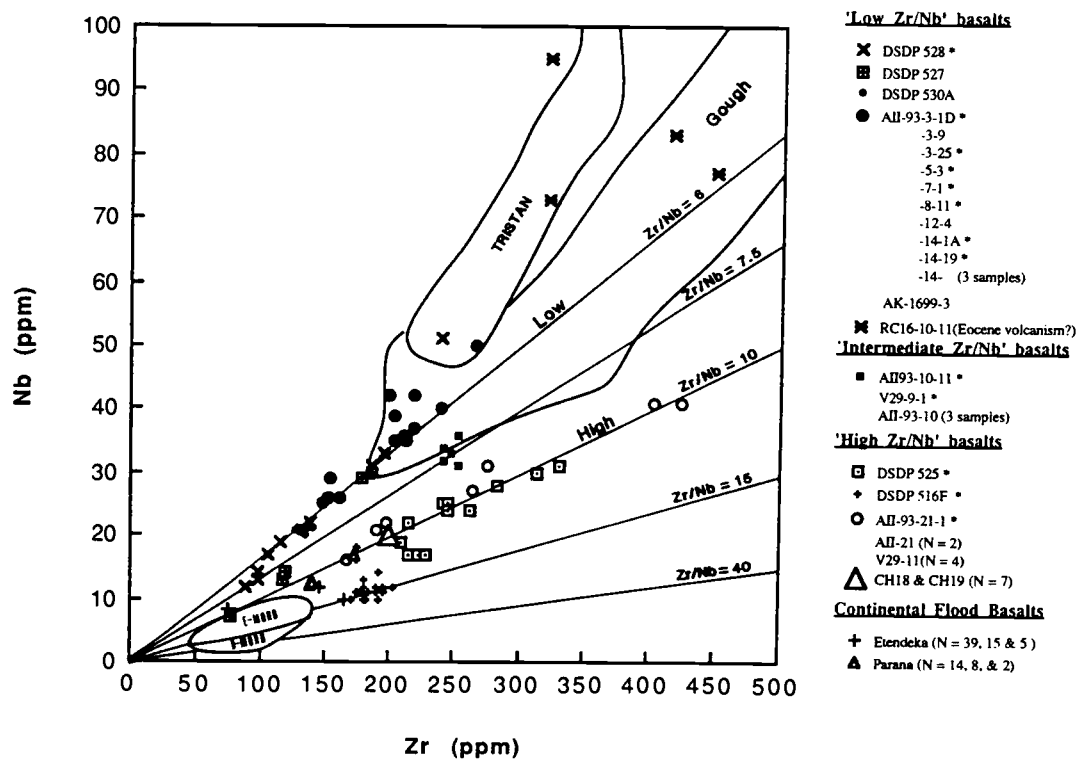
Figure II.10

of the Tristan da Cunha Zr and Nb data intersects the Zr axis, rather than the origin [Weaver et al., 1987]. Gough Island samples show a slight, but distinct decrease in Zr/Nb between the lower basalt series (about 1.0 Ma) and the upper basalt series (about 0.3 Ma) [le Roex, 1985], due possibly to the influence of decreasing degrees of partial melting.

Humphris and Thompson [1983] and Humphris et al. [1985], after Chen and Frey [1983], have suggested that as a transition to an intraplate environment occurs, low degrees and low volumes of partial melting of the surrounding depleted lithosphere (i.e., previously formed African plate) will become important in determining the composition of the volcanic trail. Spreading-axis and hot spot interactions may therefore have controlled the mixing, and relative importance, of depleted MORB, enriched OIB, and low degrees and amounts of partial melts of the depleted lithosphere, thus indirectly determining the composition of Walvis Ridge and Rio Grande Rise basalts.

As a plume rises, however, it warms the surrounding mantle material by thermal diffusion, thus lowering its viscosity sufficiently to cause large-scale entrainment and mixing of asthenospheric source material [Griffiths, 1986]. The transition to less depleted magmas within the Reunion hot spot system (i.e., decreasing MORB component) is best explained by reduction in the entrainment of upper mantle material [White et al., 1990]. Such a change in the extent of upper mantle entrainment may also have played a role in controlling the degree of enrichment of Walvis Ridge–Rio Grande Rise basalts. Sr, Nd, and Pb isotopic analyses are presently being conducted on available Walvis Ridge and Rio Grande Rise basalts, in order to determine the factors responsible for controlling temporal and spatial variations in composition [J. M. O'Connor et al., manuscript in preparation]. In conclusion, the change from high to low Zr/Nb ratios within the Walvis Ridge–Rio Grande Rise system broadly supports a model of transition from on-axis to intraplate volcanism.

ISOSTASY OF THE WALVIS RIDGE AND RIO GRANDE RISE

The transition from on-axis to intraplate hot spot volcanism within the Walvis Ridge–Rio Grande Rise system is supported by numerous gravity and geoid studies [Detrick and Watts, 1979; Bulot et al., 1984; Kogan et al.,1985; Gibert and Courtillot, 1987; Freedman, 1987; Diament and Goslin, 1987]. The gravity signatures of aseismic ridges and seamounts are sensitive to the age (i.e., strength) of the lithosphere at the time of construction. Those features which formed in an intraplate setting (i.e., old, thick seafloor) are supported by the elastic stresses produced by the bending of the plate; as the plate distributes the compensating masses over a wide area, the gravity signature measured directly over the load will be large. In contrast, volcanoes which form on young lithosphere (i.e., near a spreading-axis) will be locally supported so that the compensating masses are located directly beneath the load; the resulting gravity anomaly measured above the feature will be small.

Gravity and geoid data measured over the Walvis Ridge and the Rio Grande Rise have been correlated with bathymetry in order to determine the mechanism by which they are isostatically

compensated [Detrick and Watts, 1979; Bulot et al., 1984; Kogan et al., 1985; Gibert and Courtillot, 1987; Diament and Goslin, 1987]. Detrick and Watts [1979] have shown that from the African coast to about 3°E the Walvis Ridge is locally supported by an Airy-type thickening of the crust with a modeled crustal thickness in the range 15 km to 25 km. West of longitude 3°E, however, the Walvis Ridge is best explained by a plate model (i.e., a thin elastic plate overlying a weak fluid) with a modeled elastic thickness of between 5 and 8 km. These results are consistent with a transition from on-axis to intraplate hot spot volcanism on the Walvis Ridge at about 70 Ma.

The mechanical isostasy of the Walvis Ridge and the Rio Grande Rise has also been investigated by Bulot et al. [1984] using constraints imposed by SEASAT geoid data. In their study, the Walvis Ridge was divided into three overlapping subsections: an eastern (African coast to about 3°E), a central (about 3°E to about 0°), and a western section (about 0° to Tristan da Cunha). An Airy model calculated with a crustal thickness of 20 km is in good agreement with the experimental results obtained for both the eastern Walvis Ridge and the Rio Grande Rise. Experimental admittances using the plate model with an elastic thickness of 8 km and 6 km best fit the data from the central and western sections of the Walvis Ridge, respectively. This gradation in modeled plate thicknesses between the central and western study areas probably records the transition from on-axis to intraplate hot spot volcanism. Diament and Goslin [1987], however, have shown that the contributions of mechanical isostasy (off-axis formation) and density contrasts at depth (near-axis formation) are very different over adjoining domains along the Walvis Ridge. This can best be explained for the Walvis Ridge in terms of a rather complex history of hot spot spreading-axis interactions, as broadly documented in this study.

CHANGES IN SOUTH ATLANTIC OCEAN CIRCULATION

The transition from on-axis to intraplate hot spot volcanism within the Walvis Ridge–Rio Grande Rise may be indirectly recorded by an abrupt improvement in the oxidation state of South Atlantic bottom water at 55 to 58 Ma. Liu [1982], Liu and Schmitt [1984], Wang et al. [1986], Liu et al. [1988], and Hu et al. [1988] have proposed that under reducing conditions, Ce exists in seawater as a trivalent ion and is therefore incorporated along with the other trivalent rare earth elements (i.e., lanthanides) into seafloor sediments, by adsorption onto carbonate minerals. In contrast, under oxidizing conditions, Ce^{3+} is oxidized to Ce^{4+} and precipitates as very insoluble hydroxides. This results in depletion of Ce relative to the other trivalent rare earth elements in both seawater and sediments. Such Ce variations within marine carbonates represent a record of changes in palaeo-ocean bottom water redox conditions.

Carbonate sediment samples from DSDP 525A [Liu, 1982; Liu and Schmitt, 1984], DSDP 530A, B, located in ocean floor 20 km north of the eastern end of the Walvis Ridge [Wang et al., 1986], and DSDP 516, 516F [Hu et al., 1988] have been analyzed by the INAA technique in order to

determine downcore Ce variations. All three sites show gradual Ce depletions (i.e. reducing seawater conditions) from the late Campanian (~80 Ma) until about 55 to 58 Ma, at which time an abrupt transition to present day Ce values (i.e., oxidizing seawater conditions) occurred. Hu et al. [1988] and Liu et al. [1988] have attributed such changes in oxidation state to improvements in the circulation of South Atlantic bottom water. Breaching of the Walvis Ridge–Rio Grande Rise barrier to bottom water circulation, as a result of the divergence of the spreading-axis and the hot spot, is a probable explanation for this improvement in circulation. Widening of the South Atlantic ocean basin and subsidence of the Romanche Fracture Zone (which acted as a barrier to deep bottom water flowing between the North and South Atlantic basins), may, however, have also played significant roles.

CONCLUSIONS

Volcanism within the Walvis Ridge–Rio Grande Rise volcanic system has been shown to be fundamentally age-progressive. The origin of the recently active island of Tristan da Cunha, the Walvis Ridge and Rio Grande Rise, and the Etendeka and Parana continental flood basalts, can therefore be attributed to a common source, the Tristan plume.

The Walvis Ridge and Rio Grande Rise formed in a synchronous, age-progressive fashion along a section of the South Atlantic spreading-axis, as the African and South American plates diverged apart, astride (or in close proximity to) the Tristan hot spot. Reconstructions of the spatial relationship between the spreading-axis, the hot spot, and the evolving Walvis Ridge–Rio Grande Rise system have shown that at about 70 Ma the spreading-axis migrated to the west, away from the hot spot. This westward migration of the spreading-axis was accompanied by a northward migration over the hot spot of previously formed seafloor. As a consequence, a transition from on-axis to intraplate hot spot volcanism occurred, which resulted in the termination of Rio Grande Rise formation. Support for this conclusion is provided by the fact that on-axis basalts have higher Zr/Nb ratios in comparison to those which erupted in an intraplate situation. Changes in the spatial relationship between the spreading-axis and the hot spot may have controlled the mixing, and relative importance of, depleted MORB, enriched OIB, and partial melts of the depleted ocean lithosphere. Isostasy studies also support a transition to intraplate volcanism on the Walvis Ridge beginning at about 70 Ma.

In the light of an improved understanding of the temporal-spatial evolution of the surface expression of the Tristan plume, i.e., the Walvis Ridge–Rio Grande Rise and associated continental flood basalt fields, rotation parameters for the motion of the African plate over the Tristan hot spot have been recalculated. These reconstruction poles predict a trail for the Tristan hot spot on the African plate which agrees with the distribution of ages along the Walvis Ridge. The N-S trending eastern ridge of the Rio Grande Rise formed, in all probability, along a hot spot-fed, southward propagating spreading-axis. This portion of the Rio Grande Rise apparently does not record the actual motion of the South American plate over the hot spot. Africa/hot spots rotation parameters were therefore not

constrained to predict a trail which, on addition of South America/Africa relative motion poles, would follow the geometry of the N-S ridge of the Rio Grande Rise. Rather, the hot spot track cuts a NW-SE path across the Rio Grande Rise, following the NW-SE trending, elongated topography suggested for the rise from studies of the South Atlantic geoid. This result illustrates the critical importance of a detailed understanding of the evolution of individual hot spot systems such as the Walvis Ridge–Rio Grande Rise, in estimating reliable reconstruction poles.

The reconstructed motion of the African plate over hot spots has been extended to the North and South American plates by the addition of appropriate relative motion poles. The evolution of all significant hot spot systems on both of these plates has been discussed in detail. In order for the predicted track of the New England hot spot to pass through the region of the New England seamounts, the zero age location of this plume must be located in the vicinity of the central Atlantic spreading-axis at about 27°N. The existence of a prominent intermediate-wavelength geoid anomaly in this locality has been interpreted as supporting evidence for this conclusion. The Azores hot spot has been linked to the initiation of rifting, and consequent seafloor spreading, in the Rockall Trough.

REFERENCES

Almeida, F. F. M., Geologia e petrologia do argquipelago de Fernando do Noronha, Monogr., 13, Div. Geol. Min. Dep. Nac. Prod. Mineral., Rio de Janeiro, 1958.

Amaral, G., U. G. Cordani, K. Kawashita, and J. H. Reynolds, Potassium-argon dates of basaltic rocks from Southern Brazil, Geochim. Cosmochim. Acta, 30, 159-189, 1966.

Anderson, D. L., Hot spots, polar wander, Mesozoic convection and the geoid, Nature, 297, 391-393, 1982.

Aumento, F., Vesicularity of mid ocean pillow lavas, Can. J. Earth Sci., 8, 1315-1319, 1971.

Austin, J. A., Jr., and E. Uchupi, Continental-oceanic crustal transition off Southwest Africa, Am. Assoc. Pet. Geol. Bull., 66, 1328-1347, 1982.

Backman, J., R. A. Duncan et al., Proc. Ocean Drill. Program, Initial Rep., 115, 1085 pp., 1988.

Baker, B. H., and J. A. Miller, Geology and geochronology of the Seychelles Islands and structure of the floor of the Arabian Sea, Nature, 199, 346, 1963.

Baker, I., N. H. Gale, and J. Simons, Geochronology of the St. Helena volcanoes, Nature, 215, 1451-1454, 1967.

Barker, P. E., Tectonic evolution and subsidence history of the Rio Grande Rise, Initial Rep. Deep Sea Drill. Proj., 72, 953-976, 1984.

Barker, P. E., I. G. Gass, P. G. Harris, and R. W. LeMaitre, The volcanological report of the Royal Society expedition to Tristan da Cunha, Philos. Trans. R. Soc. London., Ser. A, 256, 439-578, 1964.

Blow, W. H., Deep Sea Drilling Project, Leg 3, Foraminifera from selected samples, Initial Rep. Deep Sea Drill. Proj., 3, 629-661, 1970.

Bolli, H. M., W. B. F. Ryan et al., Walvis Ridge-sites 362 and 363, Initial Rep. Deep Sea Drill. Proj., 40, 183-356, 1978.

Brereton, N. R., Corrections for interfering isotopes in the ^{40}Ar-^{39}Ar dating method, Earth Planet. Sci. Lett., 8, 427-433, 1970.

Bryan, W. B, and R. A. Duncan., Age and provenance of clastic horizons from hole 516F, Initial Rep. Deep Sea Drill. Proj., 72, 475-477, 1983.

Bukry, D., and M. N. Bramlette, Coccolith age determinations leg 3, Deep Sea Drilling Project, Initial Rep. Deep Sea Drill. Proj., 3, 589-612, 1970.

Bulot, A., M. Diament, M. G. Kogan, and J. Dubois, Isostasy of aseismic tectonic units in the South Atlantic Ocean and geodynamic implications, Earth Planet. Sci. Lett., 70, 346-354, 1984.

Cande, S. C., and P. D. Rabinowitz, Mesozoic sea floor spreading bordering conjugate continental margins of Angola and Brazil, Proc. Annu. Offshore Technol. Conf., 3, 1769-1776, 1978.

Cande, S. C., and P. D. Rabinowitz, Magnetic anomalies of the continental margin of Brazil, Offshore Brazil Map Ser, American Association of Petroleum Geologists, Tulsa, Okla., 1979.

Cande, S. C., J. L. LaBrecque, and W.B. Haxby, Plate kinematics of the South Atlantic: Chron 34 to present, J. Geophys. Res., 93, 13,479-13,492, 1988.

Cande, S. C., J. L. LaBrecque, R. L. Larson, W. C. Pitmann III, X. Golovchenko, and W. F. Haxby, Magnetic Lineations of the World's Ocean Basins (map). Scale: approximately 1:27,400,000 at the equator, American Association of Petroleum Geologists, Tulsa, Okla., 1989.

Chaffey, D. J., R. A. Cliff, and B. M. Wilson, Characterization of the St. Helena magma source, edited by A. D. Saunders, and M. J. Norry, Magmatism in the Ocean Basins, Spec. Publ. 42, Geol. Soc. of London, pp. 257-276, 1989.

Chave, A. D., Lower Paleocene-upper Cretaceous magnetostratigraphy, sites 525, 527, 528, and 529, Initial Rep. Deep Sea Drill. Proj., 74, 525-532, 1984.

Chen, C.-Y., and F. A. Frey, Origin of Hawaiian tholeiite and alkalic basalt, Nature, 302, 785-789, 1983.

Cherkis, N. Z., H. S. Fleming, and J. M. Brozena, Bathymetry of the South Atlantic Ocean-3°S to 40°S, Map and Chart Ser. MCH-069, Geol. Soc. of Am., Boulder, Colo., 1989.

Chevallier, L., and N. Vatin-Perignon, Volcanostructural evolution of Piton des Neiges, Reunion Island, Indian Ocean, Bull. Volcanol., 45, 287-298, 1982.

Ciesielski, P. F., Y. Kristoffersen et al., Proc. Ocean Drill. Program, Initial Rep., 114, 801 pp., 1988.

Clark, D. B., The Tertiary volcanic province of Baffin Bay, Geol. Assoc. Can. Spec. Pap., 16, 445-460, 1977.

Cordani, U. G., Idade do vulcanismo no Oceano Atlantico Sul, Bol. Inst. Geocienc. Astron., Univ. Sao Paulo, 1, 9-75, 1970.

Cordani, U. G., P. L. Sartori, and K. Kawashita, Geoquimica dos isotropes de estroncio e a evolucao da atividade vulcanica na Bacia do Parana, An. Acad. Bras. Cienc., 52, 811-818, 1980.

Cox, K. G., The role of mantle plumes in the development of continental drainage patterns, Nature, 342, 873-877, 1989.

Crough, S. T., Mesozoic hot spot epeirogeny in eastern North America, Geology, 9, 2-6, 1981.

Crough, S. T., W. J. Morgan, and R. B. Hargraves, Kimberlites: Their relation to mantle hot spots, Earth Planet. Sci. Lett., 50, 260-274, 1980.

Dalrymple, G. B., and D. A. Clague, Age of the Hawaiian-Emperor Bend, Earth Planet. Sci. Lett., 31, 317-321, 1976.

Dalrymple, G. B., and M. A. Lanphere, Potassium Argon dating: Principles, Techniques, and Application to Geochronology, W. H. Freeman, New York, 258 pp., 1969.

Dalrymple, G. B., and M. A. Lanphere, [40]Ar-[39]Ar technique of K-Ar dating: A comparison with the conventional technique, Earth Planet. Sci. Lett., 12, 300-308, 1971.

Dalrymple, G. B., and J. G. Moore, Argon 40: Excess in submarine pillow basalts from Kilaueau Volcano, Hawaii, Science, 161, 1132-1135, 1968.

Dalrymple, G. B., E. C. Alexander, Jr., M. A. Lanphere, and G. P. Kraker, Irradiation of samples for [40]Ar-[39]Ar dating using the Geological Survey TRIGA reactor, U. S. Geol. Surv. Prof. Pap., 1176, 1981a.

Dalrymple, G. B., M. A. Lanphere, and D. A. Clague, Conventional and [40]Ar-[39]Ar ages of volcanic rocks from Ojin (site 430), Nintoku (site 432), and Suiko (site 433) seamounts and chronology of

volcanic propagation along the Hawaiian-Emperor Chain, Initial Rep. Deep Sea Drill. Proj., 55, 659-676, 1981b.

Dalrymple, G. B., M. A. Lanphere, and M. S. Pringle, Correlation diagrams in ^{40}Ar-^{39}Ar dating: Is there a correct choice?, Geophys. Res. Lett., 15, 589-591, 1988.

Detrick, R. S, and A. B. Watts., An analysis of isostasy in the world's oceans: Three aseismic ridges, J. Geophys. Res., 84, 3637-3655, 1979.

Diament, M., and J. Goslin, Mechanical and thermal isostasy of submarine plateaus, (abstract), Eos Trans. AGU, 68, 1462, 1987.

Duncan, R. A., Hot-spots in the southern oceans-An absolute frame of reference for the motion of the Gondwana continents, Tectonophysics, 74, 29-42, 1981.

Duncan, R. A., Age progressive volcanism in the New England Seamounts and the opening of the central Atlantic Ocean, J. Geophys. Res., 89, 9980-9990, 1984.

Duncan, R. A., and R. B. Hargraves, ^{40}Ar-^{39}Ar geochronology of basement ages from the Mascarene Plateau, Chagos Bank, and the Maldives Ridges, Proc. Ocean Drill. Program Sci. Results, in press, 1990.

Dymond, J., Excess Ar in submarine pillow basalts, Bull. Geol. Soc. Am., 181, 1229-1232, 1970.

Emerick, C. M., and R. A. Duncan, Age progressive volcanism in the Comores Archipelago, western Indian Ocean and implications for Somali plate tectonics, Earth Planet. Sci. Lett., 60, 415-428, 1982.

Epp, D., and N. C. Smoot, Distribution of seamounts in the North Atlantic, Nature, 337, 254-257, 1989.

Erlank, A. J., and E. J. D. Kable, The significance of incompatible elements in Mid-Atlantic Ridge basalts from 45°N, with particular reference to Zr/Nb, Contrib. Mineral. Petrol., 54, 281-291, 1976.

Erlank, A. J., J. S. Marsh, A. R. Duncan, R. M. Miller, C. J. Hawkesworth, P. J. Betton, and D. C. Rex, Geochemistry and petrogenisis of the Etendeka volcanic rocks from SWA/Namibia, Spec. Publ. Geol. Soc. S. Afr., 13, 195-245, 1984.

Fleitout, L., C. Dalloubeix, and C. Moriceau, Small-wavelength geoid and topography anomalies in the South Atlantic Ocean: A clue to new hot spot tracks and lithospheric deformation, Geophy. Res. Lett., 16, 637-640, 1989.

Fodor, R. V., K. Keil, J. W. Husler, and E. H. McKee, Petrology and K-Ar age of volcanic tuff and ash from the Walvis Seamount Province, DSDP site 359, leg 39, Initial Rep. Deep Sea Drill., Proj., 39, 525-536, 1977.

Fodor, R. V., C. Corwin, and A. Rosinenberg, Petrology of Serra Geral (Parana) continental flood basalts, southern Brazil: Crustal contamination, source material, and South Atlantic magmatism, Contrib. Mineral. Petrol., 91, 54-65, 1985.

Foland, K. A., and H. Faul, Ages of the White Mountain Intrusives-New Hampshire, Vermont and Maine, U.S.A., Am. J. Sci., 277, 888-904, 1977.

Foland, K. A., L. A. Gilbert, C. A. Sebring, and J.-F. Chen, ^{40}Ar-^{39}Ar ages for plutons of the Monteregian Hills, Quebec: Evidence for a single episode of Cretaceous magmatism, Geol. Soc. Amer. Bull., 97, 966-974, 1986.

Foland, K. A., J.-F. Chen, L. A. Gilbert, and A. W. Hofmann, Nd and Sr isotopic signatures of Mesozoic plutons in northeastern North America, Geology, 16, 684-687, 1988.

Freedman, A. P., Marine geophysical applications of Seasat altimetry and the lithospheric structure of the South Atlantic Ocean, Ph.D. thesis, Mass. Inst. Technol., Cambridge, 1987.

Gartner, S., Coccolith age determinations leg 3, Deep Sea Drilling Project, Initial Rep. Deep Sea Drill. Project, 3, 613-627, 1970.

Gibert, D., and V. Courtillot, Seasat altimetry and the South Atlantic geoid, 1, Spectral analysis, J. Geophys. Res., 92, 6235-6248, 1987.

Gibert, D., V. Courtillot, and J.-L. Olivet, Seasat altimetry and the South Atlantic geoid, 2, Short-wavelength undulations, J. Geophys. Res., 94, 5545-5559, 1989.

Gilbert, L. A., and K. A. Foland, The Mont St. Hilaire plutonic complex: Occurrence of excess ^{40}Ar and short intrusion history, Can. J. Earth Sci., 23, 948-958, 1986.

Gillot, P.-Y., and P. Nativel, K-Ar chronology of the ultimate activity of Piton des Neiges, Reunion Island, Indian Ocean, J. Volcanol. Geotherm. Res., 13, 131-146, 1984.

Gillot, P.-Y., and P. Nativel, Eruptive history of Piton de la Fournaise volcano, Reunion Island, Indian Ocean, J. Volcanol. Geotherm. Res., 36, 53-65, 1989.

Griffiths, R. W., The differing effects of compositional and thermal buoyancies on the evolution of mantle diapirs, Phys. Earth Planet. Inter., 43, 261-273, 1986.

Guimaraes, I. P., A. N. Sial, and A. F. Silva Filho, Petrologia e geochimica da provincia alcalina Terciaria Fortaleza, Cera, An. Congr. Bras. Geol., Salvador 2, XXXII, 577-588, 1982.

Hartnady, C. J. H., and A. P. le Roex, Southern Ocean hot spot tracks and the Cenozoic absolute motion of the African, Antarctic, and South American plates, Earth Planet. Sci. Lett., 75, 245-257, 1985.

Hawkesworth, C. J., M. S. M. P. N. Mantovani, P. N. Taylor, and Z. Palacz, Evidence from the Parana of south Brazil for a continental contribution to Dupal basalts, Nature, 322, 356-359, 1986.

Helgason, J., Shifts of the plate boundary in Iceland: Some aspects of Tertiary volcanism, J. Geophys. Res., 90, 10,084-10,092, 1985.

Herz, N., Timing of spreading in the South Atlantic: Information from Brazilian alkalic rocks, Geol. Soc. Am. Bull., 88, 101-112, 1977.

Hu, X., Y. L. Wang, and R. A. Schmitt, Geochemistry of sediments on the Rio Grande Rise and the redox evolution of the South Atlantic Ocean, Geochim. Cosmochim. Acta., 52, 201-207, 1988. Humphris, S. E, and G. Thompson, A geochemical study of rocks from the Walvis Ridge, South Atlantic, Chem. Geol., 36, 253-274, 1982.

Humphris, S. E, and G. Thompson, Petrology and geochemistry of rocks from the Angola Basin adjacent to the Walvis Ridge: Deep Sea Drilling Project leg 75, site 530, Initial Rep. Deep Sea Drill. Proj., 75, 1099-1105, 1983.

Humphris, S. E., G. Thompson, J.-G. Schilling, and R. H. Kingsley, Petrological and geochemical variations along the mid-Atlantic Ridge between 46 S and 32 S; Influence of the Tristan da Cunha mantle plume, Geochim. Cosmochim. Acta, 49, 1445-1464, 1985.

Kent, D. V., and F. M. Gradstein, A Jurassic to recent chronology, in: The Geology of North America: The Western North Atlantic Region, DNAG Ser., vol. M, edited by B. E. Tucholke and P. R. Vogt, pp. 45-50, Geological Society of America, Boulder, Colo., 1986.

Klitgord, K. D., and H. Schouten, Plate kinematics of the central Atlantic, in: The Geology of North America: The Western North Atlantic Region, DNAG Ser., vol. M, edited by B. E. Tucholke and P. R. Vogt, pp. 351-378, Geological Society of America, Boulder, Colo., 1986.

Kogan, M. G., M. Diament, A. Bulot, and G. Balmino, Thermal isostasy in the South Atlantic Ocean from geoid anomalies, Earth Planet. Sci. Lett., 74, 280-290, 1985.

Kowsmann, R., R. Leyden, and O. Francisconi, Marine seismic investigations, southern Brazil margin, Bull. Am. Assoc. Pet. Geol., 546-557, 1977.

Kumar, N., Origin of "paired" aseismic rises: Ceara and Sierra Leone Rises in the equatorial, and the Rio Grande Rise and Walvis Ridge in the South Atlantic, Mar. Geol., 30, 175-191, 1979.

Kumar, N., and R. W. Embley, Evolution and origin of Cera Rise: An aseismic rise in the western equatorial Atlantic, Geol. Soc. Am. Bull., 88, 683-694, 1977.

Kumar, N., and L. A. P. Gamboa, Evolution of the Sao Paulo Plateau (southeastern Brazilian margin) and implications for the early history of the South Atlantic, Geol. Soc. Am. Bull, 90, 281-293, 1979.

LaBrecque, J. L.(Ed.) South Atlantic Ocean and adjacent continental margin Reg. Atlas Ser., Atlas 13, Ocean Drill. Program, College Station, Tex., 1986.

LaBrecque, J. L., J. Phillips, and J. A. Austin, The crustal age and tectonic fabric at the leg 73 sites, Initial Rep. Deep Sea Drill. Proj., 73, 791-798, 1984.

Ladd, J. W., South Atlantic sea floor spreading and Caribbean tectonics, Ph.D. thesis, 251 pp., Columbia Univ., New York, 1974.

Ladd, J. W., Relative motion of South America with respect to North America and Caribbean tectonics, Geol. Soc. Am. Bull., 87, 969-976, 1976.

Le Roex, A. P., Geochemistry, mineralogy and magmatic evolution of the basaltic and trachytic lavas from Gough Island, South Atlantic, J. Petrol., 26, 149-186, 1985.

Leyden, R., H. Asmus, S. Zembruscki, and G. Bryan, South Atlantic diapir structures, Am. Assoc. Pet. Geol. Bull., 60, 196-212, 1976.

Liu, Y.-G., Chemical element profiles by instrumental neutron activation analysis 2, Representative sediment and basalt samples taken from DSDP 678 m core, site 525A, leg 74, Walvis Ridge, M.S. thesis, Oregon State Univ., Corvallis, 1982.

Liu, Y.-G., and R. A. Schmitt, Chemical profiles in sediment and basalt samples from deep sea drilling project leg 74, hole 525A, Walvis Ridge, Initial Rep. Deep Sea Drill. Proj., 74, 713-730, 1984.

Liu, Y.-G., M. R. U. Miah, and R. A. Schmitt, Cerium: A chemical tracer for paleo-oceanic redox conditions, Geochim Cosmochim Acta, 52, 1361-1371, 1988.

MacIntyre, R. M., A. P. Dickin, A. E. Fallick, and A. N. Halliday, An isotopic and geochronological study of the younger igneous rocks of the Seychelles, Eos Trans. AGU, 66, 1137, 1985.

Manivit, M., Paleogene and upper Cretaceous nannofossils from Deep Sea Drilling Project, leg 74, Initial Rep. Deep Sea Drill. Proj., 74, 475-499, 1984.

Marsh, J. S., Basalt geochemistry and tectonic discrimination within continental flood basalt provinces, J. Volcanol. Geotherm. Res., 32, 35-49, 1987.

Martin., A. K., C. J. H. Hartnady, and S. Goodlad, A revised fit of South America and South Central Africa, Earth Planet. Sci. Lett., 54, 293-305, 1981.

Mascle, J., and J. D. Phillips, Magnetic quiet zones in the South Atlantic, Nature, 240, 80-84, 1972.

McDougall, I., The geochronology and evolution of the young volcanic island of Reunion (Indian Ocean), Geochim. Cosmochim. Acta, 35, 261-288, 1971.

McDougall, I., and R.A. Duncan, Age progressive volcanism in the Tasmantid Seamounts, Earth Planet. Sci. Lett., 89, 207-220, 1988.

McDougall, I., and T. M. Harrison, Geochronology and Thermochronology by the ^{40}Ar-^{39}Ar Method, 212 pp., Oxford University Press, New York, 1988.

McDougall, I., and C. D. Ollier, Apparent K-Ar ages from Tristan da Cunha, South Atlantic, Geol. Mag., 119, 87-93, 1982.

McDougall, I., and N. R. Ruegg, Potassium-argon dates on the Serra Geral formation of South America, Geochim. Cosmochim. Acta, 30, 191-195, 1966.

Melfi, A. J., Potassium-argon ages for core samples from Southern Brazil, Geochim. Cosmochim. Acta, 31, 1079, 1967.

Melson, W. G., and G. Thompson, Glassy abyssal basalts, Atlantic sea floor near St. Pauls Rocks: Petrography and composition of secondary clay minerals, Bull. Geol. Soc. Am., 84, 703-716, 1973.

Molnar, P., and J. Stock, Relative motions of hot spots in the Pacific, Atlantic and Indian Oceans since late Cretaceous time, Nature, 327, 587-591, 1987.

Morgan, W. J., Convection plumes in the lower mantle, Nature, 230, 42-43, 1971.

Morgan, W. J., Deep mantle convection: Plumes and plate motions, Am. Assoc. Pet. Geol. Bull., 56, 203-213, 1972.

Morgan, W. J., Hot-spot tracks and the opening of the Atlantic and Indian Oceans, in The Sea, vol. 7, pp. 443-488, Wiley Interscience, New York, 1981.

Morgan, W. J., Hot-spot tracks and the early rifting of the Atlantic, Tectonophysics, 94, 123-139, 1983.

Musset, A. E. and P. F. Barker, ^{40}Ar-^{39}Ar age spectra of basalts, Deep Sea Drilling Project site 516, Initial Rep. Deep Sea Drill. Proj., 72, 467-470, 1983.

National Geophysical Data Center, Worldwide gridded bathymetry, DBDB10, Announc. 85-MGG-01, Boulder, Colo., 1985.

Needham, H. D., D. Carre and J. C. Sibuet, Bathymetrie de la Ride de Walvis et du Bassin du Cap, Ocean Atlantique Sud, report, Dep. Geosci. Mar., Inst. Franc. de Rech. pour l'Exploitation de la Mer, Orleans, France, 1986.

Neill, W. M., Possible continental rifting in Brazil and Angola related to the opening of the South Atlantic, Nature Phys. Sci., 245, 104-107, 1973.

O'Connor, J. M., On the trail of South Atlantic hot spots: Implications for reconstructing African and South American plate motions (abstract), Eos Trans. AGU, 70, 1135, 1989.

Pearce, J. A., and M. J. Norry, Petrogenetic implications of Ti, Zr, Y and Nb variations in volcanic rocks, Contrib. Mineral. Petrol., 69, 33-47, 1979.

Ponte, F. C., and H. E. Asmus, The Brazilian marginal basins: Current state of knowledge, An. Acad. Bras. Cienc, 48 (suppl.), 215-239, 1976.

Rabinowitz, P. D., Geophysical study of the continental margin of southern Africa, Geol. Soc. Am. Bull., 87, 1643-1653, 1976.

Rabinowitz, P. D., Geophysical study of the continental margin of southern Africa, Reply, Geol. Soc. Am. Bull., 89, 793-796, 1978.

Rabinowitz, P. D., and J. L. LaBrecque, The Mesozoic South Atlantic Ocean and evolution of its continental margins, J. Geophys. Res., 84, 5973-6002, 1979.

Richards, M. A., R. A. Duncan, and V. E. Courtillot, Flood basalts and hot-spot tracks: Plume heads and tails, Science, 246, 103-107, 1989.

Richardson, S. H., A. J. Erlank, A. R. Duncan, and D. L. Reid, Correlated Nd, Sr and Pb isotope variations in Walvis Ridge basalts and implications for the evolution of their mantle source, Earth Planet. Sci. Lett., 59, 327-342, 1982.

Richardson, S. H., A. J. Erlank, D. L. Reid and A. R. Duncan, Major and trace element and Nd and Sr isotope geochemistry of basalts from the DSDP leg 74 Walvis Ridge transect, Initial Rep. Deep Sea Drill. Proj., 74, 739-754, 1984.

Saemundsson, K., Outline of the geology of Iceland, Joekull, 29, 7-28, 1979.

Samson, S. D., and E. C. Alexander, Jr., Calibration of the interlaboratory ^{40}Ar-^{39}Ar dating standard, Mmhb-1, Chem. Geol., 66, 27-34, 1987.

Schilling, J.-G., Geochemical and isotopic variation along the Mid-Atlantic Ridge axis from 79°N to 0°N, in The Geology of North America, The Western North Atlantic Region, DNAG Ser., vol. M, edited by B. E. Tucholke and P. R. Vogt, pp. 137-156, Geological Society of America, Boulder, Colo., 137-156, 1986.

Schilling, J.-G., R. H. Kingsley, and J. G. DeVine, Galapagos hot spreading center system: Spatial, petrological and geochemical variations 83°W-101°W, J. Geophys. Res., 87, 5593-5610, 1982.

Schilling, J.-G., M. Zajac, R. Evans, T. Johnston, W. White, J. D. Devine, and R. Kingsley, Petrologic and geochemical variations along the Mid-Atlantic Ridge from 29°N to 73°N, Am. J. Sci., 283, 510-586, 1983.

Schlanger, S. O., M. O. Garcia, B. H. Keating, J. J. Naughton, W. W. Sager, J. A. Haggerty, J. A. Philpotts, and R. A. Duncan, Geology and geochronology of the Line Islands, J. Geophys. Res., 89, 11, 261-11, 272, 1984.

Sclater, J. G., and D. P. McKenzie, Palaeobathymetry of the South Atlantic, Geol. Soc. Am. Bull., 84, 3203-3216, 1973.

Scrutton, R. A., Geophysical study of the continental margin of southern Africa-Discussion, Geol. Soc. Am. Bull., 89, 791-793, 1978.

Seidemann, D., Effects of submarine alteration on K-Ar dating of deep-sea igneous rocks, Geol. Soc. Am. Bull., 88, 1660-1666, 1977.

Seidemann, D., ^{40}Ar-^{39}Ar studies of deep-sea igneous rocks, Geochim. Cosmochim. Acta, 42, 1721-1734, 1978.

Sibuet, J.-C., and J. Mascle, Plate kinematic implications of Atlantic equatorial fracture zone trends, J. Geophys. Res., 83, 3401-3421, 1978.

Sibuet, J.-C., W. W. Hay, A. Prunier, L. Montadert, K. Hinz, and J. Fritsch, Early evolution of South Atlantic: Role of the rifting phase, Initial Rep. Deep Sea Drill. Proj., 75, 469-481, 1984.

Siedner, G., and J. A. Miller, K-Ar age determinations on basaltic rocks from south-west Africa and their bearing on continental drift, Earth Planet. Sci. Lett., 4, 451-458, 1968.

Siedner, G., and J. G. Mitchell, Episodic mesozoic volcanism in Namibia and Brazil: A K-Ar isochron study bearing on the opening of the South Atlantic, Earth Planet. Sci. Lett., 30, 292-302, 1976.

Srivastava, S. P., and C. R. Tapscott, Plate kinematics of the North Atlantic, in The Geology of North America: The western North Atlantic Region, DNAG Ser., vol. M, edited by B. E. Tucholke and P. R. Vogt, 379-404, Geological Society of America, Boulder, Colo., 1986.

Stock, J. M., and P. Molnar, Some geometrical aspects of uncertainties in combined plate reconstructions, Geology, 11, 697-701, 1983.

Sullivan, K. D., and C. E. Keen, Newfoundland Seamounts: Petrology and geochemistry, Geol. Assoc. Can. Spec. Pap., 16, 461-476, 1977.

Sun, S. S., R. W. Nesbitt, and A. Y. Sharaskin, Geochemical characteristics of mid-ocean ridge basalts, Earth Planet. Sci. Lett., 44, 119-138, 1979.

Svisero, D. P., H. O. A. Meyer, and H. Tsai, Kimberlites in Brazil: An initial report, in Kimberlites Diatremes, and Diamonds: Their Geology, Petrology and Geochemistry, edited by H. O. A. Meyer, and F. R. Boyd, pp. 92-100, AGU, Washington, D. C., 1979.

Taras, B. D., and S. R. Hart, Geochemical evolution of the New England Seamount chain: Isotopic and trace element constraints, Chem. Geol., 64, 35-54, 1987.

Thompson, G., A geochemical study of the low temperature interaction of seawater and oceanic igneous rocks, Eos Trans. AGU, 54, 1015-1019, 1973.

Thompson, G., and S. E. Humphris, Petrology and geochemistry of rocks from the Walvis Ridge: Deep Sea Drilling Project leg 74, sites 525, 527, and 528, Initial Rep. Deep Sea Drill. Proj., 74, 755-764, 1984.

Thompson, G., S. Humphris, and J.-G. Schilling, Petrology and geochemistry of basaltic rocks from the Rio Grande Rise, South Atlantic: Deep Sea Drilling Project, leg 72, hole 516, Initial Rep. Deep Sea Drill. Proj., 72, 457-466, 1983.

Tucholke, B. E., and N. C. Smoot, Evidence for age and evolution of Corner Seamounts and Great Meteor seamount chain from multibeam bathymetry, J. Geophys. Res., in press, 1990.

Turner, G., and P. H. Cadogan, Possible effects of ^{39}Ar recoil in ^{40}Ar-^{39}Ar dating of lunar, Proc. Lunar Sci. Conf., 5, 1601-1615, 1974.

Vandoros, P., and M. A. F. Oliveira, Sobre o fonolito de Messejana, Ceara, An. Acad. Bras. Cienco., 40, 203-206, 1968.

Vogt, P. R., and G. L. Johnson, Transform faults and longitudinal flow beneath the mid-ocean ridge, J. Geophys. Res., 80, 1399-1428, 1975.

Vogt, P. R., B. Zondek, P. W. Fell, N. Z. Cherkis, and R. K. Perry, Seasat altimetry, the North Atlantic geoid, and evaluation by shipborne subsatellite profiles, J. Geophys. Res., 89, 9885-9903, 1984.

Walker, D. A., and I. McDougall, ^{40}Ar-^{39}Ar and K-Ar dating of altered glassy volcanic rocks: The Dabi Volcanics, P.N.G., Geochem. Cosmochim. Acta., 46, 2181-2190, 1982.

Wang, Y. L., Y.-G. Liu, and R. A. Schmitt, Rare earth element geochemistry of south Atlantic deep sea sediments: Ce anomaly change at $\approx$ 54 My, Geochim. Cosmochim. Acta, 50, 1337-1355, 1986.

Weaver, B. L., N. G. Marsh, and J. Tarney, Trace element geochemistry of basaltic rocks recovered at site 516, Rio Grande rise, Initial Rep. Deep Sea Drill. Proj., 72, 451-455, 1983.

Weaver, B. L., D. A. Wood, J. Tarney, and J. L. Joron, Geochemistry of ocean island basalts from the South Atlantic: Ascension, Bouvet, St. Helena, Gough, and Tristan da Cunha, Alkaline Igneous Rocks, edited by J. G. Fitton, and B. G. J. Upton, Spec. Publ. 30, pp. 253-267, Geol. Soc. of London, 1987.

Weiss, W., Upper Cretaceous foraminiferal biostratigraphy from the Rio Grande Rise: Site 516 of leg 72, Initial Rep. Deep Sea Drill. Proj., 72, 715-721, 1983.

Wendt, I., H. Kreuser, P. Muller, U. von Rad, and H. Raschke, K-Ar ages of basalt from Great Meteor and Josephine seamounts (eastern North Atlantic), Deep Sea Res., 23, 849-862, 1976.

White, R., and D. McKenzie, Magmatism at rift zones: The generation of volcanic continental margins and flood basalts, J. Geophys. Res., 94, 7685-7729, 1989.

White, W. M., M. M. Cheatham, and R. A. Duncan, Isotope geochemistry of leg 115 basalts and inferences on the history of the Reunion mantle plume, in Proc. Ocean Drill. Program Sci. Results, in press, 1990.

Wilson, J. T., A possible origin of the Hawaiian Islands, Can. J. Phys., 41, 863-870, 1963.

York, D., Least squares fitting of a straight line with correlated errors, Earth Planet. Sci. Lett., 5, 320-324, 1969.

III. THE ST. HELENA AND WALVIS HOT SPOT SYSTEMS:
1. TIME-SPACE CONSTRAINTS ON AFRICAN PLATE MOTION

ABSTRACT

The St. Helena and Walvis hot spots are broad zones of diffuse volcanism, at least 500 km in diameter, far larger than estimated previously on the basis of the size of individual ocean islands. Two Euler poles are sufficient to reconstruct the direction of African plate over these broad hot spots (since the South Atlantic began to open), as recorded by the NE-SW trending St. Helena Seamount Chain, Walvis Ridge and Gough Lineament, and in the case of the Reunion hot spot (Indian Ocean), the Mascarene Plateau. Estimates of the angular velocity of the African plate about these poles are based on the time-space distributions of ^{40}Ar-^{39}Ar along these hot spot traces, and incorporate an uncertainty of 4.5° due to the broadness of the St. Helena and Walvis hot spots. African plate velocity appears to have decreased between ~31 and 0 Ma.

The South Atlantic spreading-axis migrated westward away from the St. Helena and Walvis hot spots, beginning between 80 and 70 Ma, resulting in a simultaneous transition to intraplate volcanism along the St. Helena Chain and the Walvis Ridge. A transitional period of overlapping on-axis and intraplate volcanism supports the existence of broad South Atlantic hot spots.

INTRODUCTION

The two longest hot spot-generated volcanic trails on the African plate, both in time and space, are the St. Helena Seamount Chain (Figure III.1a) and the sub-parallel Walvis Ridge (Figure III.1b), located in the eastern South Atlantic Ocean [e.g., Morgan, 1981]. New radiometric ages for St. Helena and Gough seamounts (Walvis Ridge) reported here lead to a better understanding of the structural evolution of these two hot spot systems and a new reconstruction of African plate motion over hot spots, since the South Atlantic began to open.

The St. Helena Seamount Chain is unique among South Atlantic hot spot trails in that it terminates at the seaward edge of the Cameroon Line, a >2,000 km long line of ocean islands and continental intrusive centers (Figure III.1a). Volcanism along this Tertiary to recent lineament does not become older with increasing proximity to the African coast [e.g. Fitton et al., 1987] and so cannot be considered a conventional extension of the St. Helena hot spot trace. Recent research suggests that the Cameroon Line is not simply a volcanic lineament, rather it is a major structural feature formed by the rejuvenation of the Adamawa Fracture Zone, a continental suture zone that has been more or less permanently rejuvenated from the late Precambrian to the present [Moreau, et al., 1987; Deruelle et al., 1989]. This is compatible with the suggestion of Morgan [1981] and Halliday et al. [1990] that the St. Helena plume was instrumental in the breakup of Africa and for the transfer of St. Helena plume components into upper mantle (i.e. fossil-St. Helena plume), which was subsequently tapped to form the Cameroon Line. A contribution of this study is to show that, despite the enigmatic character of the Cameroon Line, the St. Helena Chain represents a useful record of African plate motion. We report a

75

Figure III.1a. Bathymetry of the St. Helena Seamount Chain, after Cherkis et al. [1989]. Fracture zones and spreading-axes, after Cande et al. [1989]. Dredge and island samples analyzed in this study are shown as X's. Cameroon Line volcanism is shown in solid pattern. The bathymetry contours are at 4000 m, with the continental edge of the African coast marked by its coast line. Mercator projection.
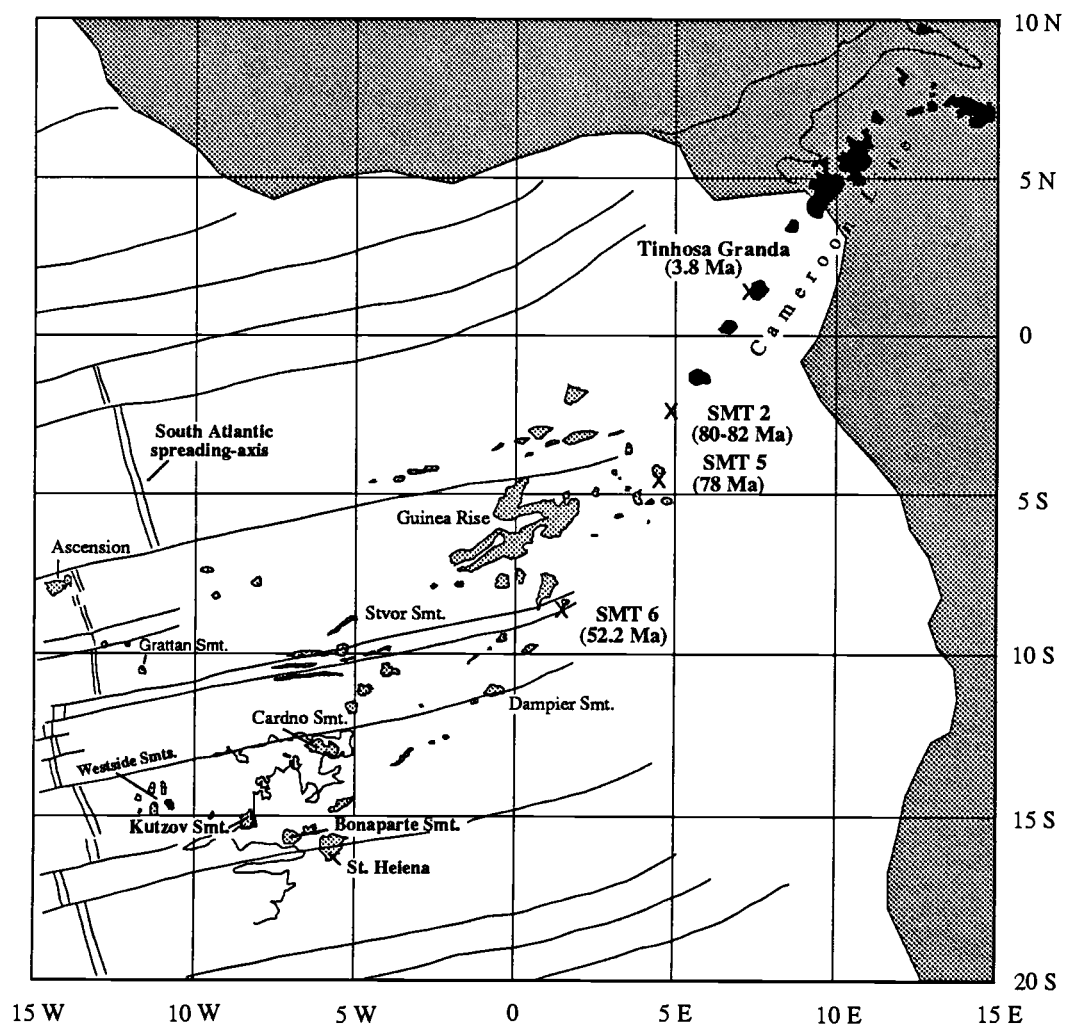
Figure III.1a

Figure III.1b. Bathymetry of the Walvis Ridge, after Cherkis et al. [1989]. The bathymetry contours are at 4000 m. Mercator projection.

78
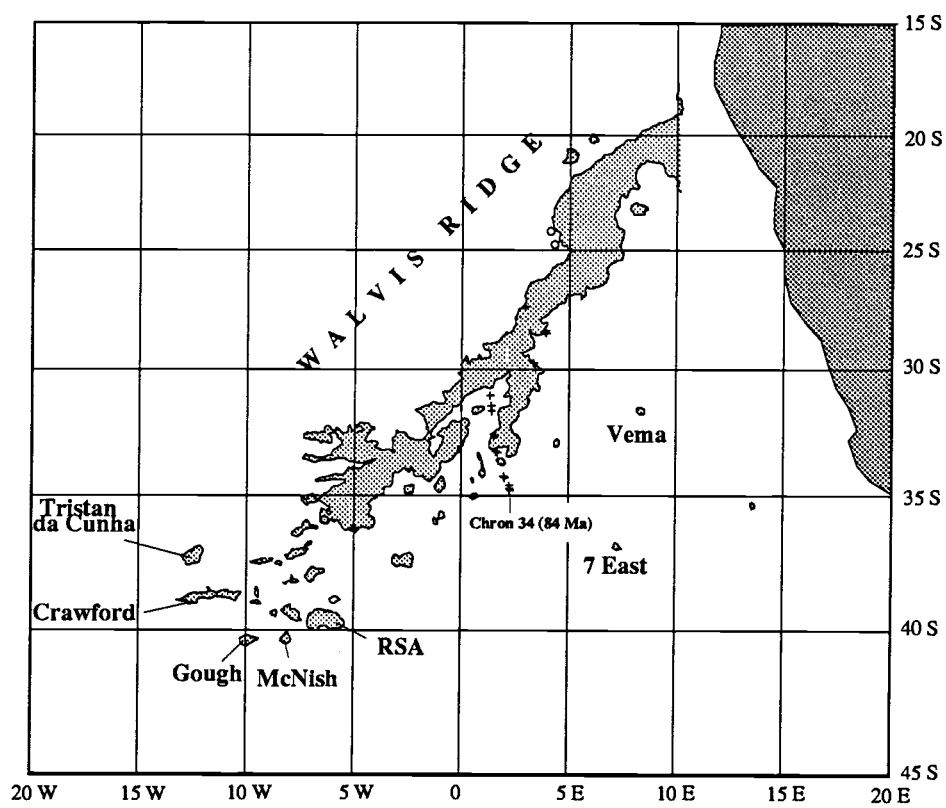
Figure III.1b

coventional K-Ar age for the island of Tinhosa Granda (Figure III.1a), confirming that it is part of the Cameroon Line.

K-Ar ages for subaerial lavas from the island of St. Helena, located on the African plate ~400-600 km to the east of the Mid-Atlantic Ridge, suggest that this island was constructed primarily between 9 and 7 Ma [Chaffey et al., 1989]. These lavas are characterized by a very high radiogenic lead component that has become progressively more pronounced since 9 Ma, probably as a result of the decreasing influence of depleted mantle material in association with waning volcanism [Chaffey, et al., 1989]. Basalts dredged from the spreading-axis to the west of St. Helena [Hanan et al., 1986] exhibit a similar St. Helena-like isotopic signature, suggesting sub-lithospheric flow of plume material from a currently active St. Helena hot spot centered beneath the island of St. Helena [e.g. Schilling et al., 1985]. A plume-ridge connection is supported by helium isotope geochemistry of the spreading axis at the latitude of St. Helena [Graham et al., unpublished manuscript].

Previous reconstructions of African plate motion over hot spots [Morgan, 1981; Duncan, 1981; and Chapter II] assumed that the islands of Tristan da Cunha and St. Helena lie close to the present-day centers of the hot spots responsible for the formation of the St. Helena Chain and the Walvis Ridge. However, models based on this assumption were not successful in matching the predicted geometries of the St. Helena and Walvis hot spots with that of the St. Helena Chain and the Walvis Ridge. In this paper we assume that the Walvis Ridge and the St. Helena Chain were generated by diffuse volcanism over a zone > 500 km in diameter, rather than by hot spot activity focussed to the diameter of an individual ocean island. Rotation parameters for African plate motion are re-evaluated on the basis of this assumption, and the combined time-space distribution of radiometric ages along the St. Helena Chain (this study), Walvis Ridge [Chapter II], Gough Lineament (this study), and the Mascarene Plateau [Duncan and Hargraves, 1990]. Calculations of angular plate velocity based on the assumption of broad hot spots incorporate a systematic uncertainty of ~500 km or 4.5°.

In an earlier study of the evolution of the Walvis Ridge-Rio Grande Rise system it was shown that the South Atlantic spreading-axis migrated westward away from the mantle-fixed Tristan hot spot beginning at about 70 Ma, resulting in a transition from on-axis to intraplate volcanism [Chapter II]. This study documents a similar such transition from on-axis to intraplate volcanism within the St. Helena hot spot system.

SAMPLE SITES

Rock samples dated by the ^{40}Ar-^{39}Ar incremental heating method were dredged from three St. Helena seamounts (Figure III.1a], RSA and McNish seamounts (Figure III.1b), and the islands of Gough and Tristan da Cunha (Figure III.1b). Samples from 7°E and Vema seamounts (Figure III.1b), located to the south of the Walvis Ridge, are also reported here as part of an ongoing study of South

Atlantic seamounts. Sample descriptions are in Appendix 2 and coordinates and brief descriptions are in Table III.1. ^{40}Ar-^{39}Ar ages of single seamounts from each of the Bahia and Pernambuco Chains [O'Connor, unpublished data] (Figure III.1c) are also included in our discussion; these ages are the initial results of a continuing study of the Brazilian Seamount Chains, the results of which will be published elsewhere.

RADIOMETRIC DATING TECHNIQUE AND RESULTS

The ^{40}Ar-^{39}Ar method is based on the generation of ^{39}Ar from ^{39}K by the irradiation of K-bearing rock samples with neutrons in a nuclear reactor. The principles, and application of this dating technique to samples effected by seafloor weathering, have been presented by Dalrymple and Lanphere [1971], Dalrymple et al. [1981a], and McDougall and Harrison [1988].

Whole rock samples were dated by the incremental heating ^{40}Ar-^{39}Ar technique at Oregon State University. Samples selected for age studies were crushed after the removal of any obvious surface weathering and vesicle fillings. The 0.5 to 1.0 mm rock fragments were retained for dating experiments, washed ultrasonically in distilled H_2O, and dried. About one gram of each sample was encapsulated in an evacuated quartz vial. Five vials were arranged around a sixth vial, containing a hornblende flux monitor of known age [520.4 Ma, Mmhb-1, Samson and Alexander, 1987] which measured the efficiency of conversion of ^{39}K to ^{39}Ar, expressed as the J-factor. Three such groups of vials were arranged vertically in an aluminium tube, which was then placed in the TRIGA Reactor at Oregon State University and irradiated for 10 hours at the 1 MW power level.

Samples and standards were placed individually in an outgassed Mo crucible, which was then heated in a high-vacuum extraction line. The standards were fused in a single heating step, while the basalts were heated incrementally in a series of five to seven steps (each of 30 min duration) and then melted during the final step. The isotopic composition of argon (^{40}Ar, ^{39}Ar, ^{37}Ar and ^{36}Ar) released from each individual heating or fusion step was measured immediately by means of an AEI MS-10S mass spectrometer, after active gases had been removed by cooling Ti-TiO$_2$ getters. The apparent ages of the individual heating steps were calculated from the measured ^{40}Ar* to ^{39}Ar ratios, after corrections for all interfering nuclear reactions had been applied using the equation of Brereton [1970]. Hence an age-temperature spectrum was obtained for each sample, based on the ^{40}Ar/^{39}Ar compositions of the gas fractions released incrementally, from low to high temperature sites. In the case of the irradiated St. Helena Seamount samples approximately one quarter of the contents of each vial was fused in a single heating step, and a total fusion age determined. Argon isotopic data and apparent ages are in Table III.2.

The most common age-temperature spectrum observed in highly altered oceanic basalts is of a middle temperature plateau bounded by higher ages at the low temperature steps, and by lower ages at the high temperature steps (e.g. Figure III.3a). Turner and Cadogan [1974] first proposed that such an

Figure III.1c. Bathymetry of the Pernambuco and Bahia volcanic lineaments, after Cherkis et al. [1989]. Fracture zones and spreading-axes are after Cande et al. [1989]. ^{40}Ar-^{39}Ar ages show are after O'Connor, unpublished data. The bathymetry contours at 4000 m. Mercator projection.
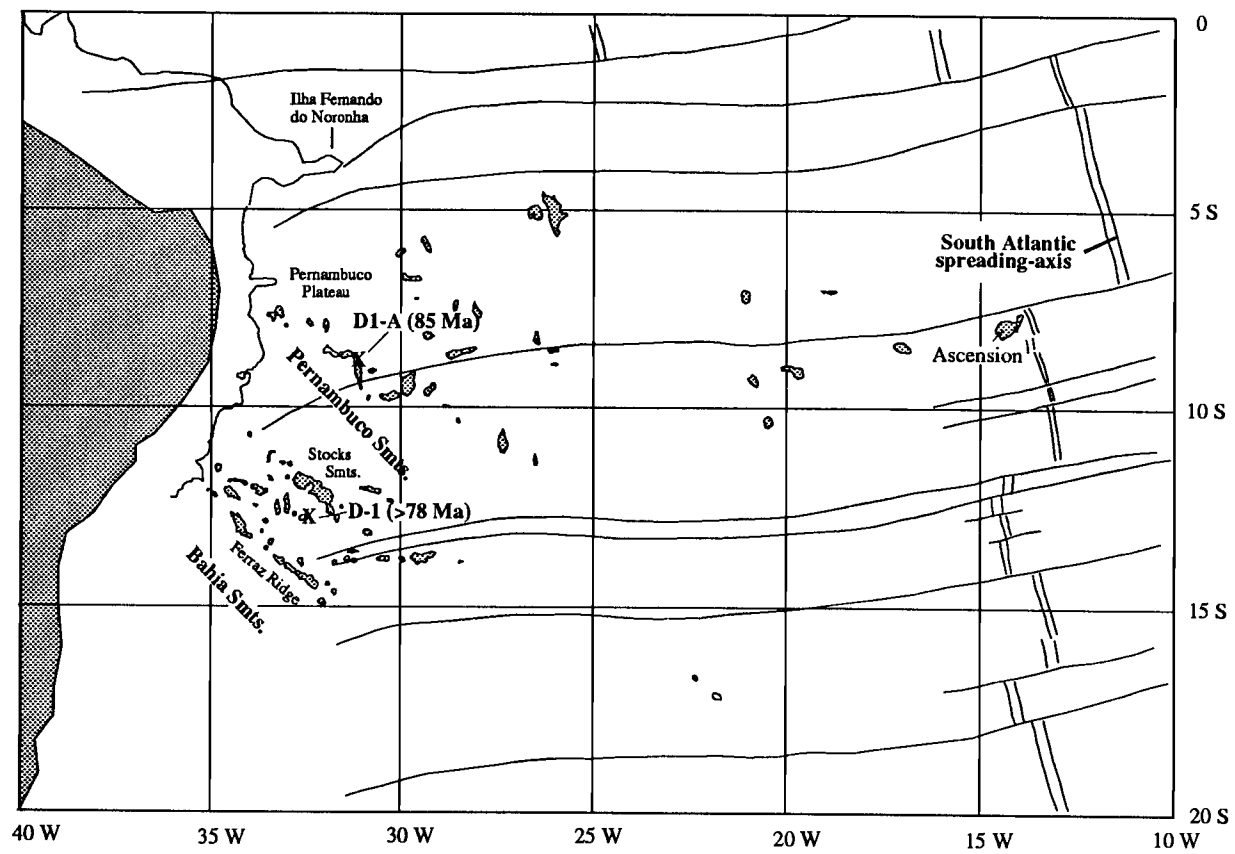
Figure III.1c

Table III.1. Location and brief description of dredged rock samples from the St. Helena Chain and the Gough Lineament

Sample	Location	Depth	Age	Description
	St. Helena Seamount AC-02			
	2° 19' 5"S; W4° 46' 4"	~1980-2000m	(80-82 Ma)	
AC-02A				highly altered volcanic rock
AC-02B				moderately altered trachyte
AC-02C				highly altered volcanic rock
AC-02E				moderately altered basalt
AC-02G				moderately altered ol, pl basalt
AC-02H				moderately altered trachyte
AC-02K				highly altered volcanic rock
AC-02I				moderately altered volcanic rock
	St. Helena Seamount AC-05			
	4° 17' 4" S; 4° 28' 7" E	~1768m	(78 Ma)	
AC-05A				moderately altered ol basalt
AC-05B				highly altered volcanic rock (alkali basalt?)
	St. Helena Seamount AC-06			
	8° 25' 6" S; 1° 33' 0" E	~1340m	(52 Ma)	
AC-06				slightly altered trachyte
	Cameroon Line (Island of Tinhosa Granda)			
	1° 21' 1" N; 7° 16' 6"E		(3.4 ± 1.4 Ma)	
TG-A-01				moderately altered volcanic rock
	Tristan da Cunha			
AG51-2-1		~2000m	(<1 Ma)	basanite
	Gough Island			
AG51-3-6		~2000m	(<1 Ma)	basalt
	McNish Seamount			
AG51-7-2	40° 10'S; 8° 33'W	3000 m	(8 Ma)	trachyte
	RSA Seamount			
AG51-12-3	31° 38'S; 8° 20'E	3000 m	(15 Ma)	mugearite (?)
	Vema Seamount			
AG51-9-1	39° 28'S; 6° 13'W	3000 m	(18 Ma)	trachyte
	7°E Seamount			
AG51-11-10	37° S; 7° E		(91 Ma)	mugearite

"inverse staircase" age-temperature profile might result from neutron-capture recoil of ^{39}Ar from K-rich to K-poor sites within fine-grained basalts, during irradiation. Because the low-temperature sites are K-rich, recoil effects may lead to the transfer of ^{39}Ar (but not ^{40}Ar*) from low temperature (i.e., alteration minerals and groundmass) to high-temperature sites (e.g., feldspar and pyroxene), resulting in a descending age-temperature release pattern. Dalrymple and Clague [1976], Seidemann [1978], and McDougall and Duncan [1988] have shown that significant amounts of ^{39}Ar may be lost from slightly altered volcanic rocks during the irradiation process. Thus, in conjunction with the loss of ^{40}Ar* discussed earlier, ^{39}Ar may also be lost from, or relocated within, a multiphase sample. Dalrymple et al. [1981b] suggested that, in cases where ^{39}Ar recoil is evident, the best age estimate for a sample comes from summing the gas composition of all the heating steps into a "recalculated" ^{40}Ar-^{39}Ar total fusion age.

Weighted mean plateau ages were calculated for samples yielding an age-temperature plateau, primarily for middle temperature heating steps. These middle temperature sites are considered to be least disturbed by the loss or addition of ^{39}Ar resulting from recoil effects, as discussed above. The slope formed by the correlation of the ^{40}Ar/^{36}Ar and ^{39}Ar/^{36}Ar ratios for selected heating steps yielded an ^{40}Ar*/^{39}Ar ratio, from which an isochron age was determined for most samples. Ideally, the ^{40}Ar/^{36}Ar intercept of such isochrons should reflect the composition of the rock at the time of crystallization, i.e., 295.5, consisting of only atmospheric argon without any contribution from potassium decay. Isochron slopes and intercepts were calculated using the least squares fitting technique of York [1969], which allows for correlated errors in both ^{40}Ar/^{36}Ar and ^{39}Ar/^{36}Ar isotopic ratios. Errors involved in measuring Ar ratios and J-factors (a typical error of 0.5% was assigned) and in making corrections for interfering nuclear reactions were combined to yield a standard deviation for each heating age. Age-temperature spectra and isochron plots are shown in Figures III.2 and III.3. Discussion of the ^{40}Ar-^{39}Ar data is in Appendix I.

A K-Ar age of 3.8 ± 1.4 Ma for a subaerial sample from the island of Tinhosa Grande (Figure III.1), confirming that it belongs to the Cameroon Line; the large uncertainty assigned to this apparent age reflects the very low percentage of radiogenic ^{40}Ar released when this sample was fused.

DISCUSSION

African plate motion over large diameter hot spots

Seamounts along the St. Helena Chain and the Gough lineament become older with increasing distance from the islands of St. Helena and Gough, respectively, as predicted by a model of African plate migration over mantle-fixed St. Helena and Walvis hot spots. The orientations and time-space distribution of dated seamounts along these chains can be combined with similar information from the Walvis Ridge, and the Mascarene Plateau (formed in the Indian Ocean by the Reunion hot spot) to

TABLE III.2. Argon Isotopic Data for Whole Rock Samples

Increment	$^{40}Ar/^{36}Ar$	$^{40}Ar/^{39}Ar$	$^{37}Ar*/^{40}Ar$	% Radiogenic ^{40}Ar	%^{39}Ar of Total	Age ± 1 σ x 10^6 years
			St. Helena Seamounts			
			Sample AC-D-02E, J = 0.00395			
1	354.3	68.98	0.0212	16.8	3.7	80.6± 6.2
2	411.9	37.69	0.0216	28.4	5.3	74.8± 1.6
3	1208.8	14.79	0.0337	75.8	27.6	78.2± 0.5
4	990.1	16.04	0.0408	70.4	25.8	78.8± 0.5
5	530.0	23.07	0.0902	44.9	8.1	72.5± 0.7
6	437.1	28.89	0.0843	33.0	7.0	66.9± 1.3
7	747.8	15.51	0.03376	63.1	22.5	68.7± 0.8
Tot. Fusion	1243.4	14.48	0.1348	77.2		78.1 ± 0.6
			Sample AC-D-02B, J = 0.00395			
1	759.3	28.31	0.0070	61.1	2.7	119.3± 1.5
2	1183.7	17.63	0.0092	75.1	3.7	91.9± 1.7
3	8701.4	11.97	0.0104	96.6	38.6	80.6± 0.4
4	2792.9	13.13	0.0108	89.5	37.4	81.9± 0.4
5	641.5	20.95	0.0136	54.0	6.0	78.9± 1.9
6	529.5	25.22	0.0197	44.3	4.0	78.0 ± 1.2
7	321.7	107.76	0.0151	8.3	7.7	62.3±1.4
Tot Fusion	1927.3	14.03	0.0215	84.8		82.8 ± 0.5
			Sample AC-D-02H, J = 0.00395			
1	866.0	23.14	0.0223	66.0	3.0	105.7± 0.9
2	4219.0	11.93	0.0164	93.1	9.1	77.5± 0.6
3	6056.7	12.1	0.0110	95.2	45.4	80.3± 0.4
4	1570.2	14.07	0.0121	81.2	16.6	79.6 ± 0.8
5	597.3	21.76	0.0179	50.6	6.5	76.9 ± 3.4
6	584.0	22.42	0.0237	49.6	10.1	77.5 ± 0.5
7	340.1	74.94	0.0155	13.2	9.3	69.4±1.4
Tot. Fusion	3823.0	12.61	0.0450	92.6		81.4 ± 0.4
			Sample AC-D-05A, J = 0.00395			
1	373.0	34.48	0.0121	20.8	1.6	50.5± 3.8
2	434.4	30.14	0.0140	32.1	3.1	67.6± 2.5
3	1382.6	13.94	0.0280	78.7	10.6	76.7± 0.5
4	3392.7	12.18	0.0330	91.5	33.7	77.8 ± 0.4
5	1352.6	14.16	0.0458	78.5	9.3	77.6 ± 0.6
6	947.3	15.77	0.0520	69.2	18.2	76.1 ± 0.5
7	424.5	33.69	0.1306	31.4	23.6	74.1 ± 0.6
Tot. Fusion	335.5	75.16	0.0199	12.1		63.5 ± 1.2
			Sample AC-D-06, J = 0.00439			
1	573.4	19.83	0.0282	48.7	0.4	74.9± 8.0
2	721.3	10.78	0.0383	59.3	0.9	49.9± 4.1
3	8037.8	6.89	0.0482	96.6	15.3	52.0± 0.2
4	10214.8	7.02	0.0381	97.3	26.6	53.3± 0.4
5	4446.9	7.2	0.0288	93.5	14.0	52.6± 0.4
6	2098.3	7.56	0.0590	86.3	12.2	51.0± 0.5
7	1957.4	7.79	0.1121	85.7	30.6	52.1 ± 0.3
Tot. Fusion	346.9	43.5	0.0245	15.0		51.0 ± 0.9

TABLE III.2 A

Increment	$^{40}Ar/^{36}Ar$	$^{40}Ar/^{39}Ar$	$^{37}Ar*/^{40}Ar$	% Radiogenic ^{40}Ar	$\%^{39}Ar$ of Total	Age $\pm 1\sigma$ x 10^6 years
			Tristan da Cunha AG51-2-1. J = 0.00242			
1	306.04	113.472	0.0037	3.5	12.6	17.1 ± 1.6
2	321.93	38.967	0.0143	8.3	13.3	14.1 ± 0.7
3	317.12	16.978	0.0445	7.1	16.2	5.3 ± 0.6
4	303.71	10.621	0.0623	3.1	12.7	1.5 ± 0.5
5	305.68	3.844	0.2225	4.9	11.1	0.8 ± 0.4
6	299.55	7.031	0.3754	4.2	34.2	1.3 ± 0.1
			Gough Island AG51-3-6 J = 0.002161			
1	158.53	116.758	0.0031	0.0	0.02	-443 ± -373
2	339.27	6.326	0.1033	13.6	0.48	3.4 ± 9.6
3	248.37	1.537	0.4408	15.9	4.7	-0.95 ± 0.6
4	267.37	1.010	0.8243	0.0	11.1	-0.19 ± 0.28
5	272.02	0.941	1.1255	0.0	15.29	-1.8 ± 0.2
6	291.59	1.952	1.1924	7.7	68.4	0.58 ± 0.07
			McNish Seamount AG51-7-1. J = 0.0027			
1	603.59	3.093	0.1140	51.7	8.1	7.8 ± 1.3
2	1082.93	2.271	0.1399	73.5	21.6	8.1 ± 0.5
3	766.78	2.556	0.2889	63.5	30.2	7.8 ± 0.1
4	541.48	3.266	0.3716	48.1	16.2	7.7 ± 0.3
5	416.18	4.879	0.2234	30.6	8.2	7.3 ± 1.5
6	394.98	4.664	1.3509	35.6	15.9	8.1 ± 0.2
			Vema Seamount AG51-12-3. J = 0.0027			
1	339.91	17.454	0.0135	13.1	2.3	11.1 ± 2.1
2	706.24	5.740	0.0137	58.2	8.3	16.2 ± 0.4
3	3730.15	3.469	0.0117	92.0	37.5	15.5 ± 0.1
4	2427.41	3.506	0.0101	87.7	27.21	14.9 ± 0.1
5	1193.07	4.210	0.0229	75.3	9.7	15.4 ± 0.3
6	809.75	4.423	0.3292	65.9	15.1	14.2 ± 0.4
			7° E Seamount AG51-11-10. J = 0.00222			
1	358.77	92.060	0.0044	17.7	0.6	64.0 ± 7.5
2	438.17	74.453	0.0055	32.6	3.7	94.7 ± 9.2
3	435.18	87.766	0.0066	32.1	10.2	109.6 ± 1.7
4	1834.47	26.914	0.0389	84.2	11.0	88.6 ± 0.6
5	3984.36	24.795	0.0435	92.9	20.4	90.0 ± 0.5
6	2131.72	25.907	0.0294	86.3	15.3	87.5 ± 0.7
7	2227.83	25.907	0.0459	86.9	38.7	88.1 ± 0.7
			RSA Seamount AG51-9-1. J = 0.00242			
1	425.54	14.469	0.0089	30.6	0.3	19.2 ± 6.1
2	1067.85	5.621	0.0134	72.3	1.3	17.7 ± 0.5
3	6885.03	4.468	0.0151	95.7	17.1	18.6 ± 0.1
4	9184.64	4.522	0.0129	96.8	15.0	19.0 ± 0.1
5	10112.14	4.547	0.0118	97.0	17.8	19.2 ± 0.2
6	8444.71	4.591	0.0125	96.5	11.5	19.2 ± 0.2
7	4985.43	4.646	0.0180	94.1	17.6	19.0 ± 0.2
8	3769.16	4.644	0.0447	92.4	19.5	18.6 ± 0.2

Here, $\lambda = 5.53$ x 10^{-10}/year. Ratios in table have not been corrected for neutron interferences.

Correction factors: $(^{36}Ar/^{37}Ar)$ Ca = 0.000264; $(^{39}Ar/^{37}Ar)$ Ca = 0.000673; $(^{40}Ar/^{39}Ar)$ K = 0.0006.

* Corrected for decay since neutron irradiation (λ ^{37}Ar = 1.975 x 10^{-2}/day).

TABLE III.2B. Age Calculations From Argon Isotopic Data

| Sample | Plateau Calculation | | | Isochron Calculation | | | Inverse Calculation | | | Total Fusion |
	Age (m.y.) ± 1σ	Steps Used	% of Total ^{39}Ar	Age (m.y.) ± 1σ	Steps Used	Intercept	Age (m.y.) ± 1σ	Steps Used	Intercept	
St. Helena Seamount 2										
AC-D-02E	78.5 ± 0.4	2, 3, 4	58.7	79.0 ± 0.9	2, 3, 4	290 ± 6.2	79.1 ± 0.9	2, 3, 4	290 ± 6.3	78.1 ± 0.6
AC-D-02B	81.6 ± 0.4	3, 4, 5, 6	86.0	80.1 ± 1.3	3, 4, 5, 6	319 ± 31.4	81.6 ± 0.7	3, 4, 5, 6	294 ± 16.1	82.8 ± 0.5
AC-D-02H	80.2 ± 0.4	3, 4, 5, 6	87.7	78.8 ± 1.0	2,3,4, 5, 6	298.2 ± 20	80.4 ± 0.5	2, 3, 4, 5, 6	284.3 ± 5.6	81.4 ± 0.4
St. Helena Seamount 5										
AC-D-05A	77.5 ± 0.4	3, 4, 5, 6	71.8	77.6 ± 0.6	3, 4, 5, 6	288 ± 10	78.2 ± 0.5	3, 4, 5, 6	278 ± 4.5	63.5 ± 1.2
St. Helena Seamount 6										
AC-D-06	52.3 ± 0.3	3, 4, 5, 6, 7	98.7	52.2 ± 0.7	3, 4, 5, 6, 7	292 ± 27	52.9 ± 0.6	3, 4, 5, 6	268 ± 21.7	51.0 ± 0.9
Tristan da Cunha										
AG51-2-1	1.3 ± 0.1	4, 5, 6	57.9	0.64 ± 0.3	4, 5, 6	301.8 ± 3.3	0.65 ± 0.3	4, 5, 6	301.8 ± 6.4	5.6 ± 0.3 *
Gough Island										
AG51-3-6	0.58 ± 0.07	6	68.4							0.25 ± 0.1*
McNish Seamount										
AG51-7-1	8.1 ± 0.05	all	100	8.1 ± 0.8	2, 3, 4, 5, 6	292.1 ± 5.6	8.2 ± 0.07	2, 3, 4, 5, 6	292.4 ± 5.3	7.9 ± 0.2*
RSA Seamount										
AG51-9-1	18.8 ± 0.1	2, 3, 4, 5, 6, 7, 8	99.7	18.7 ± 0.2	2, 3, 4, 5, 6, 7, 8	265.9 ± 51.6	18.8 ± 0.2	2, 3, 4, 5, 6, 7, 8	321 ± 331	18.9 ± 0.1*
7°E Seamount										
AG51-11-10	89.6 ± 0.5	4, 5, 6	46.8	90.4 ± 1.5	4, 5, 6	263.1 ± 43.1	91.2 ± 1.1	4, 5, 6	241.8 ± 31.0	85.4 ± 0.6*
Vema Seamount										
AG51-12-3	15.3 ± 0.1	2, 3, 4, 5, 6	97.8	15.2 ± 0.3	2, 3, 4, 5, 6	298.6 ± 26.3	15.2 ± 0.3	2, 3, 4, 5, 6	310.2 ± 25.3	15.1 ± 0.1*

* Recalculated Total Fusion Ages

Figure III.2. Age-temperature spectra, $^{40}Ar/^{36}Ar$ versus $^{39}Ar/^{36}Ar$, and $^{36}Ar/^{40}Ar$ versus $^{39}Ar/^{40}Ar$ correlation diagrams for basaltic samples from the St. Helena Seamount Chain. Age bands in spectra plots are the measured heating step ages $\pm$ 2σ. Errors on plateau ages are $\pm$ 1σ. The numbered points on the correlation diagrams correspond to the individual heating steps. Solid boxes in correlation diagrams indicate heating steps used in isochron calculations.
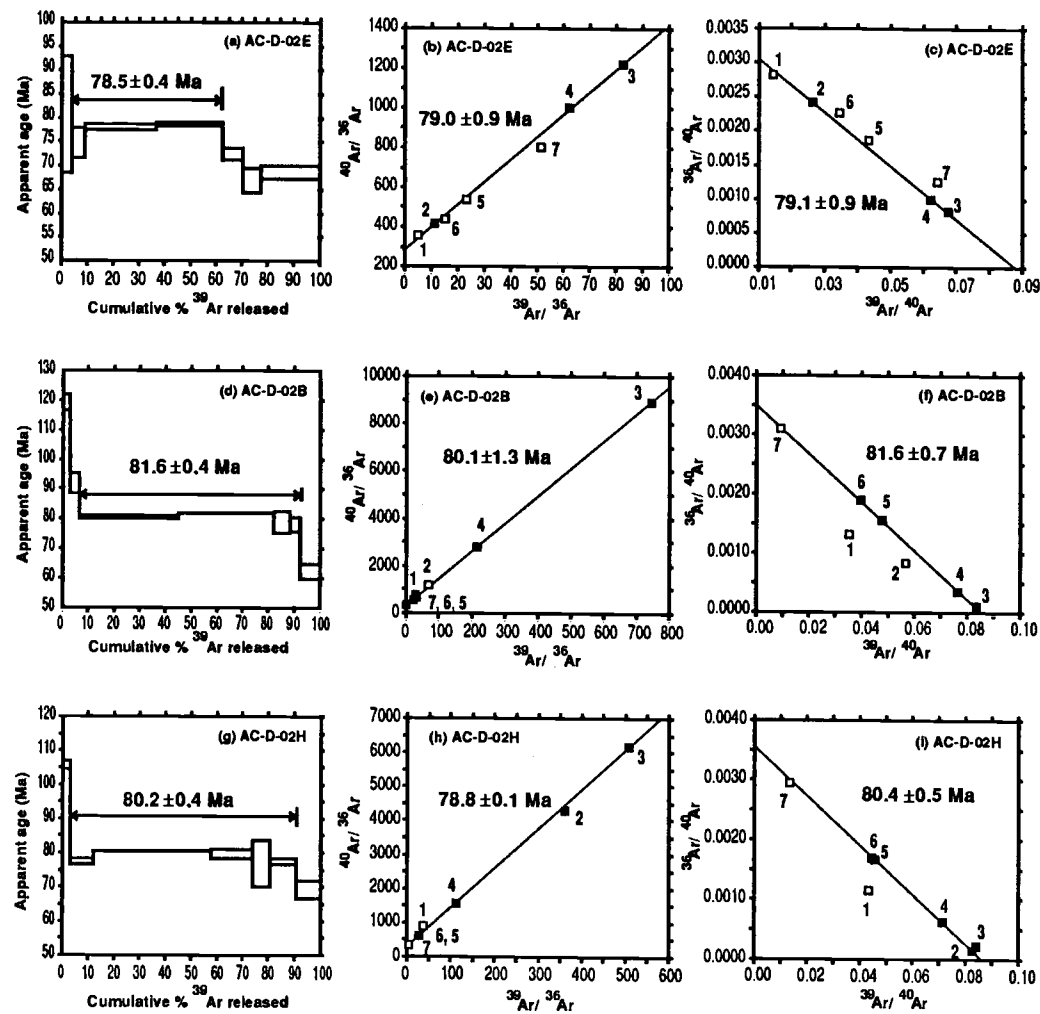
Figure III.2
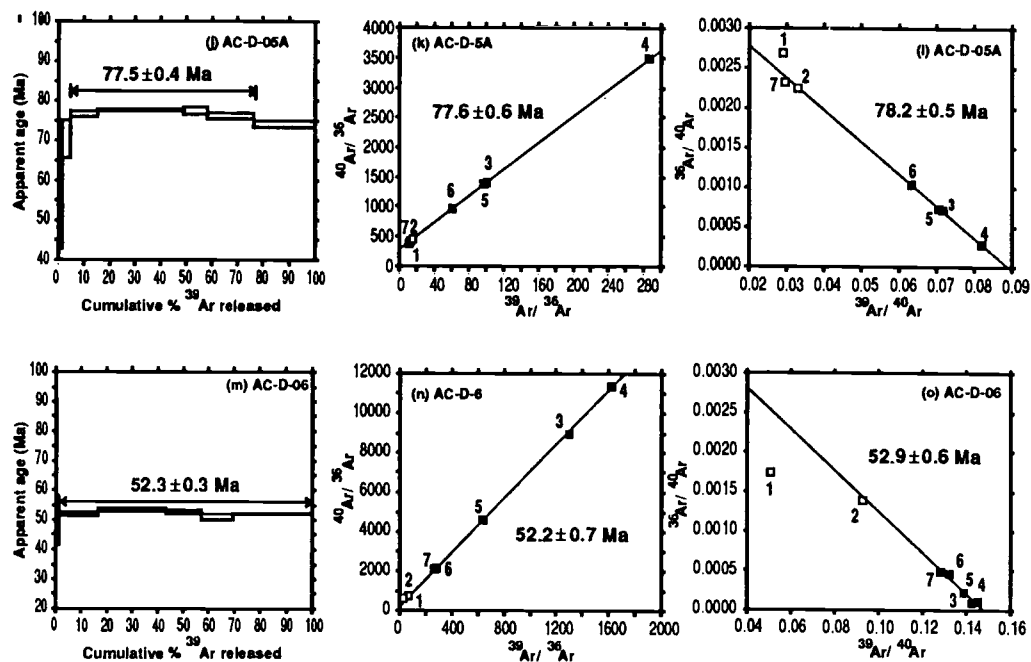
Figure III.2 (continued)

Figure III.3. Age-temperature spectra, $^{40}Ar/^{36}Ar$ versus $^{39}Ar/^{36}Ar$ and $^{36}Ar/^{40}Ar$ versus $^{39}Ar/^{40}Ar$ correlation diagrams for whole rock samples from Gough Lineament, Tristan da Cunha, and Vema and 7°E Seamounts. Other details are the same as in Figure III.2.
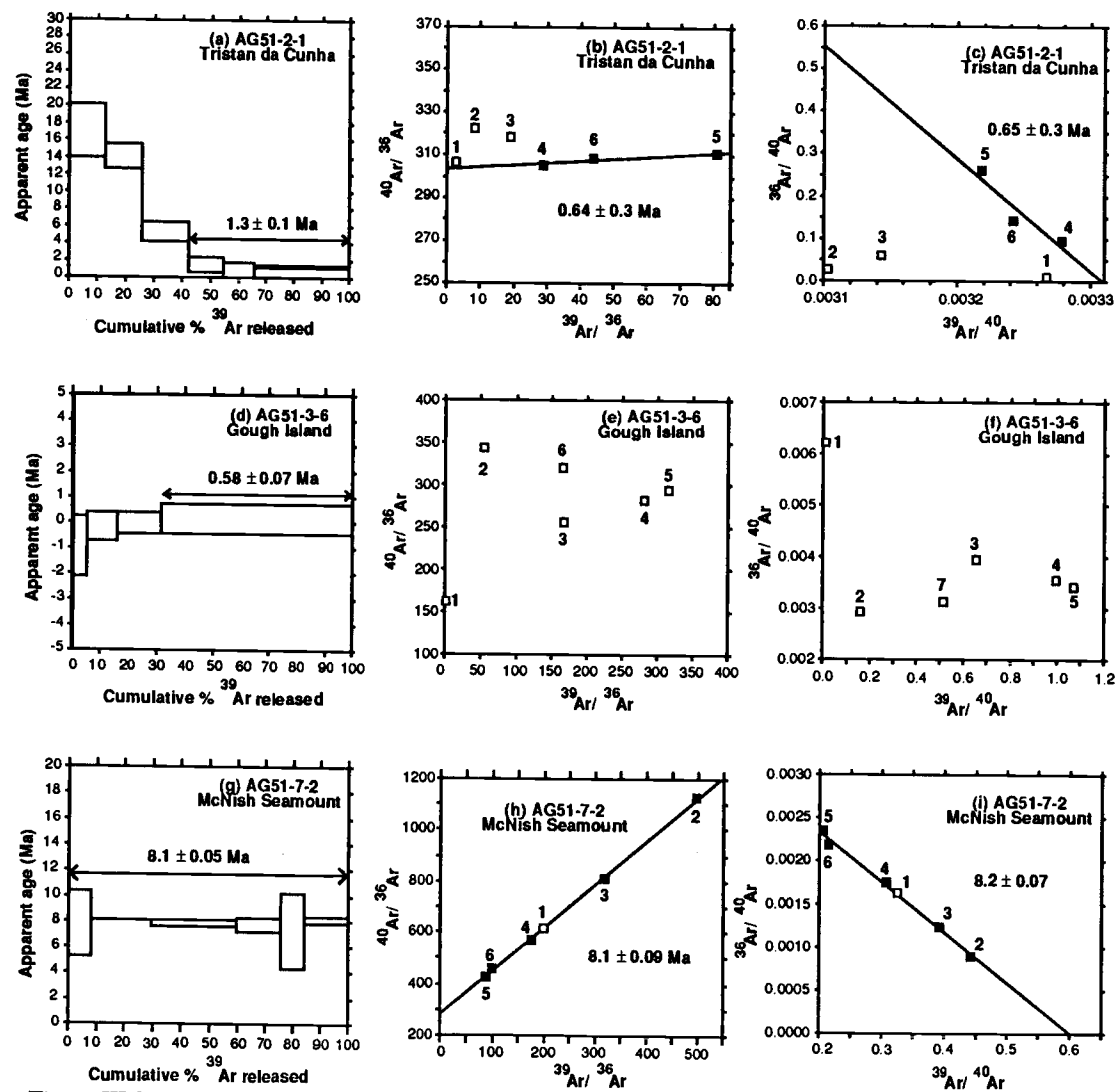
Figure III.3
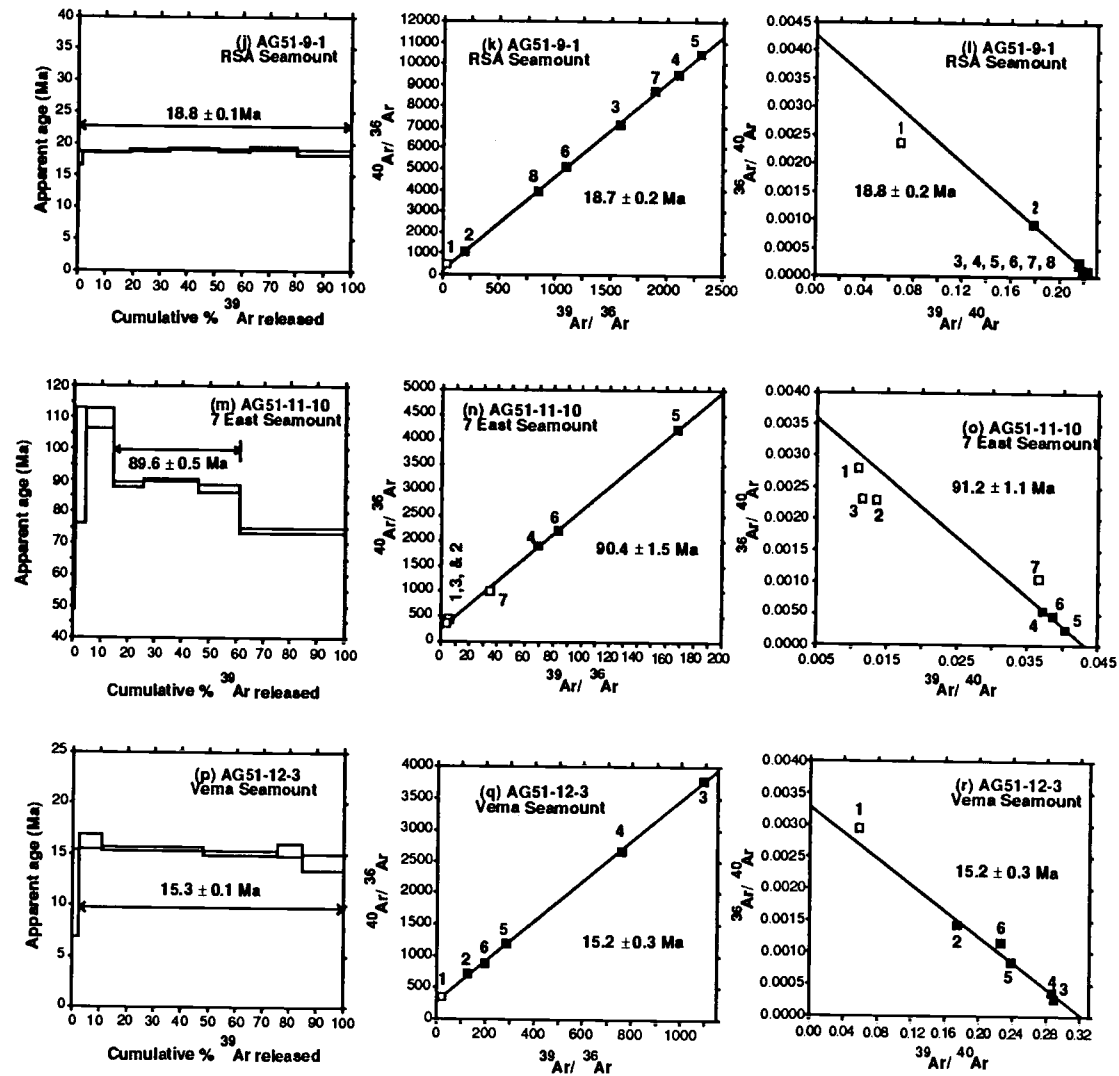
Figure III.3 (continued)

reconstruction African plate motion. The model presented below also accords with the geometry of the postulated volcanic trail of the Marion-Prince Edward hot spot, which stretches between the islands of Marion/Prince Edward and the southern tip of Madagascar.

Previous modeling has assumed that the islands of St. Helena, Tristan da Cunha, and Reunion lie close to the present-day centers of hot spots [e.g. Morgan, 1981; Duncan, 1981; and Chapter II]. Rotation poles defined on the basis of this assumption were unsuccessful in matching the modeled paths of the African plate over these hot spots, with the geometries of their respective volcanic traces, the St. Helena Chain, Walvis Ridge, and the Mascarene Plateau, respectively. For example, the predicted track of the St. Helena hot spot is offset significantly to the south of the St. Helena Seamount Chain in the model reported in Chapter II (Figure III.4a). Another problem with this model is that it predicts a sudden, probably unrealistic change in the direction of the African plate motion at ~30 Ma (Figure III.4a).

African plate motion and the case for large, diffuse hot spots

St. Helena, Bonaparte, Kutzov, and an unnamed seamount cluster (termed Westside Seamounts in this discussion) are aligned across the southwestern terminus of the St. Helena Chain (Figure III.1a). The southwestern end of the Walvis Ridge is similarly marked by an alignment of the island of Tristan da Cunha, Crawford Seamount, and Gough Island (Figure III.1b). This scattering of islands and seamounts, combined with the diffuse nature of their associated volcanic traces, is one indication that they were formed by broad diffuse hot spots. An alternative explanation is that these ocean islands and seamounts are each centered above a discrete hot spot, which is in turn linked to the St. Helena and Walvis plumes. An argument against an individual plume supplying melt to each such hot spot is that the Tristan da Cunha and Gough island are basically coeval (0 to ~1 Ma, this study and Le Roex, 1985] so making it difficult to envision the coincidental development of multiple plumes in such a localized region, at least in terms of a simple hot spot-plume model.

Another variation on the idea of broad hot spots is the possibility that the St. Helena and Walvis hot spots were initially smaller in diameter and only became very large in response to the transition from on-axis to intraplate setting (discussed in a later section), and/or a possible decrease in the velocity of the African plate (also discussed in a following section). In terms of modeling African plate motion, these variations on the theme of broad St. Helena and Walvis hot spots are not incompatible with the assumption that the centers of these hot spots are located close to Crawford and Kutzov Seamounts, respectively [O'Connor, 1989].

Two rotation poles reconstruct satisfactorily the direction of African plate migration over greater than 500 km diameter St. Helena and Walvis hot spots, in agreement with that recorded by the NE-SW orientations of their respective volcanic traces (Figure III.4). The northerly trend of the eastern

Figure III.4a. The modeled traces of African motion over hot spots (Table III.3) are shown by the heavy lines connecting the southwestern ends of the St. Helena Seamount Chain and the Walvis Ridge to the African coast. The small solid circles distributed along these lines representing the progress of the African plate at intervals of 10 Ma. Basement ages for the Walvis Ridge are from Chapter II. The DSDP 363 fossil age-range is from Bolli et al., [1978]. Dashed hot spot tracks and open circles illustrate the earlier model of Chapter II. See Figure III.5 for estimation of angular velocities used in this model. The Walvis Ridge is represented by its 400 m contour. Mercator projection.
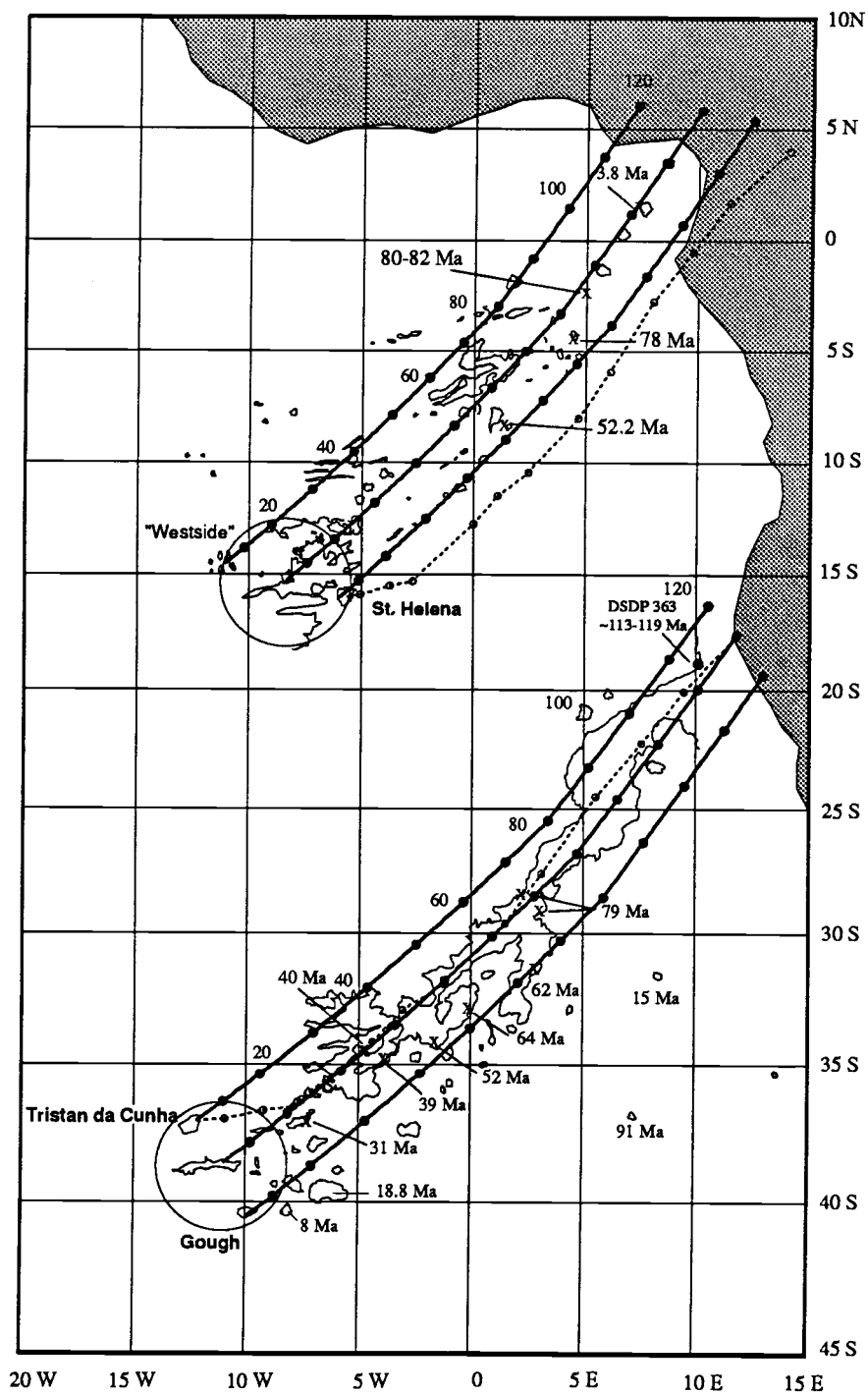
Figure III.4a

Figure III.4b. The modeled direction of African motion over the Reunion hot spot (rotation parameters in Table III.3) is illustrated by the bold line with small solid circles distributed along this line represents the progress of the African plate at intervals of 10 Ma. The dashed hot spot tracks and open circles similarly illustrate the earlier model of Chapter II. ^{40}Ar-^{39}Ar ages shown for the Mascarene plateau are from Duncan and Hargraves [1990]. The K-Ar age range for the islands of Mauritius is from McDougall [1971]. Mercator projection.

98
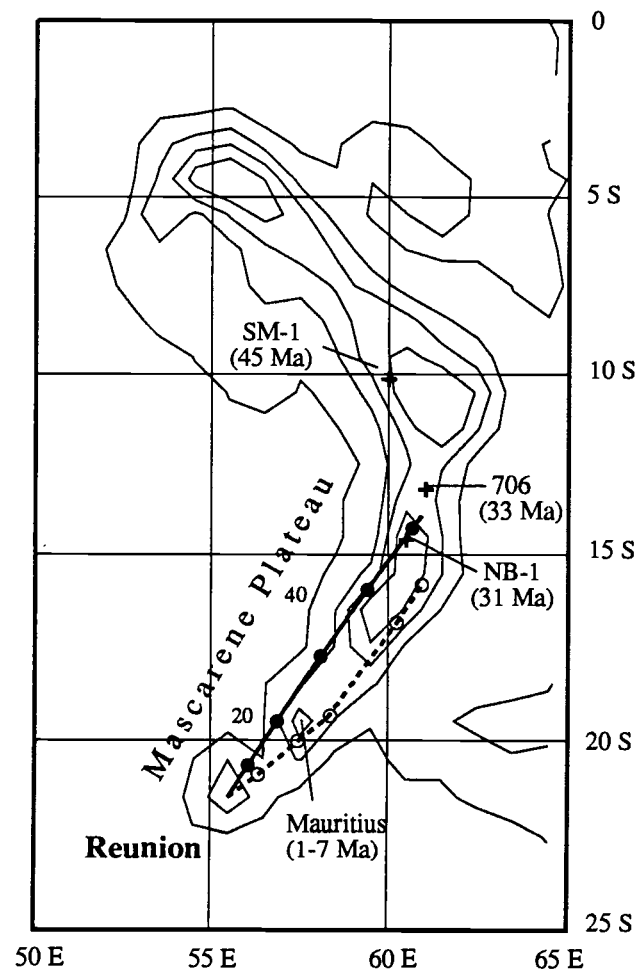
Figure III.4 b

end (i.e. older) of the Walvis Ridge (~27°S; 4°E to the African coast) suggests a change in the location of the Africa Euler pole from 37°N; 65°E to 38°N; 61°E, at approximately 80 Ma.

Supporting evidence for broad hot spots

The feasibility of broad St. Helena and Walvis hot spots is compatible with a model developed to explain anomalies in the geoid and heat flow, and the broad topographic swell, across the Cape Verde Islands [Courtney and White, 1986]. This model envisions a narrow ~150 km diameter plume of hot mantle rising upward, melting partially to form island lavas over a zone ≥ 300 km in diameter, with most plume material being deflected by the overlying plate and spreading out radially to form a mushroom-shaped head of anomalously hot mantle, some 1500 km across [Courtney and White, 1986; and White and McKenzie, 1989]. The volume and composition of melt generated by adiabatic decompression over such a hot spot is controlled by the temperature structure of the thermal plume its interaction with the overlying lithosphere [e.g., White, 1990]. While our definition of the St. Helena and Walvis hot spots is based of the size of their respective volcanic traces, the broad topographic swell, elevation heat loss, and anomalous geoid associated with these hot spots are probably greater in diameter.

A series of multiple spreading-axis jumps and propagating rifts (over a period of ~5 m.y.) at the latitudes of the islands of St. Helena and Ascension can be explained by the presence of broad, 500 km diameter St. Helena and Ascension hot spots [Brozena and White, 1990]. Although the center of the St. Helena plume lies ~400 to 600 km away, the flow of hot material away from the plume produces a large region of anomalously hot (and geochemically distinct) mantle. The topography of the spreading-axis at the latitude of Ascension Island consists of large volcanic ridges, more rugged than at the latitude of St. Helena. Brozena and White [1990] explained this difference in terms of the spreading-axis being located closer to the Ascension plume resulting in it being supplied by hotter plume material than at the latitude of St. Helena.

The existence of a broad St. Helena plume at the time of opening of the Gulf of Guinea has been invoked by Halliday et al. [1990] to explain a lead isotope anomaly in Cameroon Line lavas at the ocean/continent boundary, the diminishing lateral effects of which can be recognized as far as 400 km to either side.

Schilling et al. [1985] noted that the width of hot spot-generated geochemical and residual elevation anomalies along spreading-axes decrease with increasing distance from hot spots. An along spreading-axis geochemical anomaly width of ~1000 km is predicted by this model for the St. Helena and Walvis hot spots. This is compatible with a zone of rising magma (~ 500 km in diameter) from a mantle plume that that is also feeding a much wider zone of thermally and geochemically anomalous mantle. For example, Iceland is growing along a ~ 400 km stretch of the Mid-Atlantic spreading-axis, in association with an along axis geochemical anomaly of ~1000 km.

Previous estimates of hot spot sizes and hot spot modeling

Prior plate motion modelling has assumed that the locations and sizes of recently active oceanic islands locate the zero age centers and diameters of hot spots, e.g. Tristan da Cunha, St. Helena, and Reunion. However, as discussed above, the topographic swell, elevated heat flow, and geoid anomaly generated by hot spots can extend over a far wider area. For example, the Hawaiian swell is about 100 km across and has an average elevation of about 1 km. In the case of the Hawaiian hot spot the much greater velocity of the Pacific plate over hot spots generates immediate uplift and a large geoid anomaly at the upstream nose of the Hawaiian chain [e.g. Courtney and White, 1986; Sleep, 1990]. We postulate that radial flow of mantle from the central plume is deflected downstream, rather than forming a mushroom-like plume as described earlier for the Cape Verdes. A possible explanation for this difference between the Cape Verdes and the Hawaiian plume is that the African plate is practically stationary with respect to the Cape Verdes plume. The Walvis and St. Helena hot spots may well represent intermediate cases between the Hawaiian and Cape Verdes hot spots, explaining why the Walvis and St. Helena hot spots form > 500 km-wide volcanic chains, whereas the the Hawaiian hot spot is smaller and less diffuse. It is therefore possible to envision the St. Helena and Walvis hot spots (when located beneath the NE migrating African plate and lavas are erupting in an intraplate setting) as being > 500 km in a N-S direction, with preferential flow of deflected plume material downstream (i.e. to the east).

Calculation of plate rotation angles and sources of uncertainty

The angular velocity of the African plate since the South Atlantic opened is determined from the time-space distribution of radiometric ages along the St. Helena Chain, Walvis Ridge, and the Mascarene Plateau (Figure III.5a and III.5b). Two major sources of uncertainty are considered in these calculations, a systematic uncertainty of 4.5° or ~500 km resulting from the broadness of the St. Helena and Walvis hot spots, and the associated problem of accurately locating their present day centers.

Figure III.5a defines African plate velocity on the assumption that the Walvis and St. Helena hot spots are presently centered beneath a ~ 500 km diameter zone at the southwestern ends of the Walvis Ridge and the St. Helena Chain, and that the Reunion hot spot is centered beneath the island of Reunion. A best fitting line through all available age constraints (exclusive of the 0 to ~1 Ma age range for Tristan, Gough, and St. Helena) produces a negative intercept of ~1.5°. This can be interpreted as an indication that the centers of the Walvis and St. Helena hot spots could be ~167 km to the west of our postulated locations. An alternative explanation is that African plate velocity did indeed decreased systematically between ~31 and 0 Ma (Figure III.5a and Table III.3). The suggestion that the African plate is moving more slowly at present than during earlier times is supported by independent

Figure III.5a. Shown are ^{40}Ar-^{39}Ar ages for rock samples dredged or drilled from the St. Helena, Walvis-Gough, and Mascarene lineaments versus angles of rotation (about rotation poles in Table III.3) subtended from the centers of their respective hot spots, i.e., Crawford Seamount, Kutzov Seamount, and the island of Reunion. In the case of the Gough Lineament the rotation angles are estimated between seamounts and Gough island; this is equivalent to extrapolating seamount ages to the center of the Walvis Ridge, prior to rotating them to Crawford Seamount. Bold lines through each symbol represent an uncertainty of 4.5° assigned to account for the broadness of the hot spots. Open boxes indicate the rotation angles, listed in Table III.3, which best reconstruct African plate motion. Fossil age-range for DSDP 363 is from Bolli et al. [1978]. K-Ar ages for Mauritius are from McDougall [1971]. Regression lines are not forced through the 0 to ~1 Ma age range for Gough Island, Tristan da Cunha, and Reunion, or the ~9 to 7 Ma age-range for the island of St. Helena.
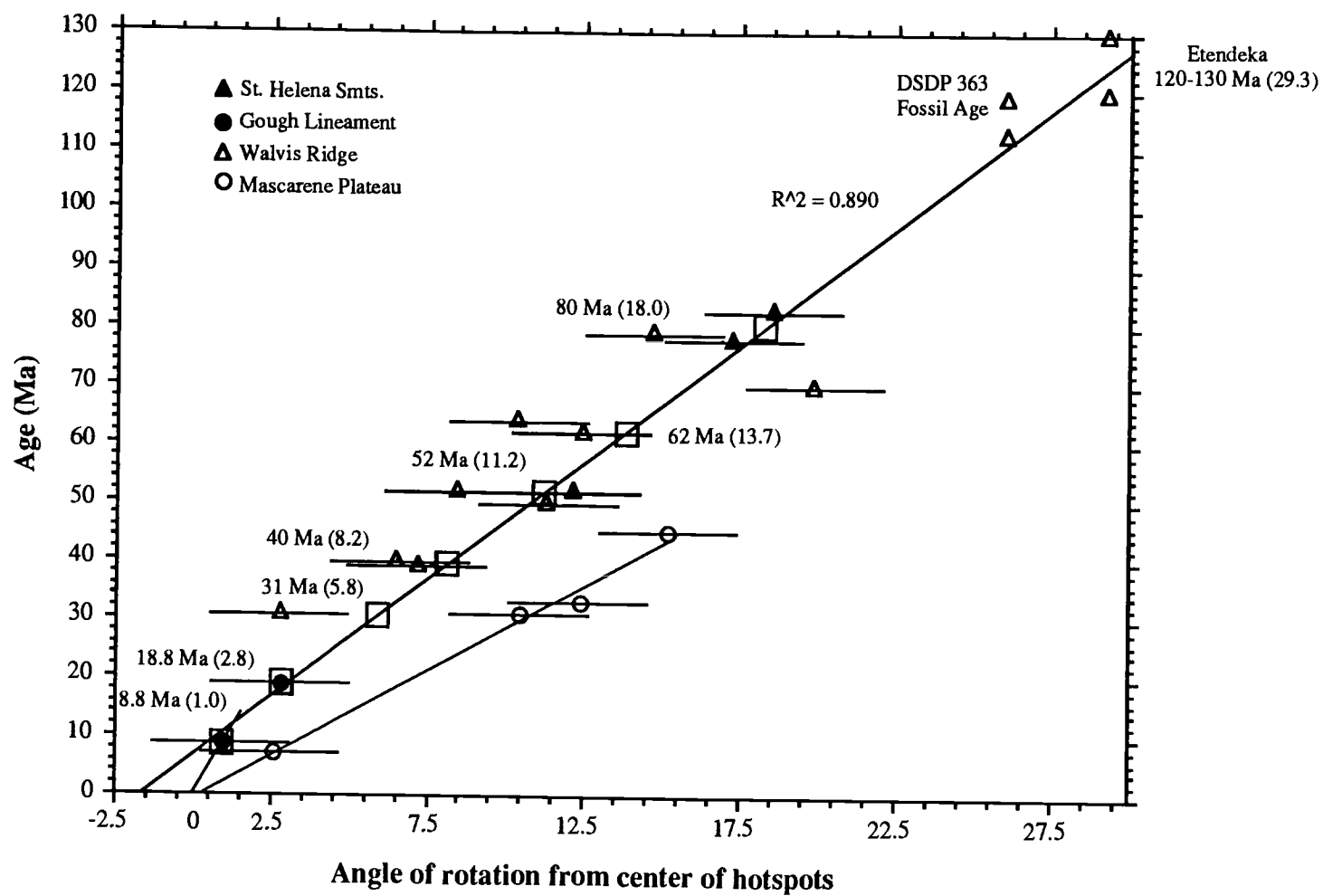
Figure III.5a

Figure III.5b. This variation diagram differs from that shown in Figures III.5a and III.5b in that the present day center of the Walvis and St. Helena hot spots are relocated 1.5° to the west of Crawford and Kutzov Seamounts, respectively, as indicated by the intercept of the fitted line through St. Helena Chain and Walvis Ridge radiometric ages shown in Figure III.5a. Other details are the same as in Figure III.5a.

Figure III.5b

St. Helena and Walvis hotspots centered 1.5° to the West

- ▲ St. Helena Smts.
- ● Gough Lineament
- △ Walvis Ridge
- O Mascarene Plateau

R^2 = 0.939

Etendeka
120-130 Ma
(30.8)

80 Ma (19.4)

62 Ma (15.0)

52 Ma (12.5)

40 Ma (9.5)

31 Ma (7.2)

18.8 (4.3)

8.8 Ma (2.5)

Age (Ma)

Angle of rotation from center of hotspots
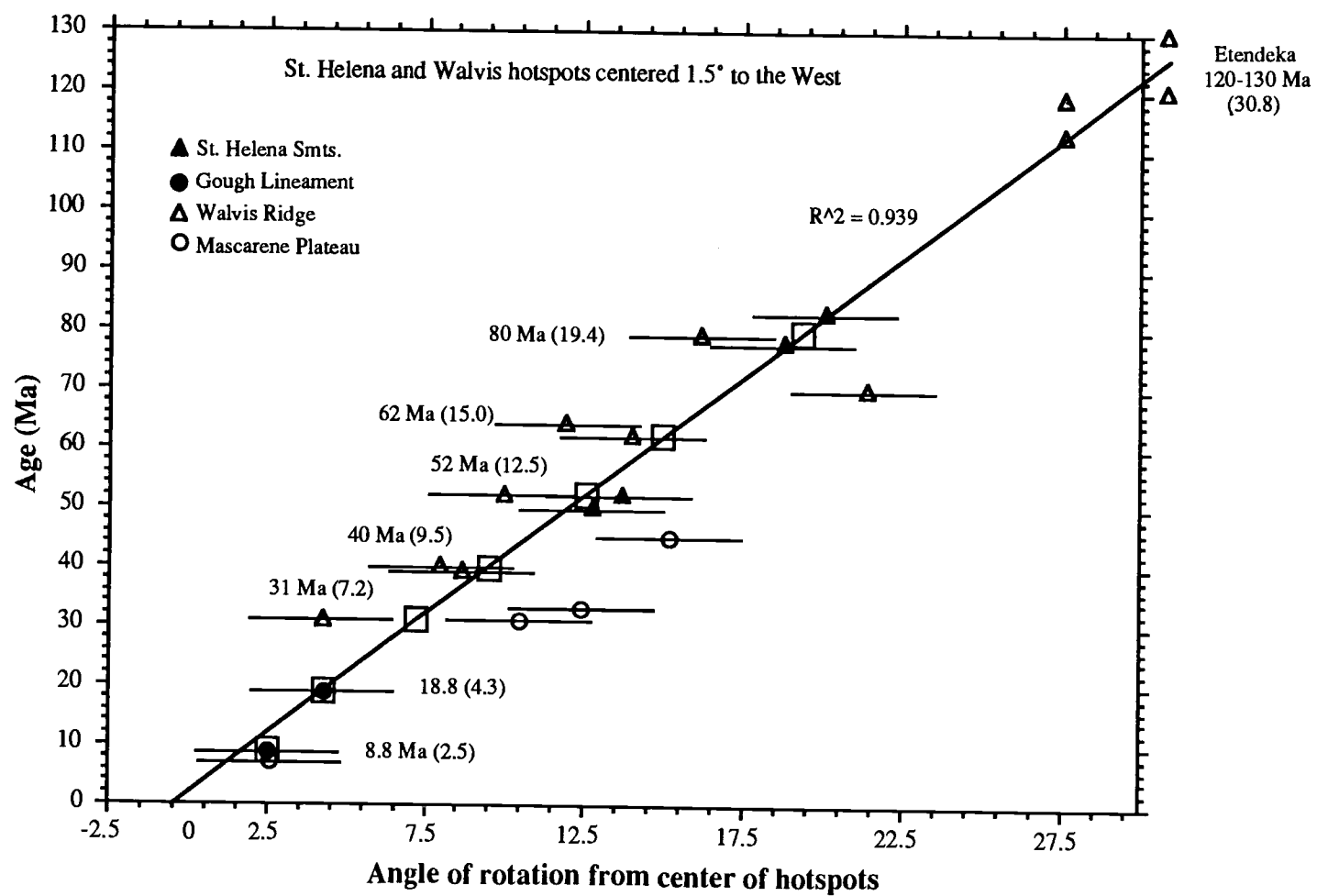
Table III.3. Finite Reconstruction Poles for African Plate Motion Over Hot Spots

Age, Ma	Latitude, °N	Longitude, °E	Angle*	Velocity (deg/m.y.)
9	38.0	-61.0	-1.0	-0.11
19	38.0	-61.0	-2.8	-0.18
31	38.0	-61.0	-5.8	-0.25
40	38.0	-61.0	-8.2	-0.27
52	38.0	-61.0	-11.2	-0.25
62	38.0	-61.0	-13.7	-0.25
80	38.0	-61.0	-18.0	-0.24
120	37.0	-65.0	-29.3	-0.28

*Negative angles indicate counterclockwise rotation.

estimates of current African velocity (i.e., 0.15 ± 0.05 deg/m.y., averaged over the past 3 m.y.) [Gripp and Gordon, 1990; Figure 1]. Pollitz [1990] has also identified a decrease in African velocity over hot spots during the period between 8 and 4 Ma, citing geologic evidence for this change along a large portion of the African plate boundary, including the Red Sea and Gulf of Aden spreading system, and the Alpine deformation zone. ^{40}Ar-^{39}Ar and K-Ar ages for the Mascarene plateau and the islands of Mauritius and Reunion are substantially offset from the line fitted through available time-space constraints, assuming the center of the Reunion hot spot is located beneath the island of Reunion. Another problem with African plate velocity calculated solely on the basis of these data is that between ~8 to 0 Ma it was ~0.3 deg/my, significantly greater than predicted by the independent estimates of African plate velocity for the past 3 m.y. [Gripp and Gordon, 1990].

Figure III.5b illustrates how rotation angles vary when the Walvis and St. Helena hot spots are relocated 1.5° to the West, as suggested by the negative intercept of the regression line fitted through all time-space data in Figure III.5a. A difficulty with this variation diagram is the lack of convincing evidence for recently formed seamounts ~1.5° km to the west of Kutzov or Crawford Seamounts. While we have selected the most elevated point of the ~300 km long Crawford Seamount as the center of the Walvis hot spot, this seamount, however, extends for ~200 km further to the west of this location in the form of a much less elevated lineament. Radiometric dating of Crawford Seamount is required in order to better distinguish between the models proposed here. Another apparent difficulty with velocities defined on the basis of Figure III.5b is again that African plate velocity between ~8 to 0 Ma was ~ 0.3 deg./m.y., significantly faster than estimated by independent estimates of current African velocity [e.g. Gripp and Gordon, 1990].

In conclusion, we consider the set of angular rotations defined in Figure III.5a as being a useful working model for reconstructing African plate motion over hot spots (Table III.3), with velocities in Figure III.5b representing a viable alternative.

Vema and 7°E Seamounts

Vema and 7°E Seamounts are located ~550 and 700 km, respectively, to the south of the Walvis Ridge, and ~500 km to the east of the C34 (84 Ma) seafloor isochron (i.e., on seafloor older than 84 Ma) (Figure III.1b). Vema Seamount (15 Ma, this study) formed in an intraplate tectonic setting as did 7°E Seamount (91 Ma, this study).

The geochemically enriched character of these seamounts confirms that they were formed by hot spots [Le Roex et al., 1990; and Le Roex et al., unpublished manuscript], although they do not appear to be related to chains of seamounts.

Figure III.6. Reconstructions of the time-space relationship between the St. Helena and Walvis hot spots, their respective volcanic traces, and the South Atlantic spreading-axis. Relative motion parameters for Africa/South America are from Shaw and Cande [1990]. Magnetic anomaly picks are from Cande et al. [1988] with pluses and small open circles representing rotated African and South American anomaly picks, respectively. Bathymetry is from Cherkis et al. [1989]. The 80 Ma age shown for the Rio Grande Rise is from O'Connor (Ar-Ar analysis, unpublished data 1989]. Mercator projection.
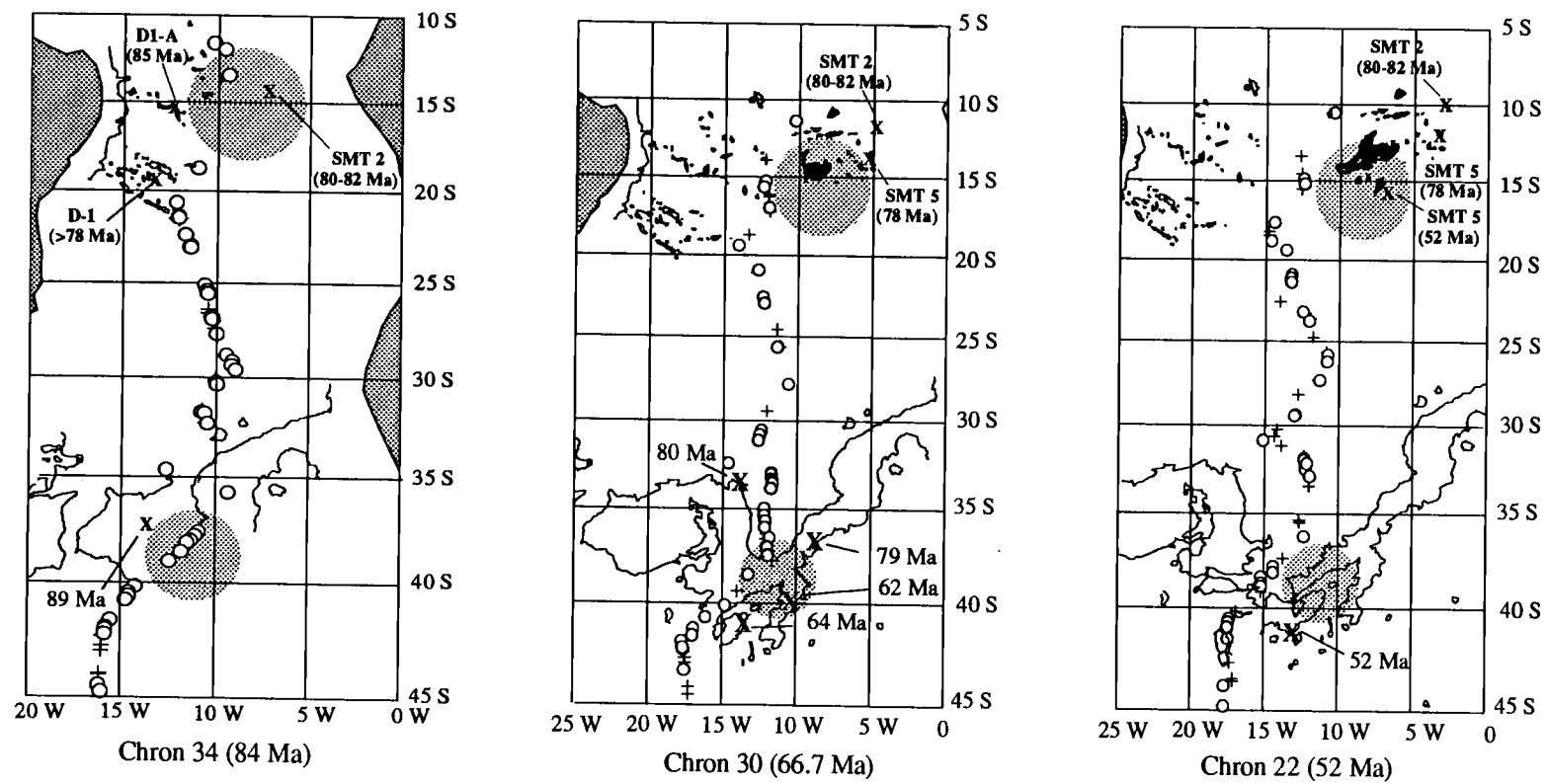
Figure III.6

INTERACTION BETWEEN THE SOUTH ATLANTIC SPREADING-AXIS AND THE ST. HELENA AND WALVIS HOT SPOTS

Reconstruction of the time-space relationship of the spreading-axis, the St. Helena hot spot, and its associated seamount chains shows that St. Helena Seamount 6 (52 Ma) formed ~500 km to the east of the South Atlantic spreading-axis, i.e., in an intraplate tectonic setting (Figure III.6); at 52 Ma the Walvis Ridge was also forming in an intraplate setting.

In contrast, St. Helena Seamounts 2 (~82 Ma) and 5 (~78 Ma) appear to have formed on, or close to, the South Atlantic spreading-axis (Figure III.6). An initial history of on-axis St. Helena hot spot volcanism is supported by the intersection of the southeastern ends of Pernambuco and Bahia Seamounts (South American plate) with the spreading-axis at chron 34 time (84 Ma) (Figure III.6). These Brazilian seamount chains are analogous to the Rio Grande Rise (South American plate), which coevolved with the Walvis Ridge while the spreading-axis was above the Walvis hot spot (Figure III.6).

The simultaneous termination of the Brazilian Seamount Chains and the Rio Grande Rise strongly suggests that the spreading-axis has migrated westward away from both the St. Helena and Walvis hot spots, beginning between 80 and 70 Ma. The low density of seafloor magnetic anomalies identified in the northern South Atlantic, however, makes it more difficult to reconstruct the relationship between the spreading-axis and the St. Helena hot spot than in the case of the relationship between the spreading-axis and the Walvis hot spot.

A transitional period of overlapping on-axis and intraplate volcanism is suggested by a chron 30 (67 Ma) reconstruction (Figure III.6), as noted previously in the case of the Walvis Ridge-Rio Grande Rise system [Chapter II]. A large, diffuse hot spot of >500 km diameter is more compatible with this wide zone of on-axis and intraplate volcanism than a more focussed point-like hot spot, typified by the size of an individual ocean island.

CONCLUSIONS

1) The St. Helena and Walvis hot spots are broad, diffuse hot spots greater than 500 km in diameter, far larger than previously estimated on the basis of the size of individual ocean islands.

2) In contrast to previous attempts, broad St. Helena and Walvis hot spots allow for the reconstruction of the direction of African motion such that it accords with the orientation of both the St. Helena Chain and the Walvis Ridge, and in the case of the Reunion hot spot, the Mascarene Plateau.

3) African rotation is constrained by the time-space distribution of radiometric ages along these volcanic lineaments and incorporates an uncertainty of ~500 km or 4.5° to allow for the broadness of the St. Helena and Walvis hot spots.

4) Our model suggests that African plate velocity decreased systematically between ~40 and 0 Ma.

5) A simultaneous transition from on-spreading-axis to intraplate volcanism is shown to have occurred along the St. Helena Seamount Chain and the Walvis Ridge between ~80 and 70 Ma, which occurred in response to the westward migration of the South Atlantic spreading-axis away from the St. Helena and Walvis hot spots, respectively.

REFERENCES

Bolli., H. Y. M., W. B. F. Ryan et al., Walvis Ridge-sites 362 and 363, Initial Rep. Deep Sea Drill. Proj., 183-356, 1978.

Brereton, N. R., Corrections for interfering isotopes in the ^{40}Ar-^{39}Ar dating method, Earth Planet. Sci. Lett., 8, 427-433, 1970.

Brozena, J. M., and R. S. White, Ridge jumps and propagations in the South Atlantic, Nature, 348, 149-152, 1990.

Cande, S. C., J. L. LaBrecque, and W. B. Haxby, Plate kinematics of the South Atlantic: Chron 34 to present, J. Geophys. Res., 93, 13,479-13,492, 1988.

Cande, S. C., J. L. LaBrecque, R. L. Larson, W. C. Pitmann III, X. Golovchenko, and W. F. Haxby, Magnetic Lineations of the World's Ocean Basins (map). Scale: approximately 1:27,400,000 at the equator, American Association of Petroleum Geologists, Tulsa, Okla., 1989.

Chaffey, D. J., R. A. Cliff, and B. M. Wilson, Characterization of the St Helena magma source, in A. D. Saunders and M. J. Norry (eds), Magmatism in the ocean basins, Geological Society Special Publication No. 42, 257-276, 1989.

Cherkis, N. Z., H. S. Fleming, and J. M. Brozena, Bathymetry of the South Atlantic Ocean-3°S to 40°S, Map and Chart Ser. MCH-069, Geol. Soc. of Am., Boulder, Colo., 1989.

Courtney, R. C., and R. S. White, Anomalous heat flow and the geoid across the Cape Verde Rise: evidence for dynamic support from a thermal plume in the mantle, Geophys. J. R. astr. Soc., 87, 815-867, 1986.

Dalrymple, G. B., and M. A. Lanphere, ^{40}Ar-^{39}Ar technique of K-Ar dating: A comparison with the conventional technique, Earth Planet. Sci. Lett., 300-308, 1971.

Dalrymple, G. B., and D. A. Clague, Age of the Hawaiian-Emperor Bend, Earth Planet. Sci. Lett., 31, 317-321, 1976.

Dalrymple, G. B., E. C. Alexander, Jr., M. A. Lanphere, and G. P. Kraker, Irradiation of samples for ^{40}Ar-^{39}Ar dating using the Geological Survey TRIGA reactor, U. S. Geol. Surv. Prof. Pap., 117, 1981a.

Dalrymple, G. B., M. A. Lanphere, and D. A. Clague, Conventional and ^{40}Ar-^{39}Ar ages of volcanic rocks from Ojin (site 430), Nintoku (site 432), and Suiko (site 433) seamounts and chronology of volcanic propagation along the Hawaiian-Emperor Chain, Initial Rep. Deep Sea Drill. Proj., 55, 659-676, 1981b.

Deruelle, B., C. Moreau, C. Nkoumbou, R. Kambou, J. Lissom, E. Njonfang, R. T. Ghogomu, and A. Nono, The Cameroon Line: Phanerozoic magmatism and the structural evolution of the African plate, A. B. Kampunzu and R. T. Lubala (eds), Blackie and Sons, London (in press) 1989.

Duncan, R. A., Hot-spots in the southern oceans-An absolute frame of reference for the motion for the Gondwana continents, Tectonophysics, 74, 29-42, 1981.

Duncan, R. A., and R. B. Hargraves, ^{40}Ar-^{39}Ar geochronology of basement ages from the Mascarene Plateau, Chagos Bank, and the Maldives Ridges, in Proc. Ocean Drill. Program Sci. Results, Vol 115, College Station TX (Ocean Drilling Program), 43-51, 1990.

Fitton, J.G., The Cameroon Line, West Africa: a comparison between oceanic and continental alkaline volcanism, Spec. Publs geol. Soc. Lond. 30, 273-291, 1987.

Gripp, A. E., and R. G. Gordon, Current plate velocities relative to the hotspots incorporating the Nuvel-1 global plate motion model, Geophys. Res. Letts., 17, 1109-1112, 1990.

Halliday, A. N., J. P. Davidson, P. Holden, C. DeWolf, D.-C. Lee, and J. Godfrey Fitton, Trace-element fractionation in plumes and the origin of HIMU mantle beneath the Cameroon Line, Nature, 347, 523-528, 1990.

Hanan, B. B., R. Kingsley, and J.-G. Schilling, Pb isotope evidence in the South Atlantic for migrating ridge-hotspot interactions, Nature, 322, 137-144, 1986.

Le Roex, A. P., Geochemistry, mineralogy and magmatic evolution of the basaltic and trachytic lavas from Gough Island, South Atlantic, J. Petrology, 149-186, 1985.

Le Roex, A. P., M. D. Kurz, and J. M. O'Connor, Geochemical characterization of Vema hotspot and seamount volcanism associated with the Gough hotspot: Implications for mantle heterogeneity beneath the South Atlantic (Abstract), Intraplate volcanism. The Reunion hot spot, Institut Physique du Globe, Paris, 12-17 November, 1990.

McDougall, I., The geochronology and evolution of the young volcanic islands of Reunion (Indian Ocean), Geochim. Cosmochim. Acta, 35, 261-288, 1971.

McDougall, I., and R.A. Duncan, Age progressive volcanism in the Tasmantid Seamounts, Earth Planet. Sci. Lett., 89, 207-220, 1988.

McDougall, I., and T. M. Harrison, Geochronology and Thermochronology by the ^{40}Ar-^{39}Ar Method, 212 pp., Oxford University Press, New York, 1988.

Moreau, C., J.-M. Regnoult, B. Deruelle, and B. Robineau, A new tectonic model for the Cameroon Line, Central Africa, Tectonophysics, 139, 317-334, 1987.

Morgan, W. J., Hot-spot tracks and the opening of the Atlantic and Indian Oceans, in The Sea, vol 7, pp 443-488, Wiley Interscience, New York, 1981.

O'Connor, J. M., On the trail of South Atlantic hot spots: Implications for reconstructing African and South American plate motions (abstract), Eos Trans. AGU, 70, 1135, 1989.

Pollitz, F. F., Two stage model of African absolute motion from 30 Myr to present, (abstract) Eos Trans. AGU, 71, 1640, 1990.

Samson, S. D., and E. C. Alexander, Jr., Calibration of the interlaboratory ^{40}Ar-^{39}Ar dating standard, Mmhb-1, Chem. Geol., 66, 27-34, 1987.

Schilling, J.-G., Upper mantle heterogeneities and dynamics, Nature, 314, 62-67, 1985.

Seidemann, D., Effects of submarine alteration on K-Ar dating of deep-sea igneous rocks, Geol. Soc. Am. Bull., 88, 1660-1666, 1978.

Shaw, P. R., and S. C. Cande, High-resolution inversion for South Atlantic plate kinematics using joint altimeter and magnetic anomaly data, J. Geophys. Res., 95, 2625-2644, 1990.

Sleep, N. H., Hotspots and mantle plumes: Some phenomonology, J. Geophys. Res., 95, 6715-6736, 1990.

Turner, G., and P. H. Cadogan, Possible effects of ^{39}Ar recoil in ^{40}Ar-^{39}Ar dating of lunar, Proc. Lunar Sci. Conf., 5, 1601-1615, 1974.

White, R., Evolution of the Reunion Hot spot, (Abstract), Intraplate volcanism. The Reunion hot spot, Institut Physique du Globe, Paris, 12-17 November, 1990.

White, R., and D. McKenzie, Magmatism at rift zones: The generation of volcanic continental margins and flood basalts, J. Geophys. Res., 94, 7685-7729, 1989.

York, D., Least squares fitting of a straight line with correlated errors, Earth Planet. Sci. Lett., 5, 320-324, 1969.

IV.   THE ST. HELENA HOT SPOT SYSTEM:
2. ISOTOPIC VARIABILITY IN RESPONSE TO MIXING OF THREE MANTLE COMPONENTS

ABSTRACT

Hyperbolic Nd-Pb, Sr-Pb, and linear Pb-Pb isotopic covariations in volcanic rocks, dredged from the St. Helena, Pernambuco, and Bahia Seamount Chains (South Atlantic Ocean) indicate a continuum of mixing between two distinct mantle components. These mantle components are characterized by the compositions of the lavas forming the island of St. Helena (i.e. HIMU) and the Walvis Ridge (i.e. EM1), respectively. Mixing between a depleted mantle component (i.e. DMM) and the HIMU–EM 1 continuum is indicated by a single St. Helena Seamount sample, which falls away from this two-component mixing array. Basalt drilled from Cretaceous seafloor formed close to the Walvis hot spot is derived from a mixture of EM1, HIMU, and DMM.

Three end-members (HIMU, EM1, and DMM) are therefore available to the St. Helena and Walvis hot spot sources, and by inference, to the majority of hot spot systems. Finally, we speculate that variability in plume temperature plays a significant role in controlling the isotopic composition of hot spot lavas, resulting in the association of predominantly EM 1-like lavas with hot and vigorous plumes and, conversely, predominantly HIMU-like lavas with cooler, less vigorous plumes.

INTRODUCTION

Diversity in Sr, Nd, and Pb isotopic ratios in lavas from ocean islands and associated seamount chains provides unequivocal evidence for long-established chemical heterogeneity in the sub-oceanic mantle. In order to explain observed mantle heterogeneity, three [Sun, 1980 and Zindler et al., 1982], four [Tatsumoto et al., 1984] or possibly five [White, 1985] chemically distinct mantle components may be required. In addition to questions regarding mantle component compositions, the origins, locations and depths in the mantle of such components, as well as associated mixing processes, are not well defined. Characterization of mantle components, the sizes of the reservoirs from which they are tapped, their geographical locations, and associated intermixing processes can, however, be constrained by investigating the evolution of seamount chains and/or ridges, particularly as they record the structural and compositional evolution of a hot spot trace over far longer time periods than in the case of individual ocean islands.

This paper contributes to this effort by investigating the isotopic compositions of lavas from the volcanic trace of the St. Helena hot spot (Figures IV.1a and IV.1b) from Cretaceous time to its present day expression at the island of St. Helena. In addition, the mantle components contributing to the composition of Walvis Ridge lavas are further constrained by the analysis of a sample drilled from Cretaceous seafloor close to the northeastern end of the Walvis Ridge (Figure IV.2).

Figure IV.1a. Bathymetry of the St. Helena Seamount Chain after Cherkis et al. [1989]. Fracture zones and spreading-axis after Cande et al. [1989]. Bathymetry contours are at 4000m. Seamount ^{40}Ar-^{39}Ar ages and island K-Ar age are from Chapter III. Mercator projection.
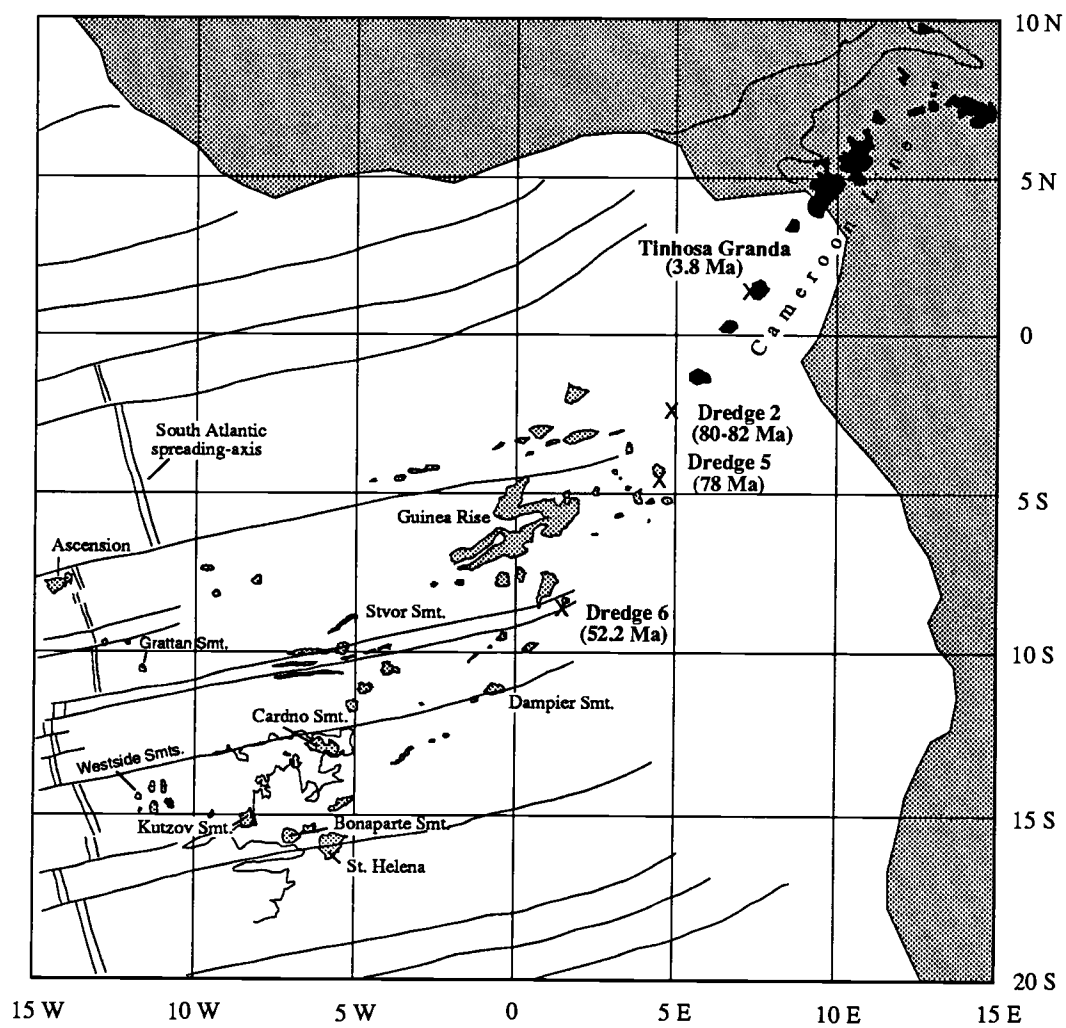
Figure IV.1a

Figure IV.1b. Bathymetry of the Pernambuco and Bahia Seamount Chains after Cherkis et al. [1989]. Fracture zones and spreading-axes are after Cande et al. [1989]. The bathymetry contours are at 4000m. Seamount radiometric ages are from O'Connor et al. (^{40}Ar-^{39}Ar analyses, unpublished data). Mercator projection.
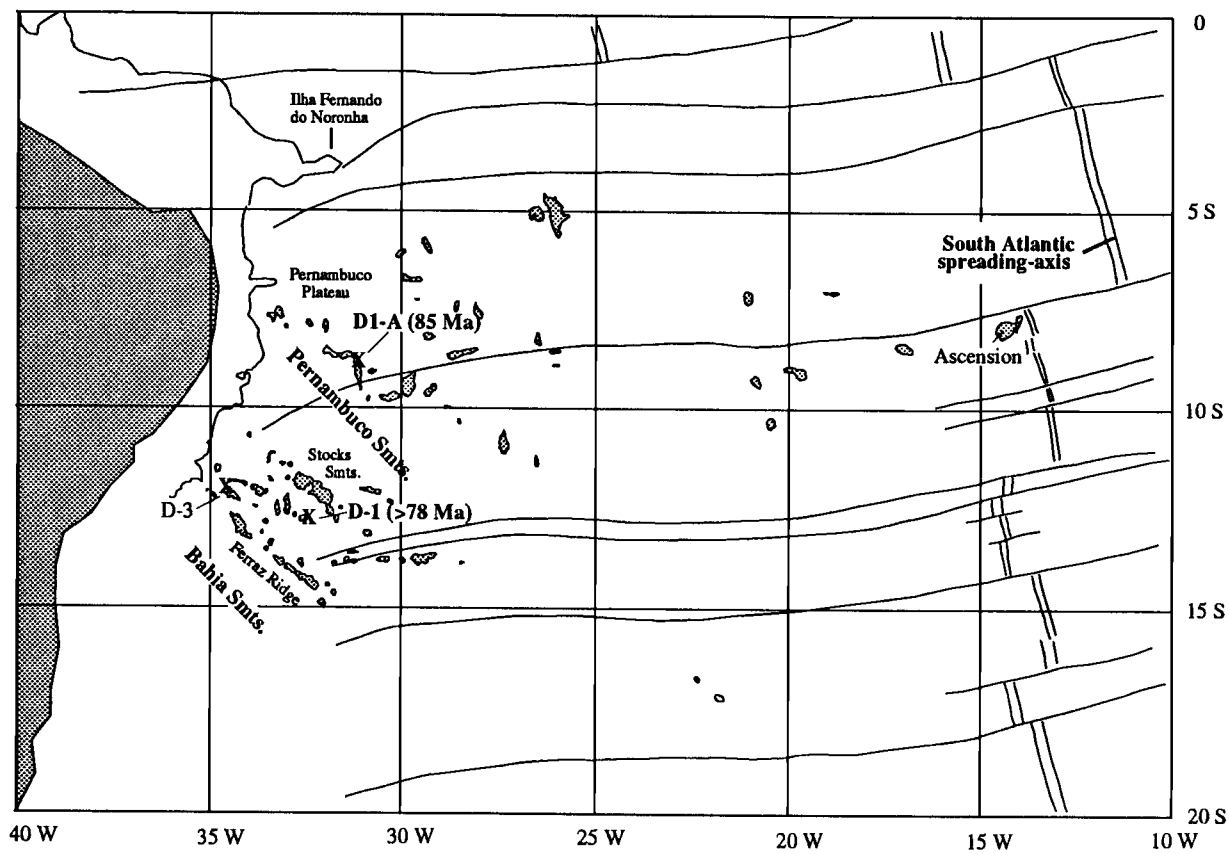
Figure IV.1b

Figure IV.2. Solid lines indicate the modeled trajectory of the African plate over > 500 km diameter St. Helena and Walvis hot spots, with solid circles indicating rate of plate migration in 10 m.y. increments [Chapter III]. ^{40}Ar-^{39}Ar ages for the Walvis Ridges are from Chapter II. The St. Helena Chain and the Walvis Ridge are sub-divided according to the tectonic setting at the time of formation, as defined in Chapter III. Mercator projection.
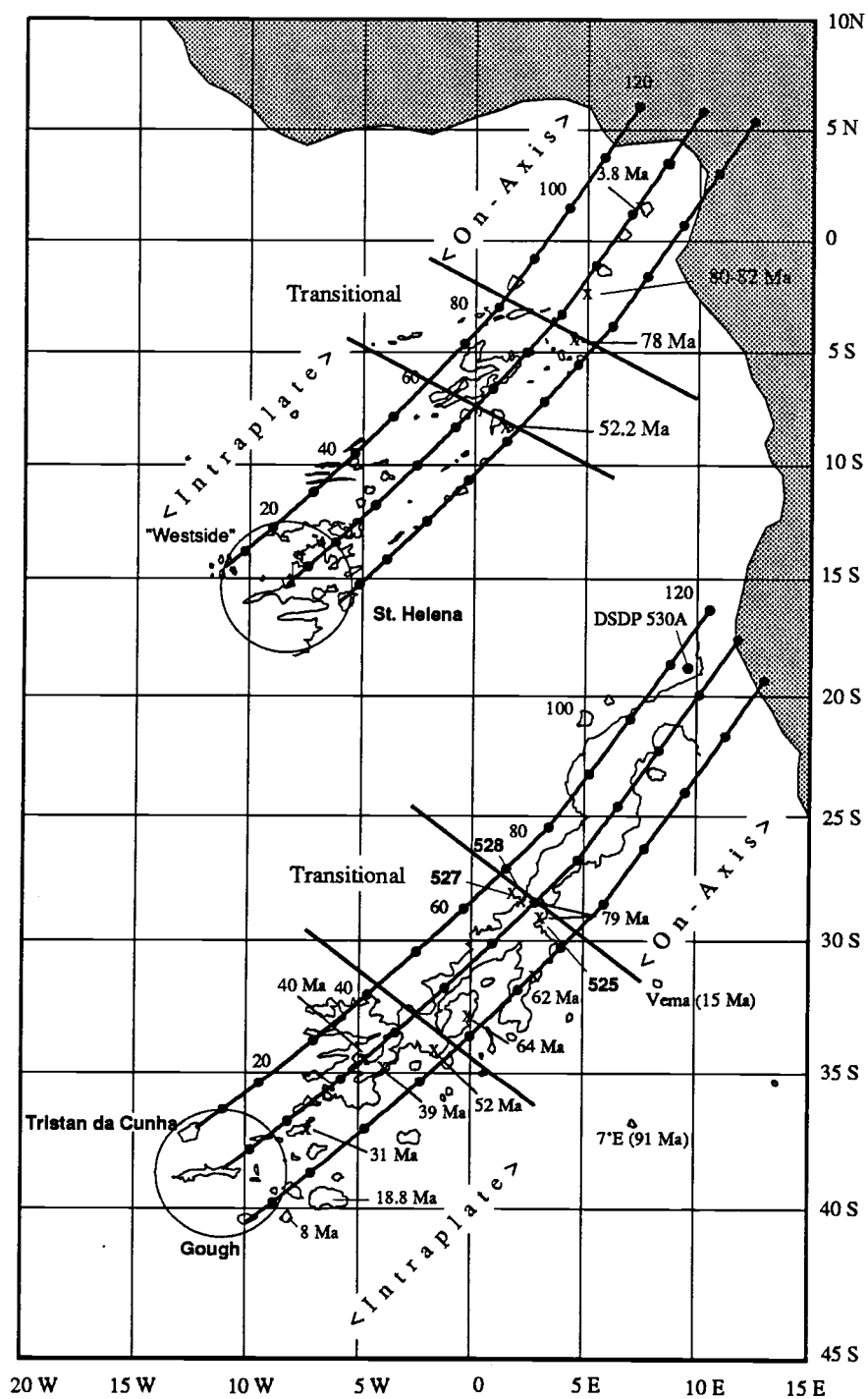
Figure IV.2

Three component mixing

The most extreme isotopic compositions of ocean island basalts may well define distinct, but internally heterogeneous mantle components or groups (e.g. White 1985). Zindler and Hart [1986], following Sun [1980] and Zindler et al. [1982], showed that most of the ocean island isotopic array can be explained in terms of mixing between three such mantle sources, HIMU, EM 1, and DMM (Figure IV.3): their terminology is followed in this discussion.

(1) HIMU mantle component, characterized by high $^{206}Pb/^{204}Pb$, low $^{87}Sr/^{86}Sr$ and moderately high $^{143}Nd/^{144}Nd$. This component is predominant on the islands of St. Helena and Tubuai, and is most pronounced on the Pacific island of Mangaia.

(2) Depleted MORB mantle (DMM) characterized by the high $^{143}Nd/^{144}Nd$ and low $^{87}Sr/^{86}Sr$ of mid-ocean ridge basalts.

(3) Enriched mantle (EM 1) intermediate in $^{87}Sr/^{86}Sr$, and high in $^{207}Pb/^{204}Pb$ and $^{208}Pb/^{204}Pb$ for a given $^{206}Pb/^{204}Pb$. This component has been defined on the basis of the Walvis Ridge [Richardson et al., 1982]; a similar component with higher $^{87}Sr/^{86}Sr$ as defined on the Pacific Island of Samoa (EM II) is not discussed further as it has not been detected in Atlantic hot spot lavas.

Hart et al. [1986], in a refinement of the Zindler and Hart [1986] model, proposed that mixing between mantle components of Tubuai (i.e. HIMU) and Walvis Ridge (EM 1) compositions, respectively, precedes mixing with other components (most probably DMM). This study reports an isotopic array that falls unequivocally along the HIMU to EM1 mixing continuum, i.e. the LoNd array of Hart et al. [1986]; mixing between DMM and this continuum is also documented. In addition, we provide evidence for the presence of the HIMU component in the volcanic products of the Walvis hot spot source. We therefore conclude that most islands and seamounts probably sample a similar continuum between two mantle components, with St. Helena and Walvis compositions being near the ends of that continuum. Although these compositions are close, but probably not equivalent to the postulated HIMU and EM 1 components, we consider them to be viable end-members for the purpose of defining mixing relationships.

Origins of mantle components

The origins of the EM 1 and HIMU sources are not yet well constrained. Suggestions for for the origin of HIMU include recycling of ancient altered oceanic crust [Hofmann and White, 1982], recycling of ancient continental crust [Allegre and Turcotte, 1985] and intra-mantle metasomatism [Zindler and Hart, 1986; Hart et al., 1986].

Based on the similarity in composition between Parana continental flood basalts and basalts drilled from the Walvis Ridge, Hawkesworth et al. [1986] suggested that the EM 1 component in South Atlantic islands originated from delamination of subcontinental mantle into the upper asthenosphere or lower lithosphere, during continental rifting. Richardson et al. [1982] considered

Figure IV.3. The DMM, HIMU, and EM 1 (which is assumed to be close to bulk silicate earth (BSE) in composition) mixing triangle of Zindler and Hart [1986; Figure 7).   BSE is defined as a primitive, undifferentiated segment of the earth's mantle.
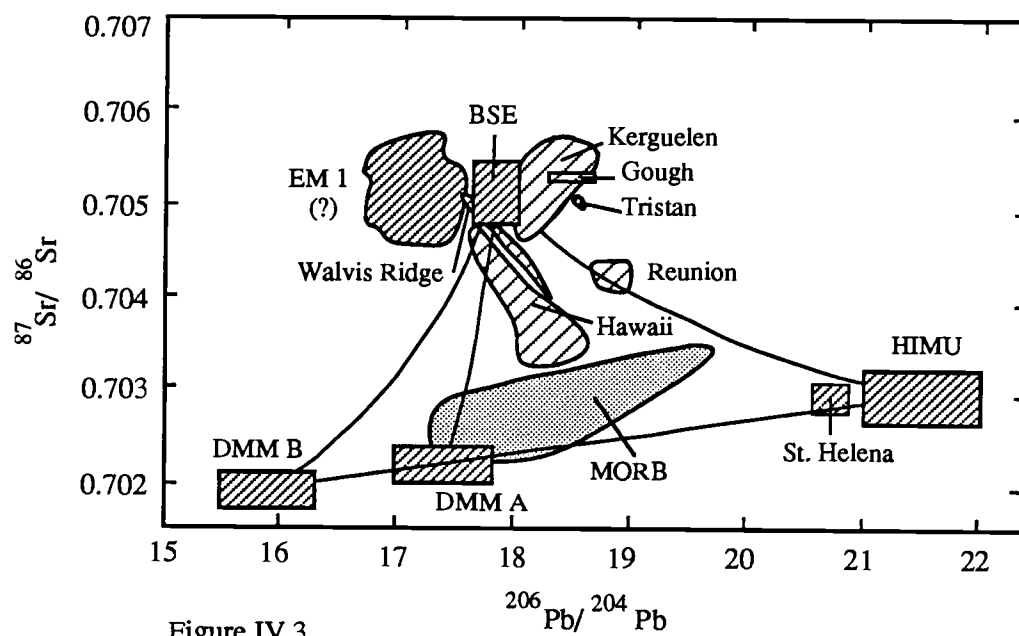
Figure IV.3

these basalts as being derived from a mantle component enriched by small volume melts and metasomatic fluids. Hart et al. [1986] noted that the Walvis Ridge component or EM1 is isotopically the most similar to bulk earth composition of proposed mantle sources and concluded that EM1 represents slightly modified primitive or bulk earth material.

Dupre and Allegre [1983a] recognized that lavas from oceanic islands in the South Atlantic and Indian Oceans have high $^{87}Sr/^{86}Sr$ ratios, and anomalously high $^{207}Pb/^{204}Pb$, $^{208}Pb/^{204}Pb$ ratios for a given $^{206}Pb/^{204}Pb$ ratio (i.e., characteristic of Walvis or EM1 lavas), which Hart [1984] termed the Dupal anomaly. Castillo [1988] noted that the southern South Atlantic is located in one of two maxima of the Dupal anomaly, which appear to be associated with large regions of low seismic velocity (LVRs) in the lower mantle; these LVRs are in turn associated with concentrations of active hot spots. Based on studies of MORBs, which sample the mantle over wide regions, he determined that the Dupal is present at intervals along the entire spreading-ridge system and concluded that the isotopic signature of MORBs primarily reflects the regional isotopic composition of the underlying mantle, rather than the influence of hot spots. Thus, the geophysical structure of the lower mantle could well be reflected in the geochemistry of erupted lavas [Castillo, 1988].

Broad, diffuse (>500 km) St. Helena and Walvis hot spots

In a companion radiometric dating study of the volcanic traces of the Walvis and St. Helena hot spots, the notion is developed that the St. Helena and Walvis hot spots are broad, diffuse zones (i.e., >500 km in diameter) of hot spot volcanism, rather than focused, point-like sources of the size of individual ocean islands or seamounts [O'Connor, 1989; and Chapter III].

Plume flux and mixing of mantle sources

The flux of melt from the Walvis plume is far greater than that from the St. Helena plume [Davies, 1988; Sleep, 1990], as indicated by the fact that the Walvis Ridge is by far the more massive volcanic edifice. We conclude our discussion by speculating that plume temperature dictates the composition of the lavas melting out of these plumes.

SEAMOUNT SAMPLES AND TECTONIC SETTING

Radiometric dating of some of the St. Helena Seamount samples analyzed in this study [Chapter III] indicates that a simultaneous transition from on-axis to intraplate tectonic setting began to affect the St. Helena and Walvis hot spot systems between ~70 and 80 Ma, as the South Atlantic spreading-axis migrated westward away from the St. Helena and Walvis hot spots (Figure IV.2). Increasing separation between the spreading-axis and the hot spots extinguished the supply of plume material to the South American plate leading to an end of construction of the Pernambuco-Bahia Chains and the Rio Grande Rise.

St. Helena Seamounts 2 and 5 have ^{40}Ar-^{39}Ar incremental heating ages of 78 Ma and 80-82 Ma, respectively (Figure IV.1). Single dredge hauls from the Bahia and the Pernambuco Seamounts have comparable ages of >78 Ma and 85 Ma, respectively (Figure IV.1b). Reconstruction of the spatial relationship between the South Atlantic spreading-axis and the St. Helena-Pernambuco-Bahia Seamount Chains at Chron 34 (84 Ma) time, indicates that these seamounts formed during a period that the spreading-axis was located close to or astride the St. Helena hot spot [Chapter III]. In contrast, St. Helena Seamount 6, which formed at 52 Ma, is much younger than surrounding seafloor and so must have formed in an intraplate tectonic setting (Figure IV.1). Sample descriptions and coordinates are in Table IV.1 and Appendix 2. Figure IV.1 illustrates the location of dredge sites.

ANALYTICAL TECHNIQUES

Sr, Nd, and Pb isotopic ratios were analyzed in the VG Sector mass spectrometer at Cornell University, following the sample preparation and analytical procedures described in Appendix 3. Prior to the measurement of isotopic ratios, samples were leached in hot, distilled 6N HCL for 1 hr to remove contamination introduced during handling and to remove the effects of seawater alteration. Major and trace element data were obtained by X-ray fluorescence spectrometry at Washington State University, following sample preparation and analytical procedures described in Appendix 3. Geochemical data are in Table IV.2.

IMPACT OF SEAWATER ALTERATION ON TRACE ELEMENT AND RADIOGENIC ISOTOPIC RATIOS

Major element data and sample descriptions clearly show that seawater has altered significantly the major element, and by inference the trace element, chemistry of the volcanic rocks dredged from the St. Helena-Bahia-Pernambuco Seamounts (Table IV.1 and IV.2). In fact, the basaltic nature of some of these samples (e.g. AC-02A, Table IV.1) can no longer be discerned. The lack of unaltered volcanic samples from the St. Helena-Bahia-Pernambuco Seamounts makes analyses of old, altered rocks unavoidable, especially as phenocrysts are also very altered.

$^{87}Sr/^{86}Sr$ ratios in submarine basalts can be increased significantly by seawater alteration [e.g. Hart, 1971; Chapman et al., 1975; Spooner, 1976; Staudigel and Hart, 1983]. Because of the very low concentrations of rare earth elements (REE) in seawater and their immobility during chemical exchange, it is generally assumed that the effects of low temperature alteration on REE patterns and Nd isotopes are negligible. Studies of altered glass [Staudigel and Hart, 1983] and hydrothermal vent waters [Michard et al., 1983] have demonstrated the immobility of the REE in the oceanic crust during hydrothermal alteration. However, Ludden and Thompson [1979] showed that REE (especially light REE) are mobile during prolonged low temperature alteration of dredged

Table IV. 1.   Location and brief description of samples from the St. Helena, Bahia, and Pernambuco
Seamounts, and DSDP Site 530A

Sample	Location	Depth	Age	Description
	St. Helena Seamount AC-02			
	2° 19' 5"S; W4° 46' 4" ~1980-2000m		(80-82 Ma)	
AC-02A				highly altered volcanic rock
AC-02B				moderately altered trachyte
AC-02C				highly altered volcanic rock
AC-02E				moderately altered basalt
AC-02G				moderately altered ol, pl basalt
AC-02H				moderately altered trachyte
AC-02K				highly altered volcanic rock
AC-02I				moderately altered volcanic rock
	St. Helena Seamount AC-05			
	4° 17' 4" S; 4° 28' 7" E ~1768m		(78 Ma)	
AC-05A				moderately altered ol basalt
AC-05B				highly altered volcanic rock (alkali basalt?)
	St. Helena Seamount AC-06			
	8° 25' 6" S; 1° 33' 0" E ~1340m		(52 Ma)	
AC-06				slightly altered trachyte
	Cameroon Line (Island of Tinhosa Granda)			
	1° 21' 1" N; 7° 16' 6"E		(3.4 ± 1.4 Ma)	
TG-A-01				moderately altered volcanic rock
	Pernambuco Seamount			
	8° 42.3'S; 31° 32.2'W ~3320m		(~85 Ma)	
RC25-15-D1-B				highly altered volcanic rock
RC25-15-D1-C				moderately altered tholeiitic or subalkaline basalt
RC25-15-D1-D				highly altered ol basalt
	Bahia Seamount			
	12° 13'S; 13° 30'W ~2726m			
RC29-05-D3				highly altered volcanic rock
	Walvis Ridge			
	19° 11.26' S; 9° 23.15' E	(Cretaceous seafloor)		
DSDP 75 530A -107-1 (54-58)				moderately altered tholeiite

Table IV.2. Geochemical data for St. Helena-Bahia-Pernambuco Seamounts and DSDP Site 530A volcanic rock samples

Major Elements	AC-02A	AC-02B	AC-02C	AC-02E	AC-02H	AC-02G	AC-02K	AC-02I	AC-05A
SiO_2	33.62	59.97	39.56	48.11	59.49				49.61
Al_2O_3	12.49	17.74	14.22	16.91	17.6				17.58
TiO_2	3.64	0.97	3.81	2.23	0.85				3.58
FeO*	9.2	6.6	10.01	6.64	6.34				9.14
MnO	0.46	0.19	0.32	0.25	0.09				0.18
CaO	20.68	2.91	16.49	11.98	3.13				8.49
MgO	1.1	0.52	0.66	0.69	0.28				4.2
K_2O	1.51	3.97	2.36	2.61	4.27				2.7
Na_2O	3.15	6.93	3.66	5.1	6.98				3.51
P_2O_5	11.0	0.801	8.26	5.24	1.27				1.26
Total	96.84	100.21	99.35	99.75	100.3				100.24

*Fe expressed as FeO

Trace Elements									
Ni	203	51	129	103	4				129
Cr	12	6	33	17	7				211
Sc	18	12	13	14	6				20
V	246	34	241	105	18				190
Ba	217	609	191	380	576				747
Rb	25	81	21	38	72				51
Sr	789	345	694	757	289				956
Zr	310	723	352	457	728				392
Y	150	59	102	69	51				36
Nb	51.5	145.4	57.2	90.6	147.8				107.6
Ga	21	25	21	23	24				17
Cu	42	9	35	26	4				46
Zn	162	132	144	90	101				114
Pb	8	9	11	5	9				5
La	87	79	83	92	76				64
Ce	90	151	102	135	173				107
Th	1	13	3	5	14				7
Zr/Nb	6	5	6.2	5	4.9				3.6

Radiogenic isotopes									
$^{87}Sr/^{86}Sr$	0.70296		0.70346			0.70363	0.70319	0.70301	0.70318
$^{143}Nd/^{144}Nd$	0.51292		0.51285			0.512788	0.51281	0.51278	0.51288
$^{206}Pb/^{204}Pb$	20.947		20.208			19.773	20.082		18.546
$^{207}Pb/^{204}Pb$	15.783		15.742			15.756	15.745		15.5
$^{208}Pb/^{204}Pb$	39.78		39.609			39.452	39.674		38.29
$^{87}Sr/^{86}Sr*$									0.70321
$^{143}Nd/^{144}Nd*$									
$^{206}Pb/^{204}Pb*$									
$^{207}Pb/^{204}Pb*$									18.614
$^{208}Pb/^{204}Pb*$									15.521
									38.355

* duplicate measurement

Table IV.2 (continued)

Major Elements

	AC-05B	AC-06	Tinhosa Granda	RC-?D1-B	RC-?D1-C	RC29-D1-D	RC29-05-D3-1	RC29-05-D3-2	RC29-05-D3-3	75-530A-107-1 (54-58)
	40.75	60.6	43.85		50.19			29.62	28.59	50.69
	9.89	18.74	10.2		15.06			10.26	10.07	15.46
	3.68	0.78	3.99		3.38			2.73	2.77	1.66
	14.1	3.28	15.26		12.39			9.05	8.94	9.79
	0.22	0.08	0.223		0.15			0.23	0.28	0.29
	14.88	4.55	13.14		10.28			33.62	33.63	10.28
	12.6	0.17	11.32		4.53			1.48	1.4	8.82
	1.22	4.12	0.14		0.86			1.58	1.47	0.13
	1.94	7.06	0.44		3.58			2.06	1.96	3.05
	1.12	1.47	1.56		0.45			1.78	1.55	0.26
	100.41	100.85	100.12		100.87			92.6	90.66	100.42

Trace Elements

	AC-05B	AC-06	Tinhosa Granda	RC-?D1-B	RC-?D1-C	RC29-D1-D	RC29-05-D3-1	RC29-05-D3-2	RC29-05-D3-3	75-530A-107-1 (54-58)
	178	14	262		32			13	24	66
	286	0	290		49			4	9	112
	22	5	26		32			6	3	39
	304	9	332		364			253	253	308
	703	868	642		135			52	51	61
	15	66	3		10			27	26	2
	781	614	506		374			425	417	258
	299	628	326		216			155	158	117
	32	45	41		36			82	59	32
	118.8	160	134.3		35.8			25.8	27.9	19.3
	11	25	16		26			23	20	16
	62	7	67		81			11	12	63
	129	121	144		116			117	127	75
	9	7	4		5			3	4	3
	83	116	99		14			42	39	19
	143	202	159		86			68	91	28
	11	13	9		2			4	2	3
	2.5	3.92	2.4		6			6	5.7	6

Radiogenic Isotopes

	AC-05B	AC-06	Tinhosa Granda	RC-?D1-B	RC-?D1-C	RC29-D1-D	RC29-05-D3-1	RC29-05-D3-2	RC29-05-D3-3	75-530A-107-1 (54-58)
	0.70295	0.70309	0.70307	0.70306	0.70302	0.70322	0.70314			0.7031
	0.51288	0.51285	0.51296	0.51282	0.51281	0.51281	0.51285			
	20.289	20.325	20.183	20.357	20.444	19.997	20.696			19.056
	15.745	15.742	15.714	15.718	15.706	15.643	15.706			15.636
	39.912	39.785	39.814	40.025	39.97	39.532	39.217			39.21
	0.70286									
	0.51293									

basalts. Cheng et al. [1987] noted variability in $^{143}Nd/^{144}Nd$ ratios due to the effects of seawater alteration in oceanic basalts dredged from the Louisville Ridge. Thus, while $^{143}Nd/^{144}Nd$ ratios are more resistant to the effects of seawater alteration than $^{87}Sr/^{86}Sr$ ratios, they can nonetheless be altered to some extent.

On the basis of the success of strong acid leaching in removing the most significant effects of seawater alteration on Sr and Nd isotopic ratios documented in the studies discussed above, we are confident that strong acid leaching has also removed the most significant effects of seawater alteration from the majority of our samples. Additional support for the success of acid leaching treatment is provided by the coherence of the majority of measured isotopic ratios in Sr, Nd, and Pb isotopic space (Figures IV.4 to IV.7). Particularly important in this regard is the fact that $^{87}Sr/^{86}Sr$ ratios are not displaced significantly toward very high values that are characteristic of the effects of seawater alteration, with the possible exception of samples AC-02C and AC-02G. The two most altered samples analyzed (AC-02A and RC29-05-D3) are significantly offset from the general trend of the St. Helena hot spot data in $^{208}Pb/^{204}Pb$ versus $^{206}Pb/^{204}Pb$ isotopic space (Figure IV.6); we attribute this to an artifact of seawater and/or hydrothermal alteration.

Due to the high degree of alteration in our samples we place little confidence in the usefulness of most trace element ratios as reliable tracers of mantle component compositions. Zr/Nb ratios are, however, widely believed to resist the effects of seawater alteration [e.g. Bienvenu et al., 1990). Zr/Nb ratios for the St. Helena-Bahia-Pernambuco Seamounts range from 2.5 to 6.2, with a mean value of 5.0 (N = 11); these low values are similar to those determined for the island of St. Helena [Chaffey et al., 1989]. In contrast to the case of the Walvis Ridge–Rio Grande Rise system (Chapter II) a transition from high to low Zr/Nb ratios with changing tectonic setting is not apparent within the St. Helena hot spot system.

RESULTS AND DISCUSSION

Isotopic ratios for rock samples dredged from St. Helena-Bahia-Pernambuco Seamounts define arrays in $^{143}Nd/^{144}Nd$ vs. $^{206}Pb/^{204}Pb$, $^{87}Sr/^{86}Sr$ vs. $^{206}Pb/^{204}Pb$, and $^{208}Pb/^{204}Pb$ vs. $^{206}Pb/^{204}Pb$ isotopic space, which extend from St. Helena Island composition (i.e., HIMU-like) toward Walvis Ridge composition (i.e., EM 1-like) (Figures IV.5 to IV.7). These arrays (referred to as Nd-Pd, Sr-Pb, and Pb-Pb in this discussion) parallel calculated mixing hyperbolae between HIMU and EM 1 end-members in Nd-Pb and Sr-Pb space, and a linear mixing line in Pb-Pb space. Following Hart et al. [1986], we interpret this as strong supporting evidence for the importance of two component mixing between HIMU and EM 1 (i.e. the LoNd array) in the generation of St. Helena-Bahia-Pernambuco Seamount lavas. The compositions of end-member components used in mixing calculations are in Table IV.3.

Figure IV.4. $^{87}Sr/^{86}Sr$ versus $^{143}Nd/^{144}Nd$ isotopic variations in St. Helena, Bahia, and Pernambuco Seamounts. The open squares represent the St. Helena-Bahia-Pernambuco data, with the solid triangle indicating the datum for the Cameroon Line island of Tinhosa Granda (Gulf of Guinea). Analytical uncertainty is within the size of symbols. Also shown are fields for Indian, Pacific, and Atlantic MORB [Dosso et al., 1988; Hamelin et al., 1984, 1985; Hamelin and Allegre, 1985; Mahoney et al., 1989; Michard et al., 1986; Price et al., 1986; White et al., 1987; and Dupre and Allegre, 1980b], Loihi Seamount [Staudigel et al., 1984], Louisville Ridge [Cheng et al., 1987], Chagos-Laccadive Ridge [White et al., 1990], St. Helena [Chaffey et al., 1989], Mangaia [Palacz and Saunders, 1986], Comores [Dupre and Allegre, 1983], San Felix [Gerlach et al., 1986], DSDP Sites 525, 527, and 528 [Richardson et al. [1982], Tristan da Cunha [LeRoex, 1990], Gough Island [LeRoex, 1985], New England Seamounts [Taras and Hart, 1987], Cape Verdes [Gerlach et al., 1988], 26°S near-axis seamounts [Castillo and Batiza, 1989], Vema, 7°E, and McNish Seamounts (Le Roex and Kurz, unpublished data). Mixing lines between DMM, EM 1 and HIMU sources are shown, with bold lines indicating the percentages of EM 1 in an EM 1–HIMU mixture, DMM in an DMM-EM 1 mixture, and DMM in a DMM–HIMU mixture. Compositions of end-member components are in Table IV.3.
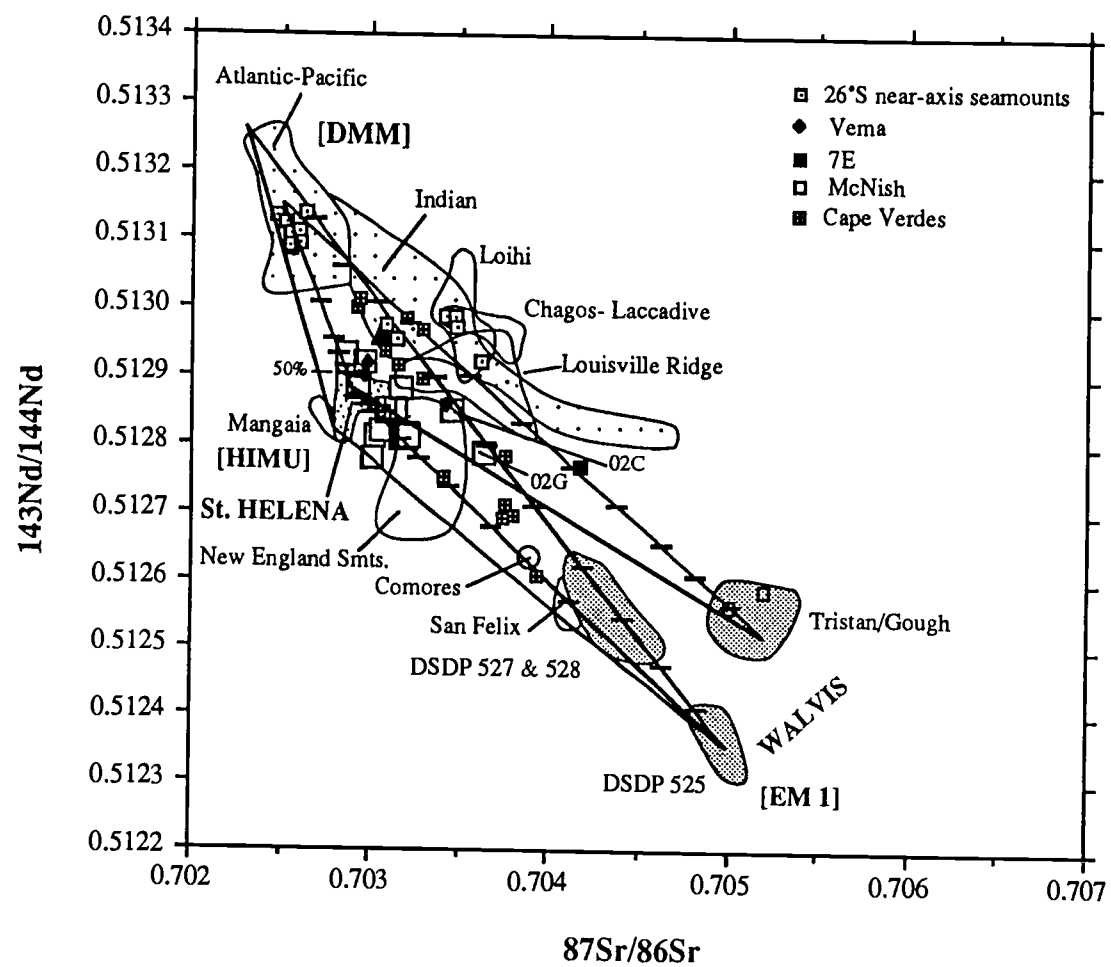
Figure IV.4

Figure IV.5. $^{143}Nd/^{144}Nd$ vs. $^{206}Pb/^{204}Pb$ variation diagram for St. Helena–Bahia–Pernambuco Seamounts. Details are the same as in Figure IV.4. Data for Tubuai is from Vidal et al., 1984. Analytical uncertainty is within size of symbols. Composition of end-member components are in Table IV.3.
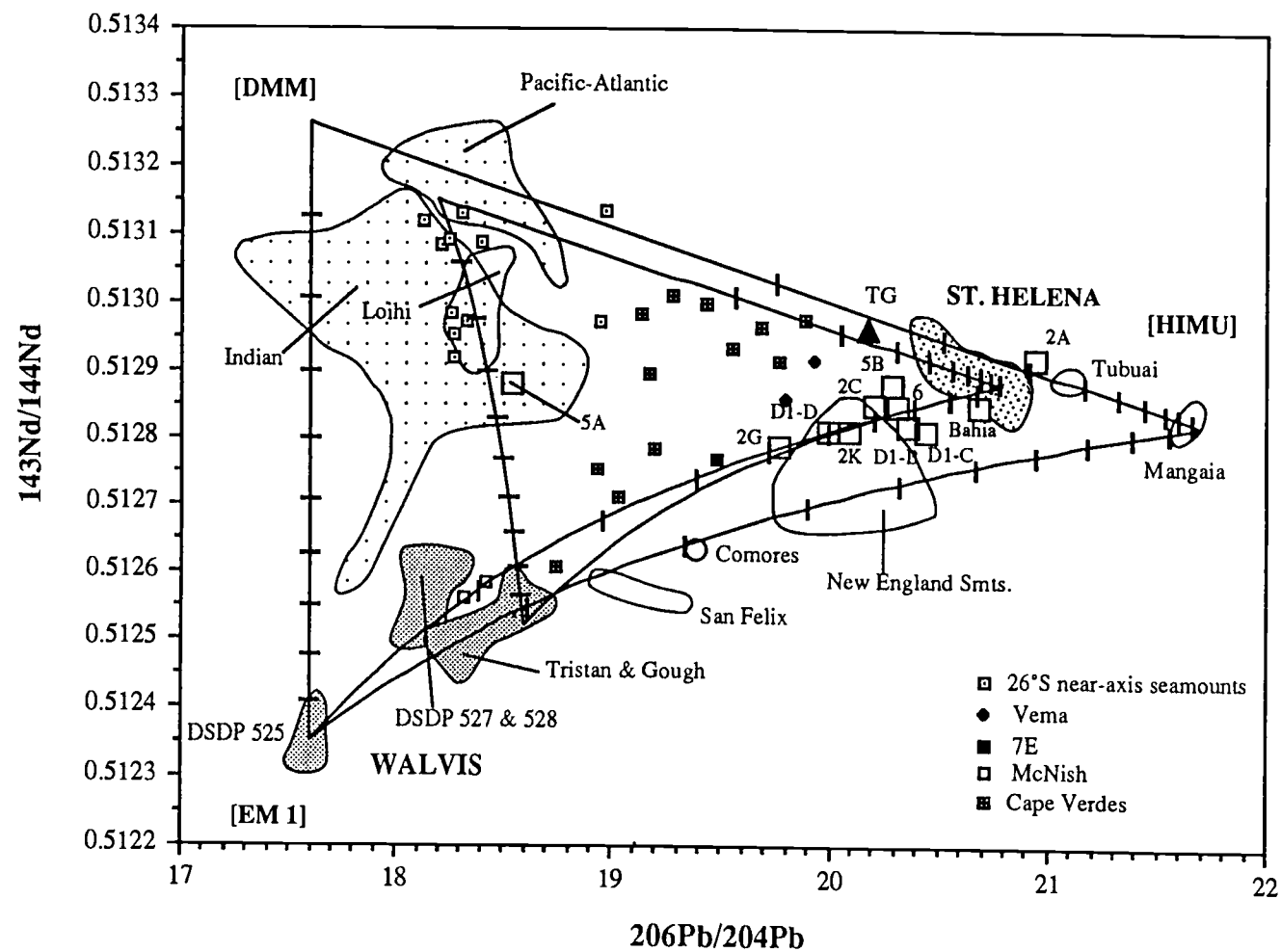
Figure IV.5

Figure IV.6. $^{206}Pb/^{204}Pb$ vs. $^{208}Pb/^{204}Pb$ variation diagram for the St. Helena-Bahia-Pernambuco Seamounts. Details are the same as in Figures IV.4 and IV.5. Data for the South Atlantic spreading-axis are from Hanan et al., 1986 and for the Walvis dredges from O'Connor and White, unpublished data. Analytical uncertainty is within size of symbols. Composition of end-member components are in Table IV.3.

Figure IV.6

Figure IV.7. ^{87}Sr/^{86}Sr vs. ^{206}Pb/^{204}Pb variation diagram for samples from the St. Helena–Bahia–Pernambuco Seamounts. Data sources and mixing lines as in Figures IV.4, IV.5 and IV.6. Analytical uncertainty is within size of symbols. Compositions of end-member components are in Table IV.3.
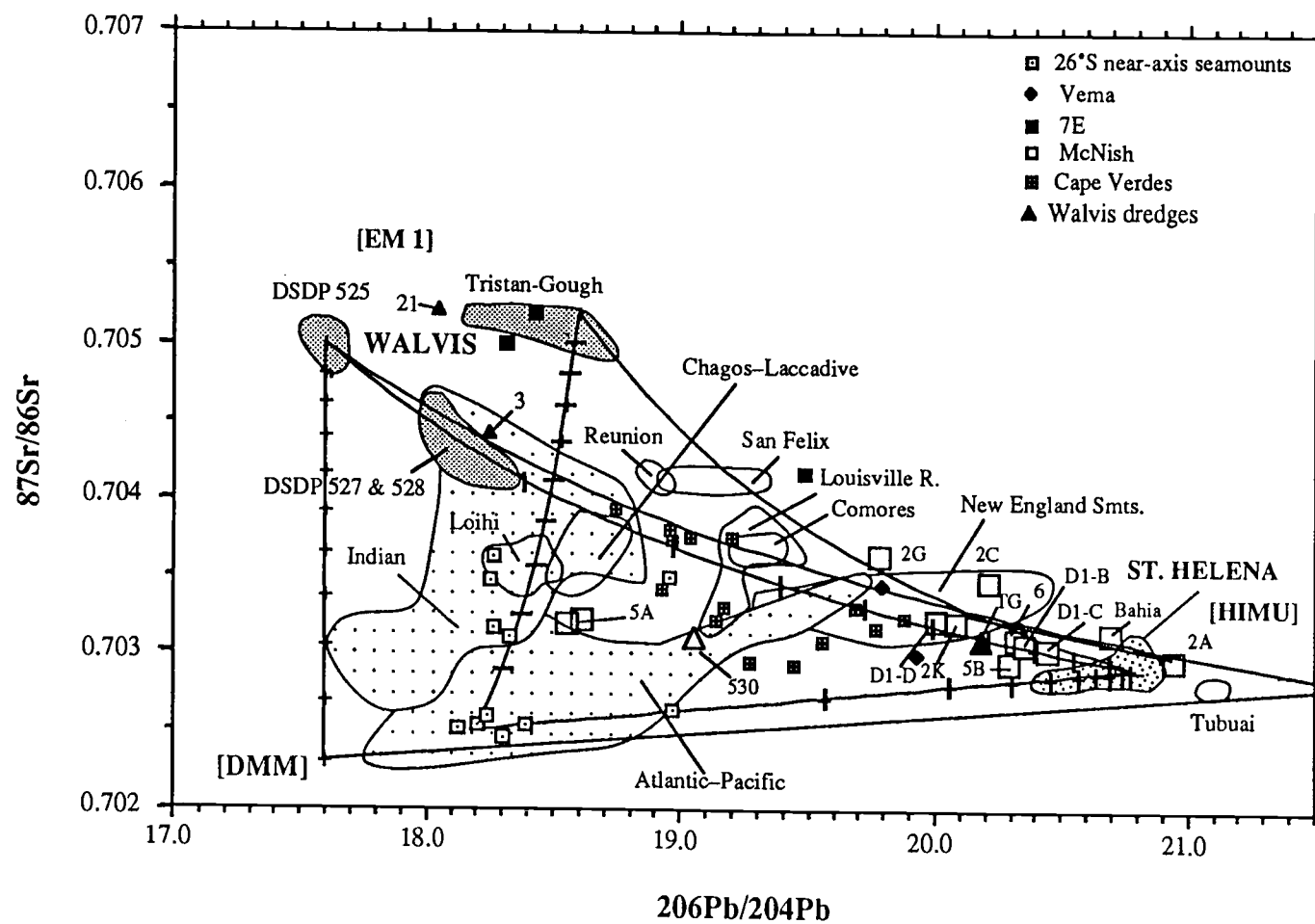
Figure IV.7

Evidence for a third mantle component
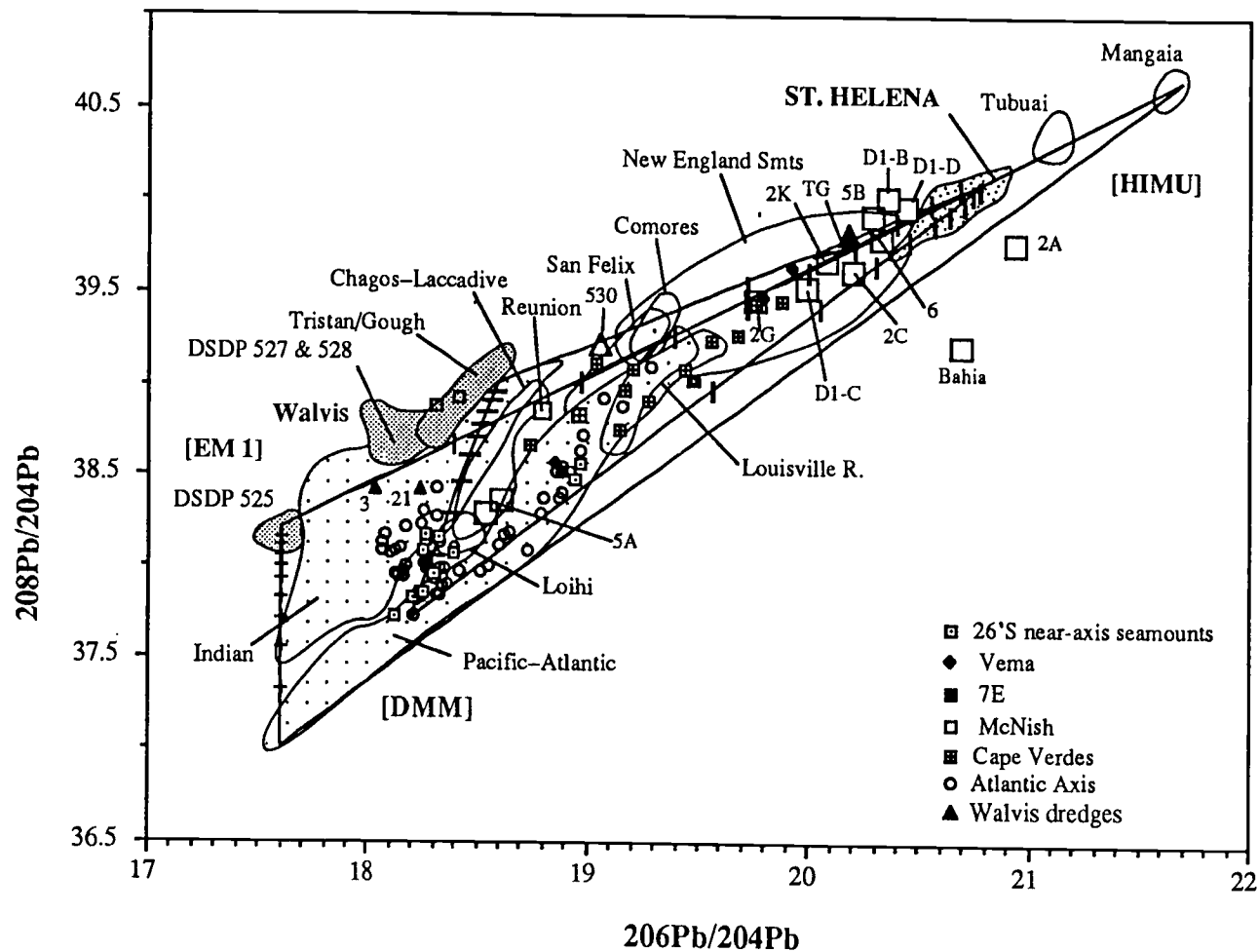
The offset of sample AC-D05A towards the DMM corner in Sr, Nd, and Pb isotopic space (similar in composition to Loihi Seamount) can be interpreted in terms of mixing between DMM and the HIMU-EM 1 mixing continuum. Following Zindler and Hart [1986] and Figure IV.3 we consider therefore the implications of three component mixing (i.e. HIMU, EM 1, and DMM,) in the generation of the isotopic variability of South Atlantic hot spot lavas.

EM 1 Heterogeneity

The isotopic composition of the EM 1 mantle component is defined by samples from a transect across a ~79 Ma region of the Walvis Ridge (DSDP Sites 525, 527, and 528, Richardson et al., 1982], and by the 0 to ~1 Ma islands of Tristan da Cunha and Gough [Le Roex, 1985; and 1990; Chapter III] (Figure IV.2). The EM 1 component as sampled along the Walvis Ridge is clearly heterogeneous and can be divided into three sub-components 1) DSDP 525, 2) DSDP 527-528, and 3) Tristan-Gough (Figures IV.4 to IV.7). DSDP 525 is characterized by having the lowest $^{206}Pb/^{204}Pb$, $^{207}Pb/^{204}Pb$, $^{208}Pb/^{204}Pb$, and $^{143}Nd/^{144}Nd$ ratios. The possibility that the pristine end-member mantle composition of EM 1 is not actually sampled by the composition of Walvis Ridge lavas cannot, however, be ruled out (e.g. Figure IV.3).

HIMU–EM 1 Continuum

As noted previously, the St. Helena-Pernambuco-Bahia Seamount data fall along a calculated hyperbolic mixing curve between HIMU and EM 1 components in Nd-Pb space (Figure IV.5). The isotopic ratios of Gough and DSDP 527 and 528 arrays also fall along this calculated mixing hyperbola. The proportion of EM 1 mixing with HIMU to form the St. Helena-Bahia-Pernambuco Seamount lavas varies between 0 and 60% (assuming that DSDP 525 represents the EM~1 component). EM 1 may well have mixed with HIMU to form the lavas on St. Helena island; if this notion is correct then approximately between 30 and 0 % EM 1 has mixed with HIMU during formation of this island. The mixing proportions discussed above are taken from mixing curves in Nd-Pb space (Figure IV.5), and are similar to those determined in Pb-Pb and Sr-Pb space (Figures IV.6 and IV.7).

Mixing between HIMU–EM 1 continuum and DMM

St. Helena Seamount dredge sample AC-05A is offset in Sr, Nd, and Pb isotopic space towards the DMM end-member, suggesting mixing between HIMU-EM 1 continuum and DMM. This mixing relationship could account for the fact that isotopic arrays for Atlantic-Pacific and Indian MORB, the Louisville Ridge (South Pacific) [Cheng et al., 1987], and the Chagos-Laccadive Ridge (Indian Ocean) [White et al., 1990] are arrayed between the HIMU-EM 1 continuum and DMM.

Table IV.3. Compositions of mantle component end-members used in mixing calculations

	Sr (ppm)	Nd (ppm)	Pb (ppm)	$^{87}Sr/^{86}Sr$	$^{143}Nd/^{144}Nd$	$^{206}Pb/^{204}Pb$	$^{208}Pb/^{204}Pb$
HIMU (St. Helena)	120	6.5	0.4	0.7029	0.51288	20.8	40.1
HIMU (Mangaia)	120	6.5	0.4	0.7028	0.51282	21.7	40.7
DMM (depleted)	12	0.65	0.04	0.7023	0.51326	17.6	37.0
DMM (enriched)	12	0.65	0.04	0.7025	0.51315	18.2	37.7
EM 1 (Tristan)	18.2	1	0.135	0.7051	0.51252	18.6	39.0
EM 1 (DSDP 525)	18.2	1	0.135	0.7050	0.51235	17.6	38.2

Sr, Nd, and Pb concentrations are from Zindler and Hart (1986)

The isotopic array for the St. Helena region intersects the HIMU-EM 1 continuum at a mixture of ~75% EM 1 and 25% HIMU, so supporting our conclusion that both HIMU and EM 1 components are both available to the St. Helena hot spot source (Figure IV.6). This assumes that the spreading axis at the latitudes of the islands of St. Helena and Tristan da Cunha is indeed being partially supplied by plume material from the St. Helena and Walvis hot spots [e.g. Schilling, 1985; Hanan et al., 1986, and Graham et al., unpublished manuscript].

Seamounts located close to the South Atlantic spreading-axis at 26°S are predominantly EM 1-like in composition [Castillo and Batiza, 1989], with involvement of HIMU also apparent in this isotopic array (Figures IV.4 to IV.7). Such near-ridge seamounts better preserve evidence for mantle heterogeneity in their region than in the case of better homogenized on-axis lavas [Castillo and Batiza, 1989]. Most pertinent to our discussion is the apparent co-existence of St. Helena and Walvis components in the same mantle source region.

Variability in lava compositions across the broad Walvis hot spot

The isotopic composition of a volcanic sample (DSDP Site 530A) drilled from seafloor located ~20 km to the north of the northeastern end of the Walvis Ridge (Figure IV.2) indicates that basalts erupted at the outer regions of the Walvis hot spot were derived from a mixture of HIMU and EM 1 components (Table IV.2; Figure IV.6); some DMM was also incorporated (Figure IV.7). Thus, all three components were present in the Walvis hot spot source during the Cretaceous.

A simple explanation for isotopic variability in melts generated by the Walvis hot spot is that HIMU melts at lower temperatures than does EM 1 (Figure IV.8). While HIMU and EM 1 are no doubt mineralogically very similar if, for example, HIMU has a higher volatile content then it would melt at lower temperatures. Unfortunately, differences between the solidus behavior of HIMU, EM 1, and DMM mantles are poorly understood.

Cape Verdes analog

Gerlach et al. [1988] showed that lavas from islands on the northern side of the Cape Verde Archipelago are predominantly HIMU, whereas lavas from Cape Verde islands ~300 km to the south contain mostly EM 1 component (Figures IV.4 to IV.7); they interpreted this zonation in lava composition in terms of a ≥ 300 km diameter hot spot. Of particular relevance to this study is their observation that HIMU lavas are related to lower temperature melting than is the case of EM 1 lavas. Chaffey et al. [1989] showed an increase in the signature of the HIMU component with time in erupted lavas on the island of St. Helena, which they interpreted in terms of preferential melting of the HIMU component as the supply of heat to the base of the lithosphere diminished.

On the basis of heat flow, bathymetry and the geoid data across the Cape Verde Islands, Courtney and White [1986] developed a convection model in which a relatively narrow column,

about 150-200 km wide, of abnormally high temperature mantle causes dynamic uplift of a swell with an elevation above surrounding seafloor of 1000-2000 m at the center (Figure IV.9). In this model, the bulk of the upwelling plume material is deflected laterally by the lithosphere and spreads out to form a 1000-2000 km diameter mushroom-shaped head with temperatures typically 100-200°C above surrounding asthenosphere. A smaller cool return flow is descending all around the outer edges of this large zone of hot mantle. The volume and composition of magma generated by adiabatic decompression over such a large hot spot is controlled by the temperature regime and circulation of the thermal plume in the asthenosphere and its interaction with the overlying lithosphere [White, 1990, White and McKenzie, 1989; and McKenzie and Bickle, 1988].

Hot spot lava heterogeneity and variable plume temperature

The following observations can now be made about Atlantic hot spot volcanism:

(1) EM 1 and HIMU components are available to the Walvis and St. Helena hot spot sources, and probably to the majority of hot spot sources,

(2) the outer edge of a broad Walvis plume is derived from a mixture of HIMU, EM 1, and DMM components,

(3) the amount of melt delivered by the Walvis hot spot is far greater than that of the St. Helena hot spot, as indicated by the relative volumes of their respective volcanic traces. Following White [1990], White and McKenzie [1989], and McKenzie and Bickle [1986], we interpret this in terms of the Walvis plume being hotter and more vigorous than the St. Helena plume.

We now speculate that these observations can be combined in a dynamic process to explain variability of HIMU, EM 1, and DMM in hot spot-generated lavas:

(1) the Walvis plume delivers large amounts of EM 1-like melt to the center of its associated hot spot trace as it is hottest at that point; the outer region of this hot spot is cooler and consequently produces less melt that is more HIMU-like.

(2) the St. Helena plume generates much less melt than in the case of the Walvis plume that is at different times/places a mix of EM 1, HIMU, and DMM, or is predominantly HIMU-like, due to the fact that it is cooler than the Walvis plume.

Supporting evidence for the viability of this model is that 7°E and Vema seamounts, located ~550 and 700 km to the south of the Walvis Ridge, respectively (Figure IV.2), are both predominantly HIMU-like in composition [Le Roex et al., unpublished manuscript], although significant amounts of EM 1 component are also evident (Figures IV.4 to IV.7). The relatively small sizes of these seamounts indicate that they were/are probably associated with cool plumes.

Figure IV.8. Schematic profile of mantle pressure versus temperature (after Klein and Langmuir, 1987). Hot plumes intersect their solidii at greater pressures, depths, and temperatures than cooler plumes, so producing more melt. This schematic assumes that HIMU melts at lower temperatures and pressures; in the case of very cool plumes EM 1 may not intersect its solidus. Thus, the hotter a plume the deeper that EM 1 (and HIMU) will start melting so increasing the possibility that the EM 1 component can dominate the composition of hot spot lavas, and/or the reservoir of HIMU in a particular volume of plume material possible becomes exhausted, as indicated by dashed lines.

lower depth of melting
so more melt produced ⟶

more EM 1-like lavas? ⟶

St. Helena   Walvis

EM 1
HIMU
EM 1
HIMU

Temperature ⟶

Pressure

?

?

cool EM 1-HIMU plume

hot EM 1-HIMU plume

EM 1 Solidus

HIMU Solidus
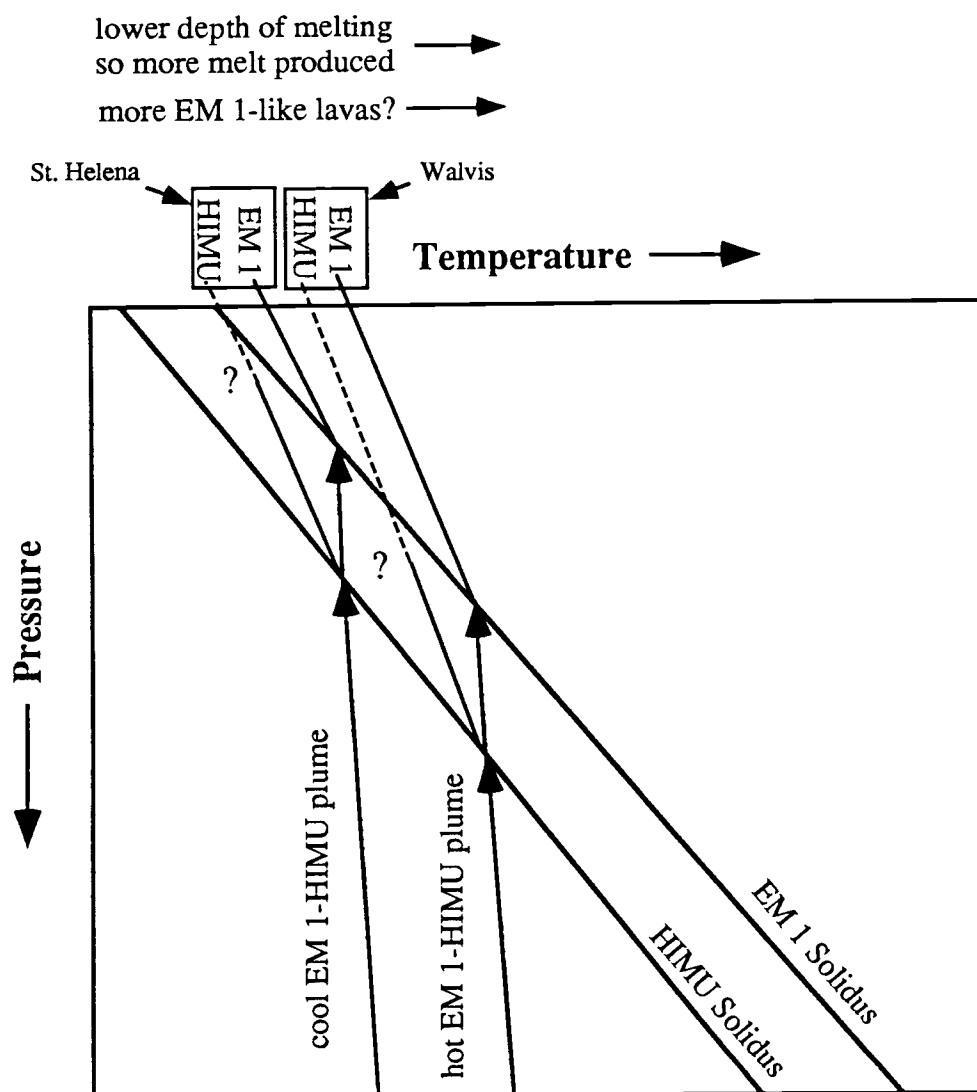
Figure IV.8

Figure IV.9. Cartoons illustrating how the proportions of HIMU, EM 1 and DMM in the lavas erupting across a hot spot might, located on a slow moving lithospheric plate, vary according to the temperature and composition of its associated plume. Theoretical temperature variations seen in cross-section through the Cape Verdes swell are from the best fitting axisymmetric convection model of Courtney and White [1986], adapted from White and McKenzie [1989]. Temperature anomalies with respect to the mean asthenosphere temperature are labeled in degrees Celsius. The narrow central rising plume, deflected laterally by the overlying plate, supplies and forms a broad mushroom-shaped head of hot material, as indicated by arrows.

HIMU-EM 1 Plume

more plume melting

HIMU <—   EM 1   —> HIMU

EM 1 and HIMU solidii
are at greater depths

km

DMM   DMM

500 km

Hot EM 1–HIMU Plume
[e.g. Walvis]

less plume melting

HIMU <—   HIMU (and EM 1)   —> HIMU

EM 1 and HIMU solidii
are at shallower depths

km

DMM   DMM

Cool EM 1–HIMU Plume
[e.g. St. Helena]

Figure IV.9a

EM 1 Plume

more plume melting

HIMU <—   EM 1   —> HIMU

0

HIMU?

-100   100   >300 ?

200
km

DMM and streaks of HIMU ?   ? DMM and streaks of HIMU

?   ?

400   ?   ?

?   ?

600

EM 1 and HIMU solidii
are at greater depths

Hot EM 1 Plume [e.g. Walvis]
500 km   HIMU entrained into core

less plume melting

HIMU <—   HIMU and EM 1   —> HIMU

0

HIMU?

-100   100   300

200
km

DMM and streaks of HIMU ?   ? DMM and streaks of HIMU

?   ?

400   ?   ?

?   ?

600

EM 1 and HIMU solidii
are at shallower depths

Cool EM 1 Plume [e.g. St. Helena]
HIMU entrained into core

Figure IV.9b

HIMU Plume

Figure IV.9c

Source compositions and variable plume temperature

We now consider three possibilities as to how EM 1 and HIMU might be made available to both the St. Helena and Walvis hot spot sources (Figure IV.9a IV.9c). The most uncomplicated explanation for the coexistence of EM 1 and HIMU components in St. Helena and Wal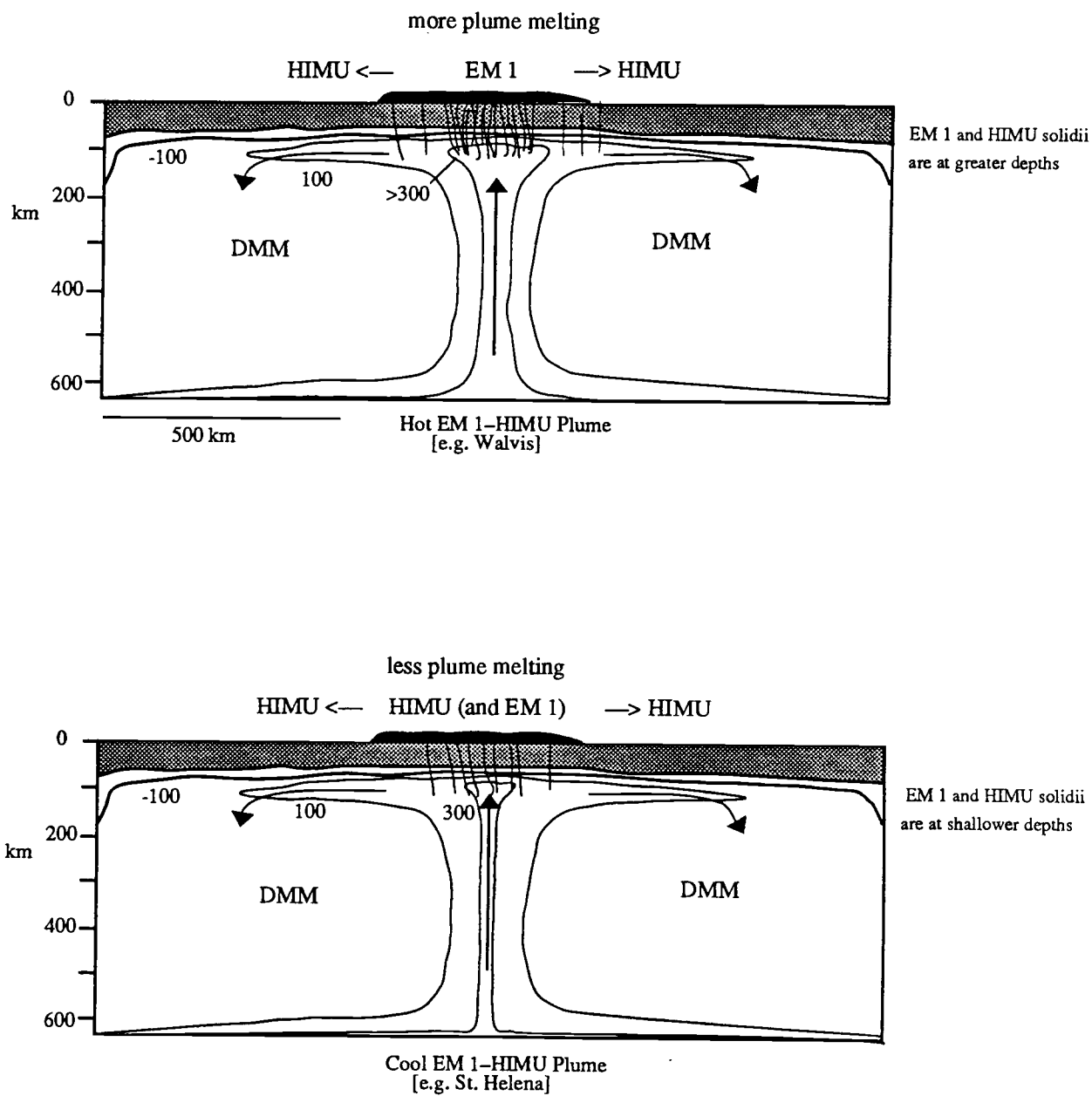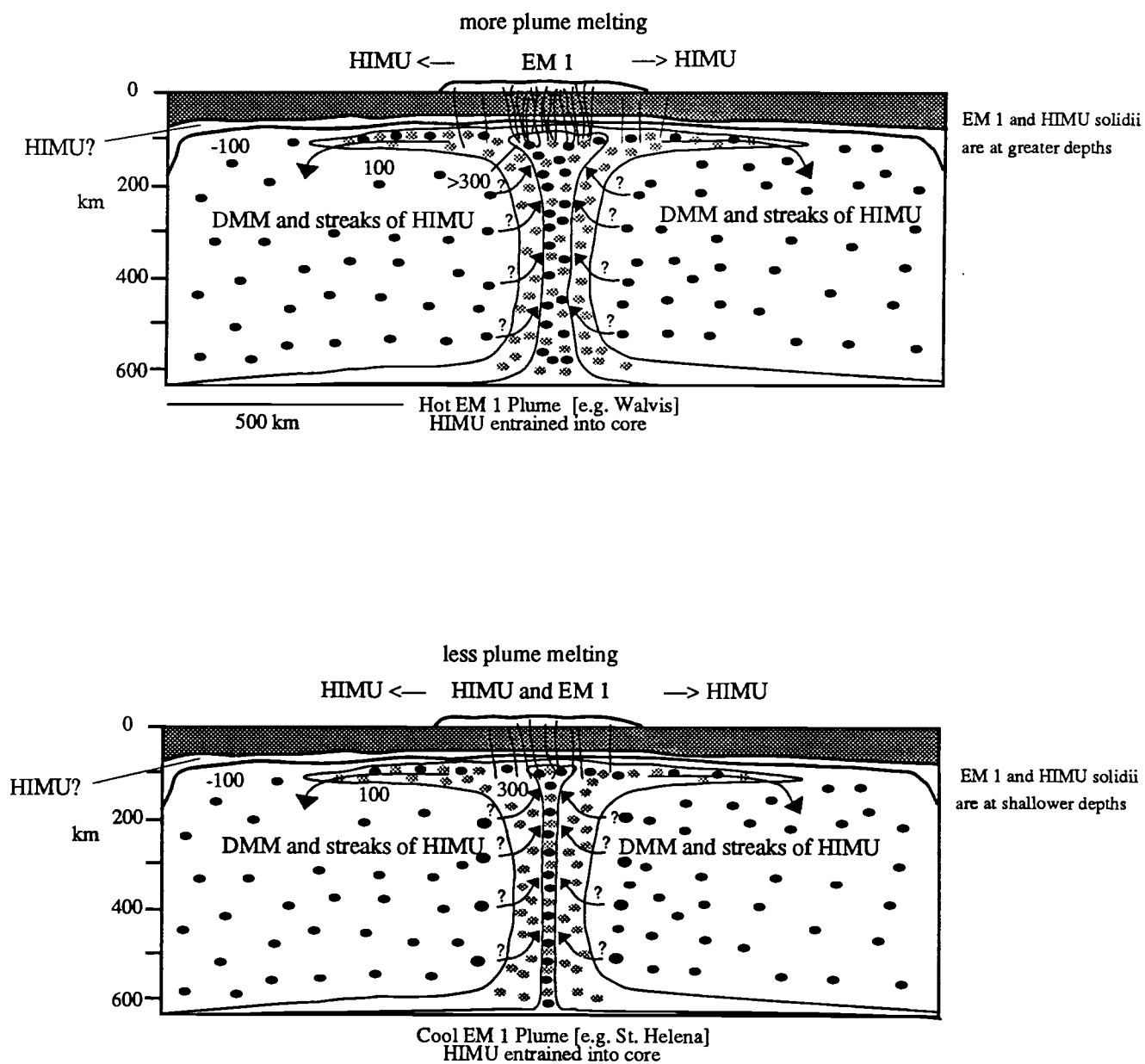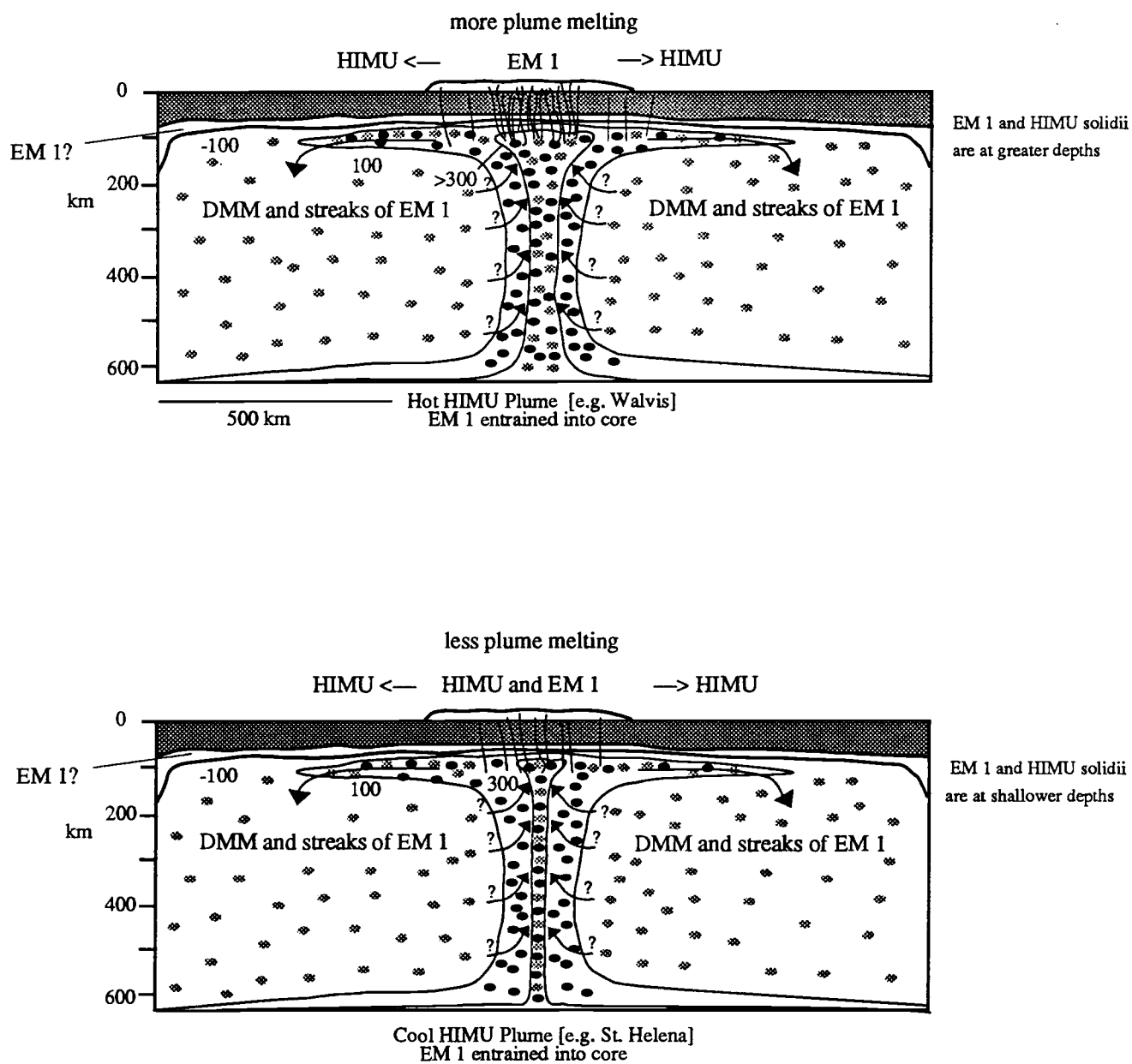vis hot spot lavas is that both components are present in plumes as they rise from the lower mantle (Figure IV.9a). Such plumes could be tapping primitive, EM 1 regions of the lower mantle, to which has been added HIMU mantle, derived from subducted oceanic or continental crust. An alternative explanation is that EM 1 and HIMU mantles are both derived from recycled components subducted into the lower mantle [e.g., Staudigel et al., 1991, following Anderson, 1982].

Assuming that HIMU mantle melts at lower temperatures than EM 1 mantle, the hotter a plume the earlier (i.e., deeper) decompression melting begins, favoring the production of an EM 1 hot spot trace, at least directly above the rising plume (Figure IV.8). This scenario would be particularly favored if the supply of HIMU in a particular volume of plume mantle becomes exhausted at a stage when EM 1 is still melting out of the plume. A cool EM 1–HIMU plume such as St. Helena or Cape Verdes produces less melt at shallower depths, resulting in the eruption of lavas ranging in composition from HIMU to a HIMU–EM 1 mixture. The HIMU component present in DSDP Site 530A lava can therefore be explained similarly in terms of decompression melting along a spreading-axis of cooler plume mantle, tapped from the outer regions of the Walvis hot spot.

Alternatively Atlantic plumes could rise from the lower mantle as either EM 1 (Figure IV.9b) or HIMU (Figure IV.9c) diapirs, with streaks of HIMU and EM 1, respectively, being entrained from the upper mantle into their cores [e.g., Griffiths and Campbell, 1990] or, possibly, to their outer edges. If either HIMU or EM 1 component is trapped in oceanic lithosphere, it might be mobilized by an EM 1 or HIMU plume, respectively. Entrainment of HIMU or EM 1 must also result in the incorporation of DMM. This more refractory, higher temperature melting component, however, probably does not melt out of the plume, except maybe in the case of a potentially very high temperature plume such as Hawaii. A difficulty with the concept of entrainment into the outer edges (as opposed to entrainment into the core) of the rising plume is that the deflected flow of plume material away from the central plume should also transport incorporated components away from the zone of plume melting (Figure IV.9). Another problem with the incorporation of either EM 1 or HIMU into a plume is that the mantle and lithosphere through which plumes ascend may become depleted in streaks or blobs of HIMU or EM 1; renewal of the HIMU or EM 1 sources in the upper mantle might, however, occur as a result of upper mantle flow. The fact that EM 1 is evident in the Pacific Basin, far removed from rifted margins may argue against a lithospheric reservoir for this component, assuming that it originates from delamination of sub-continental mantle during continental rifting [Hawkesworth, 1986].

Further evaluation of the model presented here awaits the systematic documentation of the relationship, if any, between the temperature of plumes, the isotopic compositions of their associated hot spot lavas, and the melting behavior of EM 1, HIMU and (DMM).

CONCLUSIONS

1) Sr, Nd, and Pb isotopic variability of St. Helena-Bahia-Pernambuco Seamounts indicates the existence of a mixing continuum between HIMU and EM 1 components, and for mixing between this array and DMM.

2) HIMU, EM 1 and DMM sources are available to both the St. Helena and Walvis hot spot sources.

3) Variability in plume temperature could play a significant role in controlling the isotopic composition of hot spot lavas, leading to the association of predominantly EM 1-like lavas with hot, vigorous plumes and, conversely, predominantly more HIMU-like lavas with cooler, less vigorous plumes.

REFERENCES

Allegre, C. J., and D. L. Turcotte, Geodynamic mixing in the mesosphere boundary layer and the origin of oceanic islands, Geophys. Res. Lett. 12, 207-210, 1985.

Anderson, D. L., Hot spots, polar wander, Mesozoic convection and the geoid, Nature, 297, 391-393, 1982.

Bienvenu, P., H. Bougault, J. L. Joron, M. Treuil, and L. Dmitriev, MORB alteration: Rare-earth element/non-rare-earth hygromagmaphile element fractionation, Chemical Geology, 82, 1-14, 1990.

Cande, S. C., J. L. LaBrecque, R. L. Larson, W. C. Pitmann III, X. Golovchenko, and W. F. Haxby, Magnetic Lineations of the World's Ocean Basins (map). Scale: approximately 1:27,400,000 at the equator, American association of Petroleum Geologists, Tulsa, Okla., 1989.

Castillo, P., The Dupal anomaly as a trace of the upwelling lower mantle, Nature, 336, 667-670, 1988.

Castillo, P., and R. Batiza, Strontium, neodymium and lead isotope constraints on near-ridge seamount production beneath the South Atlantic, Nature, 342, 262-265, 1989.

Chapman, H. J., E. T. C. Spooner and J. D. Smewing, $^{87}Sr/^{86}Sr$ enrichment of ophiolitic rocks from Troodos, Cyprus indicates seawater interaction, EOS 56, 1074, 1975.

Chaffey, D. J., R. A. Cliff, and B. M. Wilson, Characterization of the St. Helena Magma source, in A. D. Saunders and M. J. Norry (eds.), Magmatism in the ocean basins, Geological Society Special Publication No. 42, 257-276, 1989.

Cheng, Q., K.-H. Park, J. D. Macdougall, A. Zindler, G. W. Lugmair, H. Staudigel, J. Hawkins, and P. Lonsdale, Isotopic evidence for a hotspot origin of the Louisville Seamount Chain, in Seamounts, Islands, and Atolls, (eds. B. H. Keating, P. Fryer, R. Batiza, and G. W. Boehlert), Geophysical Monograph 43, American Geophysical Union, Washington, D.C.,1987.

Cherkis, N. Z., H. S. Fleming, and J. M. Brozena, Bathymetry of the South Atlantic Ocean-3°S to 40°S, Map and Chart Ser. MCH-069, Geol. Soc. of Am., Boulder, Colo., 1989.

Courtney, R. S., and R. S. White, Anomalous heat flow and geoid across the Cape Verde Rise: evidence for dynamic support from a thermal plume in the mantle, Geophys. J. R. ast. Soc., 87, 815-867, 1986.

Davies, G. F., Ocean bathymetry and mantle convection: 1. Large-scale flow and hotspots, J. Geophys. Res., 93, 10, 467-10, 480, 1988.

Dosso, L., H. Bougault, P. Beuzart, J. -Y. Calvez, and J. -L. Joron, The geochemical structure of the South-East Indian Ridge, Earth Planet. Sci. Letts., 88, 47-59, 1988.

Dupre, B., and C. J. Allegre, Pb-Sr isotope variation in Indian Ocean basalts and mixing phenomena, Nature, 303, 1983a.

Dupre, B., and C. J. Allegre, Pb-Sr-Nd isotopic correlation and the chemistry of the North Atlantic mantle, Nature, 286, 17-22, 1980b.

Gerlach, D. C., S. R. Hart, V. W. J. Morales, and C. Palacios, Mantle heterogeneity beneath the Nazca plate: San Felix and Juan Fernandez islands, Nature, 322, 165-169, 1986.

Gerlach, D. C., R. A. Cliff, G. R. Davies, M. Norry, and N. Hodgson, Magma sources of the Cape Verdes archipelago: Isotopic and trace element constraints, Geochim. et Cosmochim. Acta, 52, 2979-2992, 1988.

Griffiths, R. W., and I. H. Campbell, Stirring and structure in mantle starting plumes, Earth and Planet. Sci., Letts., 99, 66-78, 1990.

Hamelin, B., B. Dupre, and C. J. Allegre, Lead-strontium isotopic variations along the East Pacific Rise and the Mid-Atlantic Ridge: a comparative study, Earth Planet. Sci. Letts., 67, 340-350, 1984.

Hamelin, B., B. Dupre, and C. J. Allegre, Pb-Sr-Nd isotopic data of Indian Ocean ridges: new evidence of large-scale mapping of mantle heterogeneities, Earth Planet. Sci. Letts., 76, 288-298, 1985.

Hamelin, B., and C. J. Allegre, Large-scale regional units in the depleted upper mantle revealed by an isotope study of the South-West Indian Ridge, Nature, 315, 196-199, 1985.

Hanan, B. B., R. Kingsley, and J.-G. Schilling, Pb isotope evidence in the South Atlantic for migrating ridge-hotspot interactions, Nature, 322, 137-144, 1986.

Hart, S. R., K, Rb, Cs, Sr, and Ba contents and Sr isotope ratios of ocean floor basalts, Philos. Trans. R. Soc. London, Ser. A, 268: 573-587, 1971.

Hart, S. R., A large scale isotope anomaly in the Southern Hemisphere mantle, Nature 309, 753-757, 1984.

Hart, S. R., D. C. Gerlach, and W. M. White, A possible new Sr-Nd-Pb mantle array and consequences for mantle mixing, Geochemica et Cosmochimica Acta Vol. 50, 1551-1557, 1986.

Hawkesworth, C. J., M. S. M. Mantovani, P. N. Taylor, and Z. Palacz, Evidence from the Parana of South Brazil for a continental contribution to Dupal basalts, Nature, 356-359, 1986.

Hofmann, A. W., and W. M. White, Mantle plumes from ancient oceanic crust, earth Planet. Sci. Lett., 57, 421-436, 1982.

Klein, E. M., and C. H. Langmuir, Global correlations of ocean ridge basalt chemistry with axial depth and crustal thickness, J. Geophys. Res., 92, 8089-8155, 1987.

Le Roex, A. P., Geochemistry, mineralogy and magmatic evolution of the basaltic and Trachytic lavas from Gough Island, South Atlantic, J. Petrology, 149-186, 1985.

Le Roex, A. P., Tristan da Cunha, South Atlantic: Geochemistry and petrogenesis of a basanite-phonolite lava series, J. Petrology, 31, 779-812, 1990.

Ludden, J. N., and G. Thompson, An evaluation of the behavior of the rare earth elements during the weathering of sea-floor basalt, Earth and Planet. Sci. Letts., 43, 85-92, 1979.

Mahony, J. J., J. H. Natland, W. M. White, R. Poreda, S. H. Bloomer, R. L. Fisher, and A. N. Baxter, Isotopic and geochemical provinces of the Western Indian Ocean spreading centers, J. Geophys. Res., 94, 4033-4052, 1989.

McKenzie, D, and M. J. Bickle, The volume and composition of melt generated by extension of the lithosphere, J. Petrol., 29, 625-679, 1988.

Michard, A., F. Albarede, G. Michard, J.-F. Minster, and J. L. Charlou, Rare-earth elements and uranium in high-temperature solutions from East Pacific Rise hydrothermal vent field (13°N), Nature, 303, 795-797, 1983.

Michard, A., R. Montigny, and R. Schlich, Geochemistry of the mantle beneath the Rodriguez Triple Junction and the South-East Indian Ridge, Earth Planet. Sci. Letts., 104-114, 1986.

O'Connor, J. M., On the trail of the St. Helena hotspot: Implications for reconstructing African and and South American plate motions (Abstract), Eos Trans. AGU, 70, 1135, 1989.

Palacz, Z. A., and A. D. Saunders, Coupled trace element and isotope enrichment in the Cook-Austral-Samoa islands, southwest Pacific, Earth Planet. Sci. Letts., 79, 270-280, 1986.

Price, R. C., A. K. Kennedy, M. Riggs-Sneeringer, and F. A. Frey, Geochemistry of basalts from the Indian Ocean triple junction: implications for the generation and evolution of Indian Ocean ridge basalts, Earth Planet. Sci. Letts., 78, 379-396, 1986.

Richardson, S. H., A. J. Erlank, A. R. Duncan, and D. L. Reid, Correlated Nd, Sr, and Pb isotope variation in Walvis Ridge basalts and implications for their mantle source, Earth Planet. Sci. Letts., 59, 327-42, 1982.

Schilling, J.-G., Upper mantle heterogeneities and dynamics, Nature, 314, 62-67, 1985.

Sleep, N. H., Hotspots and mantle plumes: Some phenomonology, J. Geophys. Res., 95, 6715-6736, 1990.

Spooner, E. T. C., The strontium isotopic composition of seawater and seawater-oceanic crust interaction, Earth Planet. Sci. Lett., 31, 167-174, 1976.

Staudigel, H. and S. R. Hart, Alteration of basaltic glass: Mechanisms and significance for the oceanic crust-seawater budget, Geochim. Cosmochim. Acta 47, 337-350, 1983.

Staudigel, H., A. Zindler, S. R. Hart, T. Leslie, C.-Y. Chen, and D. Clague, The isotope systematics of a juvenile intraplate volcano: Pb, Nd, and Sr isotope ratios of basalts from Loihi seamount, Hawaii, Earth Planet. Sci. Letts., 69, 13-29, 1984.

Staudigel, H., K.-H. Park, M. Pringle, J. L. Rubenstone, W. H. F. Smith, and A. Zindler, The longevity of the South Pacific isotopic and thermal anomaly, Earth Planet. Sci. Letts., 102, 24-44, 1991.

Sun, S.-S., Lead isotopic study of young volcanic rocks from mid-ocean ridges, ocean islands, and island arcs, Phil. Trans. Roy. Soc. London A297, 409-445, 1980.

Taras, B. D., and S. R. Hart, Geochemical evolution of the New England Seamount Chain: isotopic and trace-element constraints, Chemical Geology, 64, 35-54, 1987.

Tatsumoto, M., D. M. Unruh, P. Stille, and H. Fujimaki, Pb, Sr, and Nd isotopes in oceanic basalts. In Proc. 27th Internat. Geol. Cong. 11, 485-501. Geochemistry and Cosmochemistry, VNU Science Press, 1984.

Vidal, Ph., C. Chauvel, and R. Brousse, Large mantle heterogeneity beneath French Polynesia, Nature, 307, 536-538, 1984.

White, R., and D. McKenzie, Magmatism at rift zones: The generation of volcanic continental margins and flood basalts, J. Geophys. Res., 94, 7685-7729, 1989.

White, R., Evolution of the Reunion Hotspot, (Abstract), Intraplate volcanism. The Reunion hot spot, Institut Physique du Globe, Paris, 12-17 November, 1990.

White, W. M., Sources of oceanic basalts: Radiogenic isotopic evidence, Geology 13, 115-118, 1985.

White, W. M., A. W. Hofmann, H. Puchelt, Isotope geochemistry of the Pacific Mid-Ocean Ridge basalt, J. Geophys. Res., 92, 4881-4893, 1987.

White, W. M., M. M. Cheatham, and R. A. Duncan, Isotope geochemistry of Leg 115 basalts and inferences on the history of the Reunion mantle plume, Proceedings of the Ocean Drilling Program, Scientific Results, Vol 115, 53-61, 1990.

Zindler, A, E. Jagoutz, and S. Goldstein, Nd, Sr, and Pb isotopic systematics in a three-component mantle: a new perspective, Nature 298, 519-523, 1982.

Zindler, A., and S. Hart., Chemical Geodynamics, Ann. Rev. Earth Planet. Sci., 14, 493-571, 1986.

V. CONCLUSIONS OF THESIS

The following conclusions have been drawn over the course of this study of South Atlantic hot spot volcanism:

1) The St. Helena and Walvis hot spots are both broad and diffuse (i.e. greater than 500 km in diameter), far larger than estimated previously on the basis of the sizes of individual ocean islands such as St. Helena or Tristan da Cunha.

2) Two rotation poles suffice to reconstruct the direction of African plate motion over fixed St. Helena, Walvis, and Reunion hot spots (since the South Atlantic began to open) such that predicted hot spot traces closely match their respective volcanic traces. This model incorporates the assumption that the Walvis and St. Helena hot spots are greater than 500 km in diameter.

3) African plate velocity appears to have decreased from ~0.25 deg/m.y. to ~0.11 deg/m.y. between ~31 and 0 Ma.

4) A transition from on-spreading-axis to intraplate hot spot volcanism occurred between ~80 and 70 Ma along the St. Helena Chain and the Walvis Ridge, in response to a westward migration of the South Atlantic spreading-axis away from the St. Helena and Walvis hot spots.

5) Sr, Nd, and Pb isotopic variability in rocks dredged from the St. Helena-Bahia-Pernambuco Seamounts and the island of St. Helena define a mixing continuum between HIMU and EM 1 mantle components, and for mixing between this continuum and DMM.

6) Lava drilled from Cretaceous seafloor to the north of the eastern end of the Walvis Ridge was derived from a mixture of EM 1, HIMU, and DMM mantle components.

7) Thus, EM 1, HIMU (and DMM) components are available to both the St. Helena and Walvis hot spot sources. This supports the suggestion that these components are available to the majority of hot spot systems.

8) Variability in plume temperature could play a significant role in controlling the isotopic composition of hot spot lavas, leading to the association of predominantly EM 1-like lavas with hot,

vigorous plumes and, conversely, predominantly more HIMU-like lavas with cooler, less vigorous plumes.

REFERENCES

Allegre, C. J., and D. L. Turcotte, Geodynamic mixing in the mesosphere boundary layer and the origin of oceanic islands, Geophys. Res. Lett. 12, 207-210, 1985.

Almeida, F. F. M., Geologia e petrologia do argquipelago de Fernando do Noronha, Monogr., 13, Div. Geol. Min. Dep. Nac. Prod. Mineral., Rio de Janeiro, 1958.

Amaral, G., U. G. Cordani, K. Kawashita, and J. H. Reynolds, Potassium-argon dates of basaltic rocks from Southern Brazil, Geochim. Cosmochim. Acta, 30, 159-189, 1966.

Anderson, D. L., Hot spots, polar wander, Mesozoic convection and the geoid, Nature, 297, 391-393, 1982.

Aumento, F., Vesicularity of mid ocean pillow lavas, Can. J. Earth Sci., 8, 1315-1319, 1971.

Austin, J. A., Jr., and E. Uchupi, Continental-oceanic crustal transition off Southwest Africa, Am. Assoc. Pet. Geol. Bull., 66, 1328-1347, 1982.

Backman, J., R. A. Duncan et al., Proc. Ocean Drill. Program, Initial Rep., 115, 1085 pp., 1988.

Baker, B. H., and J. A. Miller, Geology and geochronology of the Seychelles Islands and structure of the floor of the Arabian Sea, Nature, 199, 346, 1963.

Baker, I., N. H. Gale, and J. Simons, Geochronology of the St. Helena volcanoes, Nature, 215, 1451-1454, 1967.

Barker, P. E., Tectonic evolution and subsidence history of the Rio Grande Rise, Initial Rep. Deep Sea Drill. Proj., 72, 953-976, 1984.

Barker, P. E., I. G. Gass, P. G. Harris, and R. W. LeMaitre, The volcanological report of the Royal Society expedition to Tristan da Cunha, Philos. Trans. R. Soc. London., Ser. A, 256, 439-578, 1964.

Bienvenu, P., H. Bougault, J. L. Joron, M. Treuil, and L. Dmitriev, MORB alteration: Rare-earth element/non-rare-earth hygromagmaphile element fractionation, Chemical Geology, 82, 1-14, 1990.

Blow, W. H., Deep Sea Drilling Project, Leg 3, Foraminifera from selected samples, Initial Rep. Deep Sea Drill. Proj., 3, 629-661, 1970.

Bolli, H. M., W. B. F. Ryan et al., Walvis Ridge-sites 362 and 363, Initial Rep. Deep Sea Drill. Proj., 40, 183-356, 1978.

Brereton, N. R., Corrections for interfering isotopes in the ^{40}Ar-^{39}Ar dating method, Earth Planet. Sci. Lett., 8, 427-433, 1970.

Brozena, J. M., and R. S. White, Ridge jumps and propagations in the South Atlantic, Nature, 348, 149-152, 1990.

Bryan, W. B, and R. A. Duncan., Age and provenance of clastic horizons from hole 516F, Initial Rep. Deep Sea Drill. Proj., 72, 475-477, 1983.

Bukry, D., and M. N. Bramlette, Coccolith age determinations leg 3, Deep Sea Drilling Project, Initial Rep. Deep Sea Drill. Proj., 3, 589-612, 1970.

Bulot, A., M. Diament, M. G. Kogan, and J. Dubois, Isostasy of aseismic tectonic units in the South Atlantic Ocean and geodynamic implications, Earth Planet. Sci. Lett., 70, 346-354, 1984.

Cande, S. C., and P. D. Rabinowitz, Mesozoic sea floor spreading bordering conjugate continental margins of Angola and Brazil, Proc. Annu. Offshore Technol. Conf., 3, 1769-1776, 1978.

Cande, S. C., and P. D. Rabinowitz, Magnetic anomalies of the continental margin of Brazil, Offshore Brazil Map Ser, American Association of Petroleum Geologists, Tulsa, Okla., 1979.

Cande, S. C., J. L. LaBrecque, and W.B. Haxby, Plate kinematics of the South Atlantic: Chron 34 to present, J. Geophys. Res., 93, 13,479-13,492, 1988.

Cande, S. C., J. L. LaBrecque, R. L. Larson, W. C. Pitmann III, X. Golovchenko, and W. F. Haxby, Magnetic Lineations of the World's Ocean Basins (map). Scale: approximately 1:27,400,000 at the equator, American Association of Petroleum Geologists, Tulsa, Okla., 1989.

Castillo, P., The Dupal anomaly as a trace of the upwelling lower mantle, Nature, 336, 667-670, 1988.

Castillo, P., and R. Batiza, Strontium, neodymium and lead isotope constraints on near-ridge seamount production beneath the South Atlantic, Nature, 342, 262-265, 1989.

Chaffey, D. J., R. A. Cliff, and B. M. Wilson, Characterization of the St. Helena magma source, edited by A. D. Saunders, and M. J. Norry, Magmatism in the Ocean Basins, Spec. Publ. 42, Geol. Soc. of London, pp. 257-276, 1989.

Cheng, Q., K.-H. Park, J. D. Macdougall, A. Zindler, G. W. Lugmair, H. Staudigel, J. Hawkins, and P. Lonsdale, Isotopic evidence for a hotspot origin of the Louisville Seamount Chain, in Seamounts, Islands, and Atolls, (eds. B. H. Keating, P. Fryer, R. Batiza, and G. W. Boehlert), Geophysical Monograph 43, American Geophysical Union, Washington, D.C., 1987.

Chapman, H. J., E. T. C. Spooner and J. D. Smewing, $^{87}Sr/^{86}Sr$ enrichment of ophiolitic rocks from Troodos, Cyprus indicates seawater interaction, EOS 56, 1074, 1975.

Chave, A. D., Lower Paleocene-upper Cretaceous magnetostratigraphy, sites 525, 527, 528, and 529, Initial Rep. Deep Sea Drill. Proj., 74, 525-532, 1984.

Chen, C.-Y., and F. A. Frey, Origin of Hawaiian tholeiite and alkalic basalt, Nature, 302, 785-789, 1983.

Cherkis, N. Z., H. S. Fleming, and J. M. Brozena, Bathymetry of the South Atlantic Ocean-3°S to 40°S, Map and Chart Ser. MCH-069, Geol. Soc. of Am., Boulder, Colo., 1989.

Chevallier, L., and N. Vatin-Perignon, Volcanostructural evolution of Piton des Neiges, Reunion Island, Indian Ocean, Bull. Volcanol., 45, 287-298, 1982.

Ciesielski, P. F., Y. Kristoffersen et al., Proc. Ocean Drill. Program, Initial Rep., 114, 801 pp., 1988.

Clark, D. B., The Tertiary volcanic province of Baffin Bay, Geol. Assoc. Can. Spec. Pap., 16, 445-460, 1977.

Cordani, U. G., Idade do vulcanismo no Oceano Atlantico Sul, Bol. Inst. Geocienc. Astron., Univ. Sao Paulo, 1, 9-75, 1970.

Cordani, U. G., P. L. Sartori, and K. Kawashita, Geoquimica dos isotropes de estroncio e a evolucao da atividade vulcanica na Bacia do Parana, An. Acad. Bras. Cienc., 52, 811-818, 1980.

Courtney, R. S., and R. S. White, Anomalous heat flow and geoid across the Cape Verde Rise: evidence for dynamic support from a thermal plume in the mantle, Geophys. J. R. ast. Soc., 87, 815-867, 1986.

Cox, K. G., The role of mantle plumes in the development of continental drainage patterns, Nature, 342, 873-877, 1989.

Crough, S. T., Mesozoic hot spot epeirogeny in eastern North America, Geology, 9, 2-6, 1981.

Crough, S. T., W. J. Morgan, and R. B. Hargraves, Kimberlites: Their relation to mantle hot spots, Earth Planet. Sci. Lett., 50, 260-274, 1980.

Dalrymple, G. B., and D. A. Clague, Age of the Hawaiian-Emperor Bend, Earth Planet. Sci. Lett., 31, 317-321, 1976.

Dalrymple, G. B., and M. A. Lanphere, Potassium Argon dating: Principles, Techniques, and Application to Geochronology, W. H. Freeman, New York, 258 pp., 1969.

Dalrymple, G. B., and M. A. Lanphere, ^{40}Ar-^{39}Ar technique of K-Ar dating: A comparison with the conventional technique, Earth Planet. Sci. Lett., 12, 300-308, 1971.

Dalrymple, G. B., and J. G. Moore, Argon 40: Excess in submarine pillow basalts from Kilaueau Volcano, Hawaii, Science, 161, 1132-1135, 1968.

Dalrymple, G. B., E. C. Alexander, Jr., M. A. Lanphere, and G. P. Kraker, Irradiation of samples for ^{40}Ar-^{39}Ar dating using the Geological Survey TRIGA reactor, U. S. Geol. Surv. Prof. Pap., 1176, 1981a.

Dalrymple, G. B., M. A. Lanphere, and D. A. Clague, Conventional and ^{40}Ar-^{39}Ar ages of volcanic rocks from Ojin (site 430), Nintoku (site 432), and Suiko (site 433) seamounts and chronology of volcanic propagation along the Hawaiian-Emperor Chain, Initial Rep. Deep Sea Drill. Proj., 55, 659-676, 1981b.

Dalrymple, G. B., M. A. Lanphere, and M. S. Pringle, Correlation diagrams in ^{40}Ar-^{39}Ar dating: Is there a correct choice?, Geophys. Res. Lett., 15, 589-591, 1988.

Davies, G. F., Ocean bathymetry and mantle convection: 1. Large-scale flow and hotspots, J. Geophys. Res., 93, 10, 467-10, 480, 1988.

Deruelle, B., C. Moreau, C. Nkoumbou, R. Kambou, J. Lissom, E. Njonfang, R. T. Ghogomu, and A. Nono, The Cameroon Line: Phanerozoic magmatism and the structural evolution of the African plate, A. B. Kampunzu and R. T. Lubala (eds), Blackie and Sons, London (in press) 1989.

Detrick, R. S, and A. B. Watts., An analysis of isostasy in the world's oceans: Three aseismic ridges, J. Geophys. Res., 84, 3637-3655, 1979.

Diament, M., and J. Goslin, Mechanical and thermal isostasy of submarine plateaus, (abstract), Eos Trans. AGU, 68, 1462, 1987.

Dosso, L., H. Bougault, P. Beuzart, J. -Y. Calvez, and J. -L. Joron, The geochemical structure of the South-East Indian Ridge, Earth Planet. Sci. Letts., 88, 47-59, 1988.

Duncan, R. A., Hot-spots in the southern oceans-An absolute frame of reference for the motion of the Gondwana continents, Tectonophysics, 74, 29-42, 1981.

Duncan, R. A., Age progressive volcanism in the New England Seamounts and the opening of the central Atlantic Ocean, J. Geophys. Res., 89, 9980-9990, 1984.

Duncan, R. A., and R. B. Hargraves, ^{40}Ar-^{39}Ar geochronology of basement ages from the Mascarene Plateau, Chagos Bank, and the Maldives Ridges, in Proc. Ocean Drill. Program Sci. Results, Vol 115, College Station TX (Ocean Drilling Program), 43-51, 1990.

Dupre, B., and C. J. Allegre, Pb-Sr isotope variation in Indian Ocean basalts and mixing phenomena, Nature, 303, 1983a.

Dupre, B., and C. J. Allegre, Pb-Sr-Nd isotopic correlation and the chemistry of the North Atlantic mantle, Nature, 286, 17-22, 1980b.

Dymond, J., Excess Ar in submarine pillow basalts, Bull. Geol. Soc. Am., 181, 1229-1232, 1970.

Emerick, C. M., and R. A. Duncan, Age progressive volcanism in the Comores Archipelago, western Indian Ocean and implications for Somali plate tectonics, Earth Planet. Sci. Lett., 60, 415-428, 1982.

Epp, D., and N. C. Smoot, Distribution of seamounts in the North Atlantic, Nature, 337, 254-257, 1989.

Erlank, A. J., and E. J. D. Kable, The significance of incompatible elements in Mid-Atlantic Ridge basalts from 45°N, with particular reference to Zr/Nb, Contrib. Mineral. Petrol., 54, 281-291, 1976.

Erlank, A. J., J. S. Marsh, A. R. Duncan, R. M. Miller, C. J. Hawkesworth, P. J. Betton, and D. C. Rex, Geochemistry and petrogenisis of the Etendeka volcanic rocks from SWA/Namibia, Spec. Publ. Geol. Soc. S. Afr., 13, 195-245, 1984.

Fitton, J.G., The Cameroon Line, West Africa: a comparison between oceanic and continental alkaline volcanism, Spec. Publs geol. Soc. Lond. 30, 273-291, 1987.

Fleitout, L., C. Dalloubeix, and C. Moriceau, Small-wavelength geoid and topography anomalies in the South Atlantic Ocean: A clue to new hot spot tracks and lithospheric deformation, Geophy. Res. Lett., 16, 637-640, 1989.

Fodor, R. V., K. Keil, J. W. Husler, and E. H. McKee, Petrology and K-Ar age of volcanic tuff and ash from the Walvis Seamount Province, DSDP site 359, leg 39, Initial Rep. Deep Sea Drill., Proj., 39, 525-536, 1977.

Fodor, R. V., C. Corwin, and A. Rosinenberg, Petrology of Serra Geral (Parana) continental flood basalts, southern Brazil: Crustal contamination, source material, and South Atlantic magmatism, Contrib. Mineral. Petrol., 91, 54-65, 1985.

Foland, K. A., and H. Faul, Ages of the White Mountain Intrusives-New Hampshire, Vermont and Maine, U.S.A., Am. J. Sci., 277, 888-904, 1977.

Foland, K. A., L. A. Gilbert, C. A. Sebring, and J.-F. Chen, ^{40}Ar-^{39}Ar ages for plutons of the Monteregian Hills, Quebec: Evidence for a single episode of Cretaceous magmatism, Geol. Soc. Amer. Bull., 97, 966-974, 1986.

Foland, K. A., J.-F. Chen, L. A. Gilbert, and A. W. Hofmann, Nd and Sr isotopic signatures of Mesozoic plutons in northeastern North America, Geology, 16, 684-687, 1988.

Freedman, A. P., Marine geophysical applications of Seasat altimetry and the lithospheric structure of the South Atlantic Ocean, Ph.D. thesis, Mass. Inst. Technol., Cambridge, 1987.

Gartner, S., Coccolith age determinations leg 3, Deep Sea Drilling Project, Initial Rep. Deep Sea Drill. Project, 3, 613-627, 1970.

Gerlach, D. C., S. R. Hart, V. W. J. Morales, and C. Palacios, Mantle heterogeneity beneath the Nazca plate: San Felix and Juan Fernandez islands, Nature, 322, 165-169, 1986.

Gerlach, D. C., R. A. Cliff, G. R. Davies, M. Norry, and N. Hodgson, Magma sources of the Cape Verdes archipelago: Isotopic and trace element constraints, Geochim. et Cosmochim. Acta, 52, 2979-2992, 1988.

Gibert, D., and V. Courtillot, Seasat altimetry and the South Atlantic geoid, 1, Spectral analysis, J. Geophys. Res., 92, 6235-6248, 1987.

Gibert, D., V. Courtillot, and J.-L. Olivet, Seasat altimetry and the South Atlantic geoid, 2, Short-wavelength undulations, J. Geophys. Res., 94, 5545-5559, 1989.

Gilbert, L. A., and K. A. Foland, The Mont St. Hilaire plutonic complex: Occurrence of excess [40]Ar and short intrusion history, Can. J. Earth Sci., 23, 948-958, 1986.

Gillot, P.-Y., and P. Nativel, K-Ar chronology of the ultimate activity of Piton des Neiges, Reunion Island, Indian Ocean, J. Volcanol. Geotherm. Res., 13, 131-146, 1984.

Gillot, P.-Y., and P. Nativel, Eruptive history of Piton de la Fournaise volcano, Reunion Island, Indian Ocean, J. Volcanol. Geotherm. Res., 36, 53-65, 1989.

Griffiths, R. W., The differing effects of compositional and thermal buoyancies on the evolution of mantle diapirs, Phys. Earth Planet. Inter., 43, 261-273, 1986.

Griffiths, R. W., and I. H. Campbell, Stirring and structure in mantle starting plumes, Earth and Planet. Sci., Letts., 99, 66-78, 1990.

Gripp, A. E., and R. G. Gordon, Current plate velocities relative to the hotspots incorporating the Nuvel-1 global plate motion model, Geophys. Res. Letts., 17, 1109-1112, 1990.

Guimaraes, I. P., A. N. Sial, and A. F. Silva Filho, Petrologia e geochimica da provincia alcalina Terciaria Fortaleza, Cera, An. Congr. Bras. Geol., Salvador 2, XXXII, 577-588, 1982.

Halliday, A. N., J. P. Davidson, P. Holden, C. DeWolf, D.-C. Lee, and J. Godfrey Fitton, Trace-element fractionation in plumes and the origin of HIMU mantle beneath the Cameroon Line, Nature, 347, 523-528, 1990.

Hamelin, B., B. Dupre, and C. J. Allegre, Lead-strontium isotopic variations along the East Pacific Rise and the Mid-Atlantic Ridge: a comparative study, Earth Planet. Sci. Letts., 67, 340-350, 1984.

Hamelin, B., B. Dupre, and C. J. Allegre, Pb-Sr-Nd isotopic data of Indian Ocean ridges: new evidence of large-scale mapping of mantle heterogeneities, Earth Planet. Sci. Letts., 76, 288-298, 1985.

Hamelin, B., and C. J. Allegre, Large-scale regional units in the depleted upper mantle revealed by an isotope study of the South-West Indian Ridge, Nature, 315, 196-199, 1985.

Hanan, B. B., R. Kingsley, and J.-G. Schilling, Pb isotope evidence in the South Atlantic for migrating ridge-hotspot interactions, Nature, 322, 137-144, 1986.

Hart, S. R., K, Rb, Cs, Sr, and Ba contents and Sr isotope ratios of ocean floor basalts, Philos. Trans. R. Soc. London, Ser. A, 268: 573-587, 1971.

Hart, S. R., A large scale isotope anomaly in the Southern Hemisphere mantle, Nature 309, 753-757, 1984.

Hart, S. R., D. C. Gerlach, and W. M. White, A possible new Sr-Nd-Pb mantle array and consequences for mantle mixing, Geochemica et Cosmochimica Acta Vol. 50, 1551-1557, 1986.

Hartnady, C. J. H., and A. P. le Roex, Southern Ocean hot spot tracks and the Cenozoic absolute motion of the African, Antarctic, and South American plates, Earth Planet. Sci. Lett., 75, 245-257, 1985.

Hawkesworth, C. J., M. S. M. P. N. Mantovani, P. N. Taylor, and Z. Palacz, Evidence from the Parana of south Brazil for a continental contribution to Dupal basalts, Nature, 322, 356-359, 1986.

Helgason, J., Shifts of the plate boundary in Iceland: Some aspects of Tertiary volcanism, J. Geophys. Res., 90, 10,084-10,092, 1985.

Herz, N., Timing of spreading in the South Atlantic: Information from Brazilian alkalic rocks, Geol. Soc. Am. Bull., 88, 101-112, 1977.

Hofmann, A. W., and W. M. White, Mantle plumes from ancient oceanic crust, earth Planet. Sci. Lett., 57, 421-436, 1982.

Hu, X., Y. L. Wang, and R. A. Schmitt, Geochemistry of sediments on the Rio Grande Rise and the redox evolution of the South Atlantic Ocean, Geochim. Cosmochim. Acta., 52, 201-207, 1988.

Humphris, S. E, and G. Thompson, A geochemical study of rocks from the Walvis Ridge, South Atlantic, Chem. Geol., 36, 253-274, 1982.

Humphris, S. E, and G. Thompson, Petrology and geochemistry of rocks from the Angola Basin adjacent to the Walvis Ridge: Deep Sea Drilling Project leg 75, site 530, Initial Rep. Deep Sea Drill. Proj., 75, 1099-1105, 1983.

Humphris, S. E., G. Thompson, J.-G. Schilling, and R. H. Kingsley, Petrological and geochemical variations along the mid-Atlantic Ridge between 46 S and 32 S; Influence of the Tristan da Cunha mantle plume, Geochim. Cosmochim. Acta, 49, 1445-1464, 1985.

Kent, D. V., and F. M. Gradstein, A Jurassic to recent chronology, in: The Geology of North America: The Western North Atlantic Region, DNAG Ser., vol. M, edited by B. E. Tucholke and P. R. Vogt, pp. 45-50, Geological Society of America, Boulder, Colo., 1986.

Klein, E. M., and C. H. Langmuir, Global correlations of ocean ridge basalt chemistry with axial depth and crustal thickness, J. Geophys. Res., 92, 8089-8155, 1987.

Klitgord, K. D., and H. Schouten, Plate kinematics of the central Atlantic, in: The Geology of North America: The Western North Atlantic Region, DNAG Ser., vol. M, edited by B. E. Tucholke and P. R. Vogt, pp. 351-378, Geological Society of America, Boulder, Colo., 1986.

Kogan, M. G., M. Diament, A. Bulot, and G. Balmino, Thermal isostasy in the South Atlantic Ocean from geoid anomalies, Earth Planet. Sci. Lett., 74, 280-290, 1985.

Kowsmann, R., R. Leyden, and O. Francisconi, Marine seismic investigations, southern Brazil margin, Bull. Am. Assoc. Pet. Geol., 546-557, 1977.

Kumar, N., Origin of "paired" aseismic rises: Ceara and Sierra Leone Rises in the equatorial, and the Rio Grande Rise and Walvis Ridge in the South Atlantic, Mar. Geol., 30, 175-191, 1979.

Kumar, N., and R. W. Embley, Evolution and origin of Cera Rise: An aseismic rise in the western equatorial Atlantic, Geol. Soc. Am. Bull., 88, 683-694, 1977.

Kumar, N., and L. A. P. Gamboa, Evolution of the Sao Paulo Plateau (southeastern Brazilian margin) and implications for the early history of the South Atlantic, Geol. Soc. Am. Bull, 90, 281-293, 1979.

LaBrecque, J. L.(Ed.) South Atlantic Ocean and adjacent continental margin Reg. Atlas Ser., Atlas 13, Ocean Drill. Program, College Station, Tex., 1986.

LaBrecque, J. L., J. Phillips, and J. A. Austin, The crustal age and tectonic fabric at the leg 73 sites, Initial Rep. Deep Sea Drill. Proj., 73, 791-798, 1984.

Ladd, J. W., South Atlantic sea floor spreading and Caribbean tectonics, Ph.D. thesis, 251 pp., Columbia Univ., New York, 1974.

Ladd, J. W., Relative motion of South America with respect to North America and Caribbean tectonics, Geol. Soc. Am. Bull., 87, 969-976, 1976.

Le Roex, A. P., Geochemistry, mineralogy and magmatic evolution of the basaltic and trachytic lavas from Gough Island, South Atlantic, J. Petrol., 26, 149-186, 1985.

Le Roex, A. P., Tristan da Cunha, South Atlantic: Geochemistry and petrogenesis of a basanite-phonolite lava series, J. Petrology, 31, 779-812, 1990.

Le Roex, A. P., M. D. Kurz, and J. M. O'Connor, Geochemical characterization of Vema hotspot and seamount volcanism associated with the Gough hotspot: Implications for mantle heterogeneity beneath the South Atlantic (Abstract), Intraplate volcanism. The Reunion hot spot, Institut Physique du Globe, Paris, 12-17 November, 1990.

Leyden, R., H. Asmus, S. Zembruscki, and G. Bryan, South Atlantic diapir structures, Am. Assoc. Pet. Geol. Bull., 60, 196-212, 1976.

Liu, Y.-G., Chemical element profiles by instrumental neutron activation analysis 2, Representative sediment and basalt samples taken from DSDP 678 m core, site 525A, leg 74, Walvis Ridge, M.S. thesis, Oregon State Univ., Corvallis, 1982.

Liu, Y.-G., and R. A. Schmitt, Chemical profiles in sediment and basalt samples from deep sea drilling project leg 74, hole 525A, Walvis Ridge, Initial Rep. Deep Sea Drill. Proj., 74, 713-730, 1984.

Liu, Y.-G., M. R. U. Miah, and R. A. Schmitt, Cerium: A chemical tracer for paleo-oceanic redox conditions, Geochim Cosmochim Acta, 52, 1361-1371, 1988.

Ludden, J. N., and G. Thompson, An evaluation of the behavior of the rare earth elements during the weathering of sea-floor basalt, Earth and Planet. Sci. Letts., 43, 85-92, 1979.

MacIntyre, R. M., A. P. Dickin, A. E. Fallick, and A. N. Halliday, An isotopic and geochronological study of the younger igneous rocks of the Seychelles, Eos Trans. AGU, 66, 1137, 1985.

Mahony, J. J., J. H. Natland, W. M. White, R. Poreda, S. H. Bloomer, R. L. Fisher, and A. N. Baxter, Isotopic and geochemical provinces of the Western Indian Ocean spreading centers, J. Geophys. Res., 94, 4033-4052, 1989.

Manivit, M., Paleogene and upper Cretaceous nannofossils from Deep Sea Drilling Project, leg 74, Initial Rep. Deep Sea Drill. Proj., 74, 475-499, 1984.

Marsh, J. S., Basalt geochemistry and tectonic discrimination within continental flood basalt provinces, J. Volcanol. Geotherm. Res., 32, 35-49, 1987.

Martin., A. K., C. J. H. Hartnady, and S. Goodlad, A revised fit of South America and South Central Africa, Earth Planet. Sci. Lett., 54, 293-305, 1981.

Mascle, J., and J. D. Phillips, Magnetic quiet zones in the South Atlantic, Nature, 240, 80-84, 1972.

McDougall, I., The geochronology and evolution of the young volcanic island of Reunion (Indian Ocean), Geochim. Cosmochim. Acta, 35, 261-288, 1971.

McDougall, I., and R.A. Duncan, Age progressive volcanism in the Tasmantid Seamounts, Earth Planet. Sci. Lett., 89, 207-220, 1988.

McDougall, I., and T. M. Harrison, Geochronology and Thermochronology by the ^{40}Ar-^{39}Ar Method, 212 pp., Oxford University Press, New York, 1988.

McDougall, I., and C. D. Ollier, Apparent K-Ar ages from Tristan da Cunha, South Atlantic, Geol. Mag., 119, 87-93, 1982.

McDougall, I., and N. R. Ruegg, Potassium-argon dates on the Serra Geral formation of South America, Geochim. Cosmochim. Acta, 30, 191-195, 1966.

McKenzie, D, and M. J. Bickle, The volume and composition of melt generated by extension of the lithosphere, J. Petrol., 29, 625-679, 1988.

Melfi, A. J., Potassium-argon ages for core samples from Southern Brazil, Geochim. Cosmochim. Acta, 31, 1079, 1967.

Melson, W. G., and G. Thompson, Glassy abyssal basalts, Atlantic sea floor near St. Pauls Rocks: Petrography and composition of secondary clay minerals, Bull. Geol. Soc. Am., 84, 703-716, 1973.

Michard, A., F. Albarede, G. Michard, J.-F. Minster, and J. L. Charlou, Rare-earth elements and uranium in high-temperature solutions from East Pacific Rise hydrothermal vent field (13°N), Nature, 303, 795-797, 1983.

Molnar, P., and J. Stock, Relative motions of hot spots in the Pacific, Atlantic and Indian Oceans since late Cretaceous time, Nature, 327, 587-591, 1987.

Moreau, C., J.-M. Regnoult, B. Deruelle, and B. Robineau, A new tectonic model for the Cameroon Line, Central Africa, Tectonophysics, 139, 317-334, 1987.

Morgan, W. J., Convection plumes in the lower mantle, Nature, 230, 42-43, 1971.

Morgan, W. J., Deep mantle convection: Plumes and plate motions, Am. Assoc. Pet. Geol. Bull., 56, 203-213, 1972.

Morgan, W. J., Hot-spot tracks and the opening of the Atlantic and Indian Oceans, in The Sea, vol. 7, pp. 443-488, Wiley Interscience, New York, 1981.

Morgan, W. J., Hot-spot tracks and the early rifting of the Atlantic, Tectonophysics, 94, 123-139, 1983.

Musset, A. E. and P. F. Barker, ^{40}Ar-^{39}Ar age spectra of basalts, Deep Sea Drilling Project site 516, Initial Rep. Deep Sea Drill. Proj., 72, 467-470, 1983.

National Geophysical Data Center, Worldwide gridded bathymetry, DBDB10, Announc. 85-MGG-01, Boulder, Colo., 1985.

Needham, H. D., D. Carre and J. C. Sibuet, Bathymetrie de la Ride de Walvis et du Bassin du Cap, Ocean Atlantique Sud, report, Dep. Geosci. Mar., Inst. Franc. de Rech. pour l'Exploitation de la Mer, Orleans, France, 1986.

Neill, W. M., Possible continental rifting in Brazil and Angola related to the opening of the South Atlantic, Nature Phys. Sci., 245, 104-107, 1973.

O'Connor, J. M., On the trail of South Atlantic hot spots: Implications for reconstructing African and South American plate motions (abstract), Eos Trans. AGU, 70, 1135, 1989.

Palacz, Z. A., and A. D. Saunders, Coupled trace element and isotope enrichment in the Cook-Austral-Samoa islands, southwest Pacific, Earth Planet. Sci. Letts., 79, 270-280, 1986.

Pearce, J. A., and M. J. Norry, Petrogenetic implications of Ti, Zr, Y and Nb variations in volcanic rocks, Contrib. Mineral. Petrol., 69, 33-47, 1979.

Pollitz, F. F., Two stage model of African absolute motion from 30 Myr to present, (abstract) Eos Trans. AGU, 71, 1640, 1990.

Ponte, F. C., and H. E. Asmus, The Brazilian marginal basins: Current state of knowledge, An. Acad. Bras. Cienc, 48 (suppl.), 215-239, 1976.

Price, R. C., A. K. Kennedy, M. Riggs-Sneeringer, and F. A. Frey, Geochemistry of basalts from the Indian Ocean triple junction: implications for the generation and evolution of Indian Ocean ridge basalts, Earth Planet. Sci. Letts., 78, 379-396, 1986.

Rabinowitz, P. D., Geophysical study of the continental margin of southern Africa, Geol. Soc. Am. Bull., 87, 1643-1653, 1976.

Rabinowitz, P. D., Geophysical study of the continental margin of southern Africa, Reply, Geol. Soc. Am. Bull., 89, 793-796, 1978.

Rabinowitz, P. D., and J. L. LaBrecque, The Mesozoic South Atlantic Ocean and evolution of its continental margins, J. Geophys. Res., 84, 5973-6002, 1979.

Richards, M. A., R. A. Duncan, and V. E. Courtillot, Flood basalts and hot-spot tracks: Plume heads and tails, Science, 246, 103-107, 1989.

Richardson, S. H., A. J. Erlank, A. R. Duncan, and D. L. Reid, Correlated Nd, Sr and Pb isotope variations in Walvis Ridge basalts and implications for the evolution of their mantle source, Earth Planet. Sci. Lett., 59, 327-342, 1982.

Richardson, S. H., A. J. Erlank, D. L. Reid and A. R. Duncan, Major and trace element and Nd and Sr isotope geochemistry of basalts from the DSDP leg 74 Walvis Ridge transect, Initial Rep. Deep Sea Drill. Proj., 74, 739-754, 1984.

Saemundsson, K., Outline of the geology of Iceland, Joekull, 29, 7-28, 1979.

Samson, S. D., and E. C. Alexander, Jr., Calibration of the interlaboratory ^{40}Ar-^{39}Ar dating standard, Mmhb-1, Chem. Geol., 66, 27-34, 1987.

Schilling, J.-G., Geochemical and isotopic variation along the Mid-Atlantic Ridge axis from 79°N to 0°N, in The Geology of North America, The Western North Atlantic Region, DNAG Ser., vol. M, edited by B. E. Tucholke and P. R. Vogt, pp. 137-156, Geological Society of America, Boulder, Colo., 137-156, 1986.

Schilling, J.-G., R. H. Kingsley, and J. G. DeVine, Galapagos hot spreading center system: Spatial, petrological and geochemical variations 83°W-101°W, J. Geophys. Res., 87, 5593-5610, 1982.

Schilling, J.-G., M. Zajac, R. Evans, T. Johnston, W. White, J. D. Devine, and R. Kingsley, Petrologic and geochemical variations along the Mid-Atlantic Ridge from 29°N to 73°N, Am. J. Sci., 283, 510-586, 1983.

Schilling, J.-G., Upper mantle heterogeneities and dynamics, Nature, 314, 62-67, 1985.

Schlanger, S. O., M. O. Garcia, B. H. Keating, J. J. Naughton, W. W. Sager, J. A. Haggerty, J. A. Philpotts, and R. A. Duncan, Geology and geochronology of the Line Islands, J. Geophys. Res., 89, 11, 261-11, 272, 1984.

Sclater, J. G., and D. P. McKenzie, Palaeobathymetry of the South Atlantic, Geol. Soc. Am. Bull., 84, 3203-3216, 1973.

Scrutton, R. A., Geophysical study of the continental margin of southern Africa-Discussion, Geol. Soc. Am. Bull., 89, 791-793, 1978.

Seidemann, D., Effects of submarine alteration on K-Ar dating of deep-sea igneous rocks, Geol. Soc. Am. Bull., 88, 1660-1666, 1977.

Seidemann, D., ^{40}Ar-^{39}Ar studies of deep-sea igneous rocks, Geochim. Cosmochim. Acta, 42, 1721-1734, 1978.

Shaw, P. R., and S. C. Cande, High-resolution inversion for South Atlantic plate kinematics using joint altimeter and magnetic anomaly data, J. Geophys. Res., 95, 2625-2644, 1990.

Sibuet, J.-C., and J. Mascle, Plate kinematic implications of Atlantic equatorial fracture zone trends, J. Geophys. Res., 83, 3401-3421, 1978.

Sibuet, J.-C., W. W. Hay, A. Prunier, L. Montadert, K. Hinz, and J. Fritsch, Early evolution of South Atlantic: Role of the rifting phase, Initial Rep. Deep Sea Drill. Proj., 75, 469-481, 1984.

Siedner, G., and J. A. Miller, K-Ar age determinations on basaltic rocks from south-west Africa and their bearing on continental drift, Earth Planet. Sci. Lett., 4, 451-458, 1968.

Siedner, G., and J. G. Mitchell, Episodic mesozoic volcanism in Namibia and Brazil: A K-Ar isochron study bearing on the opening of the South Atlantic, Earth Planet. Sci. Lett., 30, 292-302, 1976.

Sleep, N. H., Hotspots and mantle plumes: Some phenomonology, J. Geophys. Res., 95, 6715-6736, 1990.

Spooner, E. T. C., The strontium isotopic composition of seawater and seawater-oceanic crust interaction, Earth Planet. Sci. Lett., 31, 167-174, 1976.

Srivastava, S. P., and C. R. Tapscott, Plate kinematics of the North Atlantic, in The Geology of North America: The western North Atlantic Region, DNAG Ser., vol. M, edited by B. E. Tucholke and P. R. Vogt, 379-404, Geological Society of America, Boulder, Colo., 1986.

Staudigel, H. and S. R. Hart, Alteration of basaltic glass: Mechanisms and significance for the oceanic crust-seawater budget, Geochim. Cosmochim. Acta 47, 337-350, 1983.

Staudigel, H., A. Zindler, S. R. Hart, T. Leslie, C.-Y. Chen, and D. Clague, The isotope systematics of a juvenile intraplate volcano: Pb, Nd, and Sr isotope ratios of basalts from Loihi seamount, Hawaii, Earth Planet. Sci. Letts., 69, 13-29, 1984.

Staudigel, H., K.-H. Park, M. Pringle, J. L. Rubenstone, W. H. F. Smith, and A. Zindler, The longevity of the South Pacific isotopic and thermal anomaly, Earth Planet. Sci. Letts., 102, 24-44, 1991.

Stock, J. M., and P. Molnar, Some geometrical aspects of uncertainties in combined plate reconstructions, Geology, 11, 697-701, 1983.

Sullivan, K. D., and C. E. Keen, Newfoundland Seamounts: Petrology and geochemistry, Geol. Assoc. Can. Spec. Pap., 16, 461-476, 1977.

Sun, S. S., R. W. Nesbitt, and A. Y. Sharaskin, Geochemical characteristics of mid-ocean ridge basalts, Earth Planet. Sci. Lett., 44, 119-138, 1979.

Sun, S.-S., Lead isotopic study of young volcanic rocks from mid-ocean ridges, ocean islands, and island arcs, Phil. Trans. Roy. Soc. London A297, 409-445, 1980.

Svisero, D. P., H. O. A. Meyer, and H. Tsai, Kimberlites in Brazil: An initial report, in Kimberlites Diatremes, and Diamonds: Their Geology, Petrology and Geochemistry, edited by H. O. A. Meyer, and F. R. Boyd, pp. 92-100, AGU, Washington, D. C., 1979.

Taras, B. D., and S. R. Hart, Geochemical evolution of the New England Seamount chain: Isotopic and trace element constraints, Chem. Geol., 64, 35-54, 1987.

Tatsumoto, M., D. M. Unruh, P. Stille, and H. Fujimaki, Pb, Sr, and Nd isotopes in oceanic basalts. In Proc. 27th Internat. Geol. Cong. 11, 485-501. Geochemistry and Cosmochemistry, VNU Science Press, 1984.

Thompson, G., A geochemical study of the low temperature interaction of seawater and oceanic igneous rocks, Eos Trans. AGU, 54, 1015-1019, 1973.

Thompson, G., and S. E. Humphris, Petrology and geochemistry of rocks from the Walvis Ridge: Deep Sea Drilling Project leg 74, sites 525, 527, and 528, Initial Rep. Deep Sea Drill. Proj., 74, 755-764, 1984.

Thompson, G., S. Humphris, and J.-G. Schilling, Petrology and geochemistry of basaltic rocks from the Rio Grande Rise, South Atlantic: Deep Sea Drilling Project, leg 72, hole 516, Initial Rep. Deep Sea Drill. Proj., 72, 457-466, 1983.

Tucholke, B. E., and N. C. Smoot, Evidence for age and evolution of Corner Seamounts and Great Meteor seamount chain from multibeam bathymetry, J. Geophys. Res., in press, 1990.

Turner, G., and P. H. Cadogan, Possible effects of [39]Ar recoil in [40]Ar-[39]Ar dating of lunar, Proc. Lunar Sci. Conf., 5, 1601-1615, 1974.

Vandoros, P., and M. A. F. Oliveira, Sobre o fonolito de Messejana, Ceara, An. Acad. Bras. Cienco., 40, 203-206, 1968.

Vidal, Ph., C. Chauvel, and R. Brousse, Large mantle heterogeneity beneath French Polynesia, Nature, 307, 536-538, 1984.

Vogt, P. R., and G. L. Johnson, Transform faults and longitudinal flow beneath the mid-ocean ridge, J. Geophys. Res., 80, 1399-1428, 1975.

Vogt, P. R., B. Zondek, P. W. Fell, N. Z. Cherkis, and R. K. Perry, Seasat altimetry, the North Atlantic geoid, and evaluation by shipborne subsatellite profiles, J. Geophys. Res., 89, 9885-9903, 1984.

Walker, D. A., and I. McDougall, [40]Ar-[39]Ar and K-Ar dating of altered glassy volcanic rocks: The Dabi Volcanics, P.N.G., Geochem. Cosmochim. Acta., 46, 2181-2190, 1982.

Wang, Y. L., Y.-G. Liu, and R. A. Schmitt, Rare earth element geochemistry of south Atlantic deep sea sediments: Ce anomaly change at $\approx$ 54 My, Geochim. Cosmochim. Acta, 50, 1337-1355, 1986.

Weaver, B. L., N. G. Marsh, and J. Tarney, Trace element geochemistry of basaltic rocks recovered at site 516, Rio Grande rise, Initial Rep. Deep Sea Drill. Proj., 72, 451-455, 1983.

Weaver, B. L., D. A. Wood, J. Tarney, and J. L. Joron, Geochemistry of ocean island basalts from the South Atlantic: Ascension, Bouvet, St. Helena, Gough, and Tristan da Cunha, Alkaline Igneous Rocks, edited by J. G. Fitton, and B. G. J. Upton, Spec. Publ. 30, pp. 253-267, Geol. Soc. of London, 1987.

Weiss, W., Upper Cretaceous foraminiferal biostratigraphy from the Rio Grande Rise: Site 516 of leg 72, Initial Rep. Deep Sea Drill. Proj., 72, 715-721, 1983.

Wendt, I., H. Kreuser, P. Muller, U. von Rad, and H. Raschke, K-Ar ages of basalt from Great Meteor and Josephine seamounts (eastern North Atlantic), Deep Sea Res., 23, 849-862, 1976.

White, R., and D. McKenzie, Magmatism at rift zones: The generation of volcanic continental margins and flood basalts, J. Geophys. Res., 94, 7685-7729, 1989.

White, R., Evolution of the Reunion Hot spot, (Abstract), Intraplate volcanism. The Reunion hot spot, Institut Physique du Globe, Paris, 12-17 November, 1990.

White, W. M., Sources of oceanic basalts: Radiogenic isotopic evidence, Geology 13, 115-118, 1985.

White, W. M., A. W. Hofmann, H. Puchelt, Isotope geochemistry of the Pacific Mid-Ocean Ridge basalt, J. Geophys. Res., 92, 4881-4893, 1987.

White, W. M., M. M. Cheatham, and R. A. Duncan, Isotope geochemistry of Leg 115 basalts and inferences on the history of the Reunion mantle plume, Proceedings of the Ocean Drilling Program, Scientific Results, Vol 115, 53-61, 1990.

Wilson, J. T., A possible origin of the Hawaiian Islands, Can. J. Phys., 41, 863-870, 1963.

York, D., Least squares fitting of a straight line with correlated errors, Earth Planet. Sci. Lett., 5, 320-324, 1969.

Zindler, A, E. Jagoutz, and S. Goldstein, Nd, Sr, and Pb isotopic systematics in a three-component mantle: a new perspective, Nature 298, 519-523, 1982.

Zindler, A., and S. Hart., Chemical Geodynamics, Ann. Rev. Earth Planet. Sci., 14, 493-571, 1986.

APPENDICES

APPENDIX I.

Discussion of ^{40}Ar-^{39}Ar data and apparent ages reported in Chapter III

AC-D-2E produced a reasonable plateau age of 78.5 ± 0.4 Ma Figure III.2a), which is supported by an isochron age of 79.0 ± 0.9 Ma (intercept of 290 ± 6.0) (Figure III.2b), an inverse isochron of 79.1 ± 0.9 Ma (Figure III.2c) (intercept of 290 ± 6.3), and a total fusion age of 78.1 ± 0.6 Ma . An age of 79 Ma is indicated for this sample.

AC-D-2B produced a viable plateau age of 81.6 ± 0.4 Ma (Figure III.2d), which is supported by an isochron age of 80.1 ± 1.3 Ma (Figure III.2e) (intercept of 319 ± 31), an inverse isochron of 81.6 ± 0.7 Ma (Figure III.2f) (intercept of 294 ± 16), and a total fusion age of 82.8 ± 0.5 Ma. An age of between 82 and 83 Ma is indicated for this sample.

AC-D-2H also produced a good plateau age of 80.2 ± 0.4 Ma (Figure III.2g), which is supported by an isochron age of 78.8 ± 1.0 Ma (Figure III.2h) (intercept of 298 ± 20), an inverse isochron age of 80.4 ± 0.5 Ma (Figure III.2I) (intercept of 284 ± 5.6), and a total fusion age of 81.4 ± 0.4 Ma. The best estimate of this sample is between 79 and 81 Ma.

The best overall age estimate for Seamount 2 is between 80 and 82 Ma.

AC-D-5A produced a good plateau age of 77.5 ± 0.4 Ma (Figure III.2J), which is supported by an isochron age of 77.6 ± 0.6 Ma (Figure III.2k) (intercept of 288 ± 10), an inverse isochron age of 78.2 ± 0.5 Ma (Figure III.2l) (intercept of 278 ± 5), and a total fusion age of 63.5 ± 1.2 Ma. The apparent age of this site is 78 Ma.

AC-D-06 produced an excellent plateau age of 52.3 ± 0.3 Ma (Figure III.2m), which is supported by an isochron age of 52.2 ± 0.7 Ma (Figure III.2n) (intercept is 292 ± 27), an inverse isochron age of 52.9 ± 0.6 Ma (Figure III.2o) (intercept of 268 ± 22) and a fusion age of 51.0 ± 0.9 Ma. The apparent crystallization age of this site is 52.2 Ma.

Gough Lineament

AG51-2-1 (Tristan da Cunha) produced an equivocal plateau age of 1.3 ± 0.1 Ma (Figure III.3a). This apparent age is not supported by an isochron age of 0.64 ± 0.3 Ma (Figure III.3b) (intercept of 301.8 ± 3.3) and a concordant inverse correlation age of 0.65 ± 0.3 Ma (Figure III.3c) (intercept of 301.8 ± 6.4). We consider the recalculate total fusion age of 5.6 ± 0.3 Ma as being unreliable in view of the discrepancy between, and with, plateau and isochron ages. The best age estimate for this sample ranges between 0.65 and 1.3 Ma.

AG51-3-6 (Gough Island) produced a plateau age of 0.58 ± 0.07 Ma (Figure III.3d), based on the fusion heating step. The earlier heating steps produced meaningless negative ages. We attribute this to the low yield of radiogenic Ar in this very young sample, combined with a problem with the heating filament which resulted in the initial steps being too low in temperature. Straight lines could

therefore not be fitted to the scattered heating steps in order to calculate isochron and inverse correlation ages (Figures III.3e, and III.3f). A recalculated total fusion age of 0.25 ± 0.12 Ma. Our best estimate of the age of this sample from Gough island is 0.6 Ma.

AG51-7-1 (McNish Seamount) produced a convincing plateau age of 8.1 ± 0.05 Ma (Figure III.3g). This age estimate is reinforced by an isochron age of 8.1 ± 0.9 Ma (Figure III.3h) (intercept of 292.1 ± 5.6), a concordant inverse correlation age of 8.2 ± 0.07 Ma (Figure III.3I) (intercept of 292.4 ± 5.3), and a recalculated total fusion age of 7.9 ± 0.2 Ma. An apparent age of 8.1 Ma is confidently reported for this sample.

AG51-9-1 (RSA Seamount) produced a very reliable plateau age of 18.8 ± 0.1 Ma (Figure III.3J), which is support isochron age of 18.7 ± 0.2 Ma (Figure III.3k) (intercept of 265.9 ± 51.6), an inverse correlation age of 18.8 ± 0.2 Ma (Figure III.3l) (intercept of 321 ± 331), and a recalculated total fusion age is 18.9 ± 0.1 Ma. 18.8 Ma is reliable age for this seamount sample.

7° East and Vema Seamounts

AG51-11-10 (7°East Seamount) produced a plateau age of 89.6 ± 0.5 Ma (Figure III.3m), which is supported by an isochron age of 90.4 ± 1.5 Ma (Figure III.3n) (263.1 ± 43) and an inverse correlation age of 91.2 ± 1.1 Ma (Figure III.3o) (241.8 ± 31). We consider a recalculated total fusion age of 85.4 ± 0.6 Ma to be erroneously young. The best age of this seamount sample is between 90 and 91 Ma.

AG51-12-3 (Vema Seamount) produced a convincing plateau age of 15.3 ± 0.1 Ma (Figure III.3p), which is supported by an isochron age of 15.2 ± 0.3 Ma (Figure III.3q) (intercept of 298.6 ± 26.3), an inverse correlation age of 15.2 ± 0.3 Ma (Figure III.3r) (intercept of 310.2 ± 25), and a recalculated total fusion age is 15.1 ± 0.1 Ma. An age of 15.2 Ma can reliably be assigned to this seamount sample.

APPENDIX 2

Description of samples discussed in Chapters III and IV

St. Helena Seamount 2 dredge samples are from individual cobbles which were encased in a large slab of manganese crust.

St. Helena Seamount 2

AC-02A   highly altered volcanic rock

Phenocrysts
mostly laths of plagioclase
~ 10% magnetite

Groundmass
largely altered to clays between feldspars

Comments
highly altered in terms of major element chemistry and petrography
Collophane present so explaining high P_2O_5 content
magnetite filling in voids
lot of material pulled from thin section during preparation

AC-02B   moderately altered trachyte

Phenocrysts
mostly long laths of plagioclase, some large phenocrysts of plagioclase
10% magnetite

Groundmass
clay present between feldspar laths

Comments
trachytic texture

AC-02C   highly altered volcanic rock

Phenocrysts
mostly small fine grained laths of feldspar and some large phenocrysts of feldspar
~20% magnetite

Groundmass
largely altered to clays and collophane

Comments
major element classification is not possible due to degree of alteration

AC-02E   moderately altered basalt

thin section not available
major element chemistry indicates that it is a moderately altered basalt.

AC-02H   moderately altered trachyte

Phenocrysts
mostly fine grained laths of feldspar

~10% large phenocrysts of plagioclase < 1mm
~10% magnetite
some pyroxene remaining

Groundmass
largely altered to clay

Comments
trachytic texture
feldspar appears to be albatized

AC-02G   moderately altered olivine plagioclase basalt

Phenocrysts
mostly medium sized laths of feldspar
olivine phenocrysts totally altered to iddingsite
~15% magnetite, which also fills in voids

Groundmass
altered to clays

Comments
No major element chemistry availability

AC-02K   highly altered volcanic rock

Phenocrysts
mostly laths of plagioclase
~10% magnetite
Pyroxene altered to clay

Groundmass
altered to clay

Comments
groundmass and feldspars altered to clays

AC-02I   moderately altered volcanic rock

Phenocrysts
mostly fine grained laths of feldspar
~10% magnetite
some altered pyroxenes

Groundmass
moderate alteration to clays

Comments
no major element chemistry

St. Helena Seamount 5

AC-05A   moderately altered olivine basalt

Phenocrysts
mostly composed largely of medium sized laths of feldspar, some as large as 0.5 mm
some pyroxene

Groundmass
some alteration to clays

Comments
coarse grained rock

AC-05B   highly altered volcanic rock (alkali basalt?)

Phenocrysts
~10% magnetite

Groundmass

Comments
no major element data

St. Helena Seamount 6

AC-06   slightly altered trachyte

Phenocrysts
mostly laths of feldspar
~10% magnetite

Groundmass
small degree of alteration of groundmass to clays

Comments
trachytic texture

Cameroon Line

Tinhosa Granda A-01

fairly fresh lava, some slats of plagioclase?
some fine grained pyroxene
~5% magnetite

Walvis Ridge

DSDP 530   moderately altered tholeiitic basalt

Phenocrysts
mostly long laths of feldspar
~15% magnetite
possible olivine
some relatively unaltered pyroxene

Groundmass
all altered to clay

Comments
ordinary seafloor basalt

Pernambuco Seamount

RC25-15-D1-B   highly altered volcanic rock

Phenocrysts
mostly fine grained laths of feldspar
~40% magnetite

Groundmass
all turned to clay

Comments
no major element chemistry available

RC25-15-D1-D   highly altered olivine basalt

Phenocrysts
mainly consists of medium sized laths of feldspar
some olivine
~60% magnetite

Groundmass
devitrified glass?

Comments
grain size larger than RC25-15-D1-B and RC25-15-D1-C, so a different flow unit
no major element chemistry available

RC25-15-D1-C   moderately altered tholeiitic or subalkaline basalt

Phenocrysts
mostly consists of plagioclase laths
lot of pyroxene
some olivine

Groundmass
altered to clay

Comments

Bahia Seamount

RC29-05-D3   highly altered volcanic rock

Phenocrysts
mostly feldspar laths and large calcite phenocrysts (~40%)
~50% magnetite in non-calcite phase
some pyroxene

Groundmass
mostly altered to clays
devitrified glass?

Comments
Major element classification unreliable due to alteration

APPENDIX 3.

Analytical Techniques discussed in Chapter IV

Radiogenic Isotopes (after White et al. 1990)

Rock samples were crushed in an iron platter mortar, and chips of basalts were handpicked to remove as much altered material as possible and to exclude pieces exposed to dredge, drill, and saw. After selection, all further handling was carried out in an ultraclean environment. Samples were ultrasonically cleaned in distilled water and dried; 200 mg of chips from each sample were weighed into a Teflon beaker. The samples were then leached for 1 hr in hot, distilled 6N HCL to remove contamination introduced during dredging, drilling, and handling and to remove Sr in remaining secondary phases. The samples were digested and Pb was extracted and purified with the HBr ion exchange technique described in White and Dupre (1986). The residue from the Pb extraction was converted to chloride, and Sr and Nd were extracted and purified with a BioRad AG50W-X12 and di-2-ethylhexyl orthophosphoric acid ion exchange technique (White and Patchett, 1984).

Lead was loaded on a single Re filaments with silica gel and H3P04 and analyzed in the VG Sector mass spectrometer at Cornell University. Ion beams of ^{204}Pb, ^{206}Pb, ^{207}Pb, and ^{208}Pb were simultaneously collected in four Faraday cups, and isotope were calculated after correction for differences in amplifier gain. An individual analysis consisted of 80-100 integrations of 8 s each, with base lines measured between blocks of 10 integrations. The 208Pb ion beams were typically 1-4 x 10-11 amps. To minimize sample-to-sample variations in mass fractionation during the analysis, all analyses were made at a filament temperature of 1350°C. Lead isotope ratios were corrected for fractionation by applying a 1.1°/amu correction. The correction factor was determined by repetitive analysis of NBS SRM-981, assuming values for this standard of $^{206}Pb/^{204}Pb$ = 16.937, $^{207}Pb/^{204}Pb$ = 15.493, and $^{208}Pb/^{204}Pb$ = 36.705. The 2 sigma analytical uncertainty, based on the reproducibility of the NBS-981 standard, is ± 0.012 for $^{206}Pb/^{204}Pb$, ± 0.013 for $^{207}Pb/^{204}Pb$, and ± 0.041 for $^{208}Pb/^{204}Pb$

Strontium was loaded on a single W filaments with TaCl5-HF activator, and analyzed with a dynamic triple collector technique. Ratios were corrected for mass fractionation assuming that $^{86}Sr/^{88}Sr$ = 0.1194. An ion beam intensity of ^{88}Sr was maintained near 3 x 10-11 amp during the analysis. The mean $^{87}Sr/^{86}Sr$ ratio of 58 analyses of the E&A Sr isotopic standard was 0.708020. Based on the reproducibility of this standard, the 2 sigma uncertainty is estimated at ± 0.000035.

Neodymium was loaded with a small amount of H3P04 on triple filaments consisting of Re centers and Ta sides. Analysis was performed with a dynamic quintuple collector technique that allowed measurement of the $^{143}Nd/^{144}Nd$ ratio as a monitor of data quality. Ratios were corrected for mass fractionation, assuming $^{143}Nd/^{144}Nd$ = 0.72190. An ion beam of 144Nd was maintained near 1 x 10-11 amp. The mean $^{143}Nd/^{144}Nd$ and $^{145}Nd/^{144}Nd$ ratios of 45 analyses of the La Jolla isotopic standard were 0.511840 and 0.348401, respectively. The $^{145}Nd/^{144}Nd$ ratios of samples always agreed with this value within analytical uncertainty. Based on the reproducibility of this standard, the 2 sigma analytical uncertainty of the $^{143}Nd/^{144}Nd$ ratios is estimated at ± 0.000016.

X-Ray Fluoresence Spectrometry (after Hooper and Johnson, unpublished manuscript)

Samples were reduced by tungsten carbide jaw crusher to small (~1 cm) chips. Fresh chips were hand picked to fill a 24 cc container, which was then emptied into a Tema swing mill with tungsten carbide surfaces and milled for 2 minutes. 3.5 gm of this rock powder was then weighed into a plastic mixing jar with 7.0 gms of spec. pure lithium tetraborate (Li2B4O7) and, with an enclosed plastic bead, mixed for 10 minutes. The mixed powders were emptied into graphite crucibles with internal measurements of 34.9 mm diameter by 31.8 mm high. Twenty-four filled crucibles were placed on a ceramic tray and loaded into a muffel furnace only large enough to contain the load. Fusion took 5 minutes from the time the preheated furnace returned to its normal 1000°C after loading. The ceramic plate and graphite crucibles were then removed and left to cool (10 minutes). Each disk was reground in the Tema swingmill for 35 seconds, the glass powder replaced in the graphite crucibles and refused for 5 minutes.

Following the second fusion, the cooled disks were labelled with an engraver, the lower flat surface was ground on a lap with coarse 9240) SiC grit for approximately 10 seconds, with fine

(600) SiC grit for approximately 10 seconds, finished briefly on a glass plate with fine (600) SiC grit, washed in an ultrasonic cleaner, dried, and are then ready to be loaded into the XRF spectrometer.

Use of a tungsten carbide mill resulted in significant contamination of the powder with tungsten and cobalt. Some niobium contamination has been suggested (Joron et al., 1980; Hickson and Juras, 1986) but analyses of pure vein quartz by the same preparation techniques shows no significant contamination). Hand picking of fresh chips after the use of steel hammers or hydraulic presses should prevent iron, chromium or nickel contamination.

The concentrations of the 27 elements in the unknown samples were measured by comparing the X-ray intensity for each element with the intensity of two disks each of eight international standards (USGS standards PCC-1, BCR-1, BIR-1, DNC-1, W-2, AGV-1, GSP-1 and G-2, using the values recommended by Flanagan, 1976). The 16 standard disks were run and recalibrated approximately once every three weeks or after a run of between one and two hundred unknown samples.

Two fused Li tetraborate disk samples (BCR-P and GSP-1) were used as internal standards. They are run every 28 samples routinely to provide a check on instrumental performance and provide a measure of instrument precision. Variation is given as one standard deviation expressed in oxide percent (major elements) or parts per million (trace elements), and as relative percent.

Absolute accuracy cannot be quantified exactly as no absolute standards are available. Best estimates of accuracy is derived from the standard sample calibration curves. These curves are the best straight line computer fit drawn through plots of X-ray intensity versus "theoretical intensity" (the intensity calculated from the given value from Flanagan, 1976, corrected for absorption, etc). The scatter of points about this line is a measure of accuracy of the method for each element.

For most major elements the variation between the two disks of the same standard is of the same order as their variation from the given value. The inference is that variation between different samples of standard powder or inhomogeneity resulting from the preparation of the refused beads is greater than inaccuracies caused by inadequate matrix and interference corrections. In some cases both disk values lie to the same side of the given value and here there is the possibility that the absorption corrections are less than perfect. With the exception of Na_2O, however, the total discrepancies from the given value (assuming these are perfect) are less than might reasonably be expected between two random samples collected in the field from the same rock unit-lava flow, igneous intrusion, etc.

For trace elements precision declines below 50 ppm and values below 10 ppm can be regarded as qualitative only. The precision for Ni, Cr, Sc, V, Ba, LA, and Ce is significantly less than that for Rb, Sr, Zr, Nb, Y, Ga, Cu, Zn, Pb, and Th. This correlates with the lower intensities for these elements (measured as cnts/sec/ppm) using the Rh tube. Some nickel in the Rh target exacerbates Ni precision problem.